UNIVERSITÄT
LEIPZIG

REPORT
Institute für Physik
The Physics Institutes
2018

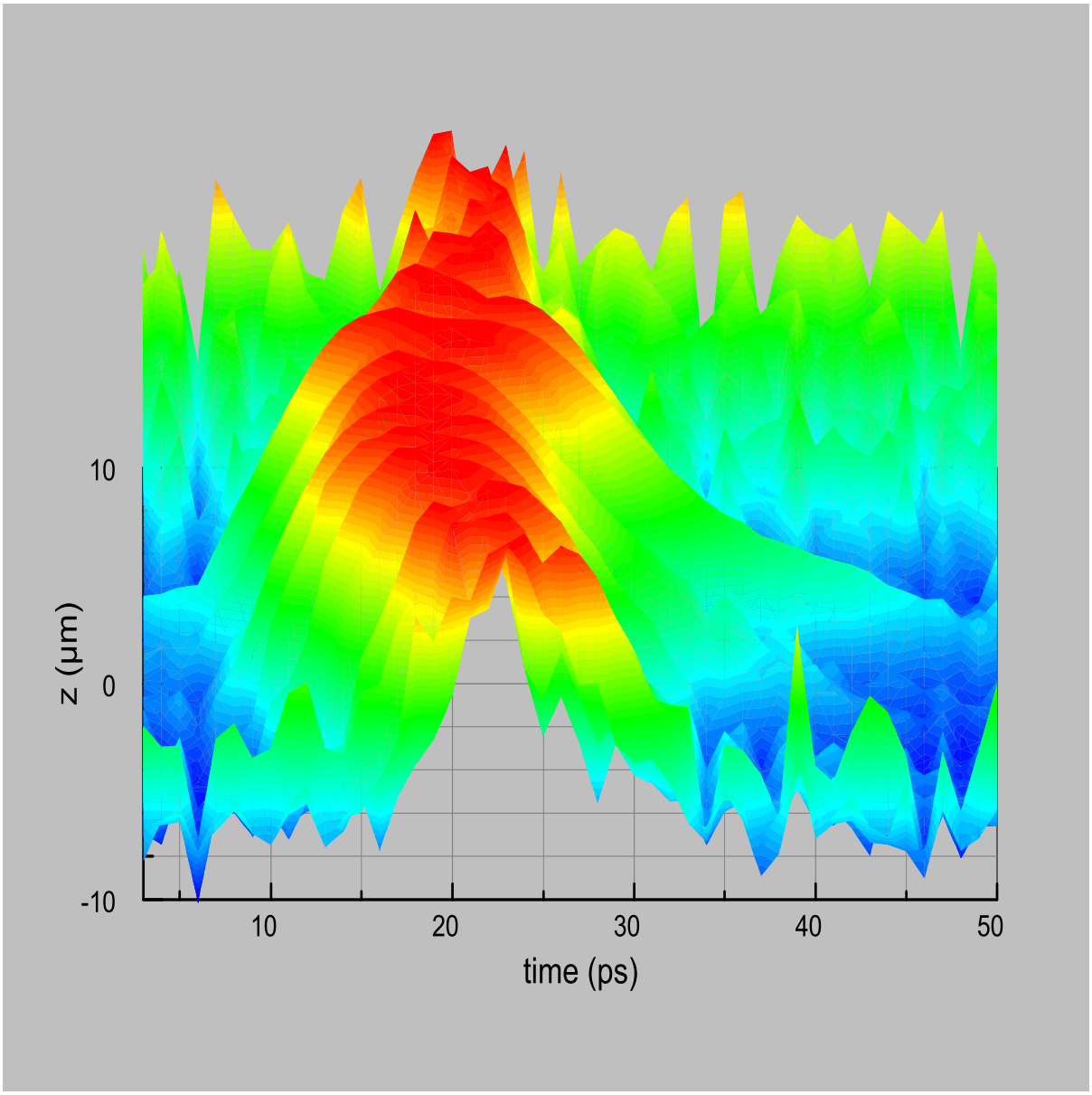

The Physics Institutes of Universität Leipzig, Report 2018
M. Grundmann (Ed.)

Technical Editor: Anja Heck

Printed in Germany by
MERKUR Druck und Kopierzentrum GmbH, Leipzig

online available at
http://nbn-resolving.de/urn:nbn:de:bsz:15-qucosa-151238

Front cover
■ Spatiotemporal evolution of a whispering gallery mode exciton-polariton Bose-Einstein condensate at 3.188 eV in a ZnO microwire after femtosecond-excitation with a one micrometer sized laser spot. The emission intensity is colour coded. Within 10 ps, the condensate spreads along the microwire axis about ± 10 μm (z-direction in the image) and was observed as long as 40 ps. ("Spatiotemporal evolution of coherent polariton modes in ZnO microwire cavities at room temperature", T. Michalsky, M. Wille, M. Grundmann, and R. Schmidt-Grund, Nano Letters **18**, 6820 (2018)).

Back cover Resent published.

Peter-Debye-Institut für Physik der weichen Materie
Felix-Bloch-Institut für Festkörperphysik
Institut für Theoretische Physik

Fakultät für
Physik und Geowissenschaften

Universität Leipzig

Peter Debye Institute for Soft Matter Physics
Felix Bloch Institute for Solid State Physics
Institute for Theoretical Physics

Faculty of Physics and Earth Sciences

Universität Leipzig

Report 2018

Addresses

Peter Debye Institute for Soft Matter Physics

Linnéstraße 5
D-04103 Leipzig, Germany
Phone: +49 341 97-32654
Fax: +49 341 97-32598
WWW: https://www.physgeo.uni-leipzig.de/fakultaet/institutebereiche/peter-debye-institut/
Mailing address: Postfach 100 920, D-04009 Leipzig, Germany

Felix Bloch Institute for Solid State Physics

Linnéstraße 5
D-04103 Leipzig, Germany
Phone: +49 341 97-32650
Fax: +49 341 97-32668
WWW: https://www.physgeo.uni-leipzig.de/fakultaet/institutebereiche/felix-bloch-institut/
Mailing address: Postfach 100 920, D-04009 Leipzig, Germany

Institute for Theoretical Physics

Brüderstraße 16
D-04103 Leipzig, Germany
Phone: +49 341 97-32420
Fax: +49 341 97-32548
WWW: https://www.physgeo.uni-leipzig.de/fakultaet/institutebereiche/theoretische-physik/
Mailing address: Postfach 100 920, D-04009 Leipzig, Germany

Preface

The 2018 Report of the Physics Institutes of the Universität Leipzig provides an overview of the structure and research activities of the three institutes.

Prof. Dr. Claudia S. Schnohr has joined the Felix Bloch Institute for Solid State Physics with her department "Structure and Properties of Complex Materials"; her specialty is X-ray spectroscopy and the investigation of local bond structure on the subnanometer scale. Dr. Johannes Deiglmayr has established an independent department for Quantum Optics at the same institute and installed his experimental setup for the high-precision quantum optical studies of Rydberg atoms and molecules.

As it is meanwhile a tradition, the Peter Debye Institute for Soft Matter Physics has organized its annual Soft Matter Day also in 2018. On July 6, all departments of the institute presented their current research in talks and posters. About one hundred scientists and students have been enjoying very lively discussions together with members of other institutes and faculties and a BBQ.

From September 24 to 26, 2018, the 9th Annual Symposium "Physics of Cancer", also supported by the graduate school BuildMoNa, brought together researchers from the worldwide pioneering groups that are investigating the mechanisms underlying cancer progression as well as diagnosis and innovative therapies. The annual BuildMoNa Symposium was held in the "Complex Nanostructures" area with focus on nanowires and their applications together with FOR1616 in Weimar. Furthermore, the proposal for a CECAM Workshop on "Active Matter and Artificial Intelligence" organized by Frank Cichos, Klaus Kroy, Fernando Peruani and Giovanni Volpe has been granted. It has meanwhile taken place from September 30 to October 02, 2019 in Lausanne, Switzerland.

The Leipzig School of Natural Sciences BuildMoNa is a platform of various faculties joining physics, chemistry and biochemistry oriented research on the nanoscale. It was established in the German Excellence Initiative and has now been formally established and funded as the first continual "Graduiertenschule" (Graduate School) of Universität Leipzig and a "Zielvereinbarung" (objective agreement) has been signed with the rectorate.

Work has successfully continued in the DFG-funded Centers of Excellence (Sonderforschungsbereiche) SFB 762 "Functionality of Oxide Interfaces" and SFB TRR 102 "Polymers under Multiple Constraints: Restricted and Controlled Molecular Order and Mobility". SFB762 will 2019 be in its last year. For the CRC Transregio 102 "Polymers under Multiple Constraints", the proposal for the third funding period has been submitted to the DFG and has been funded in the meantime. The Leipzig Labs "Physics of Tissue" and "Bionic Nano-objects" were approved by the rectorate.

Research continued in several Research Units (DFG Forschungsgruppen), Prior-

Figure 1: Signature of the objective agreement, Rektorin Prof. Schücking and Speaker of the Graduate School BuildMoNa Prof. Grundmann. (Photo by Swen Reichhold)

ity Programs (DFG Schwerpunktprogramme) and EU projects. A proposal for a new Leipzig-based DFG Research Unit on "Copper Iodide as a Multifunctional Semiconductor" was submitted and has been funded in the meantime. The International Graduate College "Statistical Physics of Complex Systems" of the Deutsch-Französische Hochschule (DFH-UFA) run by the computational physics group in cooperation with the partners Université de Lorraine in Nancy, France, Coventry University, UK, and the Institute for Condensed Matter Physis of the National Academy of Sciences of Ukraine in Lviv, Ukraine, started in January 2017, continues work in its 4th funding period.

We are grateful to all our guests for enriching this academic year with their contributions in the colloquia and within our work groups. The Felix Bloch Lecture Leipzig has been established and a colloquium talk by Theo Rasing, Radboud University Nijmegen, Netherlands on "Controlling Spin Dynamics with Light" was followed by the presentation of the Felix Bloch Early Investigator Award to Dr. Ralf Wunderlich for his work on "Nuclear hyperpolarisation in diamond". Afterwards, the unveiling of a bronze plate of Felix Bloch by the Leipzig sculptor Markus Gläser in the foyer of the Physics building was a memorable event in the presence of his son Frank Bloch and one of his grandsons from the United States (see also9.1).

Our activities and success are enabled through the generous support from various funding agencies for which we are very grateful and which is individually acknowledged in the brief reports.

Leipzig,
July 2020

F. Cichos
M. Grundmann
W. Janke
Directors

Contents

1

Structure and Staff of the Institutes

1.1 Peter Debye Institute for Soft Matter Physics

1.1.1 Office of the Director

Prof. Dr. Frank Cichos (director)

1.1.2 Molecular Nano-Photonics, Molekulare Nanophotonik [MON]

Prof. Dr. Frank Cichos

Administration and Laboratory Management

Dipl.-Phys. Andrea Kramer

Technical staff

Dipl.-Phys. Uwe Weber

PhD candidates

Alexander Fischer, M.Sc.
Martin Fränzl, M.Sc.
Jan Kiethe, M.Sc.
Santiago Muiños Landin, M.Sc.
Dipl.-Phys. Romy Schachoff
Nicola Söker, M.Sc.
Xiaoya Su, M.Sc.
Tobias Thalheim, M.Sc.

Students

Pablo Bähler Gamboa
Maike Dethloff

Nikkin Devaraju
Ena Osmic
Ricardo Rose
Matthias Volz
Fabian Welzel

1.1.3 Molecular Physics, Molekülphysik [MOP]

Prof. Dr. Friedrich Kremer

Secretary

Kerstin Lohse

Technical staff

Dipl.-Ing. (FH) Jörg Reinmuth
Dipl.-Phys. Wiktor Skokow

Academic staff

Dr. Markus Anton
Dr. Wilhelm Kossack
M. Edu. Falk Frenzel

1.1.4 Soft Matter Physics, Physik der weichen Materie [PWM]

Prof. Dr. Josef A. Käs

Secretary

Claudia Brück

Technical staff

Dr. Undine Dietrich
Dipl.-Phys. Bernd Kohlstrunk

Academic staff

Dr. Thomas Fuhs
Dr. Jörg Schnauß
Dr. David M. Smith
Prof. Dr. Mareike Zink

PhD candidates

Alice Abend, M.Sc.
Iman Elbalasy, M.Sc.
Carlotta Ficorella, M.Sc.
Martin Glaser, M.Sc.
Tom Golde, M.Sc.
Steffen Grosser, M.Sc.
Dipl.-Phys. Tina Händler
Paul Heine, M.Sc.
Philine Hietschold, M.Sc.
Kantida Juncheed, M.Sc.
Hans Kubitschke, M.Sc.
Jürgen Lippoldt, M.Sc.
Paul Mollenkopf, M.Sc.
Erik Morawetz, M.Sc.
Linda Oswald, M.Sc.
Dipl.-Phys. Carsten Schuldt
Frank Sauer, M.Sc.
Hannah-Marie Scholz-Marggraf, M.Sc.
Dimitrij Tschodu, M.Sc.
Dipl.-Phys. Enrico Warmt
Xiaofan Xie, M.Sc.
Astrid Weidt, M.Sc.

Students

Eliane Blauth
Pablo Gottheil
Klaus Jazxhi
Carlotta Ficorella
Dusan Prasevic
Frederic Renner
Hannah-Marie Scholz-Marggraf
Chelsie Steele
Cary Tutmarc
Xiaofan Xie
Pamela Yaninska

1.1.5 Biological Physics, Biologische Physik [BIP]

Prof. Dr. Claudia Mierke

Secretary

Kerstin Lohse

Technical staff

Dipl.-Ing. Kathrin Koch

PhD candidates

Stefanie Puder, M.Sc.
Dipl.-Phys. Tony Fischer
Tom Kunschmann, M.Sc.
Frank Sauer, M.Sc.

Students

Alexander Hayn
Anne-Dorette Ziems
Christian Aermes
Sebastian Ronneberger

1.1.6 Molecular Physics, Molekülphysik [MOP]

Prof. Dr. Ralf Seidel

Secretary

Kerstin Lohse

Technical staff

Dipl.-Phys. Cordula Krause
Dr. Nicole Weizenmann

Academic staff

Dr. Martin Göse
Dr. Brighton Samatanga
Dr. Saurabh Raj

PhD candidates

Pierre Aldag, M.Sc.
Dipl.-Phys. Sebastian Belau
Shikhar Gupta, M.Sc.
Florian Scheffler, M.Sc.
Selgar Henkel, M.Sc.
Patrick Irmisch, M.Sc.
Kristina Kasaciunaite, M.Sc.
Dipl.-Phys. Dominik Kauert

Felix Carstensen Kemmerich, M.Sc.
Ulrich Kemper, M.Sc.
Marius Rutkauskas, M.Sc.
Jingjing Ye, M.Sc.

Students

Brock Fergus Rupert Fettes-Leagas
Jan Kohler
Daniil Kudrin
Carlos Christian Sustay Martinez
Jonatan Meiske
Josephine Teske
Kiryl Tsiaroshyn
Joye Wittenbecher
Alexander Wulfken

1.2 Felix Bloch Institute for Solid State Physics

1.2.1 Office of the Director

Prof. Dr. Marius Grundmann (director)
Prof. Dr. Pablo Esquinazi (vice director)

1.2.2 Magnetic Resonance of Complex Quantum Solids, Magnetische Resonanz Komplexer Quantenfestkörper [MQF]

Prof. Dr. Jürgen Haase

Secretary

Sophie Kirchner

Technical staff

Gert Klotzsche
Stefan Schlayer
Horst Voigt

Academic staff

PD Dr. Marko Bertmer
Prof. Dr. Dieter Freude
Dr. Michael Jurkutat
Prof. Dr. Andreas Pöppl
Dr. Richard Reznicek

PhD candidates

Dipl.-Phys. Nina Dvoyashkina
Nataliya Georgieva, M.Sc.
Robin Gühne, M.Sc.
Seungtaik Hwang, M.Sc.
Carsten Kattinger, M.Sc.
Arafat Hossain Khan, M.Sc.
Anastasiia Kultaeva, M.Sc.
Kathrin Lorenz, M.Sc.
Dipl.-Phys. Matthias Mendt
Steven Reichardt, M.Sc.
Marufa Zahan, M.Sc.

Students

Yu-Kai Liao, B.Sc.
Manuel Lindel, B.Sc.

1.2.3 Nuclear Solid State Physics, Nukleare Festkörperphysik [NFP]

Prof. Dr. Jan Meijer

Secretary

Birgit Wendisch

Technical staff

Dipl.-Phys. Steffen Jankuhn
Carsten Pahnke
Dipl.-Ing. Joachim Starke

Academic staff

Dr.-Ing. Michael Kieschnick
Dr. Sébastien Pezzagna

PhD candidates

Sascha Becker, M.Sc.
Tobias Herzig, M.Sc.
Dipl.-Math. Roger John, B.Sc.
Tobias Lühmann, M.Sc.
Nicole Raatz, M.Sc.
Paul Räcke, M.Sc.
Clemens Scheuner, M.Sc.

Robert Staacke, M.Sc.
Ralf Wunderlich, M.Sc. (till February 2018)

Students

Mauricio Bassallo
Christoph Giese
Alexander Kühne, B.Sc.
Florian Neuhäuser, B.Sc.
Kaloyan Pavlov (till March 2018)

1.2.4 Semiconductor Physics, Halbleiterphysik [HLP]

Prof. Dr. Marius Grundmann

Secretary

Anja Heck
Sandra Meurer
Birgit Wendisch

Technical staff

Dipl.-Phys. Gabriele Benndorf
Monika Hahn
Dipl.-Ing. Holger Hochmuth
Dipl.-Phys. Jörg Lenzner
Axel Märcker
Gabriele Ramm
Roswitha Riedel
Dipl.-Ing. Ulrike Teschner

Academic staff

Dr. Robert Karsthof
Prof. Dr. Michael Lorenz
PD Dr. Rainer Pickenhain
Dr. Anna Reinhardt
Prof. Dr. Bernd Rheinländer (retired)
Dr. Peter Schlupp
Dr. Rüdiger Schmidt-Grund
Dr. Daniel Splith
Dr. Chris Sturm
Dr. Holger von Wenckstern
Dr. Chang Yang
Dr. Zhipeng Zhang

PhD candidates

Michitaka Fukumoto, M.Sc. (guest)
Oliver Herrfurth, M.Sc.
Stefan Hohenberger, M.Sc.
Tanja Jawinski, M.Sc.
Max Kneiß, M.Sc.
Evgeny Krüger, M.Sc.
Tillmann Stralka, M.Sc.
Lukas Trefflich, M.Sc.
Sofie Vogt, M.Sc.
Antonia Welk, M.Sc.
Anna Werner, M.Sc.
Vitaly Zviagin, M.Sc.

Students

Yousif Abou Leila
Michael Bar
Felix-Florian Delatowski
Sebastian Henn
Ron Hildebrandt
Florian Jung
Mizuki Kakei
Mario Klebahn
Cathatina Krömmelbein
Oliver Lahr
Sandra Montag
Andreas Müller
Sophie Müller
Andre Nabatov Sergi Ortega Micó
Eduard Rose
Fabian Schöppach
Philipp Storm
Laurenz Thyen
Christopher Walter
Benjamin Wehr
Jonathan Wernersson

1.2.5 Superconductivity and Magnetism, Supraleitung und Magnetismus [SUM]

Prof. Dr. Pablo Esquinazi

Secretary

Sandy Ehlers

Technical staff

Dr. Winfried Böhlmann
Dipl.-Krist. Annette Setzer

Academic staff

Prof. Dr. Michael Ziese
Dr. José Barzola-Quiquia
Dr. Séverine Diziain

PhD candidates

Francis Bern, M.Sc.
Lukas Botsch, M.Sc.
Johannes Küpper, M.Sc.
Christian Eike Precker, M.Sc.
Bogdan Semenenko, M.Sc.
Markus Stiller, M.Sc.

Students

Tiago Rafael Silva Cordeiro, B.Sc.
Stefan Dietel, B.Sc.
Anthony Ogbuehi
Devesh Jawla
Laetitia Paula B. Bettmann
Ratna Bahadur Bista

1.2.6 Applied Magnetic Resonance, Angewandte Magnetische Resonanz [AMR]

Prof. Dr. Rustem Valiullin
Prof. Dr. Nikolaus Weiskopf

Technical staff

Stefan Schlayer

Academic staff

PD Dr. Marko Bertmer
Prof. Dr. Harald Möller (Assoc. Mem.)

PhD candidates

Daniel Schneider, M.Sc.
Henry R.N.B. Enninful, M.Sc.

1.3 Institute for Theoretical Physics

1.3.1 Office of the Director

Prof. Dr. Wolfhard Janke (director)

Secretary

Gabriele Menge

1.3.2 Computational Quantum Field Theory, Computerorientierte Quantenfeldtheorie [CQT]

Prof. Dr. Wolfhard Janke

Academic staff

Dr. Stefan Schnabel
Dr. Jonathan Gross
Dr. Suman Majumder

PhD candidates

Johannes Bock, M.Sc.
Henrik Christiansen, M.Sc.
Momchil Ivanov, M.Sc.
Stanislav Kazmin, M.Sc.
Ravinder Kumar, M.Sc. ("co-tutelle" with Coventry University, UK)
Dipl.-Phys. Martin Marenz
Dipl.-Phys. Marco Müller
Dipl.-Phys. Hannes Nagel
Dipl.-Phys. Andreas Nußbaumer
Philipp Schierz, M.Sc.

Students

Kieran Austin
Thomas Els
Lisa Fiedler
Hans-Joachim Lange
Fabio Müller
David Oberthür
Simon Schneider
Franz Paul Spitzner
Ronja Stübe1
Dimitrij Tschodu
Tobias Weiss

Chris Allen
Jakob Bürgermeister
Adrian Häußler
Michel Michalkow

1.3.3 Quantum Field Theory and Gravity, Quantenfeldtheorie und Gravitation [QFG]

Prof. Dr. Rainer Verch (Speaker)

Prof. Dr. Gerd Rudolph (retired)

Academic staff

Prof. Dr. Rainer Verch
Priv.-Doz. Dr. Michael Bordag
Dr. Thomas-Paul Hack
Dr. Matthias Schmidt
Dr. Markus B. Fröb

PhD candidates

Tobias Diez, M.Sc.
Erik Fuchs, M.Sc.
Michael Gransee, M.Sc.
Mathias Hänsel, M.Sc.
Felix Kurpicz, M.Sc.

Students

Sandesh Bhat
Stanislaw Kazmin
Sebastian Knappe
Richard Neidhardt
Justus Neumann
Thies-Albrecht Ohst
Marie Rodal
Maik Wessling
Johannes Zähle

1.3.4 Statistical Physics, Statistische Physik [STP]

Prof. Dr. Bernd Rosenow

1.3.5 Theory of Condensed Matter, Theorie der kondensierten Materie [TKM]

Prof. Dr. Klaus Kroy (Speaker)
Prof. Dr. Jürgen Vollmer

Prof. Dr. Ulrich Behn (retired)
Prof. Dr. Dieter Ihle (retired)
Prof. Dr. Adolf Kühnel (retired)

Secretary

Susan Moreno

Academic staff

Dr. Viktor Holubec

PhD candidates

Sven Auschra, M.Sc.
Daniel Geiss, M.Sc.
Constantin Huster, M.Sc.
Dipl.-Phys. Marc Lämmel
Richard Pfaller, M.Sc.
Stefano Steffenoni, M.Sc.
Katharina Tholen, M.Sc.

Students

Ephraim Bernhardt
Paul Cervenak, B.Sc.
Daniel Dernbach, B.Sc.
Adina Hausch
Joscha Mecke, M.Sc.
Erik Rohkamm
Rojyar Rajabpour
Benjamin Streitz
Roland Wiese, B.Sc.

1.3.6 Theory of Elementary Particles, Theorie der Elementarteilchen [TET]

Prof. Stefan Hollands, PhD (Speaker)

Prof. Dr. Klaus Sibold (retired)
Dr. Daniela Cadamuro (Emmy-Noether group leader)

Academic staff

Dr. Pawel Duch (affiliated from MPI MiS)
PD Dr. Rolands Kirschner (retired)
PD Dr. Holger Perlt
PD Dr. Arwed Schiller (retired)
Dr. Jochen Zahn

PhD candidates

Mojtaba Taslimi Tehrani, M.Sc.
Vahid Toomani, M.Sc.

Students

Sami Abdallah
Christopher Allen
Shaun Brentnall
Dhiraj Kumar Deka
Sebastian Drawert
Ludwig Hoffmann
Marek Kozon
Rohan Kulkarni
Narek Papoyan
Hieu Pham
Moritz Thurmair

I

Peter Debye Institute for Soft Matter Physics

2

Molecular Nano-Photonics

2.1 Introduction

Studying dynamic processes at the level of single molecules and particles in soft materials, the group has recently started to explore the release of heat from single molecules and nanoparticles. These absorbing chromophores are able to convert optical energy into heat if their fluorescence quantum yield is low. This released heat is generating a steady state spatial temperature profile as they are embedded in a large heat bath, which is their solvent environment. This local temperature profile allows a number of new studies, which range from fundamental physical aspects of Hot Brownian Motion (HBM) to the active motion of self-propelled particles. In particular this field of research of the group addresses

- Thermally propelled particles and micromachines
- Manipulation and trapping of single nano-objects in solution
- Transmission microscopy of Rayleigh- and Mie-particles
- Manipulation of living cells by local temperature fields
- Heat conduction at the nanoscale

During the year 2018 the Molecular Nanophotonics Group has celebrated a number of achievements. Among them are:

- The group has organized the third Soft Matter Day at the Peter Debye Institute for Soft Matter Physics on July 6, 2018.
- The proposal for a CECAM Workshop on "Active Matter and Artificial Intelligence" organized by Frank Cichos, Klaus Kroy, Fernando Peruani and Giovanni Volpe has been granted. It will take place from September 30 to October 02, 2019 in Lausanne, Switzerland.
- Nicola Söker received a PhD scholarship funded by the European Social Fund (ESF), the European Union (EU) and the Free State of Saxony.
- The proposal for the third funding period of the CRC Transregio 102 "Polymers under Multiple Constraints" has been submitted to the DFG.

Collaborations with the groups of Prof. Dr. Klaus Kroy (Universität Leipzig), Prof. Dr. Michael Mertig (TU Dresden), Prof. Dr. Alois Würger (University of Bordeaux, France), Prof. Haw Yang, PhD (Princeton University, USA) and Prof. Giovanni Volpe, PhD (University of Gothenburg, Sweden) have been very fruitful

Frank Cichos

2.2 Thermophoretic trapping of single amyloid fibrils

M. Fränzl, T. Thalheim, F. Cichos, J. Posseckardt*, M. Mertig*, J. Adler† D. Huster†

*TU Dresden, Kurt Schwabe Institute of Instrumentation and Sensor Engineering Meinsberg
†Universität Leipzig, Institute for Medical Physics and Biophysics

The formation of aggregates of peptides is responsible for a number of neurodegenerative diseases linked, for example, to Alzheimer's disease or Parkinson's disease. The individual steps of this aggregation from single soluble monomers or oligomers to highly ordered, insoluble amyloid fibrils, however, are commonly hidden in the ensemble average of common measurement techniques. The heterogeneity of the ensemble at all stages of the aggregation process hides the growth details such as secondary nucleation processes or fibril fragmentation.

We recently devised an all-optically controlled trapping method [1, 2] which uses static temperature fields counteracting the Brownian motion of single amyloid fibrils freely diffusing in solution. Therefore, cover slips are provided with arrays of chromium structures with the help of laser lithography. Figure 2.1A shows a bright-field image of an array of 10 μm traps and a zoomed trap as an example. A focused 808 nm laser beam heats the chrome structure leading to a temperature gradient which pushes the amyloid fibril to colder positions due to thermophoresis (Figure 2.1B). Rotating the laser at a high frequency generates a static temperature field with its maximum at the chromium edges and the minimum in the trapping center. The amyloid fibril is thus kept in the center of the trap (Figure 2.1C).

Aβ_{40} fibrils, which are associated to Alzheimer's disease, were studied in dependence on their length to extract the translational diffusion coefficient D_t and the rotational diffusion coefficient D_r (Figure 2.1D) as well as the Soret coefficient which characterizes the strength of the trapping capability (not shown). All quantities scale as predicted from theory (see dashed lines in Figure 2.1D). To enlarge the applicability of the trap, additionally Aβ_{42} and pGlu$_3$-Aβ_{3-40} fibrils at different pH values and salt concentrations were measured. As the rotational diffusion coefficient scales with the inverse fibril length to the power of three, it provides a very sensitive measurement quantity for length changes. We measured Aβ_{40} seed fibrils in presence of monomers and monitored the rotational diffusion coefficient over time (Figure 2.1E). Fibril A does not grow over the observation time most probably due to defect fibril ends. In contrast, fibrils B and C exhibit decreasing rotational diffusion coefficients which refer to a growth rate of 0.06 nm s^{-1} for fibril B and a growth rate of 0.17 nm s^{-1} for fibril C. The growth rate of fibril C is enhanced compared to fibril B as higher pH and salt conditions resembling physiological conditions in a biological context were adjusted. The rotational diffusion

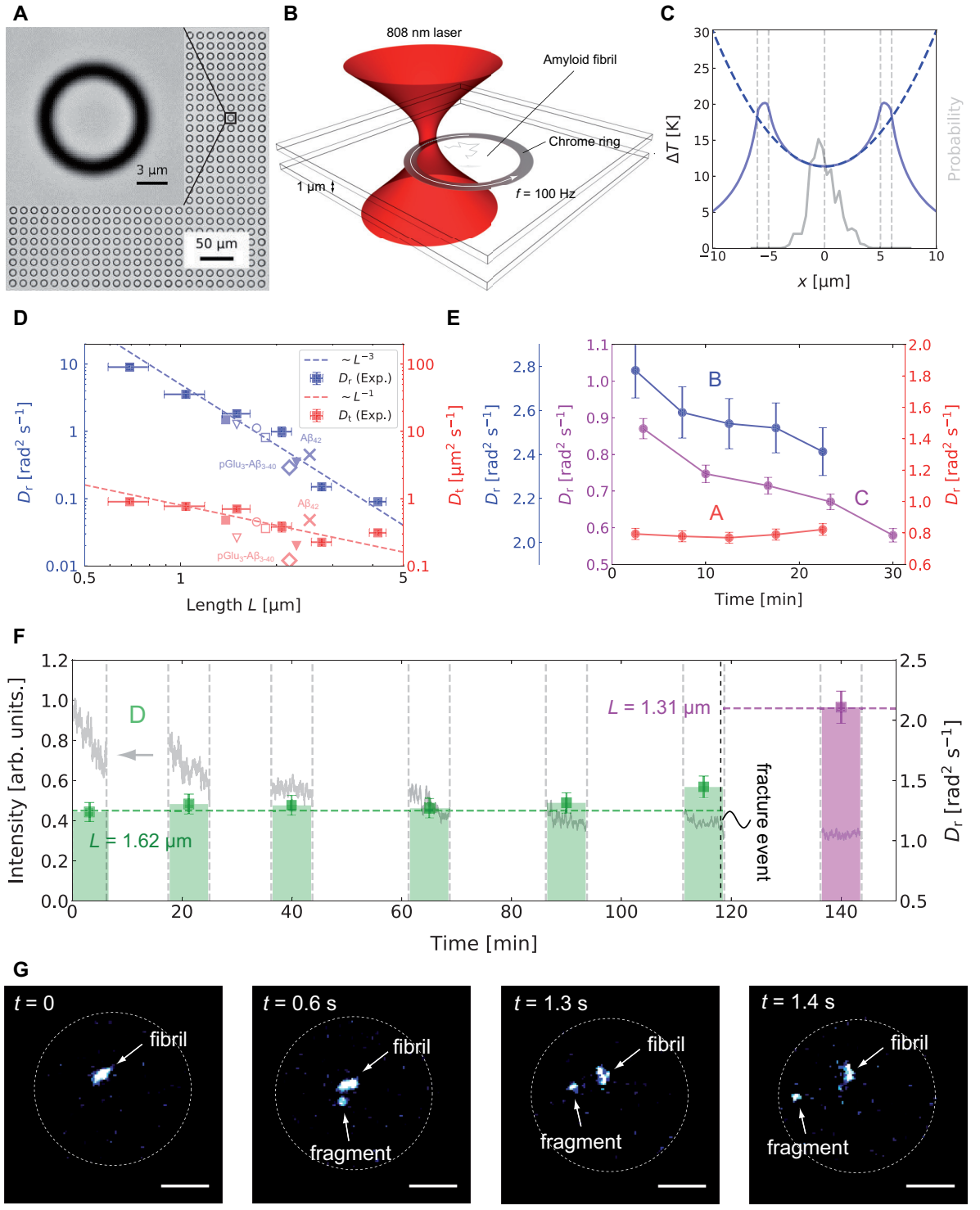

Figure 2.1: **A**) Bright field image of a 10 μm traps array and zoomed trap. **B**) Sketch of the trapping method. **C**) Temperature distribution in a thermophoretic trap. The central temperature gradient can be approximated as a harmonic trap (blue dashed line). **D**) Length dependence of the rotational and translational diffusion coefficient. **E**) Time dependence of the rotational diffusion coefficient for three fibrils. **F**) Time dependence of the rotational diffusion coefficient for a fibril in intermittent mode. **G**) Fragmentation event of fibril D from F.

coefficient is therefore an outstanding tool for the investigation of fibrillar growth processes in single fibril studies. As the used mode of the thermophoretic trap does not require feedback control of the laser for trapping the fibril, long-time studies up to several hours of single fibrils were enabled by interrupting the fluorescent excitation of the fibril's dye molecules in an intermittent mode reducing photo-bleaching (Figure 2.1F). Fibril D in Figure 2.1F shows no change of the rotational diffusion coefficient for the first 110 min. A fibril fracture event (Figure 2.1G) around minute 118, which has to our knowledge never been directly observed before, results in a sudden increase of the rotational diffusion coefficient in the next measurement period.

The thermophoretic trap together with the monitoring of the rotational diffusion coefficient thus provides an excellent combination for complex studies on molecular interactions, especially on protein and macromolecular aggregation processes for single fibrils.

The project is funded within the CRC TRR 102 "Polymers under Multiple Constraints".

[1] M. Braun, F. Cichos: ACS Nano **7**, 11200 (2013), doi:10.1021/nn404980k
[2] M. Braun et al.: PCCP **16**, 15207 (2014), doi:10.1039/C4CP01560F

2.3 Thermo-osmotic flows in electrolyte solutions

M. Fränzl, F. Cichos

In the last decade temperature gradients have become a versatile technique to manipulate nano-objects in solution, e.g., trapping of nanoparticles and macromolecules, cluster formation through hydrodynamic interactions and self-propulsion of metal-capped Janus particles. In all these examples, the motion results from thermo-osmosis: The temperature gradient alters the electric double layer along the liquid–solid interface inducing a slip flow along the interface [1, 2].

The present work addresses thermo-osmotic flows in electrolyte solutions. We locally heated a 50 nm gold film using a focused 532 nm laser within a suspension of gold tracer particles with a radius of 250 nm with various concentrations of NaCl and investigated the resulting particle transport (Figure 2.2A). For low NaCl concentrations the flow fields are in qualitative agreement with our previous results [2] in deionized water. We find increasing drift velocities with increasing NaCl concentrations. For NaCl concentrations above 10 mM a trapping of the tracer particles is observed (Figure 2.2B) suggesting an attractive electrostatic force.

In the framework of the DLVO theory the potential energy of a gold particle close to a gold surface has a secondary minimum (Figure 2.2C). With increasing salt concentration c_0 the minimum is shifted to smaller distances D. Thus, for higher NaCl concentrations the tracer particles are more likely to be found close to the gold surface. Since the thermo-osmotic slip flow is increasing with decreasing distance to the surface, the tracer particles drift velocity increases with increasing NaCl concentration. For NaCl concentrations above 10 mM the tracer particles are getting trapped at the hot spot. Currently we are investigating the influence of optical forces to the suggested electrostatic forces.

The project is funded within the DFG-ANR project "Thermoelectric Effects at the Nanoscale".

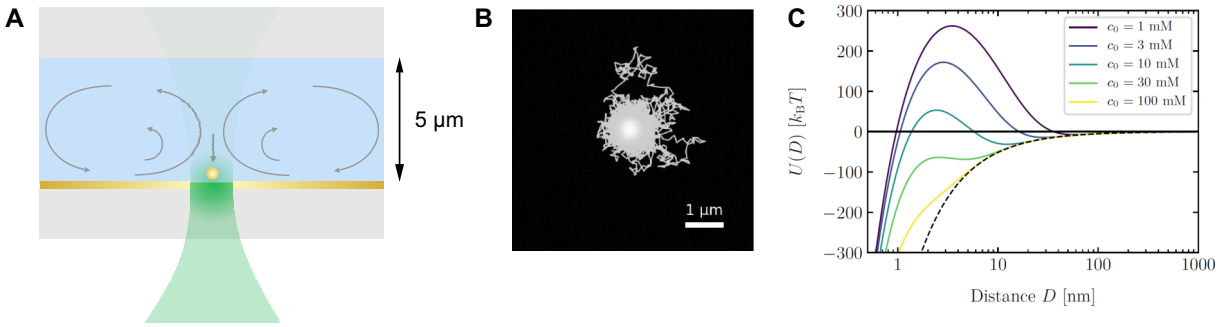

Figure 2.2: A) Sketch of the sample design. The fluid is contained between two glass cover slips with a gap of about 5 μm. The bottom glass cover slip is coated with an about 50 nm gold film and heated using a focused 532 nm laser from below. Gold nanoparticles with a radius of 250 nm are used as tracer particles. **B**) Trajectory of a gold nanparticle trapped at the hot spot. **C**) DLVO potential between a gold nanoparticle with a radius of 125 nm and a gold surface.

[1] F.M. Weinert, D. Braun: J. Appl. Phys. **104**, 104701 (2008), doi:10.1063/1.3026526
[2] A.P. Bregulla et al.: PRL **116**, 188303 (2016), doi:10.1103/PhysRevLett.116.188303

2.4 Feedback-controlled active particle assemblies

A. Fischer, F. Cichos, G. Volpe*

*University of Gothenburg, Sweden

Active particles are simple microscopic model systems for living objects such as birds, fish or people and mimic in particular the propulsion of bacteria or cells without the complexity of physical properties and chemical networks in living objects. With their bare function of self-propulsion they are, however, missing an important ingredient of life, which is sensing and feedback, that all living objects from cells up to whole organisms have in common. All of their living relatives have signaling inputs which they use to gain information on the environment. Using this external information, birds or fish can self-organize into flocks or schools and, on a microscopic level, cells may regulate gene expression. The structure formation, though, depends on the active motion of the animal and its ability to steer based on its perception of the environment. While active particles do not have such sensory inputs and feedback mechanisms built in yet, suitable control mechanisms may introduce this complexity fostering the exploration of new emergent phenomena.
We recently developed such control mechanisms for a particular new type of active particles. These active particles comprise a melamine resine particle of about one micrometer in diameter. The surface of this particle is homogeneously covered by gold nanoparticles of about 10 nm diameter at a surface coverage of 30 %. These gold nanoparticles can be heated optically by a focused laser. If this heating is asymmetric with respect to the particle center, thermo-osmotic surface flows develop and result in a self-propulsion of the particle. By controlling the heating laser position on the circumference of the particle a precise steering is achieved and by modulating the heating power different activities can be achieved.

The project considers the self-organization of such active particles by means of feedback control. In various steps we explore the importance of signaling between the environment and between the particles and its effect on a collective behavior. The experiments involve microswimmers with changing velocity due to the reaction to a virtual gradient field. Negative and positive feedback delay is included which controls aggregation or segregation of the particles, as observed for bacteria.

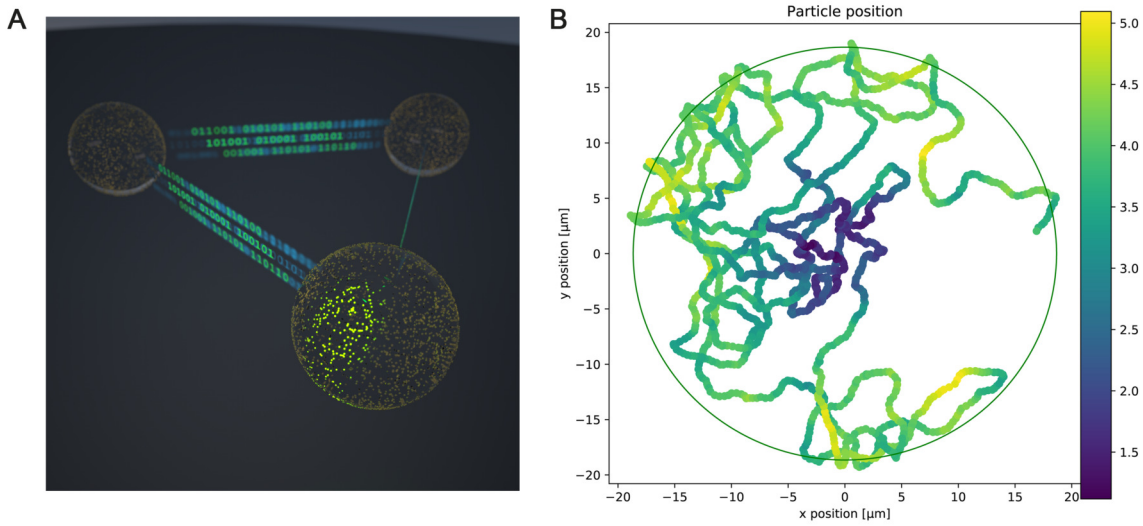

Figure 2.3: A) Artistic representation of a system of three microswimmers forming a structure due to the information flow in the feedback system. **B**) Measured path of an active swimmer in an external field adjusting its speed to the measured intensity. A positive delay is used which leads to an aggregation.

2.5 3D mapping of thermo-osmotic fluid flow fields

N. Söker, F. Cichos

Thermo-osmotic flows, the microscopic mean fluidic concentration fluxes along phase boundaries induced by gradients in local temperature, can be used as a controllable propulsion mechanism for micro- to nanoscale objects, as separation technique for macromolecules in organic solvents, potentially as the driving mechanisms of microfluidic devices and, as very recently shown, as a steering mechanism to study individual free diffusing organic macromolecules.
The phenomenon of thermo-osmosis/-phoresis happens over the span of several orders of length scales, from the average drift of dissolved ion concentrations to the migration of large organic molecules and micelles to the directed motion of micrometer-sized colloids. For the latter, only recently a discussion seems to have settled on the size dependence of the phoretic velocity of charged colloids in aqueous solution [1, 2]. To our knowledge there are only two experimental works that address the detailed microscopic liquid-flow-fields arising [3, 4].
This project aims to map the three-dimensional mean flow field induced by thermo-osmosis around micro- to nanometer-sized structures in a thin film by appropriate

optical videomicroscopy of individual metal nano tracer particles, expanding the work of Bregulla et al. [3].
The project is funded by the European Social Fund (ESF), the European Union (EU) and the Free State of Saxony.

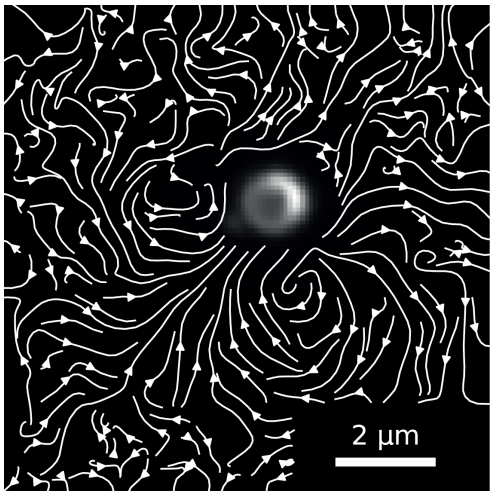

Figure 2.4: In-plane mean streamlines of gold spheres with a radius of 100 nm around a laser heated thermophoretic Janus particle with a radius of 1 μm adherent to a glass substrate.

[1] M. Braibanti et al.: PRL **100**, 108303 (2008), doi:10.1103/PhysRevLett.100.108303
[2] A. Würger: PRL **116**, 138302 (2016), doi:10.1103/PhysRevLett.116.138302
[3] A. Bregulla et al.: PRL **116**, 188303 (2016), doi:10.1103/PhysRevLett.116.188303
[4] H. Moyses et al.: Soft Matter **12**, 6357 (2016), doi:10.1039/C6SM01163B

2.6 Holographic optical tweezers

J. Kiethe, F. Cichos

Standard optical tweezers have a wide range of versatile applications and are extensively used throughout many projects in the group. As an extension to single optical tweezers, an experimental setup is developed to enable dynamic holographic optical tweezers (HOT) using a spatial light modulator (SLM) similar as in [1].
The HOT allows for the simultaneous use of multiple optical traps and control over their three-dimentional positions in the sample. Moreover, besides multiple optical traps, arbitrary structures can be realized through holographic beam shaping. The hologram computation is based on the Gerchberg–Saxton and the gratings and lenses algorithms [2]. Thus far a single steerable trap has been achieved as well as several static structures such as arrays of traps and ring structures.
In the future the HOT shall expand existing experiments. For example, it could be combined with tracking capabilities already in use in order to follow microswimmers and allow for their steering using photon nudging. Moreover, arrays of few hundreds of individual traps or laser spots can be realized.

[1] D.G. Grier: Nature **424**, 810 (2003), doi:10.1038/nature01935
[2] J. Liesener et al.: Opt. Commun. **185**, 77 (2000), doi:10.1016/S0030-4018(00)00990-1

2.7 Ballistic Hot Brownian Motion

X. Su, F. Cichos

The main goal of our research project is to explore the ultra-short time dynamics of Hot Brownian Motion down to the ballistic regime to infer for the first time the kinetic temperature of Hot Brownian Motion. To achieve this final purpose, we first started to develop an experimental setup which is capable of measuring dynamics with nanosecond time and picometer spatial resolution. During the first stages of the project we have evaluated the performance of optical tweezers in the long-time limit with the help of a camera-based detection of colloids trapped in a highly focused infrared laser beam.

We used a 1064 nm wavelength tightly-focused infrared laser as trapping laser and a white light LED for the imaging and detection of the positional fluctuations of the particle. The Brownian dynamics is characterized by the mean-squared displacement, the position autocorrelation function and the power spectral density of the positional fluctuations. All observed behaviors follow the predictions from the Stokes–Einstein relation.

For a detection with high spatial and temporal resolution, we have introduced a balanced photodiode and a knife edge prism to allow for a high resolution position detection. The difference signal from the two photodiodes is digitized with high temporal resolution by an analog-digital card. In current measurements we are able to detect a displacement of a polymer bead at ambient temperature in the optical tweezers of about 3 nm in 100 ns. With the current setup we can improve the time resolution down to 5 ns. With this experimental technique we will then be able to observe the onset of the ballistic part of isothermal Brownian Motion.

The project is funded within the DFG project "Ballistic Hot Brownian Motion".

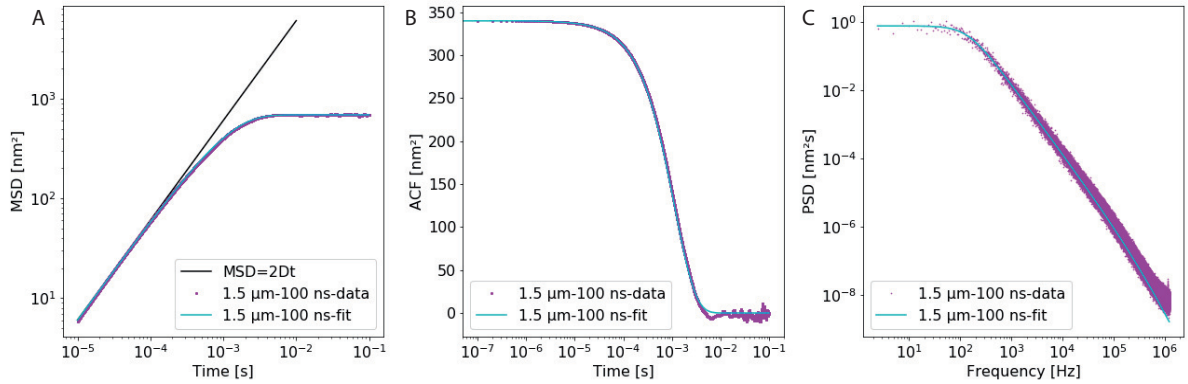

Figure 2.5: A) Mean-squared displacement as a function of time. The black line corresponds to a slope of 1 for the expected diffusive behavior. **B**) Position autocorrelation function as a function of time. **C**) Power spectral density as a function of frequency. For all three plots, the purple dots are obtained from experimental data and the cyan curves are fitting functions corresponding to the expected theoretical behavior for isothermal Brownian motion. All measurements have been carried out with 1.5 μm diameter polymer particles at a time resolution of 100 ns.

2.8 Active systems learning at the microscale

S. Muiños-Landin, F. Cichos

Living organisms are able to sense and process information about the environment they live in. They are also able to update this information in order to construct solutions for real life problems such as finding food or avoiding danger. This active adaption process, that in the long run drives the evolution of species, is the result of a short time scale evolution of the knowledge of an organism that we know as learning. At the microscale the learning is hampered by stochasticity given that the intrinsic Brownian noise makes it critical to build a feedback between stimulus and action. Here we present a system based on a self-themophoretic microswimmer that allows the application of artifical intelligence algorithms at the microscale. Using reinforcement learning we show that even under noise conditions a system is able to learn how to optimize a simple navigation task. We study the influence of noise and the situation where multiple agents can share information to carry out specific tasks. This way we show how adaptation and intelligent collective behavior can be studied using artificial microswimmer systems.

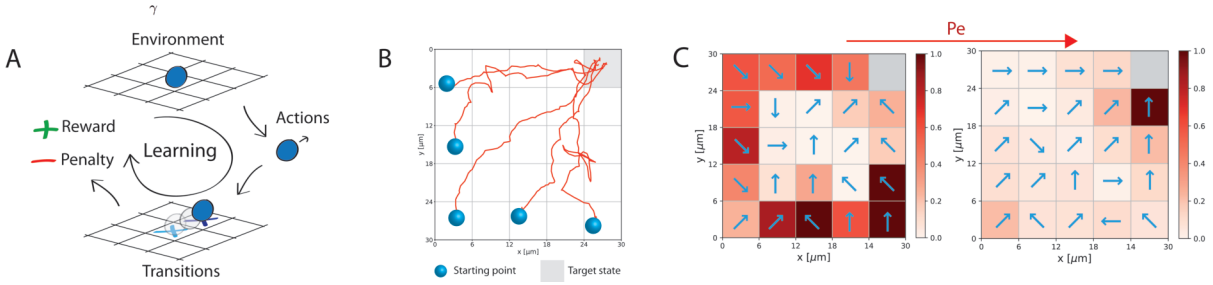

Figure 2.6: Active system learning. **A**) Reinforcement learning idea applied in our microswimmer context. The swimmer explores its environment by executing different actions that produce transitions between a set of states. The transitions are evaluated through the definition of a reward or a penalty and during the exploration the information is propagated and correlated by the system. **B**) Trajectories of the swimmer after learning. After the system has explored the environment enough in order to correlate its information on the question which is the best action to execute in each state, the system is able to navigate towards a target state independent of the starting point of the swimmer. **C**) The policy is represented by arrows indicating what is the best action to execute in each state of the gridworld. The colorscale represents the contrast between the best action in a given state and the other ones that could also be executed. It is different when the swimmer learns at different velocities, especially the states close to the edges due to the different magnitude of the role played by Brownian motion in each situation and the proximity of a penalty at the borders.

2.9 Steerable symmetric photo-phoretic microswimmers

S. Muiños-Landin, F. Cichos

Artificial microswimmers are typically asymmetric objects, where the asymmetry is important to achieve a directed propulsion along a specific direction. The asymmetry

is usually built into the geometry of the swimmer which carries out translational and rotational diffusion in the particle frame. Here we study in detail a symmetric swimmer that is propelled by self-thermophoresis. The asymmetry is introduced by an asymmetric release of energy induced by focused laser beams. This means that advanced steering schemes, such as photon nudging, become independent of rotational diffusion times, providing much more flexibility in the control of the swimmer. We analyze in detail the different experimental parameters that characterize the motion of this swimmer.

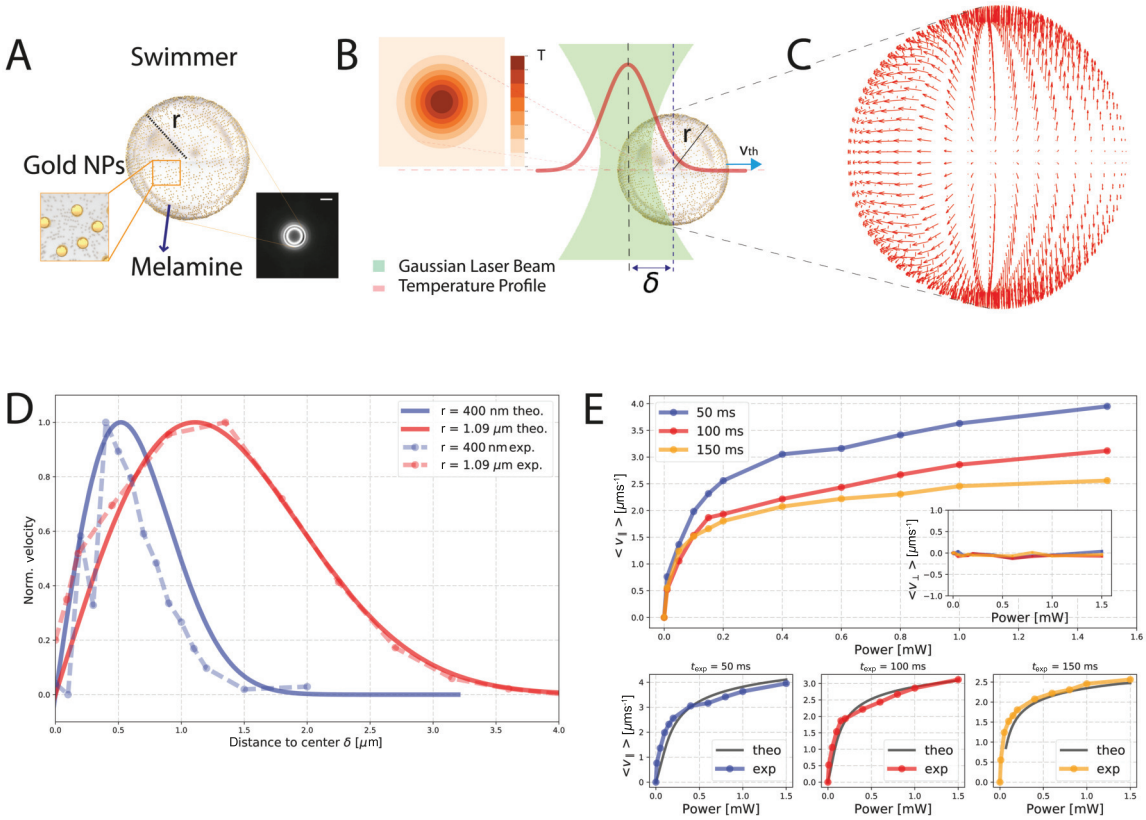

Figure 2.7: Multiparticle active system. **A**) Symmetric microswimmer made of melamine and covered homogeneously by gold nanoparticles with a radius of 10 nm on 30 % of its surface. Dark field image of the swimmer. **B**) Swimmer illuminated during active motion. A 2D Gaussian function represents the temperature increase where the laser is focused. **C**) Temperature gradient over the swimmer surface for the illumination conditions represented in B. **D**) Dependence of the velocity on the distance δ between the heating point and swimmer center for two sizes of particles. The red lines show data for a swimmer with radius $r = 400$ nm, the blue lines correspond to $r = 1.09$ μm. For both cases theory (solid lines) and experimental data (dashed lines) are shown. **E**) Mean value of the thermophoretic velocity as a function of the laser power with $\delta = 1$ μm. The values were obtained for three different exposure times $t_{exp} = 50$ ms (blue), $t_{exp} = 100$ ms (red) and $t_{exp} = 150$ ms (orange).

2.10 Funding

DFG-ANR: Thermoelectric Effects at the Nanoscale
F. Cichos in collaboration with A. Würger (University of Bordeaux, France)
DFG, CI 33/14-1

DFG SPP 1726, TP Propulsion and Interaction of Hot Brownian Swimmers
F. Cichos in collaboration with K. Kroy
DFG, CI 33/16-1 and CI 33/16-2

CRC/TRR 102, TP B10: Interaction of Single Polymer Chains in a Thermophoretic Trap
F. Cichos
DFG CRC/TRR 102

Ballistic Hot Brownian Motion
F. Cichos
DFG, CI 33/18-1

Dynamics and Control of DNA-based Hybrid Nanomachines
N. Söker
PhD Scholarship (Landesinnovationspromotion) funded by the European Social Fund (ESF), the European Union (EU) and the Free State of Saxony

Leipzig School of Natural Sciences – Building with Molecules and Nano-objects (BuildMoNa)
F. Cichos (Principal Investigator)
founded as DFG GSC 185

2.11 Organizational Duties

Frank Cichos

- Director of the Peter Debye Institute for Soft Matter Physics
- Vice Speaker of the Collaborative Research Center Transregio 102 "Polymers under Multiple Constraints"
- Member of the Scientific Advisory Board of the Kurt Schwabe Institute of Instrumentation and Sensor Engineering Meinsberg
- Member of the Steering Committee of the Graduate School BuildMoNa
- Vice Head of the Board of the Faculty for Quality Management
- Member of the Examination Board (Physics/Meteorology)
- Referee: Phys. Rev. B, Phys. Rev. Lett., Nature, Nat. Photonics, Chem. Phys. Lett., Appl. Phys. Lett., ACS Petroleum Research Fund, Medical Research Council

2.12 External Cooperations

Academic

- MPI for Intelligent Systems, Stuttgart
  Prof. Peer Fischer, PhD
- Princeton University, USA
  Prof. Haw Yang, PhD
- TU Berlin
  Prof. Dr. Regine von Klitzing
- TU Chemnitz
  Prof. Dr. Christian von Borczyskowski
- TU Dresden
  Prof. Dr. Michael Mertig
- Universität Konstanz
  Prof. Dr. Clemens Bechinger
- Universität Mainz
  Prof. Dr. Thomas Basché
- University of Bordeaux, France
  Prof. Dr. Alois Würger
- University of Gothenburg, Sweden
  Prof. Giovanni Volpe, PhD

2.13 Publications

Journals

U. Khadka, V. Holubec, H. Yang, F. Cichos: *Active particles bound by information flows*, Nat. Commun. **9**, 3864 (2018)

M. Selmke, U. Khadka, A.P. Bregulla, F. Cichos, H. Yang: *Theory for controlling individual self-propelled micro-swimmers by photon nudging II: confinement*, Phys. Chem. Chem. Phys. **20**, 10521–10532 (2018)

F. Cichos: *Thermoelectric fields hold nanoparticles*, Nat. Photonics **12**, 191–193 (2018)

M. Selmke, U. Khadka, A.P. Bregulla, F. Cichos, H. Yang: *Theory for controlling individual self-propelled micro-swimmers by photon nudging I: directed transport*, Phys. Chem. Chem. Phys. **20**, 10502–10520 (2018)

F. Schmidt, A. Magazzù, A. Callegari, L. Biancofiore, F. Cichos, G. Volpe: *Microscopic engine powered by critical demixing*, Phys. Rev. Lett. **120**, 068004 (2018)

Books

K. Kroy, F. Cichos: *Hot Brownian motion*. In: A. Bunde, J. Caro, J. Kärger, G. Vogl (eds): Diffusive spreading in nature, technology and society, Springer, Cham, 127–145 (2018)

Talks

S. Muiños-Landin, K. Ghazi-Zahedi, F. Cichos: *Active systems learning at the microscale*, APS March Meeting 2018, Los Angeles, USA, March 05–09, 2018

S. Muiños-Landin, K. Ghazi-Zahedi, F. Cichos: *Active systems learning at the microscale*, DPG Spring Meeting, Berlin, March 11–16, 2018

F. Cichos: *Feedback controlled hot microswimmers*, Seminar Talk at DLR, Institute of Materials Physics in Space, Cologne, March 21, 2018, invited

F. Cichos: *Feedback controlled hot microswimmers*, SPP 1726 Annual Meeting, Bonn, April 26–27, 2018

M. Fränzl, T. Thalheim, F. Cichos: *Single amyloid fibrils studied in a thermophoretic trap*, 5th CRC TRR 102 Minisymposium, Leipzig, June 08, 2018

F. Cichos: *Feedback controlled dynamic temperature fields*, CECAM Workshop Hot Colloids, Lyon, France, June 11–13, 2018, invited

F. Cichos: *Thermophoresis with feedback controlled temperature field*, 1st Summer School on Photothermal Effects in Plasmonics, Porquerolles, France, June 24–29, 2018, invited

N. Söker, S. Auschra, P. Cervenak, K. Kroy, F. Cichos: *Active Brownian particle under inhomogeneous activity*, Soft Matter Day, Leipzig, July 06, 2018

M. Fränzl, T. Thalheim, J. Adler, D. Huster, F. Cichos: *Single amyloid fibrils studied in a thermophoretic trap*, Soft Matter Day, Leipzig, July 06, 2018

F. Cichos: *Information controlled structure formation in artificial microswimmer*, International Conference on Control of Self-Organizing Nonlinear Systems, Warnemünde, Rostock, September 09–13, 2018, invited

M. Fränzl, T. Thalheim, J. Adler, D. Huster, F. Cichos: *Single amyloid fibrils studied in a thermophoretic trap*, Biennial Meeting of the German Biophysical Society, Düsseldorf, September 16–19, 2018

F. Cichos: *Information controlled structure formation in artificial microswimmer systems*, Colloquium at University of Gothenburg, Sweden, November 08, 2018, invited

Posters

S. Muiños-Landin, K. Ghazi-Zahedi, F. Cichos: *Active systems learning at the microscale*, APS March Meeting 2018, Los Angeles, USA, March 05–09, 2018

A. Fischer, G. Volpe, F. Cichos: *Creating sensorial delay to simulate phototaxis using thermophoresis applied to gold-coated microswimmers*, DPG Spring Meeting, Berlin, March 11–16, 2018

A. Fischer, K. Kroy, F. Cichos: *Hot Brownian motion on short time scales*, DPG Spring Meeting, Berlin, March 11–16, 2018

M. Fränzl, F. Cichos: *Optically driven thermoviscous flows*, DPG Spring Meeting, Berlin, March 11–16, 2018

S. Muiños-Landin, K. Ghazi-Zahedi, F. Cichos: *Active systems learning at the microscale*, DPG Spring Meeting, Berlin, March 11–16, 2018

N. Söker, F. Cichos: *Pair interactions of heat driven Janus particles*, DPG Spring Meeting, Berlin, March 11–16, 2018

T. Thalheim, M. Braun, F. Cichos: *Investigating compression of single DNA molecules in a thermophoretic trap*, DPG Spring Meeting, Berlin, March 11–16, 2018

A. Fischer, G. Volpe, F. Cichos: *Creating sensorial delay to simulate phototaxis using thermophoresis applied to gold-coated microswimmers*, Annual BuildMoNa Conference, Leipzig, March 19–20, 2018

M. Fränzl, F. Cichos: *Optically driven thermoviscous flows*, Annual BuildMoNa Conference, Leipzig, March 19–20, 2018

S. Muiños-Landin, K. Ghazi-Zahedi, F. Cichos: *Active systems learning at the microscale*, SPP 1726 Annual Meeting, Bonn, April 26–27, 2018

M. Fränzl, F. Cichos: *Optically driven thermoviscous flows*, 1st Summer School on Photothermal Effects in Plasmonics, Porquerolles, France, June 24–29, 2018

A. Fischer, G. Volpe, H. Yang, S. Muiños-Landin, F. Cichos: *Feedback control of active microswimmers*, 11th International Workshop on Engineering of Functional Interfaces, Wittenberg, July 01–03, 2018

M. Dethloff, N. Söker, F. Cichos: *Heat driven microswimmers at high area fractions*, Soft Matter Day, Leipzig, July 06, 2018

A. Fischer, G. Volpe, H. Yang, S. Muiños-Landin, F. Cichos: *Feedback control of active microswimmers*, Soft Matter Day, Leipzig, July 06, 2018

M. Fränzl, T. Thalheim, J. Adler, D. Huster, F. Cichos: *Single amyloid fibrils studied in a thermophoretic trap*, Soft Matter Day, Leipzig, July 06, 2018

S. Muiños-Landin, K. Ghazi-Zahedi, F. Cichos: *Active systems learning at the microscale*, Soft Matter Day, Leipzig, July 06, 2018

R. Rose, A. Heber, F. Cichos: *A photothermal detector based on liquid crystal phase transitions*, Soft Matter Day, Leipzig, July 06, 2018

M. Volz, T. Thalheim, F. Cichos: *Multiple colloidal particles in a thermophoretic trap*, Soft Matter Day, Leipzig, July 06, 2018

F. Welzel, M. Fränzl, F. Cichos: *Absolute temperature measurement of gold nanoparticles*, Soft Matter Day, Leipzig, July 06, 2018

A. Fischer, H. Yang, S. Muiños-Landin, F. Cichos: *Feedback control of active microswimmers*, International Conference NECD 18 Nonequilibrium Collective Dynamics: Bridging the Gap between Hard and Soft Materials, Potsdam, October 08–11, 2018

2.14 Graduations

Master

- Nicola Söker
  Heat driven Janus particles with spatially varying propulsion velocity
  March 2018
- Ricardo Rose
  A photothermal detector based on liquid crystal phase transitions
  September 2018

2.15 Guests

- Dr. Gopalakrishnan Balasubramanian
  Max Planck Institute for Biophysical Chemistry, Göttingen
  June 08, 2018
- Prof. Dr. Birgit Strodel
  Forschungszentrum Jülich
  June 08, 2018

3

Molecular Physics

3.1 Introduction

Our research in 2018 was focused essentially on two projects,(i) a ?Knowledge-transfer-project (Erkenntnistransfer-Projekt)? together with Prof. Veronika Strehmel, FH Krefeld and Merck KGaA in Darmstadt about ?Neue Polymermaterialien auf der Basis von funktionalisierten ionischen Flüssigkeiten für Anwendungen in Membranen? and (ii) a project on ?Broadband Dielectric and IR Spectroscopy to study molecular dynamics and order in nanometer domains of end-fixed polymers? within the Collaborative Research Center (CRC) of the universities in Halle and Leipzig, ?Polymers under multiple constraints: restricted and controlled molecular order and mobility?. In both an important progress could be achieved as demonstrated in the publications. Furthermore the book ?The scaling of relaxation processes? (Eds.: F. Kremer and A. Loidl), Springer ISBN 978-3-319-72706-6, came out in the series of ?Advances in Dielectrics (Series Editor: F. Kremer)

Friedrich Kremer

3.2 Funding

Polymers under multiple constraints: restricted and controlled molecular order and mobility - TP B08 "Broadband Dielectric Spectroscopy to study the molecular dynamics in nanometer thin layers of block copolymers"
Prof. Friedrich Kremer
DFG - SFB TRR 102-2, TP B08

3.3 Organizational Duties

Friedrich Kremer

- Principal Investigator in the "Leipzig School of Natural Sciences ? Building with Molecules and Nano-Objects" in the framework of a Graduate School funded by the "Ferderal Excellence Initiative". This supports several Ph.D. projects

3.4 External Cooperations

Academic

- Technische Universität München
  Prof. Dr. C. M. Papadakis, J. Zhang
- Leibniz-Institut für Polymerforschung Dresden
  Dr. P. Uhlmann, R. Winkler
- University of Silesia, Katowice
  Prof. Dr. M. Paluch, Dr. K. Kaminski
- Fraunhofer Institut für Mikrostruktur von Werkstoffen und Systemen IWMS, Halle
  Prof. Dr. M. Beiner
- Department of Chemical and Biomolecular Engineering, University of Tennessee, Knoxville
  Prof. Dr. J. R. Sangoro
- Hochschule Niederrhein, Institute of Organic Chemistry
  Prof. Dr. V. Strehmel

Industry

- Continental, Hannover, Germany
- Novocontrol, Hundsangen, Germany
- MERCK KGaA, Darmstadt, Germany
- EVONTA-Technology GmbH

3.5 Publications

Journals

M. Jasiurkowska-Delaporte, W. Kossack, W. K. Kipnusu, J. R. Sangoro, C. Iacob, F. Kremer, *Glassy dynamics of two poly(ethylene glycol) derivatives in the bulk and in nanometric confinement as reflected in its inter- and intra-molecular interactions*, The Journal of Chemical Physics **149**, 064501 (2018)

M. Tress, M. Vielhauer, P. J. Lutz, R. Mülhaupt, F. Kremer, *Crystallization-Induced Confinement Enhances Glassy Dynamics in Star-Shaped Polyhedral Oligomeric Polysilesquioxane-Isotactic Polystyrene (POSS-iPS) Hybrid Material*, Macromolecules **51**, 504 (2018)

M.-E. Krautwald-Junghanns, K. Cramer, B. Fischer, A. Förster, R. Galli, F. Kremer, E. U. Mapesa, S. Meissner, R. Preisinger, G. Preus, C. Schnabel, G. Steiner, T. Bartels, *Current approaches to avoid the culling of day-old male chicks in the layer industry, with special reference to spectroscopic methods*, Poultry Science **97**, 749 (2018)

Books

F. Kremer, A. Loidl (Eds.), *The scaling of relaxation processes*, Springer, 2018

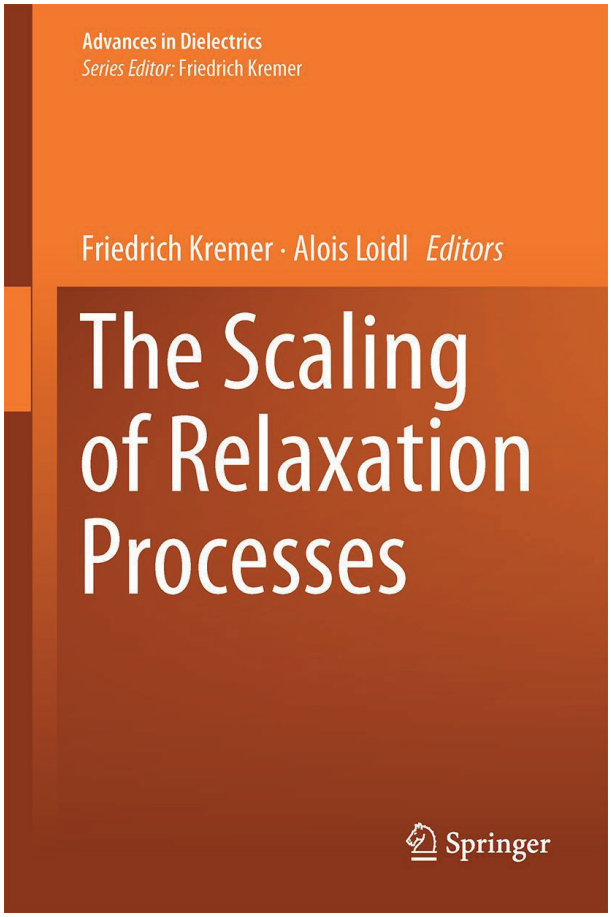

During the past two decades the experimental capabilities to study materials in an extraordinary wide spectral range at largely varying temperatures as well as pressures have enormously developed. This is especially true for Broadband Dielectric Spectroscopy (BDS) which nowadays covers the whole frequency range from 10-6 Hz up to the Far Infrared (FIR) without any gap. In addition other methods like Photon Correlation Spectroscopy (PCS), Nuclear Magnetic Resonance (NMR), Viscosimetry and mechanical Spectroscopy and even Calorimetry have also become broadband. Consequently, knowledge concerning the scaling of relaxation processes has tremendously grown and it is now common to combine different techniques in order to determine the distinct correlations and their mutual interactions in a material under study. This development has been nicely exemplified for amorphous systems being characterized by glassy dynamics which is extended from very long (106 s) to short (picoseconds) timescales, including the structural ?-relaxation (dynamic glass transition), secondary (slow and fast) ?-relaxations and the Boson peak in the Far Infrared. It is well established that structural relaxations roughly follow a Vogel-Fulcher-Tammann type of thermal activation, while secondary relaxations, at least below the glass transition temperature, can be described by an Arrhenius-like temperature dependence. Fast processes in the GHz regime seem to follow scaling predictions, while the boson peak and intramolecular vibrations are only weakly temperature dependent. The striking similarities of frequency and temperature dependencies for the large class of super-cooled liquids lead to the development of scaling approaches and theories that can model these universalities. However, often a closer inspection reveals severe discrepancies and deviations. It is the objective of this issue of ?Advances in Dielectrics? on the ?Scaling of Relaxation Processes? to summarize the current knowledge and the enormous amount of high-quality data on glassy dynamics of super-cooled liquids and to discuss it with respect to the often competing theoretical concepts.

Friedrich Kremer and Alois Loidl

Talks

F. Kremer: *Glassy dynamics in one- and two-dimensional nanometric con?nement - a comparison*, APS march meeting, Knoxville, USA, 27.02.2018

F. Kremer: *Molecular Dynamics and Charge Transport in Highly Conductive Polymerized Ionic Liquids*, invited talk, Oak Ridge National Laboratory, Los Angeles, USA, 28.02.2018

F. Kremer: *Dielectric spectroscopy with optical detection - a realistic perspective?*, 10th Conference on Broadband Dielectric Spectroscopy and its Applications, Brüssel, Belgium, 27.08.2018

F. Kremer: *Molecular dynamics at external and internal nanometric constraints*, 13th Fall Rubber Colloquium, Hannover, Germany, 06.11.2018

M. Anton: *Orientation and Order Bottle Brush Copolymers*, DPG-Spring-Meeting, Berlin, Germany, 12.03.2018

F. Kremer: *Glassy dynamics as reflected in its inter- and intra-molecular interactions*, DPG-Spring Meeting, Berlin, Germany, 15.03.2018

F. Frenzel: *Charge Transport and Glassy Dynamics in Polymeric Ionic Liquids as studied in its in Inter- and Intramolecular Interactions*, DPG-Spring-Meeting, Berlin, Germany, 15.03.2018

W. Kossack: *Temperature-dependent IR-transition moment orientational analysis applied to thin supported films of poly-?-caprolactone*, DPG-Spring-Meeting, Berlin, Germany, 15.03.2018

W. Kossack: *Infrared and dielectric spectroscopy to unravel the nature of the structural- and the secondary-relaxation in glycerol, threitol, xylitol and sorbitol*, 10th Conference on Broadband Dielectric Spectroscopy and its Applications, Brüssel, Belgium, 27.08.2018

Posters

F. Frenzel: *Multi-Phase Transition Behavior of Highly Conductive Polybromide Ionic Liquids*, DPG-Spring-Meeting, Berlin, Germany, 12.03.2019

M. Anton: *Inter- and Intramolecular Interactions in an Extraordinary Conductive Polymeric Ionic Liquid*, DPG-Spring-Meeting, Berlin, Germany, 12.03.2019

3.6 Guests

- Prof. Dr. C. Schick
  Kazan Federal University, Russia1
  09.11.-18.11.2018
- Harrouz Omar
  Université des Sciences et Technologie d'Oran, Algeria
  19.04.2018-27.04.2018

4

Soft Matter Physics

4.1 Introduction

The question how the physical properties of cells determines their individual and collective behavior lies at the heart of the research of the Soft Matter Physics group. To truly understand this question the physical properties of cells need to be investigated on multiple scales from the macroscopic tissue-level down to molecules. Biological tissues are complex structures consisting of various different cell types and extracellular matrix, that when healthy maintain a steady state. In cancer this steady state is disturbed, the cells undergo changes in their genetic and regulatory systems, but also their shape and mechanical setup changes, as well as the surrounding ECM may be restructured. These mechanical changes can act as tumor promoter in itself, while shape changes allow the transition from a jammed, solid state into an unjammed, fluid state where cells can freely move through the tissue, and escape from the primary tumor site. Our goal is to understand the underlying mechanics and emergent behavior, that could be applied to a wider range of tumors despite differences in cell type and genetic makeup. Additionally through a better understanding of composite networks of biopolymers in vitro we aim at a better understanding of the cytoskeleton in vitro.

Josef A. Käs

4.2 The two faces of enhanced stroma: Stroma acts as a tumor promoter and a steric obstacle (review)

C.T. Mierke, F. Sauer, S. Grosser, S. Puder, T. Fischer, J.A. Käs

In addition to genetic, morphological and biochemical alterations in cells, a key feature of the malignant progression of cancer is the stroma, including cancer cell motility as well as the emergence of metastases. Our current knowledge with regard to the biophysically driven experimental approaches of cancer progression indicates that mechanical aberrations are major contributors to the malignant progression of cancer. In

particular, the mechanical probing of the stroma is of great interest. However, the impact of the tumor stroma on cellular motility, and hence the metastatic cascade leading to the malignant progression of cancer, is controversial as there are two different and opposing effects within the stroma. On the one hand, the stroma can promote and enhance the proliferation, survival and migration of cancer cells through mechanotransduction processes evoked by fiber alignment as a result of increased stroma rigidity. This enables all types of cancer to overcome restrictive biological capabilities. On the other hand, as a result of its structural constraints, the stroma acts as a steric obstacle for cancer cell motility in dense three-dimensional extracellular matrices, when the pore size is smaller than the cell's nucleus. The mechanical properties of the stroma, such as the tissue matrix stiffness and the entire architectural network of the stroma, are the major players in providing the optimal environment for cancer cell migration. Thus, biophysical methods determining the mechanical properties of the stroma, such as magnetic resonance elastography, are critical for the diagnosis and prediction of early cancer stages. Fibrogenesis and cancer are tightly connected, as there is an elevated risk of cancer on cystic fibrosis or, subsequently, cirrhosis. This also applies to the subsequent metastatic process [1].

[1] C. T. Mierke et al.: NMR Biomed. **2018** 10:e3831

4.3 Glassy dynamics in composite biopolymer networks

T. Golde, C. Huster*, M. Glaser, T. Händler, H. Herrmann†‡, J.A. Käs, J. Schnauß

*Institute for Theoretical Physics, Leipzig University
†Molecular Genetics, German Cancer Research Center Heidelberg
‡Dept. of Neuropathology, University Hospital Erlangen

The cytoskeleton is a highly interconnected meshwork of strongly coupled subsystems providing mechanical stability as well as dynamic functions to cells. To elucidate the underlying biophysical principles, it is central to investigate not only one distinct functional subsystem but rather their interplay as composite biopolymeric structures. Two of the key cytoskeletal elements are actin and vimentin filaments. Here, we show that composite networks reconstituted from actin and vimentin can be described by a superposition of two non-interacting scaffolds. Arising effects are demonstrated in a scale-spanning frame connecting single filament dynamics to macro-rheological network properties. The acquired results of the linear and non-linear bulk mechanics can be captured within an inelastic glassy wormlike chain model. In contrast to previous studies, we find no emergent effects in these composite networks. Thus, our study paves the way to predict the mechanics of the cytoskeleton based on the properties of its single structural components [1].

[1] T. Golde et al.: Soft Matter **2018** 14:7970-7978

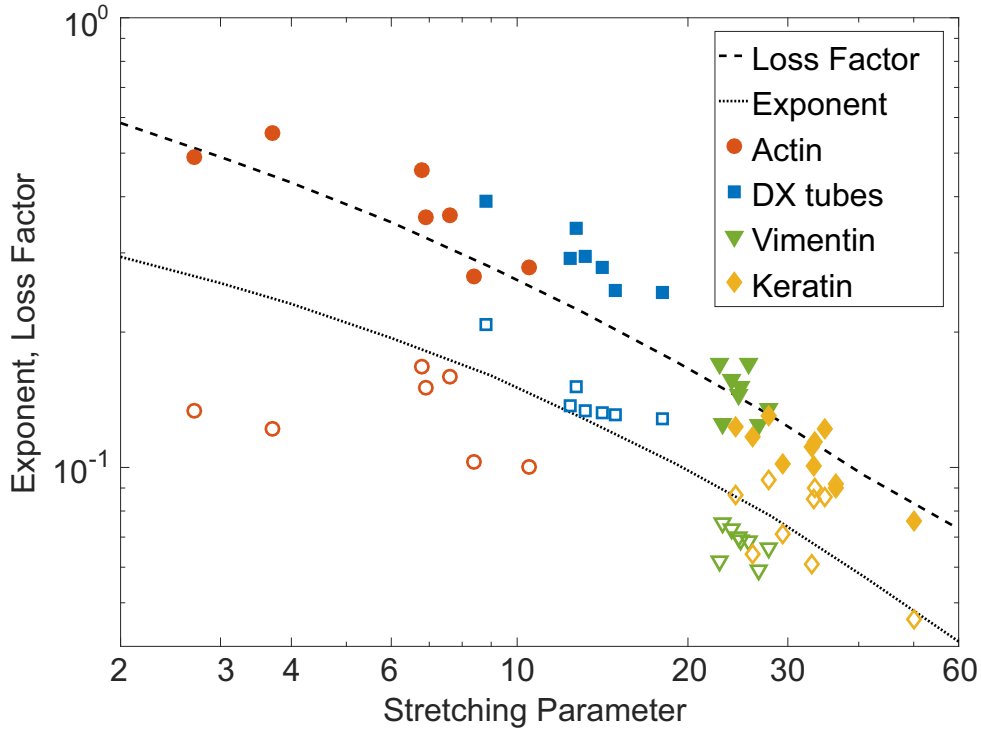

Figure 4.1: Local power law exponent of storage modulus G′ (open symbols) and loss factor tan(ϕ)=G″/G′ (solid symbols) versus stretching parameter epsilon. Each pair of data points represents one sample. The exponent was obtained from fitting G′ with a power law for frequencies smaller than the crossover between G′ and the loss modulus G″. The loss factor was obtained from fitting tan(ϕ) locally with a power law at a frequency of 1 Hz. Epsilon is the result from fitting the complex shear modulus G* to the Glassy Wormlike Chain Model for each sample. Dashed lines are the numerical results of an exemplary G*(GWLC) where all parameters except epsilon are fixed.

4.4 Direct observation and rational design of nucleation behavior in addressable self-assembly

M. Sajfutdinow[*†] W.M. Jacobs[‡], A. Reinhardt[§], C. Schneider[*], D.M. Smith[*¶]

[*]Fraunhofer Institute for Cell Therapy and Immunology, Leipzig
[†]Faculty of Chemistry and Mineralogy, Leipzig University
[‡]Department of Chemistry and Chemical Biology, Harvard University, Cambridge
[§]Department of Chemistry, University of Cambridge, Cambridge
[¶]Soft Matter Physics

To optimize a self-assembly reaction, it is essential to understand the factors that govern its pathway. Here, we examine the influence of nucleation pathways in a model system for addressable, multicomponent self-assembly based on a prototypical „DNA-brick“structure. By combining temperature-dependent dynamic light scattering and atomic force microscopy with coarse-grained simulations, we show how subtle changes in the nucleation pathway profoundly affect the yield of the correctly formed structures.

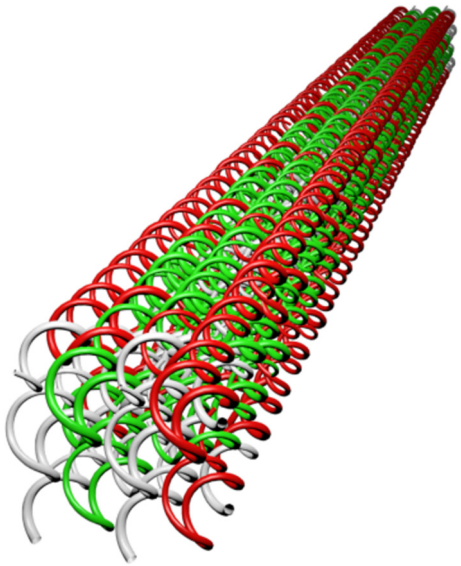

Figure 4.2: Model of „cuboid“ structure formed by the DNA Bricks method. The structure consists of 250 individual DNA oligonucleotide „bricks“, with dimensions 10 nm x 10 nm x 80 nm. Red strands represent „edge“ boundary bricks, green strands are „face“ boundary bricks.

In particular, we can increase the range of conditions over which self-assembly occurs by using stable multisubunit clusters that lower the nucleation barrier for assembling subunits in the interior of the structure. Consequently, modifying only a small portion of a structure is sufficient to optimize its assembly. Due to the generality of our coarse-grained model and the excellent agreement that we find with our experimental results, the design principles reported here are likely to apply generically to addressable, multicomponent self-assembly [1].

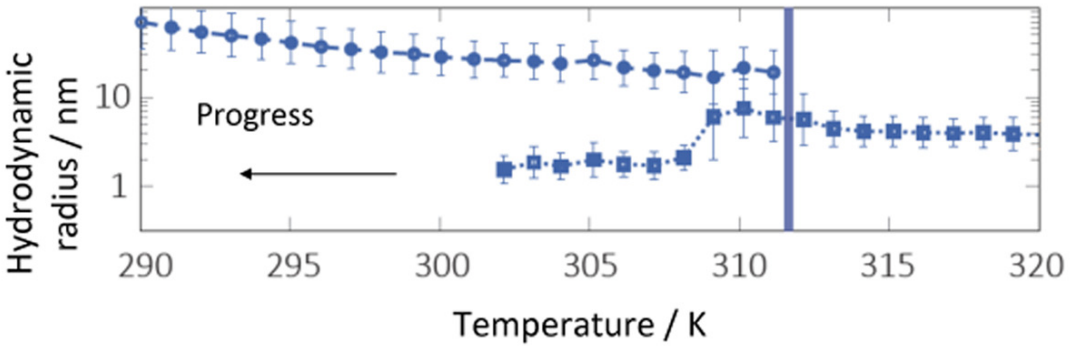

Figure 4.3: Time progression of cuboid growth, measured by Dynamic Light Scattering (DLS) at different temperatures and shown in terms of average hydrodynamic radius. A clear transition to the assembled product (hydrodynamic radius = 20 nm) is seen at approximately 312 K.

[1] M. Sajfutdinow et al.: PNAS **2018** 115(26) E5877-E5886

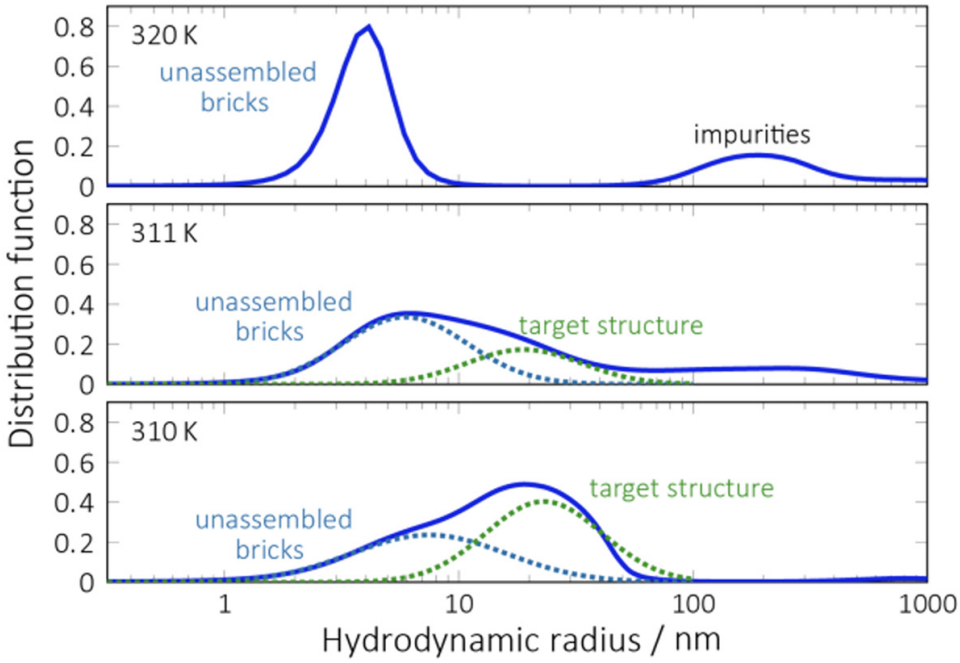

Figure 4.4: Progression of size distribution, as determined by DLS, at 3 sample temperatures. At 320 K, above the assembly threshold, the distribution is dominated by unassembled bricks (radius 2-4 nm). At the assembly threshold (311 K), a shift towards the assembled target structure is clear. Just below the threshold (310 K), the target structure (radius 20 nm) dominates the distribution.

4.5 Early adhesion of cells to ferromagnetic shape memory alloys functionalized with plasma assembled biomolecules - a single cell force spectroscopy study

M.V. Cakir, U. Allenstein, M. Zink, S.G. Mayr[*†]

[*]Leibniz Institute of Surface Engineering (IOM)
[†]Division of Surface Physics

Biomaterial performance and integration of prostheses in vivo strongly depend on the ability of cells to adhere. Plasma-assisted functionalization of smart metals with biopolymers, including plasma polymerized l-lysine (PPLL), constitutes a recently-developed promising approach to synthesize highly flexible, yet robust and strongly adherent protein coatings that support cell-biomaterial interaction. In the present study we employ single cell force spectroscopy to demonstrate that PPLL coatings promote early adhesion of fibroblast cells on the ferromagnetic shape memory alloy FePd - a promising magnetically switchable biomaterial. By varying the contact time of a cell with the substrate surface, we show that the forces and work needed to fully detach a cell increase with time and quantify bioactivity of the material. In contrast to glass and PPLL-coated glass, cell detachment from FePd requires much larger work, while a PPLL biofunctionalization further improves cell adhesion and binding affinity by an increased detachment work on short time scales. Together with a time-dependent

bond model we postulate a transition from unspecific to specific cell adhesion on FePd and PPLL-coated FePd, while on glass detachment forces are lower and level off to a saturation regime on short times prior to the expected time necessary for specific integrin-based bond formation [1].

[1] M. V. Cakir et al.: Materials & Design **2018** 158:19-27

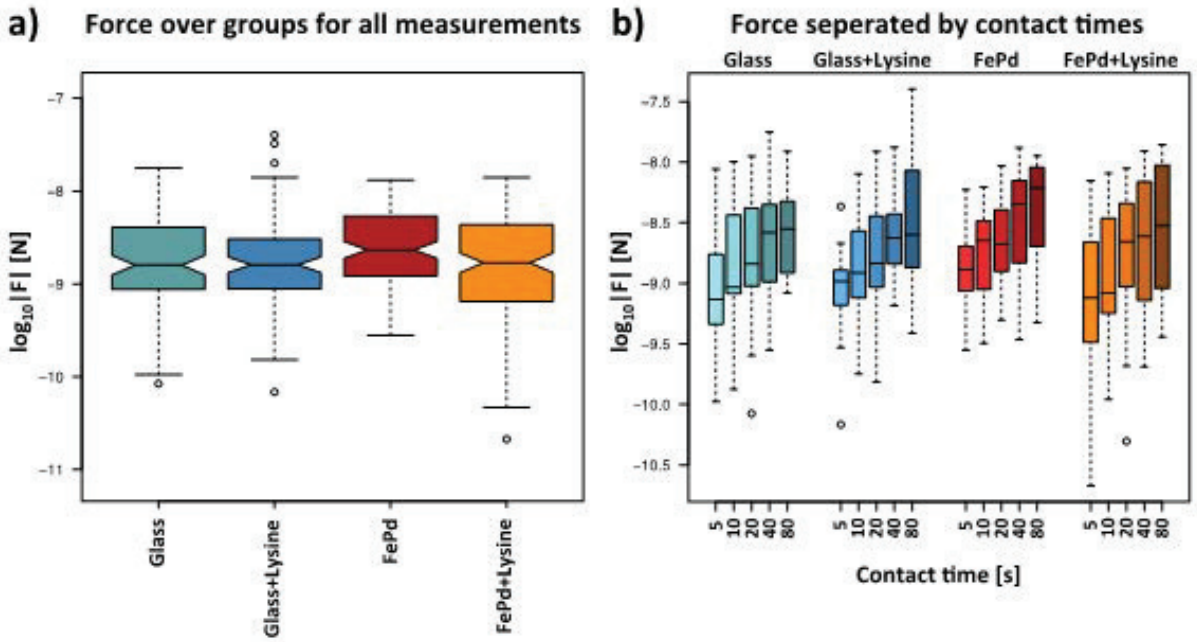

Figure 4.5: Adhesion forces of fibroblast cells to different surfaces measured by atomic force microscopy for different cell-surface contact times: a) averaged over all contact times and b) separated by contact times. Central lines represent medians, hinges represent 1^{st} and 3^{rd} quartiles, notches represent 95 % confidence intervals of medians, whiskers represent hinges ± 1.5IQR (Interquartile Range) while single points represent outliers.

4.6 Changing cell mechanics - a precondition for malignant transformation of oral squamous carcinoma cells

F. Meinhövel[*], R. Stange[†], J. Schnauß, M. Sauer[‡], J.A. Käs, T.W. Remmerbach[*§]

[*]Section of Clinical and Experimental Oral Medicine and Dept. of Oral, Maxillofacial and Facial Plastic Surgery, University Hospital, Leipzig
[†]RS Zelltechnik
[‡]Dept. of Oral Maxillofacial and Facial Plastic Surgery, SRH Zentralklinikum Suhl GmbH
[§]Griffith Institute of Health, Griffith University, Queensland, Australia

Oral squamous cell carcinomas (OSCC) are the sixth most common cancer and the diagnosis is often belated for a curative treatment. The reliable and early differentiation between healthy and diseased cells is the main aim of this study in order to improve the quality of the treatment and to understand tumour pathogenesis. Here, the optical

stretcher is used to analyse mechanical properties of cells and their potential to serve as a marker for malignancy. Stretching experiments revealed for the first time that cells of primary OSCCs were deformed by 2.9% rendering them softer than cells of healthy mucosa which were deformed only by 1.9%. Furthermore, the relaxation behaviour of the cells revealed that these malignant cells exhibit a faster contraction than their benign counterparts. This suggests that deformability as well as relaxation behaviour can be used as distinct parameters to evaluate emerging differences between these benign and malignant cells. Since many studies in cancer research are performed with cancer cell lines rather than primary cells, we have compared the deformability and relaxation of both types, showing that long time culturing leads to softening of cells. The higher degree of deformability and relaxation behaviour can enable cancer cells to traverse tissue emphasizing that changes in cell architecture may be a potential precondition for malignant transformation. Respecting the fact that even short culture times have an essential effect on the significance of the results, the use of primary cells for further research is recommended. The distinction between malignant and benign cells would enable an early confirmation of cancer diagnoses by testing cell samples of suspect oral lesions [1].

[1] F. Meinhövel et al.: Convergent Science Physical Oncology **2018** 4:034001

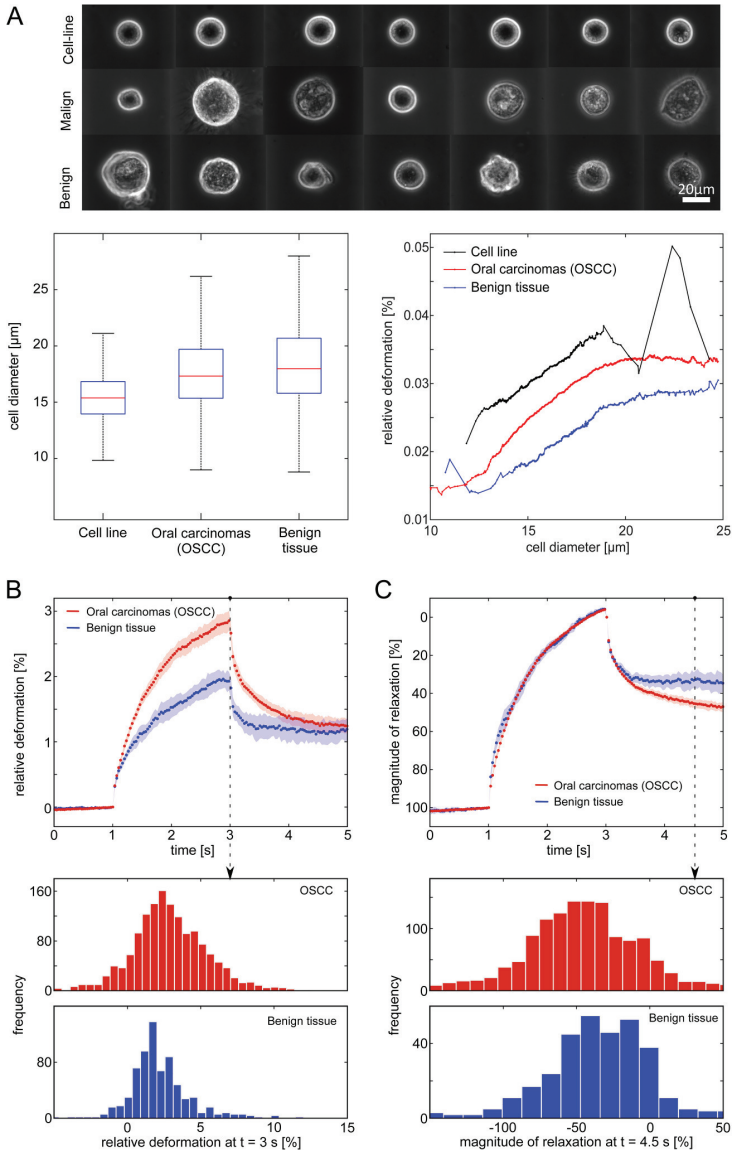

Figure 4.6: Representative examples for the diversity of cells. (A) The cells in the upper line originate from cancer cell lines (CAL27, CAL33, BHY). The cells below originate from primary cancerous tissue (middle) and primary benign tissue (bottom). The boxplot illustrates that cells originating from primary tissue are slightly larger and show a broader size distribution compared to cell lines. Cells from primary tissue as well as from cell lines display that larger cells are more deformed than smaller ones. (B) Comparing the relative deformability of primary OSCC (red; passage 0; n=1465) and benign oral epithelial tissue (blue; passage 0; n=360) reveals that malignant cells are significantly softer than their benign counterparts. At the end of the stretching (dashed line; t=3s) the counts of the relative deformations show the distribution of the maximum deformability within the distinct cell population in the according histograms. (C) The magnitude of relaxation for primary OSCC (red) and primary oral epithelial tissue (blue), derived from the relative change in ellipticity normalized to the end of stretching (t=3s), illustrates that malignant OSCC cells were still contracting after 2 s while malignant cells sem to reach a stable plateau. Representative data after a total observation time of t=4.5s are shown in the according histograms displaying the distribution of relaxation values.

4.7 Synthetic Transient Crosslinks Program the Mechanics of Soft, Biopolymer-Based Materials

J. Lorenz*, J. Schnauß, M. Glaser, M. Sajfutdinow*, C. Schuldt J.A. Käs, D.M. Smith*

*Fraunhofer Institute for Cell Therapy and Immunology, Leipzig

Actin networks are adaptive materials enabling dynamic and static functions of living cells. A central element for tuning their underlying structural and mechanical properties is the ability to reversibly connect, i.e., transiently crosslink, filaments within the networks. Natural crosslinkers, however, vary across many parameters. Therefore, systematically studying the impact of their fundamental properties like size and binding strength is unfeasible since their structural parameters cannot be independently tuned. Herein, this problem is circumvented by employing a modular strategy to construct purely synthetic actin crosslinkers from DNA and peptides. These crosslinkers mimic both intuitive and noncanonical mechanical properties of their natural counterparts. By isolating binding affinity as the primary control parameter, effects on structural and dynamic behaviors of actin networks are characterized. A concentration-dependent triphasic behavior arises from both strong and weak crosslinkers due to emergent structural polymorphism. Beyond a certain threshold, strong binding leads to a nonmonotonic elastic pulse, which is a consequence of self-destruction of the mechanical structure of the underlying network. The modular design also facilitates an orthogonal regulatory mechanism based on enzymatic cleaving. This approach can be used to guide the rational design of further biomimetic components for programmable modulation of the properties of biomaterials and cells [1].

[1] J. Lorenz et al.: Advanced Materials **2018** 1706092

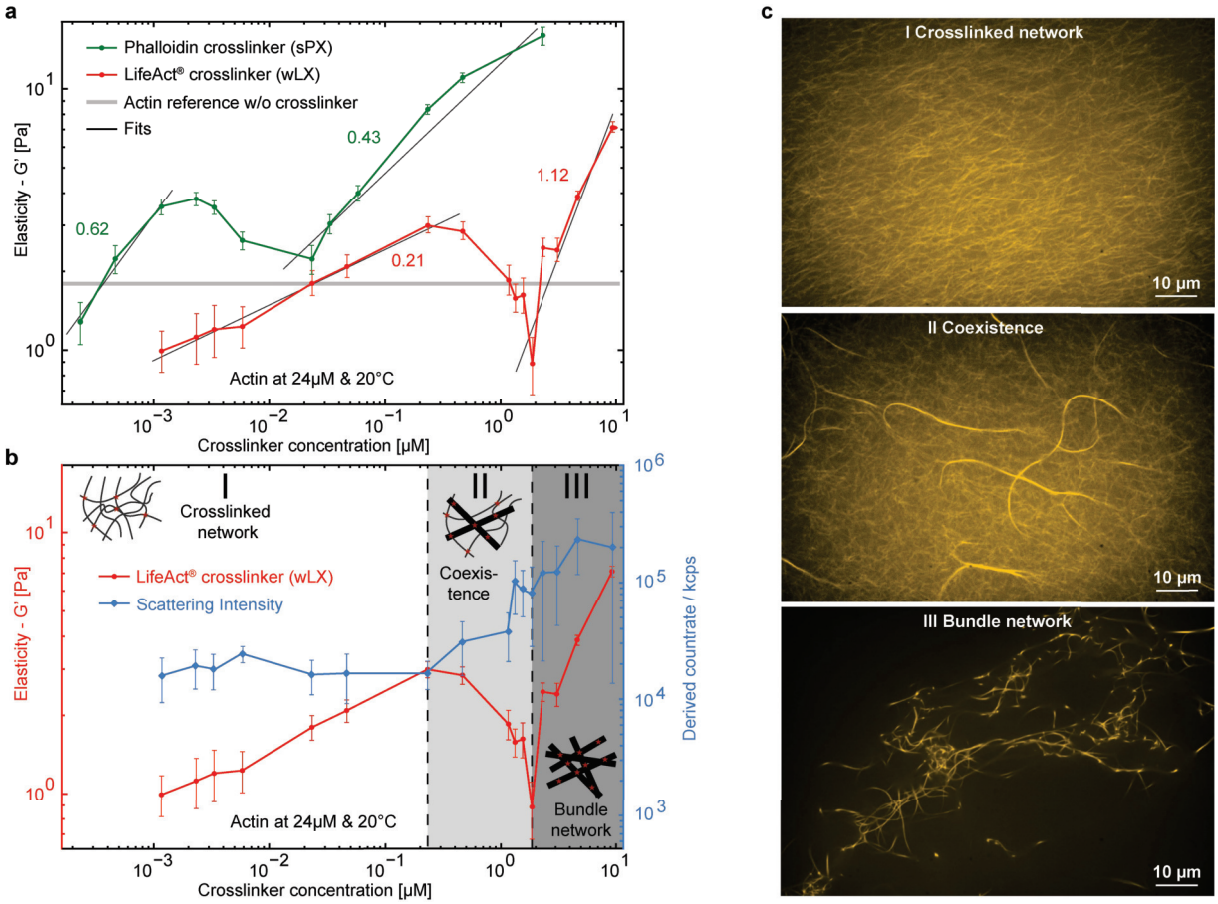

Figure 4.7: We used DNA nanotechnolgy to built synthetic, biomimetic structures able to crosslink natural biopolymers, which lend cell their mechanical stabiluty. These synthetic crosslinkers nonmonotonically influence the elasticity of actin networks. (a) Elastic moduli of actin networks were investigated for different concentrations of wLX (red) and sPX (green) crosslinkers. Both initially stiffened the networks with increasing concentration before reaching a peak, which was followed by a decrease of G' to a minimum with a subsequent monotonic increase (power-law fits (black line) and exponents are shown next to the corresponding G' increase). This nonmonotonic behavior can be attributed to different structural morphologies, which were captured by (b) light scattering (blue; error bars indicate standard deviations of the mean values) and (c) fluorescence microscopy.

4.8 Funding

Leipziger Schule der Naturwissenschaften - Bauen mit Molekülen und Nano-Objekten (BuildMoNa)
Prof. Dr. E. Hey-Hawkins, Prof. Dr. M. Grundmann und Prof. Dr. J. A. Käs
GSC 185/1

Blebbing Driven or Actin Protrusive-Force Driven Cancer Cell Migration
Prof. Dr. J. A. Käs, Prof. Dr. C. T. Mierke
DFG, KA 1116/17-1

Mechanismen Aktin-vermittelter Krafterzeugung, Morphodynamik und Motilität einzelner Zellen
Prof. Dr. J. A. Käs, Prof. Dr. K. Rottner, Prof. Dr. M. Falcke
DFG, KA 1116/14-1

Dynamisch-mechanische Manipulation and Charakterisierung von Zellen mit Hilfe magnetischer Dehnung
Prof. Dr. M. Zink
DFG, Zi-1330/2-1

FORCE - Imaging the Force of Cancer, WP 6 - Mechanical Impact of Solid Tumours on Tissues
Prof. Dr. J. A. Käs
EU Horizon 2020, 668039

Plasmaunterstützte Funktionalisierung magnetischer Kern-Schale-Nanopartikel mit Biomolekülen für die medizinische Diagnostik - BIOCOAT
Prof. Dr. M. Zink
SAB, 100259235

Organotypische Langzeitkultivierung von adultem Augengewebe zur Erforschung von Krankheiten und Wirkstoffen in vitro - EYECULTURE - TP 1
Prof. Dr. M. Zink
BMBF, 031A574A

What Holds Cancer Cells Back? (HoldCancerBack)
Prof. Dr. J. A. Käs
ERC Advanced Grant - EU Horizon 2020, 741350

Korrelative Zell-Zell-Wechselwirkung in Geweben und Gewebemodellen fur neue Ansatze in Diagnostik und Therapie: Mechanische Aspekte (KOGEME), Geräteausstattung
Prof. Dr. J. A. Käs, Prof. Dr. C. T. Mierke, Prof. Dr. T. Pompe, Prof. Dr. M. Zink
SAB, 100299919

Entwicklung einer Multiwell-Ultra High Dense Mikroelektroden- und Oszillatorenarray-Multiplexer-Plattform für räumlich-zeitlich hochaufgelöstes Monitoring zellulärer Biomechanik im Live-Modus (MUDIplex)
Prof. A. Robitzki, Prof. M. Zink, Prof. J. A. Käs, Prof. C. T. Mierke
SAB

4.9 Organizational Duties

Prof. J. A. Käs

- Senator der Universität Leipzig
- Member of the Organizing Committee: 9^{th} Annual Symposium - Physics of Cancer, Leipzig, September 2018
  involved organizers: Prof. H. Herrmann (German Cancer Research Center), Prof. B. Fabry (Friedrich-Alexander University, Erlangen-Nuremberg), Dr. Benjamin Wolf (University Hospital Leipzig), Dr. D. M. Smith (Fraunhofer Institute IZI)
- PWM Winterschool, Vítkovice, Czech Republic, February 2018
- Member of the Scientific Advisory Board of the Max Planck Institute for Medical Research
- Reviewer of the ERC Synergy Grant
- Fellow, American Physical Society
- Full Member, Saxonian Academy of Sciences

4.10 Cooperations

External Academic

- Syracuse University, USA
  Prof. M. E. Manning
- Syracuse University, USA
  Prof. J. Schwarz
- University of California Santa Barbara, USA
  Prof. M. C. Marchetti
- Harvard University, Boston, USA
  Prof. J. J. Fredberg
- King's College London, Biomedical Engineering Department, GB
  Prof. R. Sinkus
- Politecnico Milano, Italy
  Dr. R. Osellame
- Deutsche Gesellschaft für Zellbiologie (DGZ)
  Prof. Dr. H. Herrmann
- Max-Delbrück-Zentrum für molekulare Medizin
  Dr. M. Falcke
- Charité Berlin, MR Elastographie
  Prof. Dr. I. Sack
- Technische Universität Braunschweig, Zoologisches Institut
  Prof. Dr. K. Rottner
- Pathologie Hamburg-West, Institut für Histologie, Zytologie und molekulare Diagnostik
  Prof. Dr. A. Niendorf

Internal Academic, Leipzig University

- Biotechnologisch-Biomedizinisches Zentrum
  Prof. Dr. A. Robitzki
- Klinik und Poliklinik für Frauenheilkunde
  Prof. Dr. B. Aktas
- Institut für Pathologie
  Prof. Dr. L.-C. Horn
- Klinik und Poliklinik für Dermatologie, Venerologie und Allergologie
  Prof. Dr. J.-C. Simon
- Institut für Anatomie
  Prof. Dr. I. Bechmann
- Klinik und Poliklinik für Endokrinologie und Nephrologie
  Prof. M. Stumvoll
- Universitäres Krebszentrum
  Prof. F. Lordick
- Klinik und Poliklinik für Neurologie
  Dr. D. Michalski
- Rudolf-Schönheimer-Institut für Biochemie
  Prof. Dr. T. Langenhan
- Rudolf-Schönheimer-Institut für Biochemie
  Dr. I. Liebscher
- Peter-Debye-Institut for Soft Matter Physics
  Prof. Dr. C. Mierke

Industry

- RS Zelltechnik GmbH, Leipzig
  R. Stange

4.11 Publications

Journals

C. T. Mierke, F. Sauer, S. Grosser, S. Puder, T. Fischer, J. A. Käs: *The two faces of enhanced stroma: Stroma acts as a tumor promoter and a steric obstacle*. NMR Biomed. **10**, e3831 (2018)

T. Golde, C. Huster, M. Glaser, T. Händler, H. Herrmann, J. A. Käs, J. Schnauß: *Glassy dynamics in composite biopolymer networks*. Soft Matter **14**, 7970-7978 (2018)

M. C. Cakir, U. Allenstein, M. Zink, S. G. Mayr: *Early adhesion of cells to ferromagnetic shape memory alloys functionalized with plasma assembled biomolecules - a single cell force spectroscopy study*. Materials & Design **158**, 19-27 (2018)

F. Meinhövel, R. Stange, J. Schnauß, M. Sauer, J. A. Käs, T. W. Remmerbach: *Changing cell mechanics - a precondition for malignant transformation of oral squamous carcinoma cells*. Convergent Science Physical Oncology **4**, 034001 (2018)

J. Lorenz, J. Schnauß, M. Glaser, M. Sajfutdinow, C. Schuldt, J. A. Käs, D. M. Smith: *Synthetic Transient Crosslinks Program the Mechanics of Soft, Biopolymer-Based Materials*. Advanced Materials 1706092 (2018)

C. Möser, J. Lorenz, M. Sajfutdinow, D. Smith: *Pinpointed Stimulation of EphA2 Receptors via DNA-Templated Oligovalence*. Int. J. Mol. Sci. **19**, iss. 11, 3482 (2018)

M. Sajfutdinow, W. M. Jacobs, A. Reinhardt, C. Schneider, D. M. Smith: *Direct observation and rational design of nucleation behavior in addressable self-assembly*. PNAS **115**, iss. 26, E5877-5886

M. C. Engel, D. M. Smith, M. A. Jobst, M. Sajfutdinow, T. Liedl, F. Romano, L. Rovigatti, A. A. Louis, J. P. K. Doye: *Force-Induced Unravelling of DNA Origami*. ACS Nano **12**, iss. 7, 6743-6747 (2018)

Talks

T. Golde, C. Huster, M. Glaser, T. Händler, H. Herrmann, J. A. Käs, J. Schnauß: *Glassy Dynamics in Composite Biopolymer Networks*. SoftComp Workshop, Jülich, Germany, January 2018

J. Lippoldt, P. Heine, S. Grosser, L. Oswald, J. A. Käs: *Dynamics of Cell Jamming: Disentangling the Shape and Density Dependences*. PWM Winter School Vítkovice, Czech Republic, February 2018

E. W. Morawetz, E. Warmt, S. Grosser, H. Kubitschke, B. Wolf, S. Briest, M. Höckel, B. Aktas, J. A. Käs: *Cancer & E-Cadherin - a closer look*. PWM Winter School Vítkovice, Czech Republic, February 2018

S. Grosser, L. Oswald, J. Lippoldt, J. A. Käs: *Cell Motion in 3D-Aggregates is Correlated to Cell Shape*. PWM Winter School Vítkovice, Czech Republic, February 2018

F. Sauer, S. Grosser, E. Morawetz, J. A. Käs, C. T. Mierke: *Intricate features of 3D cancer cell invasion*. PWM Winter School Vítkovice, Czech Republic, February 2018

E. Warmt, S. Grosser, E. Morawetz, R. Stange, J. A. Käs: *Cortical Actin Contractility of Single Suspended Cells Might Determine Tissue Formation*. PWM Winter School Vítkovice, Czech Republic, February 2018

C. Ficorella, R. Martinéz Vazquéz, P. Heine, E. Lepera, J. Cao, R. Osellame, J. A. Käs: *Cell motility study in constriction chips*. PWM Winter School Vítkovice, Czech Republic, February 2018

P. Mollenkopf, J. Lorenz, M. Glaser, J. A. Käs, J. Schnauß, D. Smith: *Friction in isotropic polymer networks*. PWM Winter School Vítkovice, Czech Republic, February 2018

J. Lippoldt, P. Heine, S. Grosser, L. Oswald, J. A. Käs: *Dynamics of Cell Jamming: Disentangling the Shape and Density Dependences*. DPG Spring Meeting, Berlin, Germany, March 2018

F. Sauer, S. Grosser, E. Morawetz, J. A. Käs, C. T. Mierke: *Intricate features of 3D cancer cell invasion*. DPG Spring Meeting, Berlin, Germany, March 2018

T. Golde, C. Huster, M. Glaser, T. Händler, H. Herrmann, J. A. Käs, J. Schnauß: *Glassy Dynamics in Composite Biopolymer Networks*. DPG Spring Meeting, Berlin, Germany, March 2018

A. Weidt, S. G. Mary, M. Zink: *Organization of Fibronectin and NIH/3T3 Fibroblasts on Bulk Microgrooved TiO_2*. DPG Spring Meeting, Berlin, Germany, March 2018

J. A. Käs: *Why do rigid tumours contain soft cancer cells?* Physics of Life Workshop: „Merging clinical, biological and physical sciences approaches for cancer research“at BMA House, London, Great Britain, April 2018 (invited talk)

J. Schnauß: *Driving Life's Engine: from Semiflexible Components to Cell Migration & Viscoelasticity in Cell Mechanics*. Vorstellungsvortrag Juniorprofessur - Molecular Cell Biophysics & Lehrprobe, Saarbrücken, Germany, April 2018

D. M. Smith: *Bottom-up Engineering of Nanoscale Devices*. Leibniz IPHT Spring Workshop, Leipzig, Germany, April 2018

C. Tutmarc, T. Golde, M. Glaser, J. A. Käs, D. M. Smith, J. Schnauß: *Measuring reptation of biopolymer networks via biomimetic DNA probes*. DNA Mitteldeutschland, Leibniz IPHT Jena, Germany, May 2018

P. Hietschold, M. Deuflhard, S. Riedel, M. Zink, S. Mayr: *Characteristics of modified hydrogels with and without incorporated magnetic nanoparticles*. Gruppentreffen, DFG-Schwerpunktprogramm 1681, Jülich, Germany, June 2018

S. Grosser, L. Oswald, J. Lippoldt, J. A. Käs: *How Carcinomas Work: Structure and Mechanics of Multicellular Spheroids*. Soft Matter Day2018, Leipzig, Germany, July 2018

E. Warmt, S. Grosser, E. Morawetz, R. Stange, J. A. Käs: *Cortical Actin Contractility of Single Suspended Cells Might Determine Tissue Formation*. International Meeting of the German Society for Cell Biology, Leipzig, Germany, September 2018

S. Grosser, L. Oswald, J. Lippoldt, J. A. Käs: *Cell Jamming in 3D: How Can Cells in a Tumour Move?* 9^{th} Annual Symposium - Physics of Cancer, Leipzig, Germany, September 2018

P. Hietschold, S. Riedel, M. Deuflhard, M. Zink, S. Mayr: *Characteristics of modified hydrogels with and without incorporated magnetic nanoparticles*. Kolloquium, DFG-Schwerpunktprogramm 1681, Benediktbeuern, Germany, September 2018

J. A. Käs: *Cancer metastasis - A new type of unjamming transition*. Friedrich-Alexander University, Erlangen-Nuremberg, Germany, October 2018 (invited talk)

J. Lippoldt, S. Grosser, L. Oswald, M. Merkel, D. Sussman, S. Pawlizak, A. Fritsch, L. Manning, J. A. Käs: *Cell Jamming in 3D*. Erice Workshop on Self-Organization in Active Matter: from Colloids to Cells, Erice, Italy, October 2018

D. M. Smith: *Studying nucleation and mechanics of macromolecules with DNA-based mimics*. Universität Paderborn, Germany, October 2018 (invited taalk)

D. M. Smith: *Bottom-up Engineering of Nanoscale Devices to Program Macroscopic Material Properties*. Jawaharlal Nehru Centre for Advanced Scientific Research, Bangalore, India, December 2018 (invited talk)

D. M. Smith: *Bottom-up Engineering of Nanoscale Devices to Program Macroscopic Material Properties*. Dhirubhai Ambani Institute of Information and Communication Technology, Gandhinagar, India, December 2018 (invited talk)

J. A. Käs: *Comprehensive Multiscale Mechanics of Tissues: A Technology Package Reaching from Organs to Molecules*. Bruker & JPK SPM Conference and Users Meeting, Bruker BNA & JPK BioAFM Center, Berlin, Germany, December 2018

Posters

A. Weidt, S. G. Mary, M. Zink: *Organization of Fibronectin and NIH/3T3 Fibroblasts on Bulk Microgrooved* TiO_2. 14^{th} Research Festival for Life Sciences, Faculty for Medicine, Faculty for Life Sciences, Leipzig University, Germany, January 2018

H. Kubitschke, B. Wolf, E. Morawetz, L.-C. Horn, B. Aktas, U. Behn, M. Höckel, J. A. Käs: *Roadmap to Local Tumor Growth*. Research Festival for Life Sciences, Faculty for Medicine, Faculty for Life Sciences, Leipzig University, Germany, January 2018

C. Ficorella, R. Martinéz Vazquéz, P. Heine, E. Lepera, J. Cao, R. Osellame, J. A. Käs: *Cell motion through a confined micro-environment: an attempt to understand the motion of metastatic cells*. 62nd Annual Meeting Biophysical Society, San Francisco, USA, February 2018

H. Kubitschke, B. Wolf, E. Morawetz, L.-C. Horn, B. Aktas, U. Behn, M. Höckel, J. A. Käs: *Roadmap to Local Tumor Growth*. 62nd Annual Meeting Biophysical Society, San Francisco, USA, February 2018

E. Warmt, S. Grosser, E. Morawetz, J. A. Käs: *Cortical Actin Contractility of Single Suspended Cells*. DPG Spring Meeting, Berlin, Germany, March 2018

S. Grosser, L. Oswald, J. Lippoldt, J. A. Käs: *Fluid and Jammed Behaviour in Cell Spheroids*. DPG Spring Meeting, Berlin, March 2018

A. Weidt, M. Mensing, J. Lehnert, S. Mändl, M. Zink, S.G. Mayr: *Carbon implantation of TiO_2 nanotubes*. Annual BuildMoNa Conference, Graduate School BuildMoNa, Leipzig University, Germany, March 2018

E. Warmt, S. Grosser, E. Morawetz, J. A. Käs: *Cortical Actin Contractility of Single Suspended Cells*. Soft Matter Day2018, Leipzig, Germany, July 2018

F. Sauer, S. Grosser, E. Morawetz, S. Briest, L.-C. Horn, B. Aktas, C. T. Mierke, J. A. Käs: *Real Tumor Pieces and Model Cell-Aggregates Act Alike on Collagen Gels*. Soft Matter Day 2018, Leipzig, Germany, July 2018

A. Weidt, M. Mensing, J. Lehnert, S. Mändl, M. Zink, S.G. Mayr: *Carbon implantation of TiO_2 nanotubes for biomedical applications*. Soft Matter Day 2018, Leipzig, Germany, July 2018

P. Hietschold, S. Riedel, M. Zink, S. Mayr: *Characteristics of modified hydrogels with and without incorporated magnetic nanoparticles* . Soft Matter Day 2018, Leipzig, Germany, July 2018

H.-M. Scholz-Marggraf, E. Morawetz, J. Reichenbach, J. A. Käs: *Role of N-Cadherin During the Epithelial-Mesenchymal Transition*. Soft Matter Day 2018, Leipzig, Germany, July 2018

C. Ficorella, R. Martinéz Vazquéz, P. Heine, R. Osellame, J. A. Käs: *Cancer cell motility study in micro-constriction chips*. Soft Matter Day 2018, Leipzig, Germany, July 2018

E. W. Morawetz, S. Grosser, F. Sauer, T. Fuhs, B. Wolf, S. Kallendrusch, H. Kubitschke, H.-M. Scholz-Marggraf, J. Lippoldt, M. Zink, I. Bechmann, S. Briest, L.-C. Horn, B. Aktas, J. A. Käs: *The Physics of Carcinomas: Extensive Studies of the Aggressiveness of Vital Breast and Cervical Cancer Samples*. Soft Matter Day 2018, Leipzig, Germany, July 2018

H. Kubitschke, B. Wolf, E. Morawetz, L.-C. Horn, B. Aktas, U. Behn, M. Höckel, J. A. Käs: *Roadmap to Local Tumor Growth*. Soft Matter Day 2018, Leipzig, Germany, July 2018

P. Mollenkopf, J. Lorenz, M. Glaser, J. A. Käs, J. Schnauß, D. Smith: *Friction in isotropic polymer networks*. Soft Matter Day 2018, Leipzig, Germany, July 2018

P. Gottheil, S. Grosser, J. Lippoldt: *Cell Shapes in Model and Real Tissue*. Soft Matter Day 2018, Leipzig, Germany, July 2018

X. Xie, T. Fuhs, J. A. Käs: *Viscoelastic characterization of spheroid cell clusters*. Soft Matter Day 2018, Leipzig, Germany, July 2018

E. Warmt, S. Grosser, E. Morawetz, J. A. Käs: *Cortical Actin Contractility of Single Suspended Cells Might Determine Tissue Surface Tension*. International Meeting of the German Society for Cell Biology, Leipzig, Germany, September 2018

P. Hietschold, S. Riedel, M. Deuflhard, M. Zink, S. Mayr: *Characteristics of modified hydrogels with and without incorporated magnetic nanoparticles* . Kolloquium, DFG-Schwerpunktprogramm 1681, Benediktbeuern, Germany, September 2018

T. Golde, M. Glaser, C. Tutmarc, I. Elbalasy, C. Huster, G. Busteros, D. M. Smith, H. Herrmann, J. A. Käs, J. Schnauß: *The Role of Stickiness in the Rheology of Semiflexible Polymers*. 9^{th} Annual Symposium - Physics of Cancer, Leipzig, Germany, September 2018

J. Lippoldt, P. Heine, S. Grosser, L. Oswald, J. A. Käs: *Dynamics of Cell Jamming: Disentangling the Shape and Density Dependences*. 9^{th} Annual Symposium - Physics of Cancer, Leipzig, Germany, September 2018

H.-M. Scholz-Marggraf, E. Morawetz, J. Reichenbach, J. A. Käs: *Role of N-Cadherin During the Epithelial-Mesenchymal Transition*. 9^{th} Annual Symposium - Physics of Cancer, Leipzig, Germany, September 2018

F. Sauer, S. Grosser, E. Morawetz, S. Briest, L.-C. Horn, B. Aktas, C. T. Mierke, J. A. Käs: *Real Tumor Pieces and Model Cell-Aggregates Act Alike on Collagen Gels*. 9^{th} Annual Symposium - Physics of Cancer, Leipzig, Germany, September 2018

A. Weidt, M. Mensing, J. Lehnert, S. Mändl, M. Zink, S.G. Mayr: *Carbon implantation of TiO_2 nanotubes for biomedical applications*. 9^{th} Annual Symposium - Physics of Cancer, Leipzig, Germany, September 2018

C. Ficorella, R. Martinéz Vazquéz, P. Heine, R. Osellame, J. A. Käs: *Cancer cell motility study in micro-constriction chips*. 9^{th} Annual Symposium - Physics of Cancer, Leipzig, Germany, September 2018

H. Kubitschke, B. Wolf, E. Morawetz, L.-C. Horn, B. Aktas, U. Behn, M. Höckel, J. A. Käs: *Roadmap to Local Tumor Growth*. 9^{th} Annual Symposium - Physics of Cancer, Leipzig, Germany, September 2018

E. W. Morawetz, L.-C. Horn, S. Briest, B. Aktas, J. A. Käs: *Exploring Tumor Heterogeneity - Cancer Development and Invasive Traits in Primary Carcinoma Samples*. 9^{th} Annual Symposium - Physics of Cancer, Leipzig, Germany, September 2018

T. Händler, C. Tutmarc, T. Golde, M. Glaser, J. A. Käs, D. M. Smith, J. Schnauß: *Reptation in semiflexible polymer networks*. 9^{th} Annual Symposium - Physics of Cancer, Leipzig, Germany, September 2018

M. Glaser, J. Lorenz, T. Golde, J. A. Käs, J. Schnauß, D. m. Smith: *Systematic Altering of Semiflexible Biopolymer Networks via Tunable Cross-linking*. 9^{th} Annual Symposium - Physics of Cancer, Leipzig, Germany, September 2018

P. Mollenkopf, J. Lorenz, M. Glaser, J. A. Käs, J. Schnauß, D. Smith: *Friction in isotropic polymer networks*. 9^{th} Annual Symposium - Physics of Cancer, Leipzig, Germany, September 2018

E. Warmt, S. Grosser, E. Morawetz, J. A. Käs: *Cortical Actin Contractility of Single Suspended Cells*. 9^{th} Annual Symposium - Physics of Cancer, Leipzig, Germany, September 2018

4.12 Graduations

Doctorate

- Carsten Schuldt
  Semiflexible Polymer Networks and Persistence Length
  17.09.2018

Master

- Hannah-Marie Scholz-Marggraf
  Role of N-Cadherin during the Epithelial-Mesenchymal Transition
  April 2018
- Xiaofan Xie
  Viscoelastic Characterization of Multicellular Spheroids
  September 2018

Bachelor

- Thomas Lettau
  Single-cell Biomechanics for Spheroid Culture and Petri Dish Culture
  February 2018
- Rewati Limaye
  Shape of cancer cells and its use in diagnostics
  July 2018

5

Biological Physics

5.1 Introduction

The migration and invasion of cells, such as cancer cells and fibroblasts depends on their molecular, such as expression of matrix-degrading enzymes and mechanical properties, such as deformability, cytoskeletal remodeling dynamics or exertion of forces. Besides genetic, morphological and biochemical changes, the extracellular matrix stroma surrounding primary tumors seems to be a key characteristic parameter of the malignant progression of cancer, which contains migratory steps of cancer cells in order to form metastases at targeted tissues. The knowledge on the biophysical driven experimental approaches in the field of cancer research is still limited. However, there is agreement that mechanical alterations are critical regulators of the malignant progression of cancer. Thereby the mechanical sensing of the tumor surrounding stroma and the exertion of forces towards the stroma are important for determining the malignant potential of a primary tumor and subsequently of cancer cells. The impact of the tumor stroma on cancer cell motility and hence on the metastatic cascade is controversially discussed. More precisely, there are two opposite effects of the local stroma on the migration and invasion of cancer cells.

On the one hand the extracellular matrix stroma acts as tumor stroma and promotes all hallmarks of cancer that help cancer cells to overcome restrictive biological capabilities such as increased proliferation, enhanced survival and elevated migratory potential, altered metabolism and escape from programmed cell death through mechano-sensing and mechano-transduction processes, which is facilitated by increased rigidity of the stroma, possibly through the alignment of extracellular matrix fibers.

On the other hand the stroma function as a mechanical barrier for cancer cell motility in 3D extracellular matrix confinement due to structural constraints, when the pore-size is much smaller than the cell's nuclear diameter.

In detail, the mechanical properties of the tumor stroma such as the tissue matrix stiffness and its entire architectural network are the major driving factors that support or hinder the specific and optimal microenvironment for cancer cell penetration and invasion. Thus, biophysical techniques, such as magnetic tweezer, magnetic resonance elastography, cell-induced fiber displacement of the extracellular matrix, optical stretcher and nanoscale particle tracking, can be employed to determine the mechanical properties of the stroma or cells. In future approaches, these biophysical techniques need to be further developed and adapted to analyze the mechanical properties of cells

during their migration and invasion through 3D microenvironments of various matrix mechanical properties.

Prof. Dr. Claudia Tanja Mierke, Dipl. Phys. Tony Fischer

5.2 Establishment of a magnetic tweezer setup for the measurement of cellular mechanics

C. Aermes, C.T. Mierke

In order to probe the viscoelastic properties of cells, we developed a magnetic tweezer following the description of the setup presented in [1]. The magnetic tweezer is shown in figure 5.1a. It is built on top of an inverted microscope (DMI8, Leica) and enclosed by an incubation chamber. The chamber can be filled with 5% CO_2 enriched air and is equipped with a heating unit for precise temperature control of the sample. The employment of such an incubation chamber is a novel improvement over already existing magnetic tweezer setups described elsewhere [1–5]. Images are recorded with a CMOS camera (Orca Flash 4.0 V3, Hamamatsu) at a frame rate of about 40 Hz.

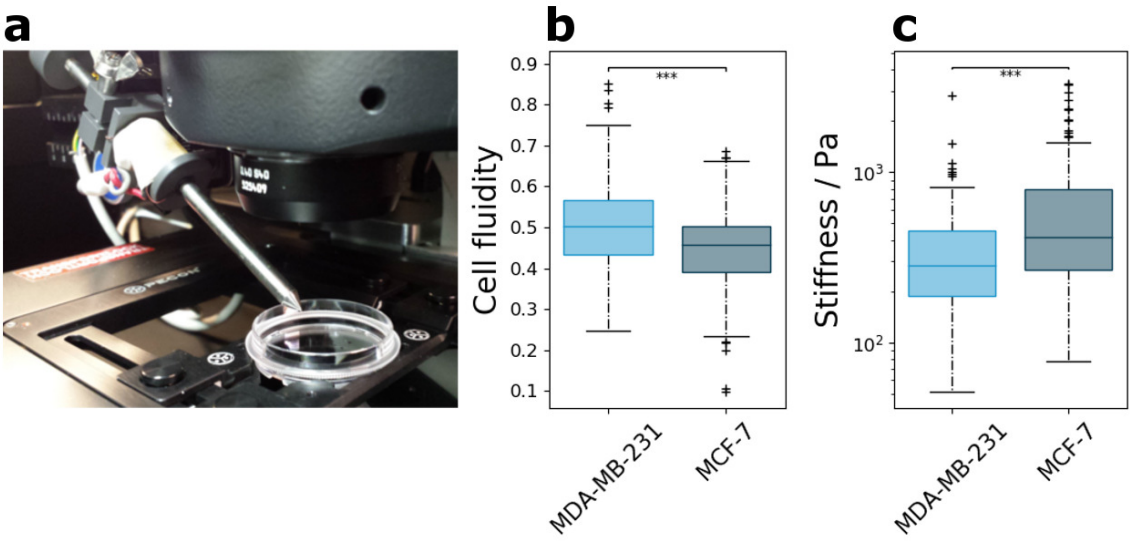

Figure 5.1: The magnetic tweezer (a) can be used to probe cell fluidity (b) and stiffness (c) of MDA-MB-231 cells (n = 159) and MCF-7 cells (n = 108). Cells were probed with a single force pulse of 1 nN magnitude and 2 s duration.

Fibronectin coated superparamagnetic beads are bound to the surface of the cells in order to probe cellular mechanics with the magnetic tweezer. Due to the coating, the beads specifically couple to integrins that in turn couple the beads to the cytoskeleton. Forces up to 10 nN can be applied to superparamagnetic beads with a diameter of 4.5 µm.

The magnetic tweezer is controlled by a custom-written LabVIEW program. The program detects and tracks beads automatically with subpixel accuracy. The beads are displaced by subjecting them to a magnetic field. Due to a dedicated feedback loop, the

force acting on the cells can be controlled with high accuracy. Using this feedback loop, it is possible to generate any time dependent force signal.

Cells can be probed with a single force pulse, a sequence of consecutive pulses, or a staircase-like sequence of pulses. Viscoelastic properties of the cell (stiffness and fluidity) are derived from creep curves in response to the applied force. Measurements with the magnetic tweezer reveal significant differences ($p < 0.05$) in the stiffness and viscoelastic state of highly invasive MDA-MB-231 cells ($n = 159$) and non-invasive MCF-7 cells ($n = 108$). In figure 5.1b and figure 5.1c, the stiffness and fluidity, respectively, of MDA-MB-231 cells and MCF-7 cells are presented. Cells were probed with a single force pulse. A constant force of one nanonewton was applied over two seconds.

In conclusion, the magnetic tweezer is a versatile tool to probe cellular mechanics. Due to the precise force control, cells can be probed with a variety of different force protocols. Significant differences in the viscoelastic parameters of different cell lines can be detected by measuring the creep response of cells with the magnetic tweezer.

[1] P. Kollmannsberger et al.: Rev. Sci. Instrum. **78**, 114301 (2007) doi:10.1063/1.2804771
[2] A.R. Bausch et al: Biophys. J. **75**, 2038 (1998) doi:10.1016/S0006-3495(98)77646-5
[3] B.G. Hosu et al.: Rev. Sci. Instrum. **74**, 4158 (2003) doi:10.1063/1.1599066
[4] T. Grevesse et al.: Sci. Rep. **5**, 9475 (2015) doi:10.1038/srep09475
[5] K.C. Johnson et al.: J. Biol. Eng. **11**, 47 (2017) doi:10.1186/s13036-017-0091-2

5.3 Establishment of Nanoscale Particle Tracking to determine Viscosity inside Cells

T. Fischer, A. Hayn, C.T. Mierke

The inside of a single cell is made up of various different proteins and polymer structures. All these different compartments and cell regions show a wide range of different mechanical properties, such as elasticity. Along with this, these cell regions possess differences in diffusivity. However, measuring elastic properties of specific cell compartments is rather difficult. Brownian motion of spherical particles can been used to determine viscoelastic properties such as viscosity [1, 2].

As our group is interested in these specific viscoelastic properties, we have done initial experminents on this subject. We used the well known MDA-MB-231 cell line for these initial experminents. Fluorescent beads are phagocytosed by these single cells. Subsequently, we record 3-dimensional image stacks of both the fluorescent beads and the cell using phase-contrast-microscopy at a frame-rate of up to 60 frames per second. An examplary racording is shown in figure 5.2a. This high frame rate allows for 3D brownian motion analysis using TrackPy [3]. A 2D projection of particles is shown in figure 5.2b. Blue denotes particles inside the cell, orange are particles classified as beeing bound to the cell membrane. Subsequently, we calculate the Ensemble Mean Squared Displacement of for example the cytoskeletal particles, as seen in figure 5.2c.

By further refining the particle classification to numerous different cell compartments, we are able to define viscosities more precisely. As seen in figure 5.3, different cell compartments show partly large differences in viscosity.

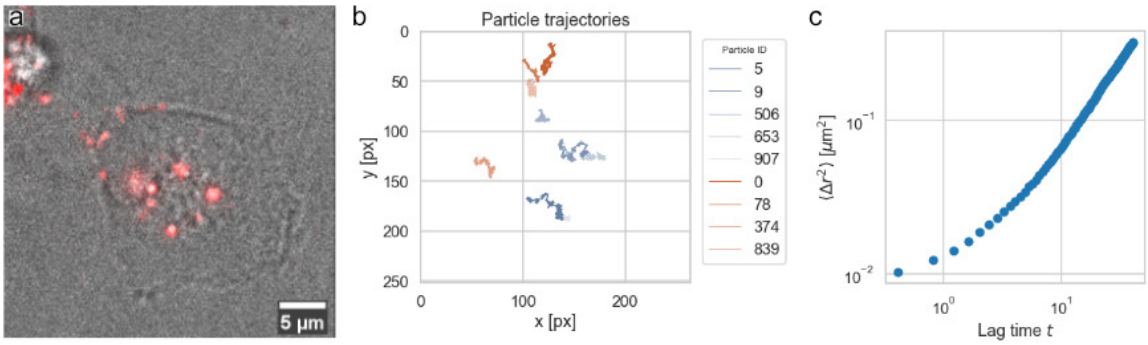

Figure 5.2: Nanoscale Particle Tracking (a) Sample image of recorded cell in grey (b) only a few detected particle trajectories are left after filtering (c) Ensemble Mean-Squared-Displacement plot

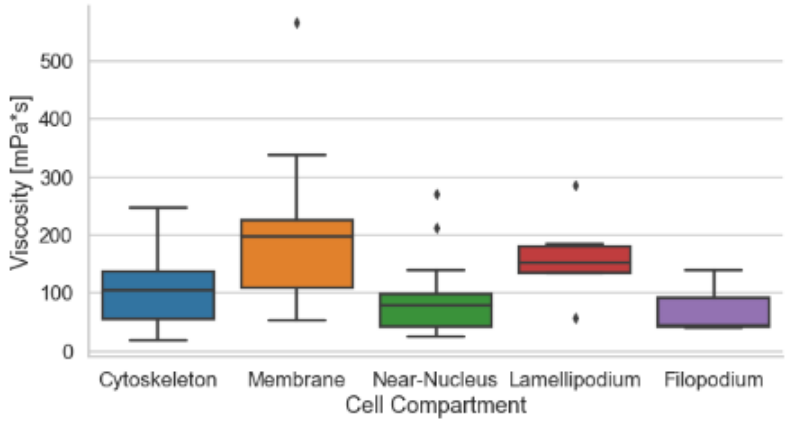

Figure 5.3: Prelaminary data shows different viscosities for particles in different cell compartments

[1] B. U. Felderhof: Physica A **147**, 533 (1988) doi:10.1016/0378-4371(88)90168-9
[2] A. N. Morozov et al.: Phys. Lett. A **46**, 375 (2011) doi:10.1016/j.physleta.2011.10.001
[3] D. B. Allan et al.: Zenodo, (2018) doi:10.5281/zenodo.1226458

5.4 Effects of Collagen-I Composition on structural and elastic properties of 3D Biomimetic ECM Models and their Influence on Cell Migration

A. Hayn, T. Fischer, C.T. Mierke

In focus of 2018 research we developed and adapted different assays to characterize tumor cell mechanics and properties. Therefor we concentrated on studies of malign and benign breast cancer cells (preferential MDA-MB-231, MCF-7 and ZR75-1 cells) that invade crafted collagen type I matrices which serve as tissue model systems. The used collagen type I is extracted from rat tail and bovine skin. We engineered collagen type I compositions that were made from solely rat tail collagen [R-collagen], solely bovine skin collagen [G-collagen] and a mixture of both collagen sources [M-collagen].

Among all compositions we crafted gels differing in collagen monomer concentration from 1.5 g/l to 3.0 g/l. Our studies showed significant differences in the invasion behavior of the used cell lines between the three used collagen compositions. At M-collagens and R-collagens the measured invasiveness and invasion depth confirm the highly aggressive character of MDA-MB-231 cancer cells and is promoted at higher collagen concentrations (2.5 g/l and 3.0 g/l). The invasiveness of MCF-7 cells is promoted at the lower concentrated M- and R-collagens, in contrary the invasion depth is promoted at higher concentrated M- and R-collagen gels. The invasiveness and invasion depth of ZR75-1 cells is inhibited in M- and R-collagens. Invasion into G-collagens surprisingly provide a generally promotion of the invasive character of all three cell lines mainly promoted at the higher collagen concentrations. Especially the - in other respects - slightly aggressive MCF-7 cells exceed the aggressiveness of high aggressive MDA-MB-231 cells and the invasion depth of MCF-7 cells is approximatively doubled compared to studies with M- and R-collagens.

To further investigate the origin of that immanent differences depending on the collagen composition used, we analyzed and characterized the collagen matrices determining pore size with confocal laser scanning microscopy [CLSM] and the mechanical properties of the gels concerning the Young's modulus, measured with scanning force microscopy [SFM]. The differences in the collagen structures (see figure 5.4), especially the intrinsic inhomogeneity of the different compositions and the correlation of collagen properties can explain the differences in the invasion behavior.

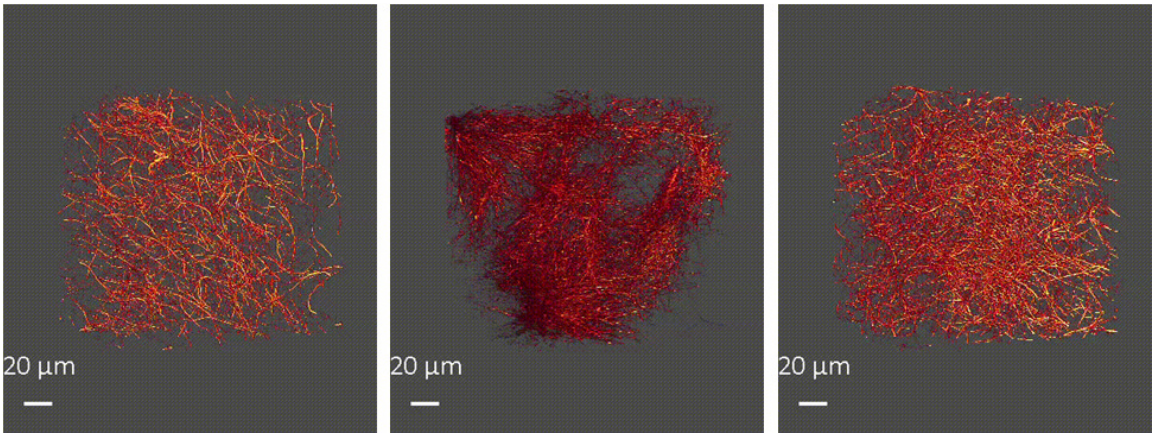

Figure 5.4: Type I collagens with different structure. Left image: collagen solely made from rat tail collagen [R-collagen] with thin, large fibrils and large spaces in between (pores). Middle image: collagen solely made from bovine skin collagen [G-collagen] with short fibrils forming very dense structures as well as some very lose compartments that form huge pores. In between the dense structures a multitude of very small pores can be seen. Right image: collagen mix containing R- and G-collagen forms relatively homogeneous structures compared to collagens solely made from R- or G-collagen. The concentration of all three examples is 2.0 g/l.

In cooperation with the Molecular biological-biochemical Processing Technology division (Prof. Robitzki, Dr. Jahnke) at the Biotechnological-Biomedical Center (BBZ), funded by the SMWK we worked to establish a migration system with the tumor cell system mentioned above and a combined assay to functionally correlate cellular mechanics with cell motility using electric cell-substrate impedance sensing [ECIS]. Therefor we are investigating tumor cells that invade collagen matrices applied on

especially manufactured chips. Each chip carries 9 culture inserts in the 96 well geometry and contains small planar electrodes made either from gold or indium tin oxide [ITO] deposited on the bottom. Due to the insulating properties of cells (especially their membranes) they behave like dielectric particles and the impedance can be measured over a frequency spectrum.

5.5 Funding

Blebbing Driven or Actin Protrusive-Force Driven Cancer Cell Migration
C.T. Mierke, J.A. Käs
DFG-MI1211/18-1

Scientific Device: Confocal Scanning Microscope with Magnetic Tweezer Device and Life Cell Imaging
C.T. Mierke
DFG-INST 268/357-1

Optical Cell Stretcher und Dual Magnetic Tweezer Cell Cluster Device: Korrelative mechanische und molekulare Zell-Zell-Wechselwirkung in Geweben und Gewebemodellen für neue Ansätze in Diagnostik und Therapie
C.T. Mierke, J.A. Käs
ESF/SAB No. 100299919

Synthese- und Analytik-Unit für die Entwicklung von Analoga für das Tumortargeting
C.T. Mierke
SMWK/SAB No. 100146227

MUDIplex
C.T. Mierke
SMWK TG70 No. 22110853

5.6 Organizational Duties

C.T. Mierke

- Referee: Cancer Research, Journal of Cell Science, Advanced Biomaterials, Acta Biomaterials, British Journal of Cancer, Journal of Pharmacy and Pharmacology, Molecular Vision, International Journal of Nanomedicine, Plos One, Eur. J. Biophysics
- Editor: Scientific Reports, Physical Biology, Frontiers Cell and Developmental Biology

5.7 External Cooperations

Academic

- University of Leipzig, Center for Biotechnology and Biomedicine (BBZ), Germany
  Prof. Dr. Andrea A. Robitzki

- Department of Paediatric Kidney, Liver and Metabolic Diseases, Hannover Medical School, Germany
  Dr. Wolfgang H. Ziegler
- GBF, National Research Center for Biotechnolog, Dept of Cell Biology, Germany
  Prof. Dr. Klemens Rottner

5.8 Publications

Journals

C.T. Mierke, F. Sauer, S. Grosser, S. Puder, T. Fischer, J.A. Käs: *The two faces of enhanced stroma: Stroma acts as a tumor promoter and a steric obstacle*, NMR Biomed. **10**, e3831 (2018) doi:10.1002/nbm.3831

Books

C.T. Mierke: Physics of Cancer, Volume 1 - Interplay between tumor biology, inflammation and cell mechanics, 2nd Ed. (IOP Publishing, Leipzig 2018)

C.T. Mierke: Physics of Cancer, Volume 2 - Cellular and microenvironmental effects, 2nd Ed. (IOP Publishing, Leipzig 2018)

Talks

T. Fischer, A. Hayn, C.T. Mierke: *Microenvironment influences migration of cancer cells in 3D*, Soft Matter Day, Leipzig, Germany, July 2018

A. Hayn, T. Fischer, C.T. Mierke: *Inhomogeneities in 3-Dcollagen matrices impact matrix mechanical properties*, Soft Matter Day, Leipzig, Germany July 2018

A. Hayn, T. Fischer, C.T. Mierke: *Biophysikalische Methoden zur Charakterisierung physikalischer Eigenschaften von Zellen*, BBZ Doktoranden-Kolloqium, Leipzig, Germany November 2018

T. Fischer, C.T. Mierke: *Influence of matrix and cellular properties on human cancer cell migration in 3D biomimetic matrices*, DPG-Frühjahrstagung, Berlin, Germany March 2018

S. Puder, T. Kunschmann, C.T. Mierke: *Effect of Arp2/3 on 3D migration and cellular mechanical properties*, DPG-Frühjahrstagung, Berlin, Germany March 2018

Posters

T. Kunschmann, S. Puder, C.T. Mierke: *The influence of Rac1 on motility into 3D extracellular matrices and mechanical properties*, DPG-Frühjahrstagung, Berlin, Germany March 2018

T. Fischer, A. Hayn, C.T. Mierke: *3D pore size of collagen matrices as a robust measure of scaffoldtopology*, Soft Matter Day, Leipzig, Germany July 2018

6

Molecular Biophysics

6.1 Introduction

The research of the Molecular Biophysics group aims at dissecting the mechanisms and physical principles of biological nanomachines that are involved in the processing of nucleic acids. To this end the groups uses single-molecule methods in particular force spectroscopy as well as advanced fluorescence spectroscopy. This allows to observe structural states as well as the real-time dynamics of just a single nanomachine at a time. Considerable efforts are dedicated to the further development of the single-molecule technologies. Additionally, the group aims at building artificial nanomachines and nanostructures by using DNA as a programmable material. Particularly, three-dimensional DNA nanostructures are employed as molecular templates in order to fabricate electronic devices from inorganic materials by self-assembly. The following specific topics have been pursued in 2018:

- Combined force spectroscopy and single-molecule fluorescence approaches
- Target recognition by CRISPR-Cas enzymes
- Mechanisms of molecular motors that are involved in cellular DNA break repair
- DNA templated synthesis of complex metallic nanostructures and their electric characterization
- Hierarchical drug delivery systems based on DNA nanostructures
- Mechanics of small molecule binding to DNA

The group was part of the Collaborative Research Center (CRC) TRR 102 "Polymers under Multiple Contraints" as well as the Biomolecular Assembled Circuits (BAC) path of the cluster of excellence "Center for Advancing Electronics Dresden" (cfaed, TU Dresden). Main funding of the group is provided by an ERC consolidator grant.

Ralf Seidel

6.2 Cooperation of molecular motors during dsDNA repair

K. Kasaciunaite*, F. Fettes*, M. Levikova†, P. Cejka‡, R. Seidel*

*Peter Debye Institute for Soft Matter Physics, University of Leipzig, Germany
†Institute of Molecular Cancer Research, University of Zurich, Switzerland
‡Institute for Research in Biomedicine (IRB), Università della Svizzera Italiana, Switzerland

Double strand DNA (dsDNA) break repair by homologous recombination in eukaryotes is a complex process that is not well understood at the molecular level. A main step of this process is the 5´-strand resection at the DNA break. In yeast, one resection mechanism involves the cooperation of two molecular motors: the RecQ helicase Sgs1 and the nuclease-helicase Dna2. These proteins unwind DNA in opposite directions while the produced single stranded DNA (ssDNA) is protected by the ssDNA binding protein RPA. To gain insight into the potentially synergistic cooperation by these motors we utilized magnetic tweezers. This technique allows stretching single DNA molecules and, this way, monitoring the conversion of dsDNA to ssDNA by a change of the DNA length in real-time. We first characterized nuclease-dead Dna2 and Sgs1 individually. Dna2 showed processive unidirectional unwinding of long fragments being strictly dependent on the presence of RPA. In contrast, Sgs1 alone displayed gradual DNA unwinding being terminated by frequent spontaneous DNA rezipping events. In the presence of RPA, the unwinding velocity of Sgs1 was markedly shifted towards lower velocities and the helicase could also close the DNA by gradual rewinding rather than rezipping. When reconstituting the full DNA resection process in vitro using wt Dna2, Sgs1 and RPA, an overall long-range and slow unidirectional DNA unwinding (Dna2-like) was observed. On top of this process, shorter repetitive opening and closing events (Sgs1-like) appeared. Furthermore, the presence of Dna2 reverted the RPA-induced velocity reduction of Sgs1. These data suggest the formation of a Sgs1-Dna2 complex

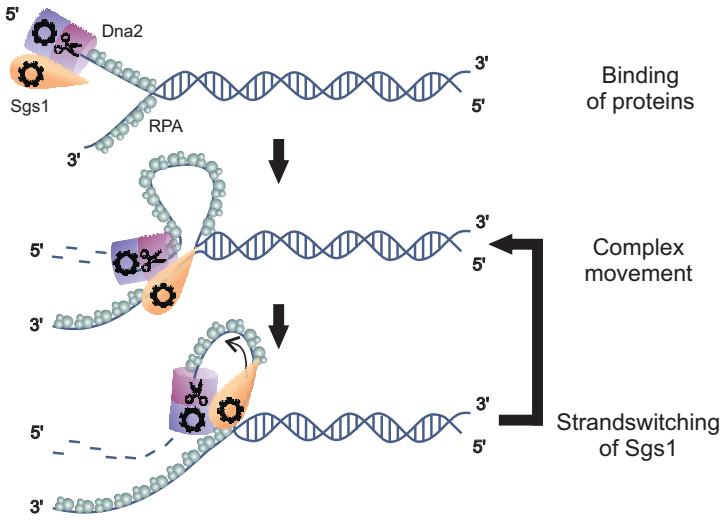

Figure 6.1: Model for DNA end resection by the two molecular motor proteins Sgs1 and Dna2 which use opposite polarities to move along DNA.

in which Sgs1 unwinds the dsDNA and feeds the resulting ssDNA for degradation into Dna2 (Fig. 6.1). While formation of such a resection complex is similar to the well-known prokaryotic counterpart RecBCD, the coupling between the eukaryotic enzymes appears to be considerably weaker.

[1] K. Kasaciunaite, F. Fettes, M. Levikova, P. Daldrop, R. Anand, P. Cejka, R. Seidel: EMBO J.**e101516**, (2019)

6.3 Decision making in CRISPR-Cas complexes

M. Rutkauskas*, I. Songailiene†, T. Sinkunas†, S. Wittig‡, C. Schmidt‡, V. Siksnys†, R. Seidel*

*Peter Debye Institute for Soft Matter Physics, University of Leipzig, Germany
†Institute of Biotechnology, Vilnius University, Lithuania
‡HALOmem, Martin-Luther-University Halle-Wittenberg, Germany

CRISPR-Cas adaptive immunity of Type I and Type II systems relies on surveillance complexes that recognize invader DNA and dedicate it for degradation. The surveillance complexes harbour a crRNA that promotes target recognition by base pairing with a complementary target strand. The formed crRNA:DNA heteroduplex is called R-loop (Fig. 6.2). In the Cascade surveillance complexes of Type IE CRISPR-Cas systems R-loop formation over the whole recognition sequence causes "locking" - a structural rearrangement of the complex. This allows the recruitment of the Cas3 helicase-nuclease that finally degrades the target DNA. It was previously shown that modular nature of the multisubunit complex Cascade allows to incorporate crRNAs of altered length, such that the recognition sequence is potentially extended or shortened. This raises significant interest in the field of genome engineering and gene editing because complexes that can recognize longer sequences may be used as more accurate molecular instruments in genetics and medicine.

In this study we investigated the target recognition process of Cascade complexes from *St. thermophilus* with shortened and extended crRNAs. To this end we employed single molecule DNA supercoiling to directly observe R-loop formation. For all Cascade variants the length of the formed R-loop corresponded to the spacer length of the crRNA, i.e. the longest obtained R-loop had 57 base pairs (bp). The R-loop length was however not correlated to R-loop stability. Complexes with shortened crRNAs did not get locked at all and thus did not support DNA degradation by Cas3. The locked state of complexes with crRNAs extended by 12 nucleotides (nt) and 24 nt was as stable as the wild type (wt) complex and DNA degradation occurred at unaltered rate. Complexes with increased crRNA length of 6 nt and 18 nt exhibited a drastically increased R-loop stability, albeit the target degradation by Cas3 was almost abolished. For the wt Cascade complex locking occured when the R-loop extends at least over 28 bp of the 32 bp. For the complexes with extended crRNAs, we therefore tested whether "locking" and DNA degradation occurred at the wt R-loop length or whether it required a significantly longer R-loop. All Cascades with extended crRNAs formed "unlocked" R-loops on targets containing 26 bp match but formed "locked" R-loops

on 32 bp or longer targets. Thus, the decision to "lock" the R-loop and to degrade target DNA is made at the fixed position from the PAM independently on the length of the crRNA. Therefore, complexes with extended crRNAs will not exhibit an increased target specificity. These findings have impact for the genome engineering community because applying Cascade complexes with extended crRNAs may lead to increased off-targeting (Fig. 6.2).

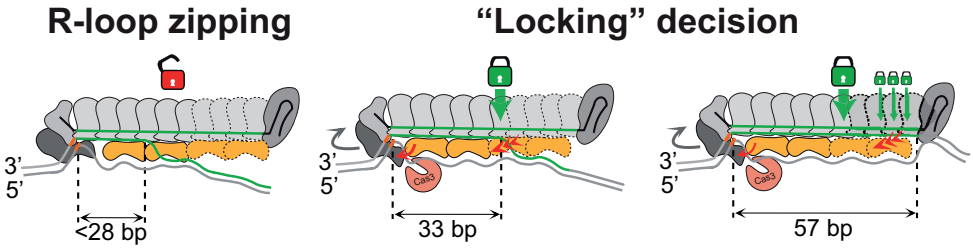

Figure 6.2: Model of the decision making process by Cascade complexes with elongated spacers. The Cascade complexes form R-loops in a zipper-like fashion starting from the PAM. The R-loops are unlocked, i.e. reversible if they are shorter than 28 bp (left). R-loops that exceed 28 bp in length become locked independent of the spacer length (middle). For complexes with elongated spacers, R-loops can extend over the full spacer length. Protein contacts to the R-loop at the PAM distal end provide an additional R-loop stabilization (right).

6.4 Anticooperative Binding Governs the Mechanics of Ethidium-Complexed DNA

J. Dikic*, R. Seidel*

*Peter Debye Institute for Soft Matter Physics, University of Leipzig, Germany

In this project we used single-molecule mechanical experiments to investigate structural aspects of small molecule (ethidium bromide, EtBr) binding to DNA [1]. The ethidium moiety can intercalate (bind) in between two stacked base pairs (Fig. 6.3a), thereby increasing the base-pair distance by about 0.34 nm and untwisting the DNA by about 28° per intercalated molecule. The intercalation has so far been thought to obey a neighbor-exclusion model, in which only every other intercalation side can by occupied by the intercalator. In our experiments we carefully studied how the apparent mechanical properties, in particular the stretch rigidity and the twist rigidity, of DNA change when complexed with ethidium.

By recording force-extension curves using magnetic tweezers on single DNA molecules in presence of EtBr (Fig. 6.3b) we observed a decreased apparent DNA stretch rigidity (Fig. 6.3c). Previous reports attributed this to an altered mechanical rigidity of the complexed DNA itself, which was however not in agreement with our data (light blue line in Fig. 6.3c). Alternatively, we considered additional force-induced intercalation during which the equilibrium constant for the ethidium intercalation becomes increased with force. Thus ethidium intercalation becomes facilitated at elevated force, which causes an additional force dependent DNA lengthening and thus an apparent stretch softening of the DNA.

Careful modelling based on a neighbor exclusion model (non-cooperative model) could well describe the stretch softening of the DNA at low but not at high intercalator concentrations (blue dashed line in Fig. 6.3c). Persistent stretch softening at high intercalator concentrations indicated further force-dependent intercalation. This could be modelled (see red line in Fig. 6.3c) by assuming intercalation into nearest neighbor sites in an anti-cooperative manner using a McGhee-von Hippel binding isotherm for ligand binding to lattices. Thus intercalation next to a site that is already covered by an intercalator is not strictly forbidden but unfavorable and restricted to much higher concentrations. Therefore, force-induced intercalation persisted throughout the testable EtBr concentration range and was dominating the apparent stretch rigidity of intercalator-complexed DNA. This effectively masked underlying changes of the mechanical properties of the intercalator-complexed DNA itself.

In addition to the DNA stretch mechanics, we investigated also the DNA twist mechanics. The apparent twist rigidity was found to be considerably reduced in presence of the intercalator. This behavior was similar to stretching and could also be explained by the anti-cooperative intercalation mode of the ethidium moiety.

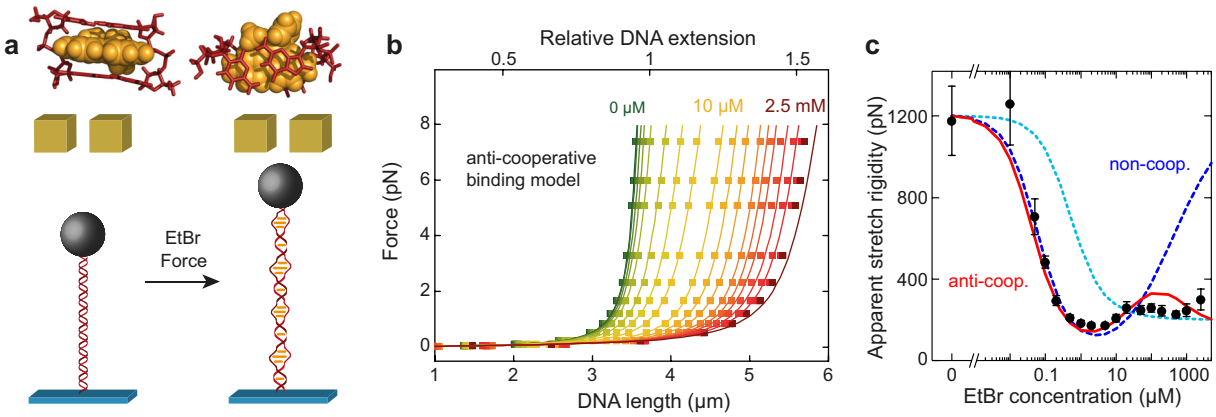

Figure 6.3: Stretch-mechanics of DNA in presence of an intercalating molecule. (a) In presence of EtBr, the ethidium moiety (shown in yellow in the crystallographic structure) can intercalate in between two stacked DNA base pairs (shown in brown). This leads to an elongation of the DNA contour length. External force as applied with magnetic tweezers can induce additional intercalation by ethidium. (b) Force-extension curves of dsDNA in presence of increasing intercalator concentrations (filled squares). Visible is a DNA length increase as well as an apparent stretch softening at the high forces with increasing EtBr concentration. Solid lines are predictions from force-dependent anti-cooperative ethidium intercalation into DNA. (c) Apparent stretch rigidity extracted from the force extension curves (filled circles) compared to predictions from anti-cooperative (red line) and non-cooperative ethidium intercalation (blue dashed line).The light blue dashed line shows a prediction assuming a reduced stretch rigidity of the ethidium complexed DNA itself.

[1] J. Dikic, R. Seidel: Biophys J.**116**, 1394 (2019)

6.5 DNA mold templated assembly of conductive gold nanowires

T. Bayrak[*], S. Helmi[†], J. Ye[†], D. Kauert[†], J. Kelling[‡], T. Schönherr[*], R. Weichelt[§], A. Erbe[*], R. Seidel[†]

[*]Institute of Ion Beam Physics and Materials Research, Helmholtz-Zentrum Dresden-Rossendorf, Germany

[†]Peter Debye Institute for Soft Matter Physics, University of Leipzig, Germany

[‡]Department of Information Services and Computing, Helmholtz-Zentrum Dresden-Rossendorf, Germany

[§]Physical Chemistry, TU Dresden, Germany

On the nanoscale, fundamental properties and potential applications are greatly influenced by the size and shape of the material. There is a tremendous boost in the field of DNA nanotechnology in fabricating complex and atomically-precise nanostructures in a fully programmable manner. "DNA Origami" takes advantage of base complementarity of individual short oligonucleotides, to fold a long "scaffold strand" into almost any continuous 2D or 3D shape. This idea has inspired the usage of DNA nanostructures as templates for guiding and structuring the deposition of metals. We previously introduced a new concept of a DNA mold-based particle synthesis that allows the fabrication of inorganic nanoparticles with programmable shape. We demonstrated the concept by fabricating a 40 nm long rod-like gold nanostructure with a quadratic cross-section [1]. We expanded the capabilities of the mold-based particle synthesis to demonstrate the synthesis of uniform conductive gold nanowires with 20-30 nm diameters [2]. By programming the specific interaction between DNA mold monomers we can produce large linear mold superstructures that are subsequently filled with metal (see Fig. 6.4). Using electron beam lithography individual nanowires could be contacted for electric measurements. Conductance measurements over a temperature range from room to low temperatures showed that a sizeable fraction of these wires is indeed metallically conductive (Fig. 6.4).

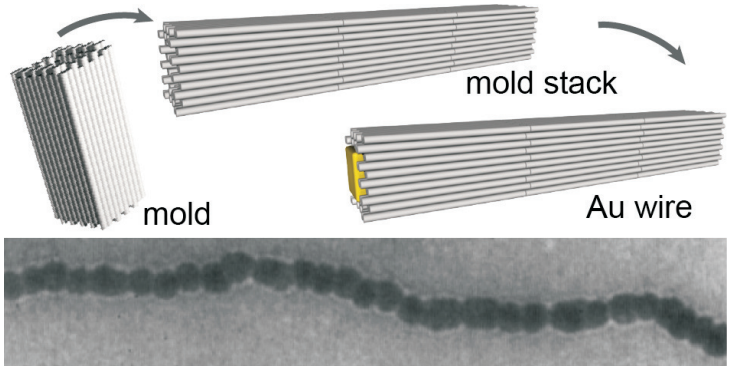

Figure 6.4: (top) Scheme and TEM image of the metallic wire formation. Two seed-preloaded mold monomers with specfic interface designs are mixed together to allow the formation of long linear mold tubes. After the seeded growth within this structure, the empty cavity of the mold chain is filled with gold nanoparticles of 25 nm diameter. (bottom) TEM image demostrated the correct formation of the gold wire and the homogenous growth of the gold nanoparticles.

[1] S. Helmi, C. Ziegler, D.J. Kauert, R. Seidel: Nano Lett. **14**, 6693 (2014)
[2] T. Bayrak, S. Helmi, J. Ye, D. Kauert, J. Kelling, T. Schönherr, R. Weichelt, A. Erbe, R. Seidel: Nano Lett. **18(3)**, 2116-2123 (2018)

6.6 DNA Origami and Layer-by-Layer Microcarrier Hybrid System for Drug Delivery

F. Scheffler[*†], M. Brueckner[†], J. Ye[*‡], R. Seidel[*‡], U. Reibetanz[†]

[*]Peter Debye Institute for Soft Matter Physics, University of Leipzig, Germany
[†]Institute for Medical Physics and Biophysics, Medical Faculty Leipzig, Germany
[‡]Center for Advancing Electronics Dresden, TU Dresden, Germany

DNA origami nanostructures have been under intensive investigation the last decade. Their structural versatility and ease of functionalization make them a promising tool for enhanced drug delivery. Unfortunately, their structural stability under physiological conditions is nowadays not fully understood and controversially discussed. For an enhanced protection of the DNA origami on the endocytotic pathway we integrated them into a super-ordinated carrier system of Layer-by-Layer (LbL) microparticles. The initial characterization of the systems composition was done by flow cytometry and zeta potential measurements. After finding suitable conditions for the integration of DNA origami molds into the polymeric multilayer of LbL microcarriers, we focused on the structural stability under different pH and enzymatic conditions. Overall, an enhanced stability of the integrated DNA origami under a broad spectrum of pH values, against isolated enzymes and even under in vitro conditions on the endocytotic pathway was derived. Further, we showed the enhanced uptake of DNA origami on LbL microcarriers compared to free origami and integrated a model agent (bovine serum albumin) into the cavity of the used structures to deliver it into mammalian cells.

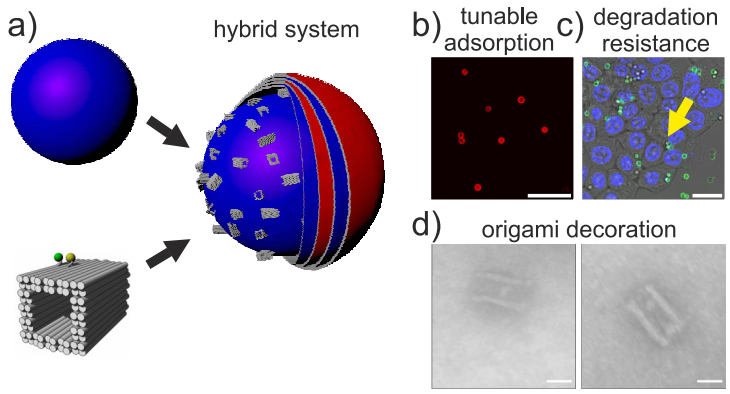

Figure 6.5: a) Scheme of the design of the hybrid carrier. DNA Origami was integrated in the polymeric shell of the LbL microcarriers and covered by 4 additional layers of biopolymers. b) The number of DNA origami per microcarrier can be finely tuned. c) The additional layers of biopolymers protect the DNA origami from degradation in live cell application. d) Either one or two bovine serum albumins can be implemented into the cavity by specific binding sites.

The high potential of this system was shown by further functionalizing the microcarrier surface with a supported lipid bilayer for the subsequent integration of antibodies for a delivery into specific tissue.

6.7 Funding

Quantitative understanding of target recognition on DNA based on directional zipping processes
Prof. Ralf Seidel
ERC Consolidator Grant 2016
Grant Agreement number: 724863-ZIPgeting-ERC-2016-COG (2017- 2022)

A DNA origami-brick system for the fabrication of nanoelectronic elements
Prof. Ralf Seidel
DFG - SE 1646/8-1 (2017-2020)

Structure-function analysis of a molecular switch for long-range diffusion on DNA
Prof. Ralf Seidel
Icahn School of Medicine at Mount Sinai, New York, GZ: 5 R01 GM111507-02 (2015-2018)

Research funding within the Exzellenzcluster "Center for Advancing Electronics Dresden", Path D: Biomolecular-Assembled Circuits
Prof. Ralf Seidel
DFG - EXC 1056 (2015-2018)

Probing structural transitions of single-polymer chains with mechanical stress
Prof. Ralf Seidel
DFG - SFB TRR 102-2, TP B13 (2015-2019)

6.8 Organizational Duties

Ralf Seidel

- Principal Investigator in the "Leipzig School of Natural Sciences - Building with Molecules and Nano-Objects"
- Principal Investigator in the SFB-Transregio 102 "Polymers under multiple constraints: restricted and controlled molecular order and mobility"
- Board member of the Division of Physics in Life Sciences of the European Physical Society
- Co-Leader of the BAC path within the Exzellenzcluster "Center for Advancing Electronics Dresden"
- Manuscript reviewing for Nature, Cell, Nat. Mol. Struct. Biol., Nat. Commun., Nano Lett., Nucleic Acids Res., Nanoscale

Brighton Samatanga

- Manuscript reviewing for Nucleic Acids Research

Saurabh Raj
- Manuscript reviewing for Micromachines, Sensors

6.9 External Cooperations

Academic

- Vilnius University, Lithuania
  Prof. Virginijus Siksnys
- University of Bristol, UK
  Prof. Mark Szczelkun
- Icahn School of Medicine at Mount Sinai, USA
  Prof. Aneel Agarwal
- Zurich University, Swizerland
  Prof. Petr Cejka
- Skolkovo Institute of Technology, Russia
  Prof. Konstantin Severinov
- Martin-Luther-Universität Halle-Wittenberg, Germany
  Prof. Jörg Kreßler
- Helmholtz-Zentrum Dresden-Rossendorf, Germany
  PD Dr. habil. Artur Erbe
- Technische Universität Dresden, Germany
  Prof. Alexander Eychmüller
- Imperial College London, UK
  Dr. Tom Ouldridge
- Institut für Medizinische Physik und Biophysik, Germany
  PD Dr. Uta Reibetanz

6.10 Publications

Journals

A. Krivoy, M. Rutkauskas, K. Kuznedelov, O. Musharove, C. Rouillon, K. Severinov, R. Seidel: *Primed CRISPR adaptation in escherichia coli cells does not depend on conformational changes in the cascade effector complex detected in vitro*, Nucleic Acids Res. **46** (8), 4087-4098 (2018)

T. Bayrak, S. Helmi, J. Ye, D.J. Kauert, J. Kelling, T. Schönherr, R. Weichelt, A. Erbe, R. Seidel: *DNA mold templated assembly of conductive gold nanowires*, Nano Lett. **18** (3), 2116-2123 (2018)

Talks

R. Seidel: *Insights into target recognition by CRISPR-Cas complexes from single-molecule mechanical measurements*, Physik-Kolloquium, Universität Bielefeld, Bielefeld, Germany, January 2018

R. Seidel: *DNA origami templated metal nanostructures*, Functional DNA Nanotechnology Workshop 2018, Rom, Italy, June 2018

R. Seidel: *A kinetic model for off-target recognition by Cascade, CRISPR 2018*, Vilnius, Lithuania, June 2018

J. Ye: *Nano-electronic components built from DNA templates*, Cfaed, BAC-retreat, Rathen, Germany, June 2018

P. Irmisch, R. Seidel: *Modelling DNA-strand displacement reactions in the presence of base-pair mismatches*, Soft Matter Day, Leipzig, Germany, July 2018

K. Kasaciunaite, F. Fettes, M. Levikova, P. Cejka, R. Seidel: *Cooperation of molecular motors during dsDNA repair*, Soft Matter Day, Leipzig, Germany, July 2018

B. Samatanga, I. Mogila, G. Tamulaitis, V. Siksnys, R. Seidel: *RNA processing and activation of type IIIA CRISPR-Cas systems*, Biennial Meeting of the German Biophysical Society, Düsseldorf, Germany, September 2018

R. Seidel: *Studying interactions of proteins with ribonucleic acids using mechanical forces*, Workshop Modern Methods of RNP Analysis, Universität Regensburg, Regensburg, Germany, October 2018

U. Kemper, R. Seidel: *Towards self-assembled magnetic nanostructures*, DNA Mitteldeutschland, Potsdam, Germany, November 2018

J. Ye: *Nano-electronic components built from DNA templates*, NanoNet PhD Seminars, Dresden, Germany, November 2018

R. Seidel: *Mechanistic Insights into target recognition by CRISPR-Cas effector complexes*, BBZ Methodological Workshop Series - Genome editing technologies, Universität Leipzig, Germany, December 2018

Posters

F. Engert, R. Seidel, U. Reibetanz: *Layer-by-Layer - DNA Origami hybrid System*, 14. Research Festival for Life Sciences, Leipzig, Germany, January 2018

P. Aldag, J. Madariaga, I. Songailiene, M. Rutkauskas, V. Siksnys, R. Seidel: *Correlated Single Molecule Twist and Fluorescence Measurements on CRISPR-Cas Systems*, Biophysical Society Meeting, San Francisco, USA, February 2018

D.J. Kauert, R. Seidel: *High Speed Mechanical Measurements based on DNA Origami Torque Sensors*, 62nd Annual Meeting of the Biophysical Society, San Francisco, USA, February 2018

K. Kasaciunaite, F. Fettes, M. Levikova, P. Cejka, R. Seidel: *Cooperation of DNA helicases during dsDNA end resection*, Biophysical Society Meeting, San Francisco, USA, February 2018

P. Aldag, J. Madariaga, I. Songailiene, M. Rutkauskas, V. Siksnys, R. Seidel: *Correlated Single Molecule Twist and Fluorescence Measurements on CRISPR-Cas Systems*, Les Houches Fluorescence Winter School, Les Houches, France, March 2018

F. Engert, R. Seidel, U. Reibetanz: *A Hierarchical Carrier System based on DNA Origami and Layer-by-Layer Microcarriers*, Annual Conference of the Graduate School BuildMoNa, Leipzig, Germany, March 2018

B. Samatanga, I. Mogila, G. Tamulaitis, V. Siksnys, R. Seidel: *RNA processing and activation of type IIIA CRISPR-Cas system*, RNA 2018, Berkeley, USA, June 2018

F. Engert, M. Brueckner, J. Ye, R. Seidel, U. Reibetanz: *A Hierarchical Carrier System based on DNA Nanostructures and Layer-by-Layer Microcarriers*, Functional DNA Nanotechnology Workshop, Rome, Italy, June 2018

J. Ye, R. Weichelt, U. Banin, A. Eychmüller, R. Seidel: *Nano-electronic components built from DNA templates*, Functional DNA Nanotechnology, Rome, Italy, June 2018

B. Samatanga, I. Mogila, G. Tamulaitis, V. Siksnys, R. Seidel: *RNA processing and activation of type IIIA CRISPR-Cas systems*, CRISPR 2018, Vilnius, Lithuania, June 2018

S. Henkel, J. Dikic, R. Seidel: *Mechanistic insight into target recognition process by TALEs*, Soft Matter Day, Leipzig, Germany, July 2018

J. Ye, R. Weichelt, U. Banin, A. Eychmüller, R. Seidel: *Nano-electronic components built from DNA templates*, BioMolecular Electronics conference, Madrid, Spain, August 2018

J. Ye, R. Weichelt, U. Banin, A. Eychmüller, R. Seidel: *Nano-electronic components built from DNA templates*, IHRS NanoNet Annual Workshop, Bad Gottleuba, Germany, September 2018

P. Irmisch, R. Seidel: *Modelling DNA-strand displacement reactions in the presence of base-pair mismatches*, 24th International Conference on DNA Computing and Molecular Programming, Jinan City, China, October 2018

6.11 Graduations

Master

- Patrick Irmisch
  Characterizing and modelling DNA-strand displacement reactions in the presence of base pair mismatches
  March 2018
- Brock Fergus Rupert Fettes-Leagas
  A Highly Parallel Magnetic Tweezers Setup for Single Molecule Spectroscopy
  October 2018

Bachelor

- Joey Wittenbecher
  Quantification of the target-binding of CRISPR-Cas Enzymes and Comparison with the theoretical modeling
  January 2018

6.12 Guests

- Prof. Mark Szcelkun
  University of Bristol, UK
  01.03.2018 until 03.03.2018
- Georgij Kostiuk
  Vilnius University, Lithuania
  04.03.2018 until 16.03.2018 and 26.08.2018 until 14.09.2018
- Dario Pragliola
  Universität Zürich, Schweiz
  01.05.2018 until 31.10.2018
- Alfonso Brenlla
  St. Andrews, UK
  11.-15.6.2018
- Gintautas Tamulaitis
  Vilnius University, Lithuania
  12.09.2018 until 14.09.2018
- Mahdi Bagherpoor-Helabad
  FU Berlin
  25.09.2018
- Dr. Sebastian Staacks
  RWTH Aachen
  06.11.2018

II

Felix Bloch Institute for Solid State Physics

7

Magnetic Resonance of Complex Quantum Solids

7.1 Introduction

The electronic properties of quantum-solids in which the electrons exhibit strong correlations with each other or with the lattice are particularly rich and will be of special importance in future functional materials. In addition, such solids are challenging for experiment, as well as theory, as the more than twenty five-year history of high-temperature superconductivity shows: we still do not understand the electronic structure of these systems. One particular aspect of strongly correlated electronic materials is their tendency towards nano-scale electronic phase separation. Even in perfect lattices, electronic nano-structures can form. The investigation of such materials requires the use of methods that can give detailed information. Here, magnetic resonance, on nuclei and electrons, is of particular interest as they not only have atomic scale resolution, but also yield bulk information in contrast to surface techniques. We explore the properties of these materials with tailored new techniques at the frontiers of magnetic resonance. For example, we are the leading laboratory when it comes to NMR at highest pressures and magnetic fields.

Jürgen Haase

7.2 Bulk Charge Ordering in the CuO_2 Plane of the Cuprate Superconductor $YBa_2Cu_3O_{6.9}$ by High-Pressure NMR

S. Reichardt, M. Jurkutat, R. Guehne, J. Kohlrautz, A. Erb*, J. Haase

*Walter-Meißner-Institute for Low Temperature Research, Walther-Meißnerstr. 8, 85748 Garching, Germany

Cuprate superconductors still hold many open questions, and recently, the role of symmetry breaking electronic charge ordering resurfaced in underdoped cuprates as a phenomenon that competes with superconductivity. Here, unambiguous nuclear magnetic resonance (NMR) proof (Fig. 7.1) is presented for the existence of local charge

ordering in nearly optimally doped $YBa_2Cu_3O_{6.9}$, even up to room temperature. Increasing pressure and decreasing temperature leads to the highest degree of order in the sense that the two oxygen atoms of the unit cell of the CuO_2 plane develop a charge difference of about 0.02 holes, and order throughout the whole crystal. At ambient conditions, a slightly smaller charge difference and a decreased order is found. Evidence from literature data suggests that this charge ordering is ubiquitous to the CuO_2 plane of all cuprates. Thus, the role of charge ordering in the cuprates must be reassessed.

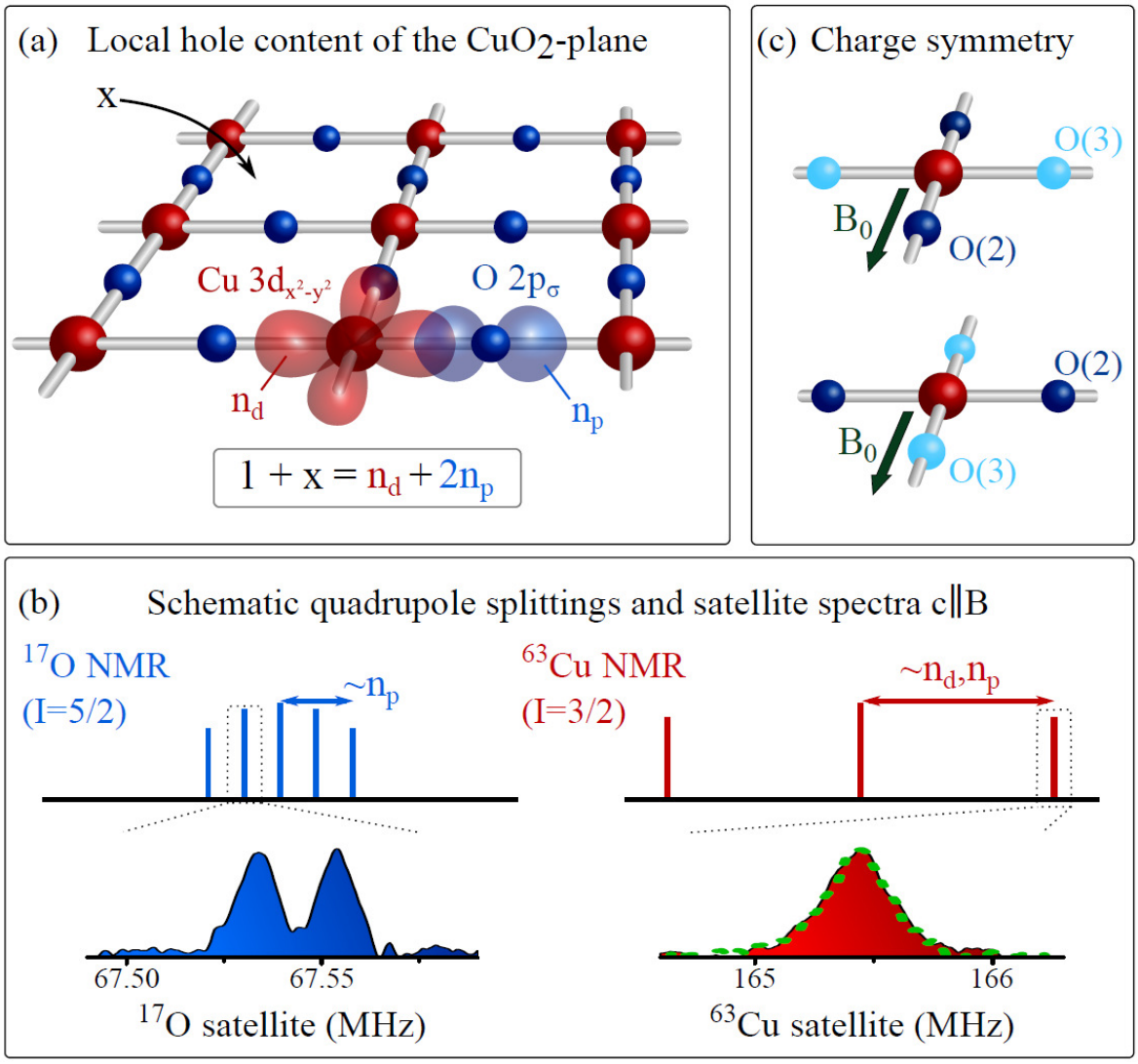

Figure 7.1: Nuclear magnetic resonance (NMR) and charge distribution in the CuO_2 plane. (a) $^{63,65}Cu$ and ^{17}O NMR can measure the hole contents of the bonding orbitals; (b) quadrupole splittings and satellite spectra c ||B; (c) charge symmetry.

7.3 Alkane/alkene mixture diffusion in sliicalite-1 studied by MAS PFG NMR

N. Dvoyashkina, D. Freude, A.G. Stepanov*, W. Böhlmann, R. Krishnar†, J. Kärger, J. Haase

*Novosibirsk State University, Pirogova Str. 2, Novosibirsk, 630090, Russia
†Van't Hoff Institute for Molecular Sciences, University of Amsterdam, Science Park 904, 1098, XH Amsterdam, The Netherlands

The diffusivity of n-alkanes and n-alkenes (C2 to C6) and their mixtures in silicalite-1 was studied by magic-angle spinning pulsed field-gradient nuclear magnetic resonance (MAS PFG NMR) at the temperatures of 273 K, 313 K and 373 K. It could be proved that there is no significant difference between the diffusivities of alkanes, alkenes and their mixtures for equal carbon numbers and equal total loading. The diffusivities of the alkanes, alkenes and their mixtures are found to monotonically decrease with increasing carbon number, in agreement with the results obtained in MD simulations with n-alkanes in silicalite-1.

7.4 Nitric Oxide Adsorption in MIL-100(Al) MOF Studied by Solid-State NMR

A.H. Khan, B. Barth*, M. Hartmann*, J. Haase, M. Bertmer

*Erlangen Catalysis Resource Center (ECRC), Friedrich-Alexander-Universität Erlangen-Nürnberg, 91058 Erlangen, Germany

Adsorption of nitric oxide (NO) in the metal-organic framework (MOF) MIL-100(Al) is studied by solid-state NMR. Owing to a modified synthesis, no extraframework benzenetricarboxylate is present on the cost of a small amount of extraframework $Al(OH)_3$ as evident from ^{27}Al, ^{1}H, as well as heteronuclear correlation spectra. Five-coordinated aluminum sites represent about 50% of the aluminum in a dehydrated sample, which remain open for adsorption. With increasing NO loading, a decrease of five-coordinated aluminum with a subsequent increase of six-coordinated aluminum site intensity is found. Additionally, ^{1}H spin-lattice relaxation time T_1 is decreasing with an increasing amount of NO, which also supports the NO interaction with the MOF because of the paramagnetism of NO. Fourier-transform infrared spectroscopy data further hint at Al-NO interactions.

7.5 Elucidating the Formation and Transformation Mechanisms of the Switchable Metal-Organic Framework ELM-11 by Powder and Single-Crystal EPR Study

A. Kultaeva, V. Bon*, M.S. Weiss†, A. Pöppl, S. Kaskel*

*Technische Universität Dresden, Department of Inorganic Chemistry, Bergstrasse 66, 01069 Dresden, Germany
†Helmholtz-Zentrum Berlin für Materialien und Energie, Macromolecular Crystallography Group, Albert-Einstein-Straße 15, 12489 Berlin, Germany

The effect of the synthesis conditions on the structure and guest-responsive properties of a 'gate pressure' metal-organic framework (MOF) with composition [Cu(4,4'-bipy)$_2$(BF$_4$)$_2$]n (4,4'-bipy = 4,4'-bipyridine), also known as ELM-11 (ELM = elastic layer material) was investigated. Two different batches of ELM-11, synthesized from water-methanol and water-acetonitrile solutions, have been entirely characterized by PXRD, nitrogen (77 K) and carbon dioxide (195 K) physisorption, elemental analysis, DRIFT, TG, and SEM. Both ELM-11 samples were studied by electron paramagnetic resonance (EPR) spectroscopy in order to follow the change in the local structure of the copper ion during the activation and resolvation. Continuous wave X-band EPR measurements on powder samples provided an elongated octahedral coordination symmetry of the cupric ions and revealed different axial ligands in the as-synthesized and activated forms in both bulk samples of ELM-11. One of the procedures was amended in order to slow down the crystallization that allows isolation of single crystals of two polymorphic modifications of Cu-4,4'-bipyridine coordination polymers, namely [Cu(4,4'-bipy)$_2$(CH$_3$CN)$_2$](BF$_4$)$_2$ and [Cu$_2$O(4,4'-bipy)$_3$(CH$_3$CN)$_4$](BF$_4$)$_2$, one of which shows a crystal structure similar to that of ELM-11. Further single-crystal EPR experiments on the as-synthesized material [Cu(4,4'-bipy)2(CH$_3$CN)$_2$](BF$_4$)$_2$ revealed the orientation of the g tensor of the cupric ions and proved that layers of acetonitrile-synthesized ELM-11 are arranged perpendicularly to the crystallographic c axis.

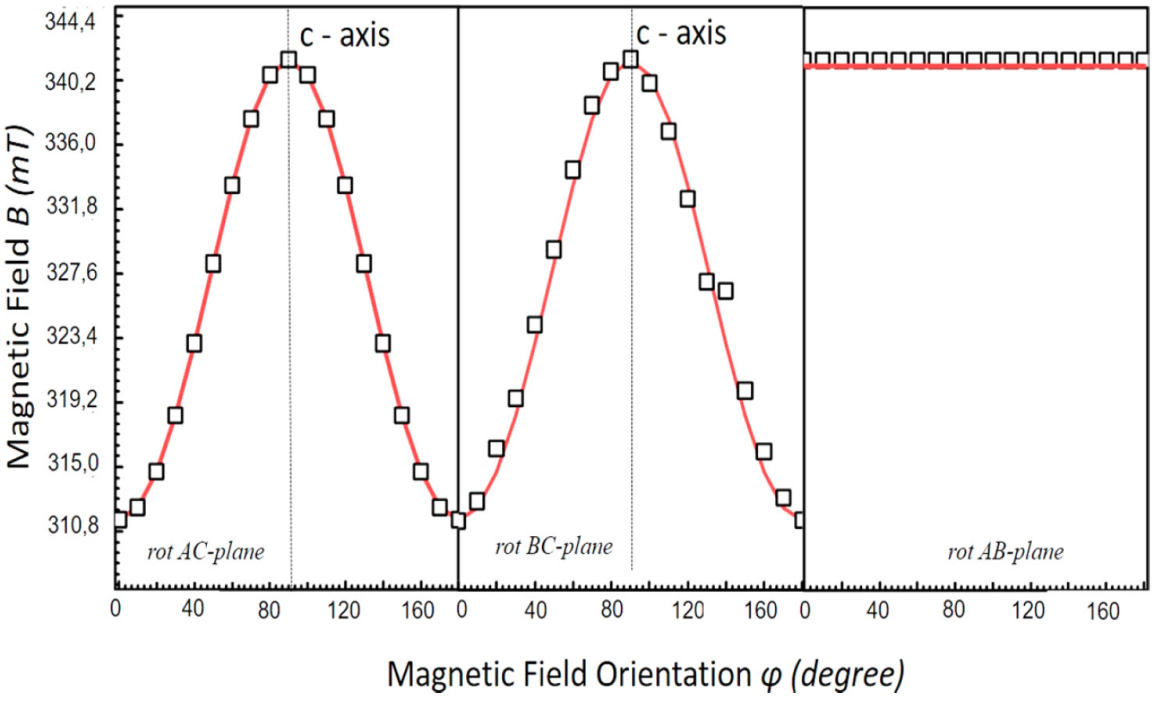

Figure 7.2: EPR angular-dependent resonancefields positions of the Cu^{2+} species in a synthesized $_{Acet}$ELM-11 single crystal for a rotation of B_0 inAC, BC, and AB planes. The red solid line shows the simulated angular dependences.

7.6 Funding

Energy efficient MOF-based Mixed Matrix Membranes for CO_2 Capture
Prof. Dr. Jürgen Haase
EU, 608490

Anwendungen der NMR-Spektroskopie zur Erforschung von Struktur-Beweglichkeits-Beziehungen an nanoporösen Wirt-Gast-Systemen im konzentrierten Einsatz mit dem Micro-Imaging
Prof. Dr. Jürgen Haase, Prof. Dr. Jörg Kärger
DFG, HA 1893/17-1

Metalle unter extremen Bedingungen
Prof. Dr. Jürgen Haase
DFG, HA 1893/12-1

Micro-Imaging transienter Konzentrationsprofile von Gastgemischen in Zeolithkristallen
Prof. Dr. Jürgen Haase, Prof. Dr. Jörg Kärger
DFG, HA 1893/15-1

Deuterium-Festkörper-NMR und ^1H MAS PFG NMR-Untersuchungen der Beweglichkeit des Wirtsgerüsts und der Gastmoleküle in nanoporösen Materialien
Prof. Dr. Jürgen Haase
DFG, HA 1893/16-1

EPR spectroscopy of paramagnetic centers and adsorption complexes in porous metal organic frameworks: Development and application of dielectric resonators and microresonators for investigations of small single crystals
Prof. Dr. Andreas Pöppl
DFG PO 426/11-2

Monitoring adsorption induced transformations of MOFs at a molecular level by in situ EPR spectroscopy
Prof. Dr. Andreas Pöppl
DFG PO 426/13-1

7.7 Organizational Duties

Professor Dr. Jürgen Haase

- Dean of the Faculty
- Vice Director of the Magnetic Resonance Center Leipzig
- Board Member of the Heisenberg Gesellschaft e. V.
- Full Member of the Saxonian Academy of Sciences in Leipzig
- Member of the German Physical Society
- Member of the American Physical Society
- Member of the 'ICAM Board of Goveners' of the Institute for Complex Adaptive Matter

- Referee: Physical Review, Science, IOP, German-Israeli Foundation for Scientific Research and Developement

Prof. Dr. Andreas Pöppl
- Referee: Journal of Magnetic Resonance, Journal of the American Chemical Society, Physical Chemistry Chemical Physics, Chemical Physics Letters
- Project Reviewer: German-Israeli Foundation for Scientific Research and Development

Prof. Dr. Dieter Michel
- Full Member of the Saxonian Academy of Sciences in Leipzig
- Member of the German Physical Society
- Member of the Society of German Chemists
- German Coordinator of the German-Russian Centre 'Applied and Computational Physics (ACOPhys)' at the St. Petersburg State University
- Member at the International Advisory Committee of the International Meeting of Ferroelectricity
- Member at the International Advisory Committee of the European Meeting of Ferroelectricity
- Member at the International Advisory Committee of the Conference 'NMR of Condensed Matter St. Petersburg'
- Member of the German-Israeli Foundation for Scientific Research and Developement
- Referee: Physical Review, Journal of Physics: Condensed Matter, Langmuir, Journal of Magnetic Resonance, Phys. Stat. Sol., Materials Chemistry and Physics, German-Israeli Foundation for Scientific Research and Developement

Prof. Dr. Rolf Böttcher
- Referee: Physical Review, Journal of Physics: Condensed Matter, Langmuir, Journal of Magnetic Resonance

7.8 External Cooperations

Academic

- Technical University Munich, Physics Department, Crystal Lab, Garching, Germany
  Prof. Dr. Andreas Erb
- Washington University, St. Louis, MO, USA
  J. Schilling, M. Conradi
- Victoria University, Physics Department,Wellington, New Zealand
  Dr. Grant V. M.Williams
- University of Illinois at Urbana-Champaign, Department of Physics, USA
  Prof. Dr. C. P. Slichter
- University of New South Wales, School of Physics, Sydney, Australia
  Prof. Dr. O. Sushkov
- Martin-Luther-Universität Halle-Wittenberg, Halle, Germany
  Dr. H. T. Langhammer

- Kazan State University, Tartastan, Russian Federation
  Prof. Dr. E. N. Kalabukhova
- Universität Erlangen-Nürnberg, Erlangen Catalysis Resource Center - ECRC, Erlangen, Germany
  Prof. Dr. Martin Hartmann
- Université du Maine, Laboratoire de Physique de l'Etat Condenseé, Le Mans, France
  Prof. Dr. A. Kassiba
- University of Vilnius, Faculty of Physics, Vilnius, Lithuania
  Prof. Dr. J. Banys
- University of Illinois at Chicago, USA
  Prof. Dr. D. K. Morr
- Skolkovo Institute of Science and Technology, Moscow, Russia and Institute for Theoretical Physics, University of Heidelberg, Heidelberg, Germany
  Prof. Dr. Boris V. Fine
- Boreskov Institute of Catalysis, Novosibirsk, Russia Novosibirsk State University, Novosibirsk, Russia
  Dr. Alexander G. Stepanov
- Institute of Physics, St. Petersburg State University, St. Petersburg, Russia
  Prof. Dr. Elena V. Charnaya
- Ruhr-University Bochum, Bochum, Germany
  R. A. Fischer

Industry

- NMR-Service GmbH, Erfurt, Germany
  M. Braun
- Bruker BioSpin GmbH, Rheinstetten, Germany
  F. Engelke

7.9 Publications

Journals

M. Avramovska, D. Pavicevic, J. Haase: *Properties of the electronic fluid of superconducting cuprates from ^{63}Cu NMR shift and relaxation*, arXiv.org, Condensed Matter (2018) 1-7

L. Borchardt, D. Leistenschneider, J. Haase, M. Dvoyashkin: *Revising the Concept of Pore Hierarchy for Ionic Transport in Carbon Materials for Supercapacitors*, Adv. Energy Mater. 8 (2018)

C. Chmelik, M. Liebau, M. Al-Naji, J. Möllmer, D. Enke, R. Gläser, J. Kärger: *One-Shot Measurement of Effectiveness Factors of Chemical Conversion in Porous Catalysts*, ChemCatChem 10 (2018) 5602-5609

N. Dvoyashkina, D. Freude, A. G. Stepanov, W. Böhlmann, R. Krishnar, J. Kärger, J. Haase: *Alkane/alkene mixture diffusion in silicalite-1 studied by MAS PFG NMR*, Microporous Mesoporous Mater. 257 (2018) 128-134

N. Dvoyashkina, C.F. Seidler, M. Wark, D. Freude, J. Haase: *Proton mobility in sulfonic acid functionalized mesoporous materials studied by MAS PFG NMR diffusometry and impedance spectroscopy*, Microporous Mesoporous Mater. 255 (2018) 140-147

M. Dvoyashkin, N. Wilde, J. Haase, R. Gläser: *Diffusion of methyl oleate in hierarchical micro-/mesoporous TS-1-based catalysts probed by PFG NMR spectroscopy*, RSC Adv. 8 (2018) 38941-38944

S. Hwang, R. Semino, B. Seoane, M. Zahan, C. Chmelik, R. Valiullin, M. Bertmer, J. Haase, F. Kapteijn, J. Gascon, G. Maurin, J. Kärger: *Revealing the Transient Concentration of CO_2 in a Mixed-Matrix Membrane by IR Microimaging and Molecular Modeling* Angew. Chem. Int. Ed. 57 (2018) 5156-5160

S. Hwang, A. Gopalan, M. Hovestadt, F. Piepenbreier, C. Chmelik, M. Hartmann, R.Q. Snurr, J. Kärger: *Anomaly in the chain length dependence of n-alkane diffusion in ZIF-4 metal-organic frameworks*, Molecules 23 (2018) 668

A.H. Khan, B. Barth, M. Hartmann, J. Haase, M. Bertmer: *Nitric oxide adsorption in MIL-100(Al) MOF studied by solid-state NMR*, J. Phys. Chem. C 122 (2018) 12723-12730

A. Kultaeva, T. Biktagirov, P. Neugebauer, H. Bamberger, J. Bergmann, J. van Slageren, H. Krautscheid, A. Pöppl: *Multifrequency EPR, SQUID, and DFT Study of Cupric Ions and Their Magnetic Coupling in the Metal-Organic Framework Compound $_{3\infty}$[Cu(prz-trz-ia)]*, J. Phys. Chem. C 122 (2018) 26642-26651

A. Kultaeva, V. Bon, M.S. Weiss, A. Pöppl, S. Kaskel: *Elucidating the Formation and Transformation Mechanisms of the Switchable Metal-Organic Framework ELM-11 by Powder and Single-Crystal EPR Study*, Inorg. Chem. 57 (2018) 11920-11929

A. Lauerer, R. Kurzhals, H. Toufar, D. Freude, J. Kärger: *Tracing compartment exchange by NMR diffusometry: Water in lithium-exchanged low-silica X zeolites*, J. Magn. Reson. 289 (2018) 1-11

D. Michel: *Magic-Angle Spinning NMR and Molecluar Mobility in Heterogeneous Systems*, Appl. Magn. Reson. 49 (2018) 537-552

R. Pickenhain, M. Schmidt, H. von Wenckstern, G. Benndorf, A. Pöppl, R. Böttcher, M. Grundmann: *Negative-U Properties of the Deep Level E3 in ZnO*, Phys. Stat. Solidi B 255 (2018)

S. Reichardt, M. Jurkutat, R. Guehne, J. Kohlrautz, A. Erb, J. Haase: *Bulk charge ordering in the CuO_2 plane of the cuprate superconductor $YBa_2Cu_3O_{6.9}$ by high-pressure NMR*, Condensed Matter 3 (2018) 23/1 - 23/16

M. Simenas, M. Ptak, A.H. Khan, L. Dagys, V. Balevicius, M. Bertmer, G. Völkel, M. Maczka, A. Pöppl, J. Banys: *Spectroscopic Study of $[(CH_3)_2NH_2][Zn(HCOO)_3]$ Hybrid Perovskite Containing Different Nitrogen Isotopes*, J. Phys. Chem. C 122 (2018) 10284-10292

R. Wunderlich, J. Kohlrautz, B. Abel, J. Haase, J. Meijer: *Investigation of room temperature multispin-assistend bulk diamond (13)C hyperpolarization at low magnetic fields*, J. Phys. Cond. Matter 30 (2018) 305803

7.10 Graduations

Doctorate

- Steven Reichardt
  title
  February 2018
- Nina Dvoyashkina
  title
  April 2018

Master

- Manuel Lindel
  Nuclear Magnetic Resonance of Zintl phase Deuterides
  March 2018

8

Nuclear Solid State Physics

8.1 Introduction

An absolute prerequisite for the manufacture of quantum computers in a solid state is the precise positioning of individual qubits with suitable properties. If the nitrogen–vacancy (NV) centre in diamond is to be used as a qubit, the deterministic implantation of individual N ions is necessary, as well as the transformation of the implanted N into a negatively charged NV centre. While the first requirement is a technical problem and the developments from our institute quickly led to first solutions, the second problem was of a very difficult character. It had to be understood, how the NVs are formed and how the defects could be caused, how a permanent negative charge could be achieved and how the diamond could be annealed as optimally as possible in order to achieve a long coherence time. Also it had to be checked if and how other defects or foreign atoms like H influence the diamond properties. If you are travelling in a multiparameter space and no strategies or solutions are recognisable, you have to learn from the biologists or physicians. They almost always have this problem because of the most complex living matter. Their solution strategy is simple: try out as many different methods and substances as possible and hope that a remedy against a disease, for example, is the right one. A screening procedure was used to investigate the effects of different foreign atoms as quickly as possible: The 100 kV implanter was rebuilt in a way that it allows to change energy and ion type in only a few minutes. Using shadow masks it was then possible to test many different substances and combinations on a diamond sample. Besides many new colour centres, important properties for an optimal doping of diamond could be found.

As a physicist you don't like to admit it, but sometimes it actually helps to learn from the strategies of our colleagues in biochemistry and medicine, which often seem random to us.

All these nice results are only possible thanks to our funding agencies, to whom we would like to express our deepest gratitude in particular the VolkswagenStiftung, the Deutsche Forschungsgemeinschaft (DFG), the European Social Fund (ESF), the European Union (EU), and the Senatsausschuss Wettbewerb (SAW) Project of the Leibniz Association.

Jan Meijer

8.2 Creation of diamond thin films by an ion-cut method

C. Scheuner, T. Lühmann, M. Kieschnick, J. Küpper*, L. Trefflich†, S. Pezzagna, M. Grundmann†, J. Meijer

*Division of Superconductivity and Magnetism
†Division of Semiconductor Physics

The properties of the negatively charged nitrogen–vacancy (NV) centre are very promising for its use as a quantum system in applied sciences. One application may be the sensing of microwaves or magnetic fields as demonstrated by Chipaux et al. [1]. For these applications an increased detection efficiency or a decreased measurement time is desirable. This can be realized by a Purcell enhancement of the NV fluorescence using optical cavities. To build these cavities we use Diamond thin films with thicknesses of below 200 nm produced by an ion-cut method.

Ion-cut method means that a bulk diamond is irradiated with ions of homogeneous energy. These ions create the greatest damage near to their stopping depth and therefore produce a highly damaged layer in a certain depth. Since diamond has a relatively sharp transition to form graphite at a certain damage concentration, this effect can be exploited to produce diamond thin films.

To create an optical cavity the diamond thin film needs to be fabricated with high accuracy in roughness and thickness. To achieve this the damage distribution of the ion beam in diamond was simulated with `SRIM` [2]. This program models the interaction of the ions with the target but does not take into account damage accumulation. Therefore the resulting damage distribution is afterwards scaled with a model taking into account defect saturation and swelling [3]. The main feature of this model is a probability of recombination of interstitials with vacancies linearly increasing with the ion dose. A comparison between the scaled data and the `SRIM` output is shown in Fig. 8.1**(a)**.

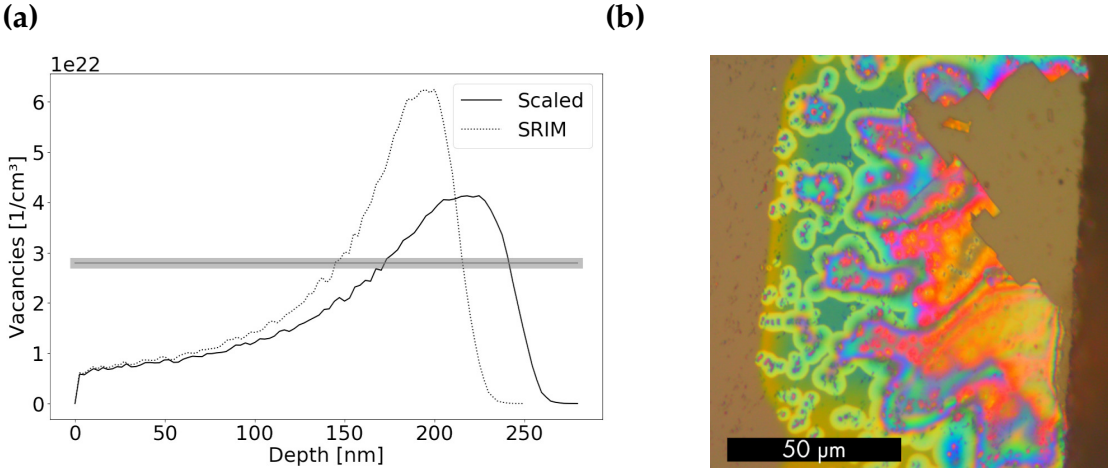

Figure 8.1: (a) Simulation of the vacancy distribution over the penetration depth for H at an energy of 35 keV and a fluence of 1.5×10^{17} cm^{-2} with `SRIM` and a high dose scaling of the vacancy distribution. This scaling is taking into account defect saturation and damage induced swelling. The horizontal line represents the graphitisation threshold. **(b)** Freestanding membrane after O etching, indicated by interference in white light, similar to Newton rings.

Following the irradiation of the bulk diamond, it was annealed in a high-temperature vacuum oven to enhance the transition sharpness between diamond and graphite. After this, a dark spot of graphitized material could be seen. To lift off the diamond thin film the graphite needed to be removed. This was done with heating up the diamond in an O atmosphere, where the graphite oxidizes at lower temperatures as the diamond and thus gets removed without significant damage of the diamond thin film. This creates a free-standing diamond membrane, shown in Fig. 8.1**(b)**. This membrane is than broken with a needle and the diamond fragments can be lifted on a glass slide.

The resulting fragments of the diamond thin film have been characterized using atomic force microscopy (AFM) and photoluminescence (PL) spectroscopy to check their quality. We found that the thickness is close to the value predicted by the simulation and the surface roughness is close to untreated diamond. The PL spectra showed that there is a reduction in NV luminescence but the remaining crystal damage is low. In the future, we need to improve the parameters in order to get a greater NV luminescence.

[1] M. Chipaux et al.: Appl. Phys. Lett. **107**, 233502 (2015), doi:10.1063/1.4936758
[2] J.F. Ziegler et al.: Nucl. Instrum. Meth. Phys. Res. B **268**, 1818 (2010), doi:10.1016/j.nimb.2010.02.091
[3] B.A. Fairchild et al.: Adv. Mater. **24**, 2024 (2012), doi:10.1002/adma.201104511

8.3 Quantum and classical light emitters in silicon: Impurities and complex defects for nanophotonics

T. Herzig, W. Redjem*, G. Cassabois*, E. Rousseau*, V. Jacques*, A. Benali†, M. Abbarchi†, S. Pezzagna, J. Meijer

*Laboratoire Charles Coulomb (L2C), CNRS-UMR 5221, Université de Montpellier, France
†Institut Matériaux-Microélectronique-Nanosciences de Provence (IM2NP), CNRS-UMR 7334, Aix-Marseille Université, France

The steady demand of better performing computers requires continual improvement of processing power and faster data transfer. Hitherto this was possible by decreasing structure sizes of microelectronic components ("Moore's law") or by establishing new designs (e.g. 3D-ICs, FinFETs, etc.) on Si-based microchips. This process is drawing to an end by the so called interconnect bottleneck problem. When the feature sizes of integrated circuits (IC) become too small, the signal delay is no longer dictated by the gate switching time but by the wiring delay [1]. Since this physical limitation is inevitable, new designs for next generation computers are needed. One of the most anticipated concepts is the utilization of quantum computing and nanophotonics in Si.

Si has been the main material in semiconductor fabrication for decades, attributable to its physical properties and the high amount of natural resources, which makes it very inexpensive. But due to its indirect bandgap, radiative transitions in Si are highly improbable which makes it unsuitable for optoelectronical applications. But by modifying the crystal structure, one can suppress the non-radiative transitions and therefore enhance the light extraction from Si itself. This can be achieved by e.g. the creation of specific defects with ion implantation techniques. In our project, we

investigate the generation and properties of a defect in the Si lattice, called G-centre. This defect has a sharp zero-phonon line (ZPL) at around $\lambda \approx 1280\,\text{nm}$, matching the optical telecommunications O-band wavelength with low transmission losses, and a broad phonon sideband (PSB) to lower energies (Fig. 8.2). It consists of one interstitial

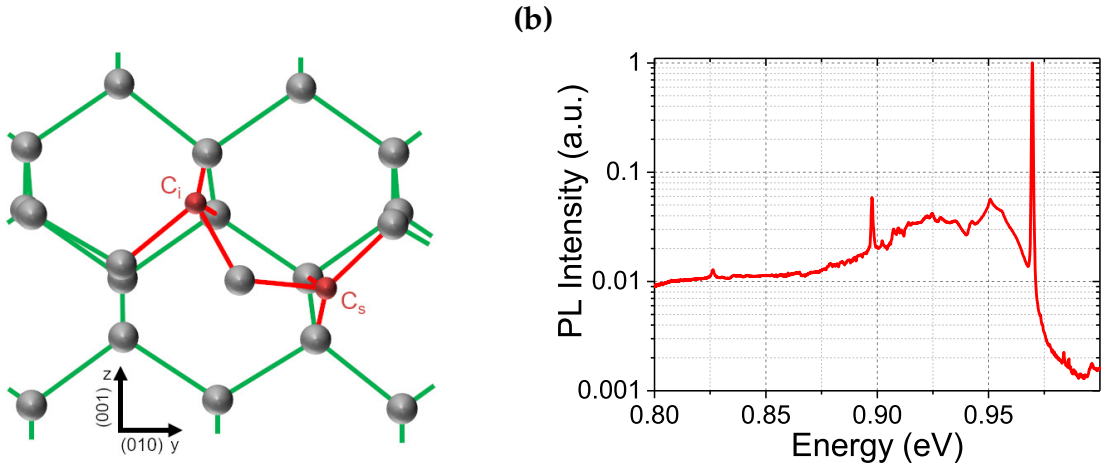

Figure 8.2: (a) B-configuration of a G-centre as depicted in [2]. Note the prominent interstitial C_i and substitutional C_s atoms. **(b)** Typical photoluminescence (PL) spectrum of an ensemble of G-centres. Note the sharp ZPL at $E \approx 0.97\,\text{eV}$ or $\lambda \approx 1280\,\text{nm}$, respectively, and the PSB to lower energies.

C_i and one substitutional C_s atom within the Si lattice and occurs in four different configurations, depending on the orientation of the C atoms in the lattice [2]. It was first observed in the early 1960s after high-energy electron irradiation of n-type Si [3] and later identified as a bistable C pair by electron paramagnetic resonance (EPR), optically detected magnetic resonance (ODMR), and infrared (IR) absorption measurements [4].

To generate these defects, a 100 kV accelerator with a source of negative ions by Cs sputtering (SNICS) (Fig. 8.3) is used for implantation of different isotopes (e.g. $^{12}C_1$, $^{13}C_1$, $^{28}Si_1$) with energies between $(5-100)\,\text{keV}$ and ion fluences ranging from $\left(10^9-10^{16}\right)\,\text{cm}^{-2}$. After rapid thermal annealing ($T = 1000\,^\circ\text{C}$ for 20 s at N_2 atmosphere) to incorporate the C atoms into the Si lattice, a high-energy irradiation with light ions, performed at the LIPSION Singletron accelerator with focusing setup and microbeam scanning system, leads to the C_i–C_s pair. Beside the investigation of the best implantation conditions, we also examine the influence of e.g. doping or photonic structures on the generation and yield of G-centres.

Since start of the project we have been able to characterise the saturation power of an ensemble of G-centres. We investigated the recombination dynamics, leading to a new value for the lifetime of the state of $\tau = 5.9\,\text{ns}$ at low temperature (Fig. 8.4**(a)**). According to theoretical modelling of the vibronic spectrum, we estimated the spatial extension of the electronic wave function in a G-centre to $\sigma = 1.6\,\text{Å}$ (Fig. 8.4**(b)**). Moreover, the temperature dependence of the emission spectrum and recombination dynamics was recorded [5], leading to new insights of the characteristics of this fascinating defect. With this knowledge, we want to entrench a method for straightforward production of lasers, light-emitting diodes (LED) and single-photon sources directly within Si itself, to herald the start of a new and revolutionary design for Si-based photonic and quantum devices.

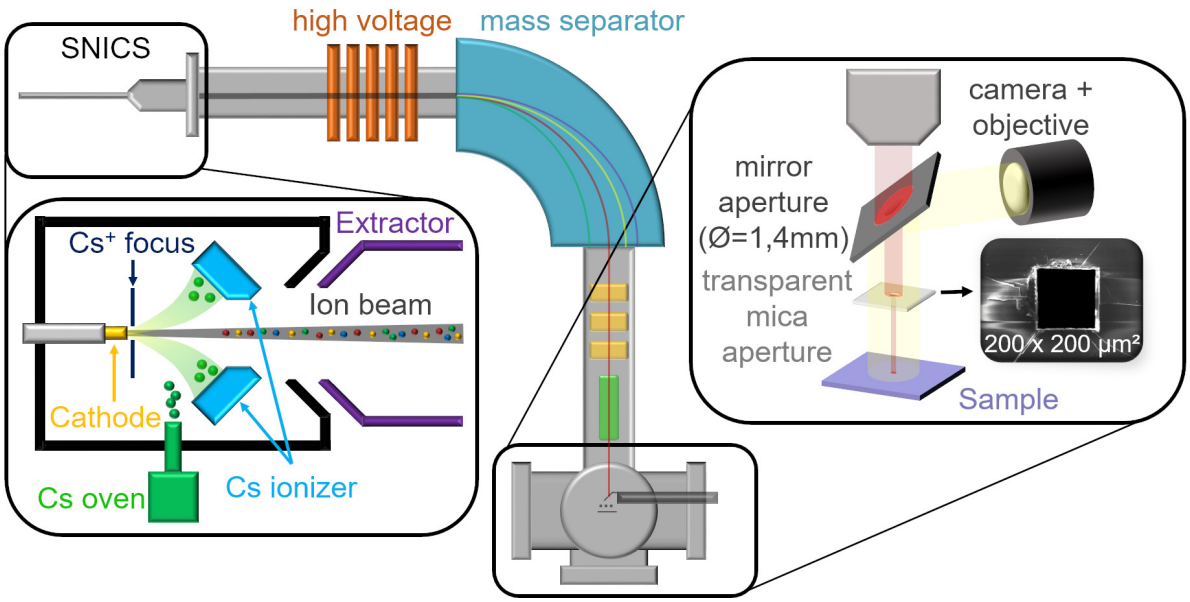

Figure 8.3: 100 kV implanter with a SNICS and an aperture system within the sample chamber for collimating the ion beam, allowing spatial selective ion implantation with µm resolution.

(a) **(b)**

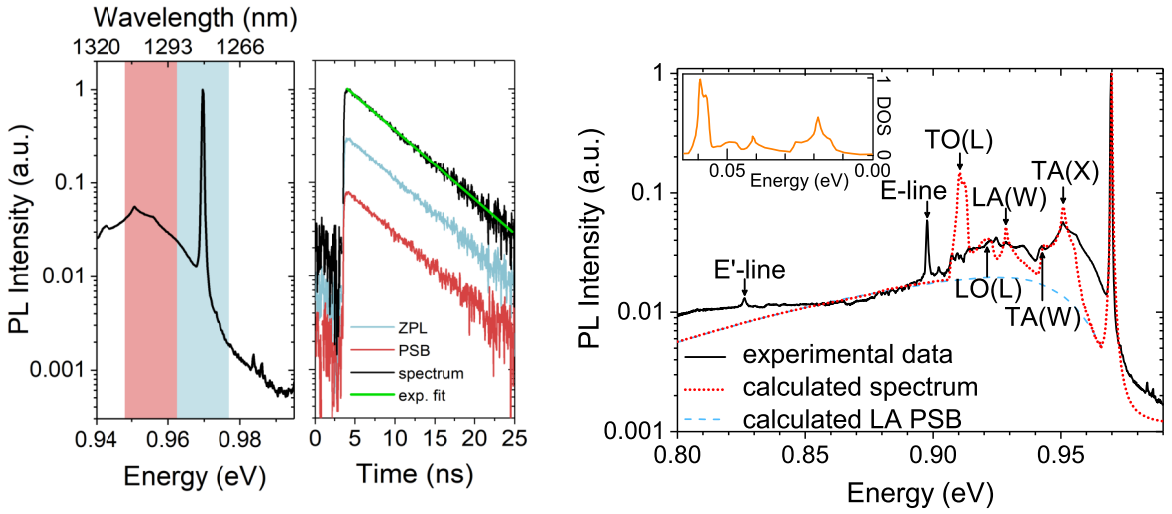

Figure 8.4: **(a)** Photoluminescence (PL) spectrum and lifetime of an ensemble of G-centres measured at $T = 10\,\mathrm{K}$. The *red* and *blue* shaded areas indicate the spectral width of the two bandpass filters used for spectrally selective time-resolved measurements of the ZPL (*blue*) and the PSB (*red*). The same lifetime of $\tau = 5.9\,\mathrm{ns}$ for the ZPL as well as for the PSB indicates the same microscopic origin. **(b)** Theoretical approach based on nonperturbative calculations of the acoustic phonon sideband and an ad hoc inclusion of zone-edge phonons. This model provides a direct estimation of the spatial extension of the electronic wave function in a G-center ($\sigma = 1.6$ Å) [5].

[1] L. Pavesi: J. Phys.: Condens. Matter **15**, R1169 (2003), doi:10.1088/0953-8984/15/26/201
[2] D. Timerkaeva et al.: J. Appl. Phys. **123**, 161421 (2018), doi:10.1063/1.5010269

[3] G.D. Watkins et al.: Phys. Rev. **121**, 1001 (1961), doi:10.1103/physrev.121.1001
[4] L.W. Song et al.: Phys. Rev. B **42**, 5765 (1990), doi:10.1103/physrevb.42.5765
[5] C. Beaufils et al.: Phys. Rev. B **97**, 035303 (2018), doi:10.1103/physrevb.97.035303

8.4 Microscopic structure elucidation of coffee charcoal particles (*Coffea Arabica* L.) in comparison to activated medicinal charcoal using scanning electron microscopy

C. Vissiennon[*†], A. Iphöfer[†], St. Jankuhn

[*]Institute for Medical Physics and Biophysics
[†]Repha GmbH Biologische Arzneimittel, Langenhagen

Coffee charcoal is described as the milled, roasted to blackening outer seed parts of green dried *Coffea Arabica* L. fruits and was introduced into medical practice by A. Heisler in 1937 [1]. Within a traditional herbal medicinal product (Myrrhinil-Intest) it is used since several decades for the treatment of intestinal disorders. So far mainly adsorptive properties were thought to mediate therapeutic effects in coffee charcoal preparations in similarity to medicinal (activated) charcoal. However, previous pharmacological studies revealed significant effects of a coffee charcoal extract on cell signaling especially within the cytokine/chemokine signaling pathway in human macrophages.

Aim of the present study was to produce electron scanning microscopic images of coffee charcoal and active charcoal particles in order to compare the microscopic constitution with regard to surface structure, porosity and presence of pore ducts.

Thus, images were obtained using the scanning electron microscope (SEM) tools of the dual beam microscope (DBM) Nova NanoLab 200/600 of the FEI Comp. in the low voltage mode at 5 kV. Samples (activated charcoal and coffee charcoal particles) were fixated on a double-sided adhesive tape and sputter-coated with Au.

The obtained images allow better characterization of the particle texture (see Fig. 8.5). The porosity and presence of pore ducts were found to be different between the samples, whereby the particle size of activated charcoal was apparently smaller and porosity increased compared to coffee charcoal particles which appeared also revealed less distinct pore ducts. These observations suggest that adsorptive properties might be different in coffee charcoal samples and additional pharmacological effects on cell function contribute to the observed therapeutic effects. These observations are in line with findings from H. Riedel who found a much lower adsorptive capacity of coffee charcoal compared to activated charcoal [2].

[1] A. Heisler: Hippokrates **8**, 1247 (1937)
[2] H. Riedel: Klin. Wochenschr. **18**, 609 (1939), doi:10.1007/BF01777865

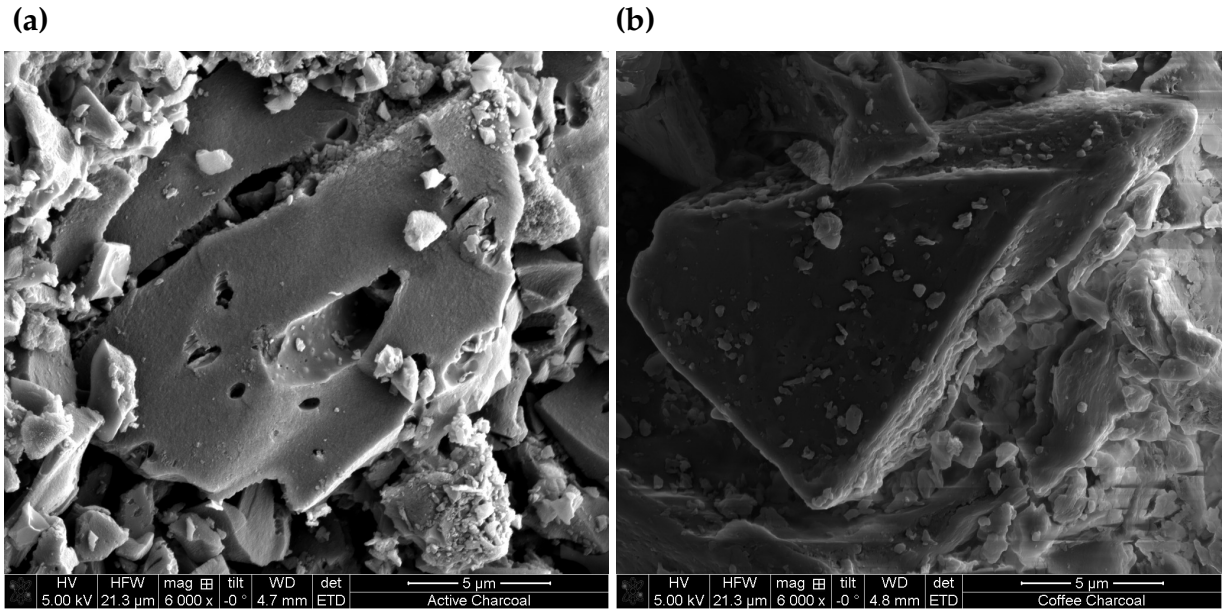

Figure 8.5: SEM images of **(a)** activated charcoal, **(b)** coffee charcoal.

8.5 Image charge detection statistics

P. Räcke[*†], R. Staacke[*], J.W. Gerlach[†‡], D. Spemann[†‡], J. Meijer[*†]

[*]Division of Nuclear Solid State Physics
[†]Leibniz Joint Lab "Single Ion Implantation", Leipzig
[‡]Leibniz Institute of Surface Engineering e.V. (IOM), Leipzig

In the Leibniz Joint Lab "Single Ion Implantation", a collaboration with the Leibniz Institute of Surface Engineering e.V., we continued the development of experimental techniques for deterministic ion implantation. The central focus is the development of image charge detection (ICD), an approach for the non-perturbative detection of ions on the way to the sample. In our labs, image charge detector prototypes were developed and used for the detection of ion bunches as a model system for highly charged ions. First results of these experiments were published in 2018 [1]. The investigations continued with quantitative measurements of detection and error rates of the ICD system, also leading to a recent publication [2]. By measuring 6×10^4 Fourier spectra of identical single ion bunch passages, the statistical distributions of signal and noise were analysed (see Fig. 8.6). The probability density functions can be modelled with a generalised gamma distribution at each frequency. This is useful for the characterisation of the noise and signal properties and to determine detection and error rates. It is shown that the false positive error rate can be minimised at the cost of detection rate, but this does not impair the fidelity of a deterministic implantation process. Independent of the ion species, at a signal-to-noise ratio (SNR) of 2 (corresponding to 1100 Ar^{2+} ions), a false positive error rate of 0.1 % is achieved, while the detection rate is about 22 %. In conclusion, even at very small SNR, a pre-detection method like ICD is suitable for deterministic ion implantation. Future work must be focused on optimising the noise performance of the ICD system to reach sensitivities close to single elementary charges.

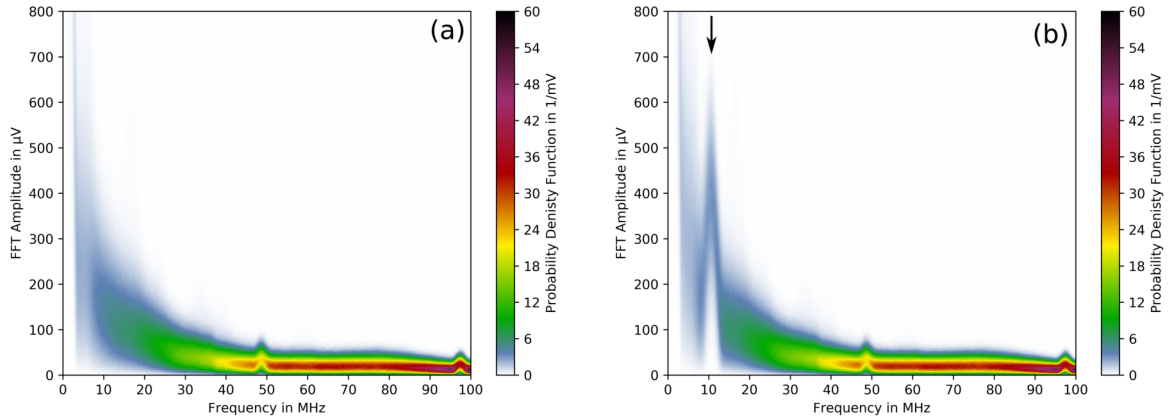

Figure 8.6: Normalised histograms as a measurement of the probability density function of the fast Fourier transform (FFT) amplitudes at all frequencies up to 100 MHz: **(a)** noise, **(b)** with 10 keV Ar^{2+} ion bunch signal at f = 10.55 MHz (arrow) and 13.5 nA continuous beam current, i.e. SNR = 2. Reproduced from [2] in compliance with the CC BY 3.0 license [3].

[1] P. Räcke et al.: Sci. Rep. **8**, 9781 (2018), doi:10.1038/s41598-018-28167-6
[2] P. Räcke et al.: J. Phys. D: Appl. Phys. (accepted manuscript), doi:10.1088/1361-6463/ab1d04
[3] creativecommons.org/licenses/by/3.0/

8.6 Biofilms on the in- and outside of long-term jugular vein catheters placed in horses

A. Reinert*, A. Mottl†, St. Jankuhn

*Institute of Veterinary Anatomy
†University Hospital for Horses

In human and veterinary clinics, especially in intensive care, long-term intravenous catheters are port devices implanted in large veins to inject medications, parenteral nutrition, blood products/fluids or to perform blood tests. In horses, long-term jugular vein catheters (JVC) are used for this purpose. The catheter usually lays for several days. The longer it is placed, the higher is the risk for vessel wall inflammations and venous thrombosis (thrombophlebitis). Infection can complicate and enhance this venous disorder and can induce vessel wall rupture or systemic sepsis. The catheter insertion site serves as a portal for bacteria and fungi that get access to the vein and adhere to the surface of the carrier. It is reported that, depending on the coating of the catheter, the inner site is lined by a biofilm already 24 h after its placement. The biofilm consists of polysaccharides, fibrin, fibronectin or laminin and is produced by microorganisms and the host. Microorganisms within the biofilm are protected against defense mechanisms of the host and antibiotics. Therefore, the biofilm and vein thrombi within the catheters are the most important pathogenic sites of catheter-born infections, serving as a growing medium for microorganisms.

The project aim the detection of biofilms on the inner and outer site of jugular vein catheters 24 h after placement. Therefore, in the jugular vein (neck) of 16 horses a polyurethane catheter (Extended Use MILACATH, Long Term Catheter, 12G/14G × 13cm, Mila International, Inc.) was implanted. The insertion site was previously disinfected after standard clinical procedure. The JVC was removed after 24 h and its tip was cut off and divided longitudinally in half. The two pieces were fixed in 4 % formalin and stored at 4 ℃ until their preparation for scanning electron microscopy (SEM). Therefore, samples were washed in buffer, treated with 1 % OsO_4 for 1 h at 4 ℃, dehydrated in ethanol, dried in a critical-point-dryer and sputter-coated with Ag or Au. SEM pictures of different amplification of the in- and outside of the JVC were taken at the dual beam microscope (DBM) Nova NanoLab 200/600 of the FEI Comp. (see Fig. 8.7).

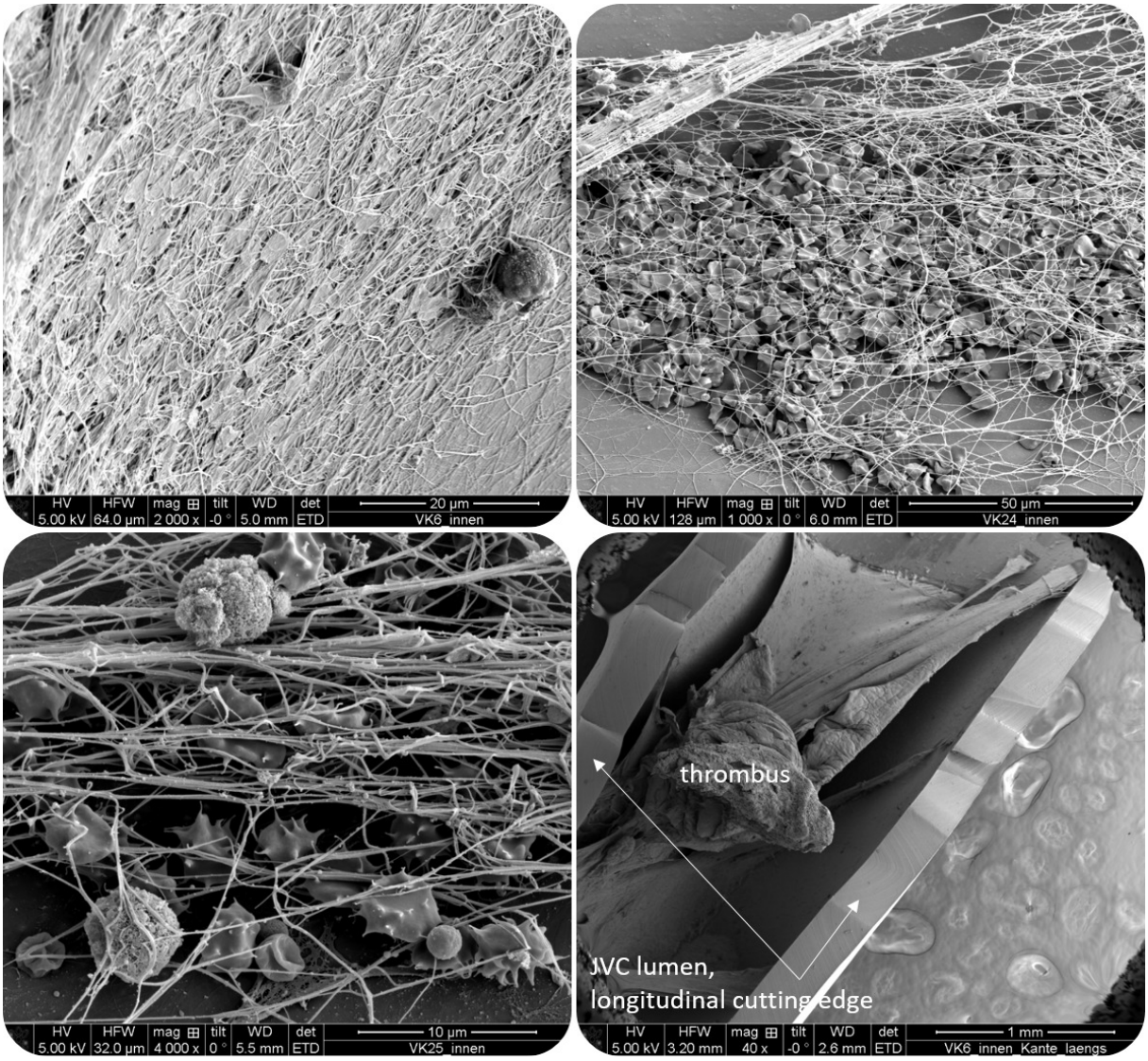

Figure 8.7: SEM pictures of the surface of long-term JVC placed in horse veins for 24 h. A biofilm is present consisting of blood clothing products (especially fibrin), embedded blood cells and bacteria.

In all the 16 catheters, a biofilm on the inside and the outside was present. The biofilm consists of blood clothing products (especially fibrin), embedded blood cells

and bacteria. The determination of the bacteria and probably fungi will be finally done by microbiologists. The biofilm lining the inner side of the catheter seems to be slightly more pronounced. However, the variation of the total area covered by a biofilm is very variable between the catheters. Further, in three catheters a thrombus was present.

The SEM data confirm that the use of long-term jugular vein catheters increase the risk for local and systemic complications in horses. Further, the obtained pictures provide morphological information about the microorganisms growing on the carrier and have therefore diagnostic potential.

[1] C. Müller et al.: Tierärztl. Prax. G **44**, 187 (2016), doi:10.15653/TPG-140417
[2] T.E. Geraghty et al.: Vet. Rec. **164**, 227 (2009), doi:10.1136/vr.164.8.227
[3] D.P.M. Dias et al.: Can. Vet. J. **54**, 65 (2013)
[4] A. Schoster: Schweiz. Arch. Tierheilkd. **159**, 477 (2017), doi:10.17236/sat00126
[5] M. Gominet et al.: APMIS **125**, 365 (2017), doi:10.1111/apm.12665

8.7 Room temperature multispin-assisted bulk diamond ^{13}C hyperpolarisation at low magnetic fields

R. Wunderlich, J. Kohlrautz*, B. Abel†, J. Haase*, J. Meijer

*Division of Magnetic Resonance of Complex Quantum Solids
†Leibniz Institute of Surface Engineering e.V. (IOM), Leipzig

In this work we investigated the time behaviour of the polarisation of bulk ^{13}C nuclei in diamond above the thermal equilibrium. This nonthermal nuclear hyperpolarisation is achieved by cross relaxation (CR) between two N related paramagnetic defect species in diamond in combination with optical pumping. The decay of the hyperpolarisation at four different magnetic fields is measured. Furthermore, we use the comparison with conventional nuclear resonance measurements to identify the involved distances of the nuclear spin with respect to the defects and therefore the coupling strengths. Also, a careful look at the linewidth of the signal give valuable information to piece together the puzzle of the hyperpolarisation mechanism. Moreover we can argue that a coupling to sufficient far away spins is necessary for a nuclear spin transport and bulk polarisation. This could have a tremendous impact on future hyperpolarisation application e.g. in nano diamonds, which could be more efficient with spin impurities (see Fig. 8.8).

8.8 Tin-vacancy in diamonds for luminescent thermometry

M. Alkahtani*, I. Cojocaru*, X. Liu*, T. Herzig, J. Meijer, J. Küpper, T. Lühmann, A.V. Akimov*, P.R. Hemmer*

*Institute for Quantum Science and Engineering, Texas A& M University, College Station, TX, USA

Colour centres in diamonds have shown promising potential for luminescent thermometry. So far, the nitrogen–vacancy (NV) colour centre has demonstrated a high

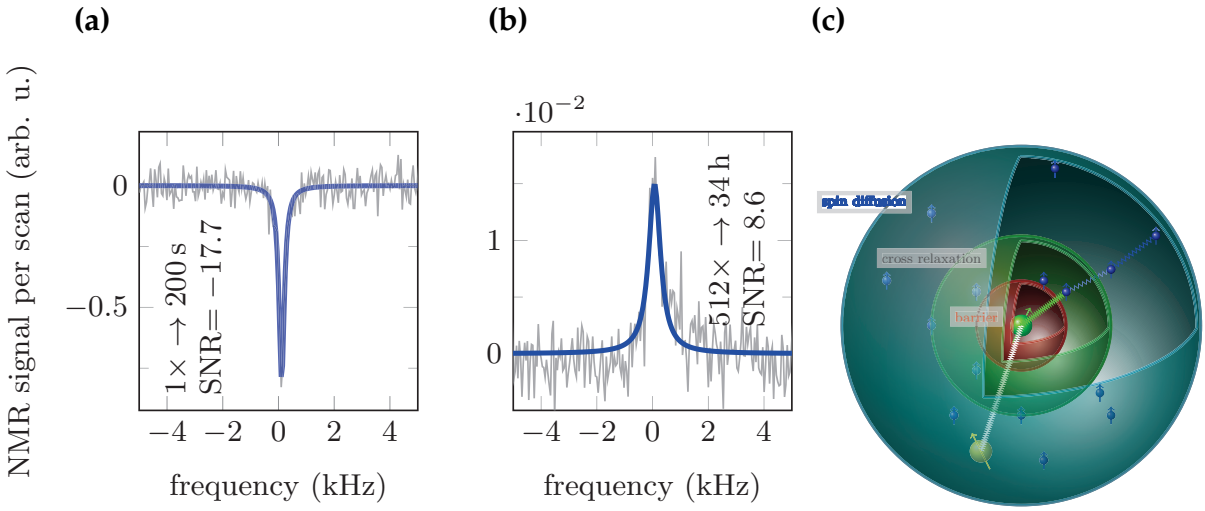

Figure 8.8: Comparison of nuclear magnetic resonance (NMR) ^{13}C spectra of a single scan after hyperpolarisation during 200 s irradiation at a stabilised field of 49.38 mT **(a)** and an accumulation over 512 scans separated by 240 s (over all 34 h accumulation time) in quasi-thermal equilibrium **(b)**. In the latter case no signal can be found after a single scan. Note the opposite sign but the even better signal to noise ratio (SNR) in the hyperpolarised case (SNR −17.7 **(a)** to 8.6 **(b)**). **(c)** Sketch of the hyperpolarisation mechanism in the picture of CR between a P1 and NV centre (*yellow* and *green* spin). The defect is surrounded by a diffusion barrier (*red*) and a spherical shell of direct coupled ^{13}C spins (*green*). The electronic spin of one defect centre is coupled to a nearby ^{13}C nuclear spin (*blue* spins), which leads to a polarisation transfer to the latter. This polarisation can diffuse in the bulk via the dipolar ^{13}C network. The range of spin diffusion is indicated by the outer sphere (*blue*).

sensitivity for optical temperature monitoring in biological systems. However, the NV centre requires microwave excitation which can cause unwanted heating, and the NV is also sensitive to non-axial magnetic fields, both of which can result in inaccurate temperature measurements. To overcome this drawback, the silicon–vacancy (SiV) and germanium–vacancy (GeV) colour centres in diamonds have recently been explored and have shown good optical temperature sensitivity owing to the temperature dependent wavelength optical zero-phonon line. Here, we report optical temperature measurements using the recently discovered tin–vacancy (SnV) colour centre in diamond and show sensitivity better than 0.2 K in 10 s integration time. Also, we compare the relative merits of SnV with respect to SiV and GeV for luminescent thermometry. These results illustrate that there are likely to be many future options for nanoscale thermometry using diamonds [1].

[1] M. Alkahtani et al.: Appl. Phys. Lett. **112**, 241902 (2018), doi:10.1063/1.5037053

8.9 Screening and engineering of colour centres in diamond

T. Lühmann, N. Raatz, R. John, M. Lesik*, J. Rödiger†, M. Portail‡, D. Wildanger§, F. Kleißler¶, K. Nordlund‖, A. Zaitsev**, J.-F. Roch†, A. Tallaire††‡‡, J. Meijer, S. Pezzagna

[*]Laboratoire Aimé Cotton, CNRS, Université Paris-Sud and Ecole Normale Supérieure de Cachan, Orsay, France
[†]Fraunhofer Heinrich Hertz Institute, Berlin
[‡]Centre de Recherche sur l'Hétéro-Epitaxie et ses Applications, Valbonne, France
[§]Kassel
[¶]Department of NanoBiophotonics, Max Planck Institute for Biophysical Chemistry, Göttingen
[‖]Department of Physics and Helsinki Institute of Physics, University of Helsinki, Helsinki, Finland
[**]The College of Staten Island, City University of New York, Staten Island, NY, USA
[††]Laboratoire des Sciences des Procédés et Matériaux, Université Paris 13, Sorbonne Paris Cité, CNRS, Villetaneuse, France
[‡‡]IRCP Paris, Paris, France

We present a high throughput and systematic method for the screening of colour centres in diamond with the aim of searching for and reproducibly creating new optical centres down to the single defect level, potentially of interest for a wide range of diamond-based quantum applications. The screening method presented here should, moreover, help to identify some already indexed defects among hundreds in diamond [1] but also some promising defects of a still unknown nature, such as the recently discovered ST1 centre [2]. We use ion implantation in a systematic manner to implant several chemical elements. Ion implantation has the advantage of addressing single atoms inside the bulk with defined depth and high lateral resolution, but the disadvantage of producing intrinsic defects. The implanted samples are annealed in vacuum at different temperatures (between 600 ℃ and 1600 ℃ with 200 ℃ steps) and fully characterised at each step in order to follow the evolution of the defects: formation, dissociation, diffusion, re-formation and charge state, at the ensemble level and, if possible, at the single centre level. We review the unavoidable ion implantation defects (such as the GR1 and 3H centres), discuss ion channeling and thermal annealing and estimate the diffusion of the vacancies, N and H. We use different characterisation methods best suited for our study (from widefield fluorescence down to subdiffraction optical imaging of single centres) and discuss reproducibility issues due to diamond and defect inhomogeneities. N is also implanted for reference, taking advantage of the considerable knowledge on nitrogen–vacancy (NV) centres as a versatile sensor in order to retrieve or deduce the conditions and local environment in which the different implanted chemical elements are embedded. We show here the preliminary promising results of a long-term study and focus on the elements O, Mg, Ca, F and P from which fluorescent centres were found [3].

[1] A.M. Zaitsev: *Optical properties of diamond* (Springer, Berlin 2001), doi:10.1007/978-3-662-04548-0
[2] R. John et al.: New J. Phys. **19**, 053008 (2017).
[3] T. Lühmann et al.: J. Phys. D: Appl. Phys. **51**, 483002 (2018), doi:10.1088/1361-6463/aadfab

8.10 Single-photon emitters in lead-implanted single-crystal diamond

S. Ditalia Tchernij[*†], T. Lühmann, T. Herzig, J. Küpper, A. Damin[‡], S. Santonocito[*], M. Signorile[‡], P. Traina[§], E. Moreva[§], F. Celegato[§], S. Pezzagna, I.P. Degiovanni[§], P. Olivero[*†], M. Jakšić[¶], J. Meijer, P.M. Genovese[†§], J. Forneris[†¶]

[*]Physics Department and "NIS" Inter-departmental Centre, University of Torino, Torino, Italy
[†]Istituto Nazionale di Fisica Nucleare (INFN), Sez. Torino, Torino, Italy
[‡]Chemistry Department and "NIS" Inter-departmental Centre, University of Torino, Torino, Italy
[§]Istituto Nazionale di Ricerca Metrologica (INRiM), Torino, Italy
[¶]Ruđer Bošković Institute, Zagreb, Croatia

We report on the creation and characterisation of Pb-related colour centres in diamond upon ion implantation and subsequent thermal annealing. Their optical emission in the photoluminescence (PL) regime consists of an articulated spectrum with intense emission peaks at 552.1 nm and 556.8 nm, accompanied by a set of additional lines in the (535 – 700) nm range. The attribution of the PL emission to stable Pb-based defects is corroborated by the correlation of its intensity with the implantation fluence of Pb ions. PL measurements performed as a function of sample temperature (in the (143 – 300) K range) and under different excitation wavelengths (i.e., 532 nm, 514 nm, 405 nm) suggest that the complex spectral features observed in Pb-implanted diamond might be related to a variety of different defects and/or charge states. The emission of the 552.1 nm and 556.8 nm lines is reported at the single-photon emitter level, demonstrating that they originate from the same individual defect. This work follows from previous reports on optically active centres in diamond based on group-IV impurities, such as Si, Ge, and Sn. In perspective, a comprehensive study of this set of defect complexes could bring significant insight on the common features involved in their formation and opto-physical properties, thus offering a basis for the development of a new generation of quantum-optical devices [1].

[1] S. Ditalia Tchernij et al.: ACS Photonics **5**, 4864 (2018), doi:10.1021/acsphotonics.8b01013

8.11 Photoelectrically detected magnetic resonance on nitrogen–vacancy centres

S. Becker, J. Meijer

To achieve the ambitious goals that were conceived for the nitrogen–vacancy (NV) centre in the field of quantum computation a number of obstacles have to be overcome. One of these obstacles is the read out of the spin state of single NV centres that are located close enough together so that they can interact with each other. The established

optical read out method [1] for NV centres has in addition to its poor collection efficiency additionally the inherent problem that its resolution limit (which is set by the Abbe limit) is notably to high for read out of single centres that are close enough to each other to couple. A photoelectrical read out by photoelectrically detected magnetic resonance (PDMR) like it is shown in [2, 3] has a resolution limit that is low enough to solve the aforementioned problem and in addition has a signifficant higher collection efficiency.

The PDMR mechanism is based on a drop in the generated photocurrent from the NV centres caused by the depopulation of one of the centres spin states by scanning microwaves in an appropriate frequency range. The exploitation of the structure of the energy states makes this possible. The NV centre has a triplet ground and excited state. Situated between them are two metastable singlet state. A photon of appropriate wavelength can excite the centre, lifting an electron into the excited state. If a second photon is absorbed fast enough before the centre decays, the electron is lifted into the conduction band of the diamond, where due to an applied electric field it contributes to a photocurrent that can be detected. If the centre decays before a second photon is absorbed, it will relax either directly to the ground state from where the centre is immediately ready to absorb another photon or over the metastable singlet states. In the latter case the electron is shelved. During this shelving time no other electron can be lifted up and so the centre remains idle. Because the direct decay is preferred by the $ms = 0$ state and the shelving decay by the $m_s = \pm 1$ state, a frequent repetition of this process will lead to a larger contribution to the photocurrent, if the centre is in the $m_s = 0$ state then it being in the $m_s = \pm 1$ state. Since the centres spin state can be controlled by applying microwaves of appropriate frequency this difference in the photocurrent can be detected, and the spin state of the NV centre can be read out. We applied this technique to ensembles of NV centres, where we could measure a contrast in the spectrum of 2.9 % (see Fig. 8.9). This contrast is limited by the background

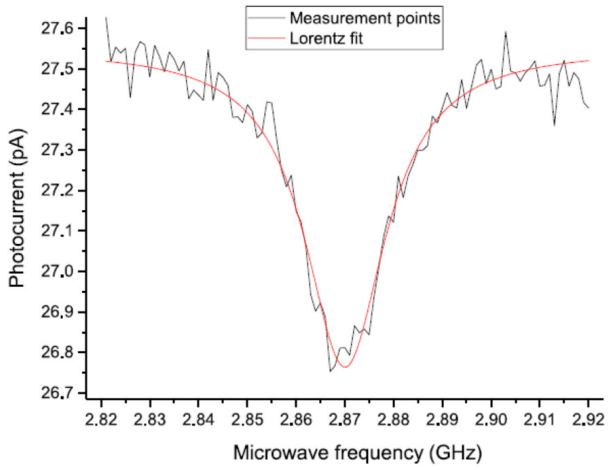

Figure 8.9: Spectrum of a PDMR measurement. Microwave are scanned in a range of 200 MHz around the resonant frequency at which a drop in the photocurrent can be observed.

signal of substitutional N atoms in the diamond as well as by a precise timing of laser and microwave pulses. Using purer samples or suppressing the signal from the substitutional N atoms as well as applying pinpoint pulses to the sample will boost the detection limit to single NV centres. By fabricating contacts in the range of tens of nanometers and a precise NV generation we will be able to scale up quantum logic

gates to a new dimensions.

[1] A. Gruber et al.: Science **276**, 2012 (1997), doi:10.1126/science.276.5321.2012
[2] E. Bourgeois et al.: Nat. Commun. **6**, 8577 (2015), doi:10.1038/ncomms9577
[3] P. Siyushev et al.: Science **363**, 728 (2019), doi:10.1126/science.aav2789

8.12 Funding

Utilization of Ion Accelerators for Studying and Modelling of Radiation Induced Defects in Semiconductors and Insulators
Prof. Dr. J. Meijer
IAEA: CRP F11016

DIAmond Devices Enabled Metrology and Sensing (DIADEMS)
Prof. Dr. J. Meijer
EU: FP7-ICT-2013.9.7 611143

Joint Lab "Einzelionenimplantation": "Sensorik mit einzelnen Atomen"
Prof. Dr. Dr. h.c. B. Rauschenbach/Prof. Dr. J. Meijer
Leibniz-Gemeinschaft/EU

Diamond Materials for Quantum Application: Ultraprecise deterministic doping of diamond
Prof. Dr. J. Meijer
DFG: FOR1493

ECR-Ionenquelle
Prof. Dr. J. Meijer
DFG: HBFG

Kontrollierte Erzeugung von Defekt-Induziertem Magnetismus (DIM) in graphit- und diamantbasierten Filmen
Prof. Dr. J. Meijer/Prof. Dr. P. Esquinazi
DFG: ME 1564/11-1

Quanten und klassische Lichtquellen in Silizium: Verunreinigungen und komplexe Defekte für die Nanophotonik
Dr. S. Pezzagna, Prof. Dr. J. Meijer
DFG: ULYSSES

Leipzig School of Natural Sciences - Building with Molecules and Nano-objects (BuildMoNa)
Prof. Dr. M. Grundmann, Prof. Dr. J. Meijer

Engineering Single Atoms for Quantum Technologies
Prof. Dr. J. Meijer
DAAD: 57319788

Integration of Molecular Components in Functional Macroscopic Systems: Coupling color centers into macroscopic quantum systems with an atomic nano-assembler
Prof. Dr. J. Meijer
VolkswagenStiftung

Functionalized Nanodiamonds for Biomedical Research and Therapy
Prof. Dr. J. Meijer
VolkswagenStiftung

EXMAD – Extreme Sensitive Magnetometry using Nitrogen–Vacancy Centers in Diamond
Prof. Dr. U.L. Andersen/Prof. Dr. J. Meijer
The Danish Council for Strategic Research

Advancing Science and TEchnology thRough dIamond Quantum Sensing (ASTERIQS)
Prof. Dr. Jan Meijer
EU: H2020-FETFLAG-2018-3 820394

Herstellung und Optimierung von Quantenobjekten für die Mikrowellen-Sensorik (MICROSENS)
Prof. Dr. Jan Meijer
BMBF: 16KIS0831

8.13 Organizational Duties

S. Becker

- Session Chair: Annual BuildMoNa Conference, Leipzig, 19.–20.03.2018

J. Meijer

- Member Study Commission (Physics): Faculty of Physics and Earth Sciences, Universität Leipzig
- Member PhD Board: Faculty of Physics and Earth Sciences, Universität Leipzig
- Principal Investigator: Graduate School BuildMoNa, Universität Leipzig
- Member User Selection Panel for the Ion Beam Center: Helmholtz-Zentrum Dresden–Rossendorf
- Member Advisory Board: ISTAC Croatian Nuclear Science
- Session Chair: Diamond Workshop SBDD XXIII, Hasselt, Belgium, 07.–09.03.2018
- International Organising Committee: 16th International Conference on Nuclear Microprobe Technology and Applications, Guildford, Surrey, UK, 08.–13.07.2018
- Referee: Several journals

S. Pezzagna

- Referee: Several journals

P. Räcke

- Speaker Doctoral Candidates Committee: Graduate School BuildMoNa, Universität Leipzig
- Doctoral representative: Graduate Centre Mathematics/Computer Science and Natural Sciences, Research Academy Leipzig, Universität Leipzig

- Session Chair: Annual BuildMoNa Conference, Leipzig, 19.–20.03.2018

8.14 External Cooperations

Academic

- City University of New York, College of Staten Island, Department of Engineering Science and Physics, USA
  Assoc. Prof. Dr. A.M. Zaitsev
- Centre National de la Recherche Scientifique (CNRS), École normale supérieure (ENS), Laboratoire Aimé Cotton (LAC), Cachan, France
  Prof. Dr. J.-F. Roch
- Centre National de la Recherche Scientifique (CNRS), Laboratoire des Sciences des Procédés et des Matériaux (LSPM), Fabrication Processes of Advanced Materials (PEMA), Paris, France
  Prof. Dr. J. Achard
- Commissariat à l'énergie atomique et aux énergies alternatives (CEA), Institut Rayonnement Matière de Saclay (IRAMIS), Service de Physique de l'Etat Condensé (SPEC), Quantronique, Saclay, France
  Prof. Dr. D. Esteve
- ETH Zürich, Physikdepartement, Laboratorium für Festkörperphysik, Spin Physics and Imaging, Switzerland
  Prof. Dr. C. Degen
- Fraunhofer-Institut für Angewandte Festkörperphysik Freiburg, Mikro- und Nanosensoren
  Dr. C.E. Nebel
- Humboldt-Universität zu Berlin, Mathematisch-Naturwissenschaftliche Fakultät I, Institut für Physik, AG Nanooptik
  Prof. Dr. O. Benson
- Hungarian Academy of Sciences, Wigner Research Centre for Physics, Institute for Solid State Physics and Optics, Budapest, Hungaria
- Interuniversitair Micro-Electronica Centrum (imec) Leuven, Belgium
- Julius-Maximilians-Universität Würzburg, Fakultät für Chemie und Pharmazie, Institut für Organische Chemie
  Prof. Dr. A. Krüger
- Leibniz-Institut für Oberflächenmodifizierung e.V. Leipzig
  Prof. Dr. Dr. h.c. B. Rauschenbach, Prof. Dr. B. Abel
- Leibniz-Universität Hannover, Institut für Anorganische Chemie, AK Analytik
  Prof. Dr. C. Vogt
- Ludwig-Maximilians-Universität München, Fakultät für Physik, Experimentelle Quantenphysik
  Prof. Dr. H. Weinfurter
- Max-Planck-Institut für biophysikalische Chemie Göttingen, Karl-Friedrich-Bonhoeffer-Institut, Abt. NanoBiophotonik
  Prof. Dr. Dr. h.c. St.W. Hell

- Technische Universität München, Walter Schottky Institut, E25: Spins and Defects in Semiconductors
  Prof. Dr. M.S. Brandt
- Università di Torino, Dipartimento di Fisica Sperimentale, Gruppo di Fisica dello Stato Solido
  Prof. Dr. E. Vittone
- Universität Basel, Department of Physics, Quantum-Sensing Lab, Switzerland
  Prof. Dr. P. Maletinsky
- Universität Kassel
- Universität Konstanz, Mathematisch-Naturwissenschaftliche Sektion, Fachbereich Physik, Lehrstuhl für Ultrakurzzeitphysik und Photonik
  Prof. Dr. A. Leitenstorfer
- Universität Leipzig, Medizinische Fakultät, Institut für Medizinische Physik und Biophysik
  Prof. Dr. E. Donath, Dr. I. Estrela-Lopis, Priv.-Doz. Dr. U. Reibetanz
- Universität Mainz, Fachbereich Physik, Mathematik und Informatik, Institut für Physik, Arbeitsgruppe Quanten-, Atom- & Neutronenphysik (QUANTUM)
  Prof. Dr. F. Schmidt-Kaler, Priv.-Doz. Dr. K. Singer
- Universität Stuttgart, Fakultät Mathematik und Physik, 3. Physikalisches Institut
  Prof. Dr. J. Wrachtrup
- Universität Ulm, Fakultät für Naturwissenschaften, Institut für Quantenoptik
  Prof. Dr. F. Jelezko
- Universität Ulm, Fakultät für Naturwissenschaften, Institut für Theoretische Physik, Controlled Quantum Dynamics Group
  Prof. Dr. M.B. Plenio
- University of Warwick, Department of Physics, Condensed Matter Physics, Magnetic Resonance Cluster, Coventry, UK
  Prof. Dr. M. Newton
- Universität Wien
- Westfälische Wilhelms-Universität Münster, Physikalisches Institut
  Prof. Dr. R. Bratschitsch

Industry

- ARTTIC Paris, France
- attocube systems AG München
- Element Six Ltd. Shannon, Co. Clare, Ireland
- THALES Research & Technology Palaiseau, France

8.15 Publications

Journals

M. Alkahtani, I. Cojocaru, X. Liu, T. Herzig, J. Meijer, J. Küpper, T. Lühmann, A.V. Akimov, P.R. Hemmer: *Tin-vacancy in diamonds for luminescent thermometry*, Appl. Phys. Lett. **112**, 241902:1–5 (2018)
doi:10.1063/1.5037053

C. Beaufils, W. Redjem, E. Rousseau, V. Jacques, A.Y. Kuznetsov, C. Raynaud, C. Voisin, A. Benali, T. Herzig, S. Pezzagna, J. Meijer, M. Abbarchi, G. Cassabois: *Optical properties of an ensemble of G-centers in silicon*, Phys. Rev. B **97**, 035303:1–12 (2018)
doi:10.1103/PhysRevB.97.035303

S. Becker, N. Raatz, St. Jankuhn, R. John, J. Meijer: *Nitrogen implantation with a scanning electron microscope*, Sci. Rep. **8**, 32:1–6 (2018)
doi:10.1038/s41598-017-18373-z

M. Brueckner, St. Jankuhn, E.-M. Jülke, U. Reibetanz: *Cellular interaction of a layer-by-layer based drug delivery system depending on material properties and cell types*, Int. J. Nanomed. **13**, 2079–2091 (2018)
doi:10.2147/ijn.s153701

S. Ditalia Tchernij, T. Lühmann, T. Herzig, J. Küpper, A. Damin, S. Santonocito, M. Signorile, P. Traina, E. Moreva, F. Celegato, S. Pezzagna, I. Degiovanni, P. Olivero, M. Jakšić, J. Meijer, P. Genovese, J. Forneris: *Single-photon emitters in lead-implanted single-crystal diamond*, ACS Photonics **5**, 4864–4871 (2018)
doi:10.1021/acsphotonics.8b01013

R. Ganassin, C. Merker, M.C. Rodrigues, N.F. Guimarães, C.S.C. Sodré, Q. da Silva Ferreira, S.W. da Silva, A.S. Ombredane, G.A. Joanitti, K.R. Py-Daniel, J. Zhang, C.-S. Jiang, P.C. de Morais, E. Mosiniewicz-Szablewska, P. Suchocki, J.P.F. Longo, J. Meijer, I. Estrela-Lopis, R.B. de Azevedo, L.A. Muehlmann: *Nanocapsules for the co-delivery of selol and doxorubicin to breast adenocarcinoma 4T1 cells in vitro*, Artificial Cells, Nanomedicine, and Biotechnology **46**, 2002–2012 (2018)
doi:10.1080/21691401.2017.1408020

S. Grawe, S. Augustin-Bauditz, H.-C. Clemen, M. Ebert, S.E. Hammer, J. Lubitz, N. Reicher, Y. Rudich, J. Schneider, R. Staacke, F. Stratmann, A. Welti, H. Wex: *Coal fly ash: linking immersion freezing behavior and physicochemical particle properties*
Atmos. Chem. Phys. **18**, 13903–13923 (2018), doi:10.5194/acp-18-13903-2018

P. Happel, T. Waag, M. Schimke, S. Schweeberg, A. Muzha, K. Fortak, D. Heesch, L. Klask, M. Pilscheur, F. Hoppe, T. Lenders, J. Meijer, G. Lepperdinger, A. Krueger: *Intrinsically ^{32}P-Labeled Diamond Nanoparticles for In Vivo Imaging and Quantification of Their Biodistribution in Chicken Embryos*, Adv. Funct. Mater. **28**, 1802873:1–9 (2018)
doi:10.1002/adfm.201802873

D. Heesch, D. Rogalla, T. Lenders, J. Meijer, P. Happel: *Implantation of defined activities of phosphorus 32 with reduced target damage*, Rev. Sci. Instrum. **89**, 113304:1–5 (2018)
doi:10.1063/1.5019014

B. Krause, T. Meyer, H. Sieg, C. Kästner, P. Reichardt, J. Tentschert, H. Jungnickel, I. Estrela-Lopis, A. Burel, S. Chevance, F. Gauffre, P. Jalili, J. Meijer, L. Böhmert, A. Braeuning, A.F. Thünemann, F. Emmerling, V. Fessard, P. Laux, A. Lampen, A. Luch: *Characterization of aluminum, aluminum oxide and titanium dioxide nanomaterials using a combination of methods for particle surface and size analysis*, RSC Adv. **8**, 14377–14388 (2018)
doi:10.1039/c8ra00205c

T. Lühmann, N. Raatz, R. John, M. Lesik, J. Rödiger, M. Portail, D. Wildanger, F. Kleißler, K. Nordlund, A. Zaitsev, J.-F. Roch, A. Tallaire, J. Meijer, S. Pezzagna: *Screening and engineering of colour centres in diamond*, J. Phys. D: Appl. Phys. **51**, 483002:1–24 (2018)
doi:10.1088/1361-6463/aadfab

P. Räcke, D. Spemann, J.W. Gerlach, B. Rauschenbach, J. Meijer: *Detection of small bunches of ions using image charges*, Sci. Rep. **8**, 9781:1–10 (2018)
doi:10.1038/s41598-018-28167-6

Y. Schlussel, T. Lenz, D. Rohner, Y. Bar-Haim, L. Bougas, D. Groswasser, M. Kieschnick, E. Rozenberg, L. Thiel, A. Waxman, J. Meijer, P. Maletinsky, D. Budker, R. Folman: *Wide-Field Imaging of Superconductor Vortices with Electron Spins in Diamond*, Phys. Rev. Appl. **10**, 034032:1–6 (2018)
doi:10.1103/physrevapplied.10.034032

T. Unden, N. Tomek, T. Weggler, F. Frank, P. London, J. Zopes, C. Degen, N. Raatz, J. Meijer, H. Watanabe, K.M. Itoh, M.B. Plenio, B. Naydenov, F. Jelezko: *Coherent control of solid state nuclear spin nano-ensembles*, npj Quantum Inf. **4**, 39:1–6 (2018)
doi:10.1038/s41534-018-0089-8

L. Veith, J. Böttner, A. Vennemann, D. Breitenstein, C. Engelhard, J. Meijer, I. Estrela-Lopis, M. Wiemann, B. Hagenhoff: *Detection of ZrO_2 Nanoparticles in Lung Tissue Sections by Time-of-Flight Secondary Ion Mass Spectrometry and Ion Beam Microscopy*, Nanomaterials **8**, 44:1–15 (2018)
doi:10.3390/nano8010044

A.M. Wojciechowski, M. Karadas, A. Huck, C. Osterkamp, St. Jankuhn, J. Meijer, F. Jelezko, U.L. Andersen: *Camera-limits for wide-field magnetic resonance imaging with a nitrogen-vacancy spin sensor*, Rev. Sci. Instrum. **89**, 031501:1–8 (2018)
doi:10.1063/1.5010282

A.M. Wojciechowski, M. Karadas, C. Osterkamp, St. Jankuhn, J. Meijer, F. Jelezko, A. Huck, U.L. Andersen: *Precision temperature sensing in the presence of magnetic field noise and vice-versa using nitrogen-vacancy centers in diamond*, Appl. Phys. Lett. **113**, 013502:1–5 (2018)
doi:10.1063/1.5026678

R. Wunderlich, J. Kohlrautz, B. Abel, J. Haase, J. Meijer: *Investigation of room temperature multispin-assisted bulk diamond ^{13}C hyperpolarization at low magnetic fields*, J. Phys.: Condens. Matter **30**, 305803:1–6 (2018)
doi:10.1088/1361-648x/aacc32

Z. Yang, F. Shi, P. Wang, N. Raatz, R. Li, X. Qin, J. Meijer, C. Duan, C. Ju, X. Kong, J. Du: *Detection of magnetic dipolar coupling of water molecules at the nanoscale using quantum magnetometry*, Phys. Rev. B **97**, 205438:1–6 (2018)
doi:10.1103/physrevb.97.205438

Talks

C. Beaufils, W. Redjem, E. Rousseau, V. Jacques, A. Yu Kuznetsov, C. Raynaud, C. Voisin, A. Benali, T. Herzig, S. Pezzagna, J. Meijer, M. Abbarchi, G. Cassabois
Optical Properties of an Ensemble of G-Centers in Silicon
16th International Conference on Nuclear Microprobe Technology and Applications, Guildford, Surrey, UK, 08.–13.07.2018

S. Becker, N. Raatz, S. Jankuhn, R. John, J. Meijer
Production of nitrogen vacancy centres with a scanning electron microscope
Diamond Workshop SBDD XXIII, Hasselt, Belgium, 07.–09.03.2018

S. Becker, N. Raatz, S. Jankuhn, R. John, J. Meijer
Nitrogen Implantation with a Scanning Electron Microscope
16th International Conference on Nuclear Microprobe Technology and Applications, Guildford, Surrey, UK, 08.–13.07.2018

S. Ditalia Tchernij, F. Picollo, P. Traina, E. Moreva, I.P. Degiovanni, T. Herzig, J. Küpper, S. Pezzagna, G. Prestopino, M. Marinelli, E. Milani, C. Verona, G. Verona-Rinati, N. Skukan, M. Jakšić, M. Genovese, J. Meijer, P. Olivero, J. Forneris
Formation of novel optical centers in diamond upon ion implantation and annealing
Diamond Workshop SBDD XXIII, Hasselt, Belgium, 07.–09.03.2018

A.M. Jakob, V. Schmitt, B.C. Johnson, V. Mourik, S.G. Robson, P. Räcke, F. Stopp, K. Groot-Berning, A. Morello, J. Meijer, D. Spemann, F. Schmidt-Kaler, D.N. Jamieson
High Precision Deterministic Ion Implantation for Large-Scale Arrays of Single Donor Qubits in Silicon
Silicon Quantum Electronics Workshop, Sydney, Australia, 13.–15.11.2018

D. Lehmann
Die Atombombe — sieben Etappen von einer Utopie zum Sündenfall der Physik
Seminar, Arnold-Sommerfeld-Gesellschaft e. V., Leipzig, 15.02.2018, invited

L. Mayer, T. Debuisschert, A. Tallaire, J. Achard, S. Pezzagna, J. Meijer, L. Toraille, M. Lesik, L. Rondin, J.-F. Roch
Magnetic Sensing with Nitrogen-Vacancy Centers in Diamond
Journées Science et Progrès de la F2S: Les technologies quantiques: En route vers les applications, Paris, France, 11.01.2018

J. Meijer
A scheme to realize a quantum computer based on coupled NV *and P1 centers in diamond*
5th International Conference on Time Series and Forecasting, Granada, Spain, 19.–21.09.2018, invited

J. Meijer
Interaction of a SSQ with Light and Quantum Error Correction
Adiabatic Quantum Computing and Quantum Simulation
Deterministic Single Ion Implanation Based on Predetection Methods
SRIM/CSRIM Simulations
Joint ICTP-IAEA Advanced School on Ion Beam Driven Materials Engineering: Accelerators for a New Technology Era (smr 3236), Trieste, Italy, 01.–05.10.2018, invited

S. Pezzagna, J. Meijer
Technological challenges to create solid state quantum devices in diamond
Diamond Workshop SBDD XXIII, Hasselt, Belgium, 07.–09.03.2018, invited

N. Raatz, T. Lühmann, R. John, J. Meijer, S. Pezzagna
Colour centres implanted in CVD and HPHT IIa diamonds: do hydrogen play a role?
European Materials Research Society Fall Meeting, Warsaw, Poland, 17.–20.09.2018

P. Räcke
Deterministic ion implantation: how to count single ions
Annual Conference of the Graduate School BuildMoNa, Leipzig, 19.–20.03.2018

P. Räcke, D. Spemann, J.W. Gerlach, B. Rauschenbach, J. Meijer
A Concept for Deterministic Ion Implantation by Image Charge Detection
16th International Conference on Nuclear Microprobe Technology and Applications, Guildford, Surrey, UK, 08.–13.07.2018

Posters

T. Herzig, N. Raatz, J. Meijer, G. Cassabois, M. Abbarchi, S. Pezzagna
Creation of quantum light sources in silicon using spatial selective ion implantation of high lateral resolution
22nd International Conference on Ion Implantation Technology, Würzburg, 16.–21.09.2018

R. John, J. Meijer
Possible coupling of implanted europium to nitrogen vacancy centres in diamond
Diamond Workshop SBDD XXIII, Hasselt, Belgium, 07.–09.03.2018

R. John, J. Meijer
Possible coupling of implanted europium to nitrogen vacancy centres in diamond
Annual Conference of the Graduate School BuildMoNa, Leipzig, 19.–20.03.2018

P. Räcke, J.W. Gerlach, B. Rauschenbach, S. Robson, A.M. Jakob, D.N. Jamieson, J. Meijer, D. Spemann
Status Report of a Deterministic Ion Implantation System for Large-Scale Dopant Array Engineering in Arbitrary Substrates
Silicon Quantum Electronics Workshop, Sydney, Australia, 13.–15.11.2018

S.G. Robson, P. Räcke, A.M. Jakob, D. Spemann, V. Mourik, V. Schmitt, B.C. Johnson, J.C. McCallum, J. Meijer, A. Morello, D.N. Jamieson
Deterministic ion implantation at room temperature for large-scale Si : P *quantum*

computing devices
Silicon Quantum Electronics Workshop, Sydney, Australia, 13.–15.11.2018

C. Scheuner, N. Raatz, P. Räcke, S. Jankuhn, S. Pezzagna, C. Trautmann, J. Meijer
Development of Nano Apertures for Ion Beam Collimation
16th International Conference on Nuclear Microprobe Technology and Applications, Guildford, Surrey, UK, 08.–13.07.2018

I. Weigelt, K. Reimann, E. Kirilina, J. Meijer, S. Jankuhn, T. Arendt, M. Morawski
Quantification and cellular localization of iron in brain of patients with Parkinson's disease and age-matched controls
14th Leipzig Research Festival for Life Sciences, Leipzig, 19.01.2018

V. Zviagin, P. Huth, C. Sturm, D. Spemann, S. Mändl, J. Lenzner, A. Setzer, J. Meijer, R. Denecke, P. Esquinazi, M. Grundmann, R. Schmidt-Grund
Optical and Magnetic Properties of Spinel Type Ferrites in Relation to their Crystallographic Order
DPG-Frühjahrstagung, Berlin, 11.–16.03.2018

Patents

B. Burchard, P.D. Esquinazi, J. Meijer
Graphit-Supraleiter und dessen Anwendung
WO 2018/185306 A1

8.16 Awards

T. Herzig
Best Student Poster
22nd International Conference on Ion Implantation Technology, Würzburg, 16.–21.09.2018

P. Räcke
First Presentation Prize
Annual Conference of the Graduate School BuildMoNa, Leipzig, 19.–20.03.2018

C. Scheuner
Best Poster Prize
16th International Conference on Nuclear Microprobe Technology and Applications, Guildford, Surrey, UK, 08.–13.07.2018

R. Wunderlich
Felix Bloch Early Investigator Award
Universität Leipzig, Felix Bloch Institute for Solid State Physics, 23.10.2018

8.17 Graduations

Doctorate

- R. Wunderlich
  Nukleare Hyperpolarisation im Diamanten mittels Stickstoff-Fehlstellen-Zentren und komplexer Vier-Spin-Kopplung
  February 2018

Bachelor

- K. Pavlov
  Ion beam optics simulation and experimental comparison of the 3 MeV LIPSION accelerator in Leipzig
  March 2018

8.18 Guests

- Prof. Dr.-Ing. P. Glösekötter
  Fachhochschule Münster, Fachbereich Elektrotechnik und Informatik, Steinfurt
  22.10.2018
- D. Holmes
  University of Melbourne, Faculty of Science, School of Physics, Experimental Condensed Matter Physics, Parkville, VIC, Australia
  09.09.–05.10.2018
- Assoc. Prof. R. Ishihara
  Delft University of Technology, Faculty of Electrical Engineering, Mathematics and Computer Science, Department of Quantum & Computer Engineering, Quantum Integration Technology; QuTech, Delft, The Netherlands
  09.05.2018
- Dr. A.M. Jacob
  University of Melbourne, Faculty of Science, School of Physics, Experimental Condensed Matter Physics, Parkville, VIC, Australia
  20.07.–27.08.2018
- Prof. Dr. F. Jelezko
  Universität Ulm, Fakultät für Naturwissenschaften, Institut für Quantenoptik
  06./07.05.2018
- S. Robson
  University of Melbourne, Faculty of Science, School of Physics, Experimental Condensed Matter Physics, Parkville, VIC, Australia
  06.08.–06.09.2018
- Prof. Dr. D. Suter
  Technische Universität Dortmund, Fakultät Physik, Experimentelle Physik III, Hochauflösende Spektroskopie
  16.–18.07.2018

- Dr. A. Wickenbrock
  Johannes-Gutenberg-Universität Mainz, Fachbereich Physik, Mathematik und Informatik, Institut fü r Physik, Quanten-, Atom- und Neutronenphysik (QUANTUM), AG Budker; Helmholtz-Institut Mainz
  06./07.05.2018
- Prof. Dr. J. Wrachtrup
  Universität Stuttgart, Fakultät Mathematik und Physik, 3. Physikalisches Institut
  06./07.05.2018

9

Semiconductor Physics

9.1 Introduction

Our research report gives you a summery of the recent activities and discoveries of the Semiconductor Physics group. We hope it finds your interest and gives you a scientific stimulus. Among others, you will find novel findings on fundamental aspects of optical activity and the gyrotropy tensor using KTP as model material, ultrafast time-resolved ellipsometry on ZnO, sesquioxide alloys and strained heterostructures in the $(In,Al,Ga)_2O_3$ system and experimental evidence for exceptional 'Voigt' points and their topology in anisotropic ZnO-based microcavities among other topics.

A highlight of the year was the first Felix Bloch Lecture Leipzig on "Controlling Spin Dynamics with Light" delivered by Prof. Theo Rasing from the Institute of Molecules and Materials of Radboud University Nijmegen. Afterwards, a bronze plate with the portrait of Felix Bloch by Leipzig sculptor Markus Gläser was unveiled in the foyer of the physics building in the presence of Felix Bloch's son Frank and grandson Elias.

We have developed and experimentally investigated our theory of pseudomorphic

strain in heterostructures with arbitrary interface orientation for rhombohedral/trigonal (and thus also hexagonal) and monoclinic (and thus also orthorhombic, tetragonal and cubic) crystal classes.

This is of particular relevance for $(Al,Ga)_2O_3$ layers on (monoclinic) β-Ga_2O_3 and (rhombohedral) α-Al_2O_3 substrates. The pulsed laser deposition used for the fabrication of such heterostructures has been ameliorated with the concept of continuous vertical composition spreads through the use of elliptically segmented targets (Chap. 9.2); for this work Max Kneiß has received the BuildMoNa Award 2019 (first prize).

We like to draw your attention to the fact that a long-standing issue has been solved within a fruitful cooperation with Humboldt Universität. The Schottky contact between a noble metal oxide (PtO_x) and an oxide semiconductor (zinc-tin-oxide, ZTO) is indeed proven to be of Schottky-type since due to reduction of the noble metal oxide, the contact contains a pure metal layer. Connected to the role of oxygen vacancies is a long paper summarizing many years of DLTS research on the E3 level in ZnO.

We are largely indebted to our funding agencies in particular Deutsche Forschungsgemeinschaft (DFG). We are grateful for the continued funding of Sonderforschungsbereich SFB 762 "Functionality of Oxide Interfaces" that runs in its final period (2016–2019) and our project on nanowire heterostructures in the Forschergruppe FOR 1616 "Nanowire Optoelectronics" which has concluded by now (2015–2018). Sächsische Aufbaubank (SAB) is supporting our efforts on combinatorial pulsed laser deposition within the new project COSIMA (2017–2020) that has enriched our group with a Müller matrix ellipsometer, a low-temperature Hall effect wafer prober and a new laboratory for combinatorial pulsed laser deposition. Our project on flexible oxide electronic circuits is funded in the DFG SPP FFLexCom (SPP 1796) and has been renewed (2015–2021). Work has begun in the ZONE project on (Mg,Zn)(O,N) thin films in a joint ANR-DFG project together with CNRS-CRHEA, Valbonne. The work of our students, researchers and guests together with our academic and industrial partners near and far was fruitful and enjoyable and thus it is with great pleasure that the Semiconductor Physics Group presents their progress report.

Leipzig,
March 2019

Marius Grundmann

9.2 Pulsed laser deposition with radially segmented targets for compositional gradients in growth direction

M. Kneiß, P. Storm, G. Benndorf, M. Grundmann, H. von Wenckstern

For researchers growing and studying functional layers, the precise control of the composition of thin film in devices is highly desired. Be it impurity doping for conductivity control, ternary alloy compositions for devices utilizing heterostructures, such as quantum-well LEDs or infrared photodetectors as well as MODFETS, or composition graded buffer layers to compensate for lattice mismatches towards cost-effective substrate materials [1]. Pulsed laser deposition (PLD) is a powerful tool for the growth of highly crystalline thin film layers mostly transferring the stoichiometry of the employed target material to the layer deposited. Therefore, to induce a variation of the thin film composition, the composition of particle flux needs to be adjustable, which is an established method for techniques such as molecular beam epitaxy or metal-organic chemical vapor deposition. In PLD, this requires the use of a different target or complicated multi-beam [2] or mirror setups [3].

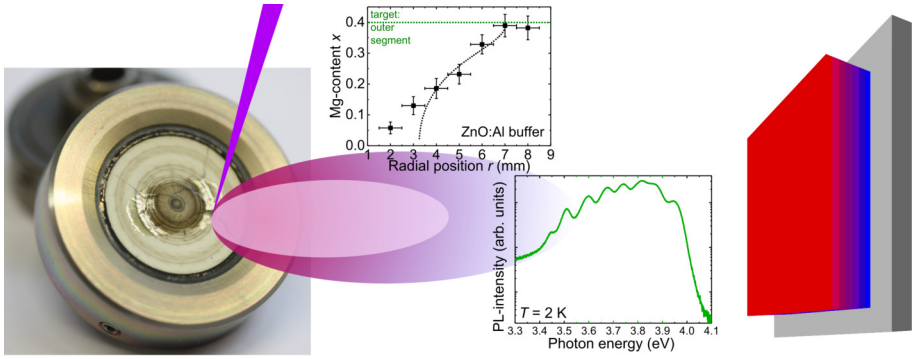

Figure 9.1: Elliptically-segmented $Mg_{0.4}Zn_{0.6}O$/ZnO target used in this study after several depositions. The schematic on the right shows the variation of the Mg content in growth direction. The inset graphics show the low-temperature photoluminescence spectrum of such a composition-graded thin film and the incorporated Mg-content in dependence on the radial position of the laser spot on the target determined for homogeneous layers.

Until now, the variation of the particle flux composition was not possible in PLD by ablating a single target only, not to speak of a continuous composition grading in growth direction of a thin film. We already have reported about a continuous composition spread technique employing segmented targets that resulted in a lateral composition variation on the substrate wafer [4]. However, thin films with a well-defined and controllable composition as well as composition gradients in growth direction are not possible with this technique. Both of these issues can be addressed by an approach employing radially-segmented targets which we have developed [5], in particular we use elliptically-segmented targets where the inner segment has a different composition than the outer segment, see also Figs. 9.1 and 9.2.

In our standard PLD approach, the target would be rotated and the radial position of the laser spot on the target surface changed continuously to ensure a homogeneous ablation of the target surface. For the novel technique, we fix the radial position of

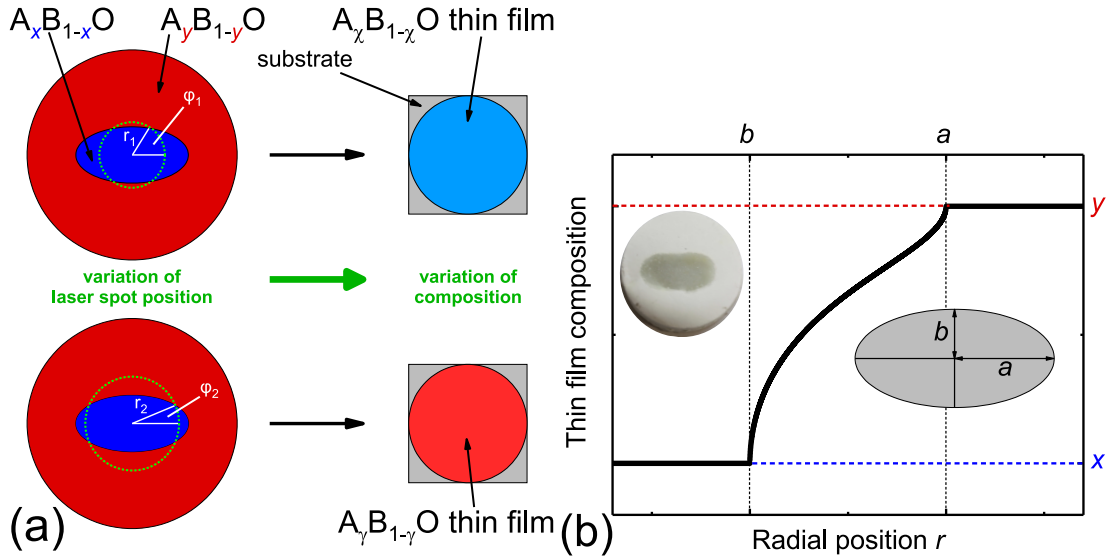

Figure 9.2: (a) Schematic depiction of the increase of path length ratio of the track of the laser spot in the outer segment to the inner segment when the radial position of the laser spot is increased from r_1 to r_2 on a rotating target. The corresponding change in the average particle flux composition in the PLD plasma results in different thin film compositions χ and γ for the two radial positions. (b) Expected thin film composition in dependence on the radial position r of the laser spot on the target assuming an ideal point-like laser spot and stoichiometric transfer of the target material. The inset shows the $Mg_{0.4}Zn_{0.6}O$/ZnO target prior to deposition.

the laser spot such that the laser ablates a circular track on the target surface, see also Fig. 9.2 (a). The laser now ablates alternatingly the outer and the inner segment of the target, such that the particle flux composition is changing constantly between the stoichiometry of outer and inner segment. The thin film composition resulting from this circular ablation is given by the time-average of the particle flux composition, which in turn is given by the path length ratio of the laser spot between outer and inner segment of the target. Calculating the expected thin film composition theoretically, assuming an ideal point-like laser spot and a stoichiometric transfer from the target, gives the curve displayed in Fig. 9.2 (b) enabling a continuous variation of the thin film composition. This both enables the deposition of homogeneous thin films with any desired cation ratio between that of the inner and outer segment as well as the growth of layers with a composition gradient in growth direction when the radial position is varied in-situ. We therefore call this technique vertical continuous composition spread (VCCS). We employed an elliptically-segmented $Mg_{0.4}Zn_{0.6}O$/ZnO target (shown in the inset in Fig. 9.2 (b) prior to and in Fig. 9.1 after several depositions). We have grown both homogeneous $Mg_xZn_{1-x}O$ thin films with a thickness of ≈ 40 nm on Al-doped ZnO buffer layers as well as layer systems with a step-graded composition variation in growth direction. We could show that we can vary the Mg-content in the thin films within the whole composition range of the target with reasonable agreement of the radial dependence to the model theory, see Fig. 9.3 (a). From low-temperature photoluminescence (PL) measurements, it was further confirmed that a homogeneous distribution of Mg-atoms in the layers occurred. The broadening of the excitonic emission of the alloy layers (Fig. 9.3 (b)) is similar to thin films grown by conventional PLD, literature data and model curves. X-ray diffraction and atomic force microscopy confirmed similar struc-

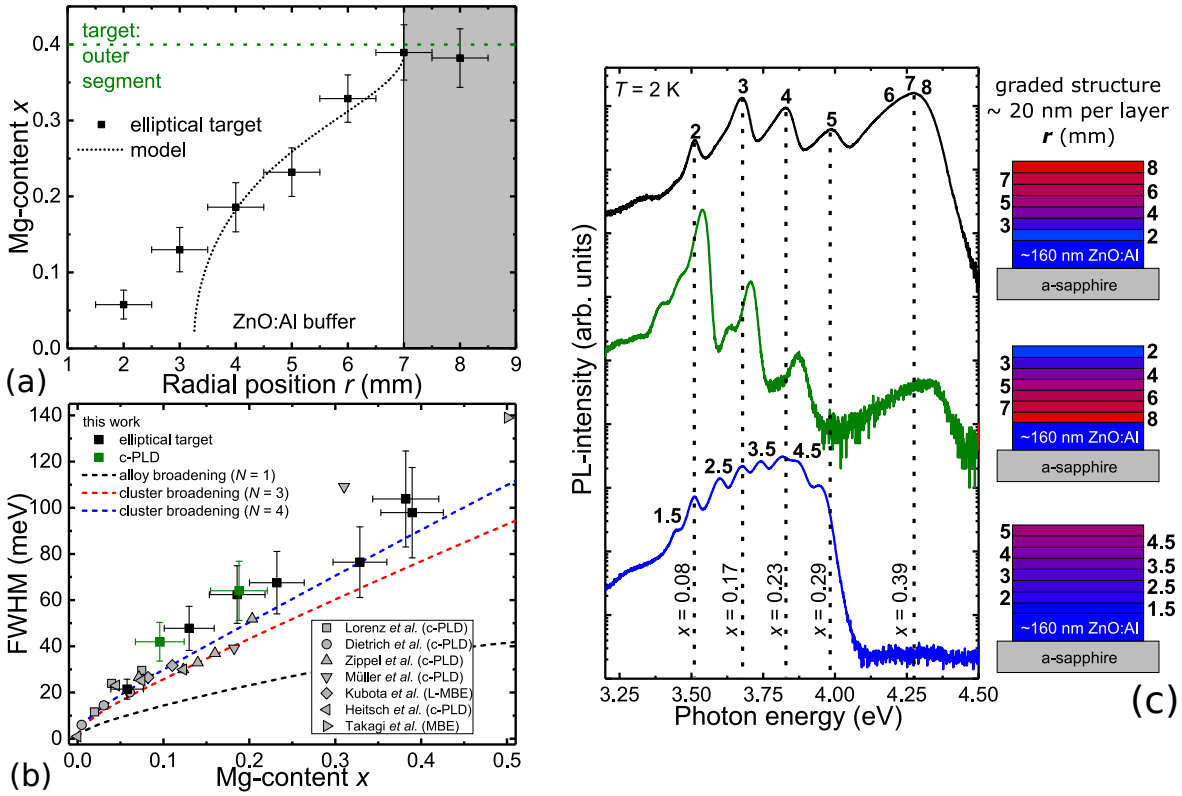

Figure 9.3: (a) Mg-content x of homogeneous $Mg_xZn_{1-x}O$ layers on Al-doped ZnO buffer layers in dependence on the radial position r. The ideal model curve of the expected composition is given as black dashed line. (b) Broadening (full width at half maximum FWHM) of the excitonic emission peak in low-temperature PL spectra of the homogeneous layers in dependence on their Mg-content and in comparison to literature values [6–12] as well as samples grown by conventional PLD. Dashed lines are theoretical models for alloy broadening. (c) Low temperature PL spectra of thin films with composition gradient in growth direction. Schematic of the structures are given next to the spectra with the corresponding value of r for each layer.

tural and surface quality of our layers compared to conventional PLD (not shown). In low-temperature PL measurements of the step-graded $Mg_xZn_{1-x}O$ thin films, excitonic emission peaks could be identified for each layer (Fig. 9.3 (c)). Their energetic positions are in agreement with the expected Mg-content for the respective radial positions. Even narrow graded thin films with well-pronounced emission peaks corresponding to each layer in the structure are possible (Fig. 9.3 (c) lowest curve). Therefore, a significant diffusion of Mg-atoms between the single layers can be excluded. With this, we have clearly demonstrated that we have developed a practically applicable PLD technique for the growth of homogeneous layers with any desired composition as well as composition gradients in growth direction. Since nearly any alloy system or impurity dopant is within the reach of this technique, there are numerous applications possible, such as strain engineering, dopant profiling, the creation of discrete material libraries or precise band gap engineering for heterostructures.

[1] Inoue *et al.*, IEEE Trans. Electron Devices **55**, 483 (2008)
[2] Eason *et al.*, J. Phys. D: Appl. Phys. **47**, 034007 (2014)
[3] Fischer *et al.*, Rev. Sci. Instrum. **83**, 043901 (2012)

[4] von Wenckstern *et al.*, CrystEngComm **15**, 10020 (2013)
[5] Kneiß *et al.*, ACS Comb. Sci. **20**, 643 (2018)
[6] Takagi *et al.*, Jpn. J. Appl. Phys. **42**, L401 (2003)
[7] Heitsch *et al.*, J. Appl. Phys. **101**, 083521 (2007)
[8] Müller *et al.*, J. Appl. Phys. **107**, 013704 (2010)
[9] Kubota *et al.*, Appl. Phys. Lett. **90**, 141903 (2007)
[10] Lorenz *et al.*, Thin Solid Films **518**, 4623 (2010)
[11] Zippel *et al.*, J. Lumin. **130**, 520 (2010)
[12] Dietrich *et al.*, New J. Phys. **12**, 033030 (2010)

9.3 Strain in pseudomorphic rhombohedral/trigonal heterostructures

M. Grundmann

Epitaxial heterostructures are the basis of basically all modern devices. Generally, they involve materials with different lattice constants, leading to pseudomorphic strain for layer thickness below the onset of plastic relaxation. First this has been investigated for cubic materials, such as silicon and III-V semiconductors, also representing the simplest case. Then, wurtzite-based heterostructures were investigated for GaN- and ZnO-based heterostructures; here polar, non-polar and semi-polar directions arise [1]. Recently, monoclinic heterostructures based on β-Ga_2O_3 were theoretically treated by us [2].

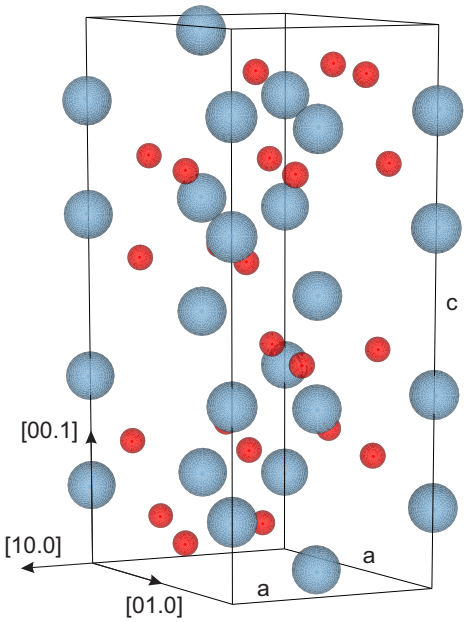

Figure 9.4: One sixth of the hexagonal unit cell of rhombohedral α-Al_2O_3 (oxygen atoms are shown in red, aluminum atoms in blue). The crystal directions and lattice constants are indicated. Figure prepared with VESTA [4].

Here, we discuss pseudomorphic heterostructures of corundum-structure materials, i.e. in particular rhombohedral, α-phase $(Al,Ga)_2O_3$ layers on alumina [3]. The usual unit cell of alumina is depicted in Fig. 9.4.

We have calculated analytically, in the framework of linear elastic continuum theory, the epitaxial in-plane and out-of-plane strain components for pseudomorphic growth of rhombohedral heterostructures for all substrate orientations, including the c-, a-, m-, n-, and r-planes [3]. Numerical examples were given for the sesquioxide semiconductor system of Al-rich $(Al,Ga)_2O_3/Al_2O_3$. From the deformation of the unit cell, various X-ray peak positions and lattice plane tilts have been calculated. In Fig. 9.5 the r-plane (out-of-plane) lattice constant is depicted for pseudomorphic and fully relaxed growth on r-plane alumina.

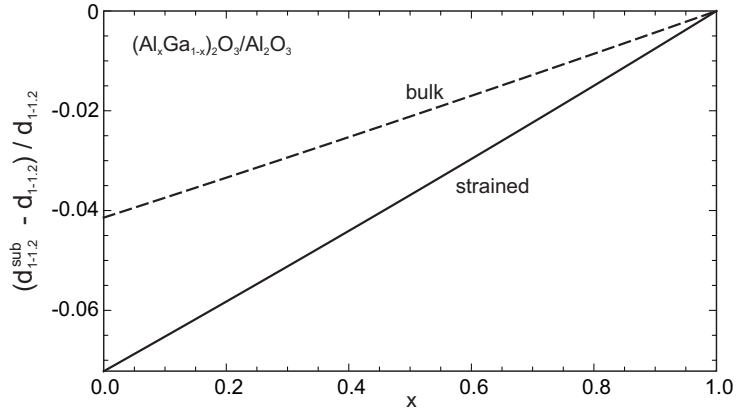

Figure 9.5: Bulk/relaxed and pseudomorphically strained r-plane (out-of-plane) lattice constant relative to the substrate lattice constant of α-phase $(Al_xGa_{1-x})_2O_3$ on r-plane Al_2O_3.

We note that by setting the elastic constant C_{14} to zero, our theory covers as well the simpler case of hexagonal (wurtzite) heterostructures discussed in [1].

[1] M. Grundmann, Jesús Zúñiga-Pérez, *Pseudomorphic ZnO-based heterostructures: from polar through all semipolar to nonpolar orientations*, phys. stat. sol. (b) **253**, 351–360 (2016)
[2] M. Grundmann, *Strain in Pseudomorphic Monoclinic Ga_2O_3-based Heterostructures*, phys. stat. sol. (b) **254**, 1700134 (2017)
[3] M. Grundmann, *Elastic Theory of Pseudomorphic Monoclinic and Rhombohedral Heterostructures*, J. Appl. Phys. **124**, 185302:1-10 (2018)
[4] K. Momma, F. Izumi, *VESTA 3 for three-dimensional visualization of crystal, volumetric and morphology data*, J. Appl. Crystallogr. **44**, 1272–1276 (2011)

9.4 Pseudomorphic growth of $(Al_{1-x}Ga_x)_2O_3$ thin films on R-plane sapphire

M. Lorenz, S. Hohenberger, E. Rose, M. Grundmann

Single-crystalline α-$(Al,Ga)_2O_3$ is interesting for the fabrication of high-quality semiconductor and dielectric heterostructures due to the similar ionic radii and the availability of high-quality sapphire substrates [1]. From the literature review published in

[1], a clear gap is visible for epitaxial growth of α-$(Al_{1-x}Ga_x)_2O_3$ films on the Al-rich side. Therefore, the aim of this work [1] was to demonstrate coherent pseudomorphic growth of α-$(Al_{1-x}Ga_x)_2O_3$ films on R-plane (01.2) sapphire substrates. Eventually, such thin films can be used in dielectric superlattices.

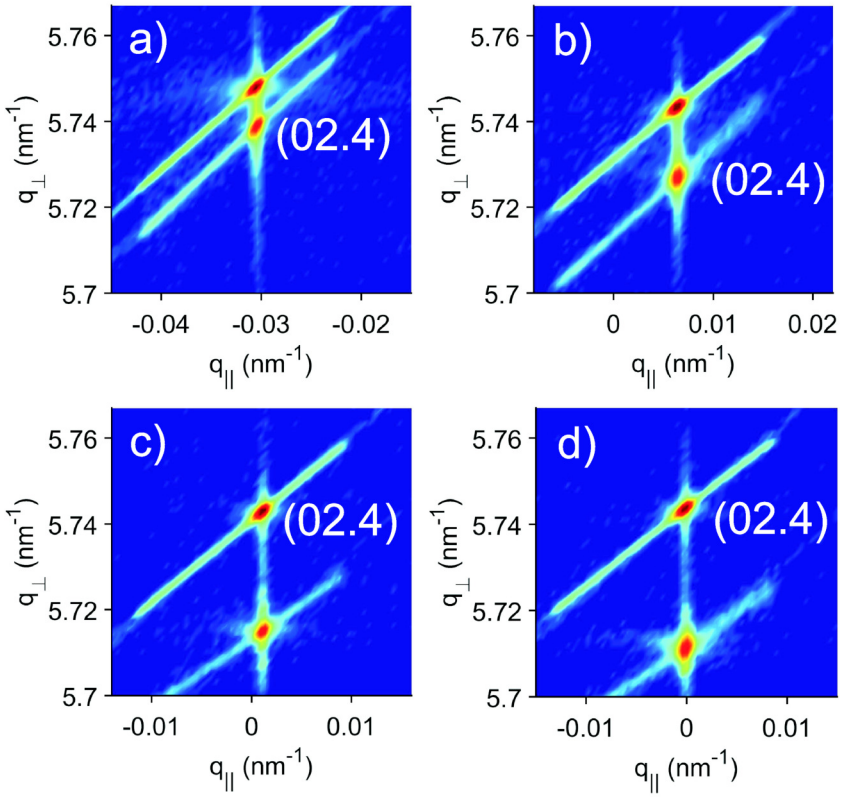

Figure 9.6: RSMs around symmetric (02.4) reflections, measured with the fast frame-based option of the PIXcel^{3D} detector of samples with increasing Ga-content, i.e. increasing peak splitting: a) x = 0.0209, b) x = 0.0377, c) x = 0.0635, and d) x = 0.0745. The more intense upper peak stems from the substrate in all maps. Figure adopted from [1].

Atomically smooth, pseudomorphic $(Al_{1-x}Ga_x)_2O_3$ thin films were grown for $0 \leq x < 0.08$ on R-plane sapphire (01.2) by pulsed laser deposition. The laser targets with nominal Ga-contents x = 0, 0.1, and 0.2 were sintered pellets pressed from high purity Al_2O_3 and Ga_2O_3 powders. The oxygen partial pressure during growth was optimized to 10^{-3} mbar. The growth temperature obtained by the CO_2 laser heater was varied between 500°C and 1,000°C. Substrates were single-side epi polished r-plane sapphire (01.2) single crystals (10×10×0.5 mm^3). Films up to 720 nm thickness show atomically stepped surfaces with monolayer terraces, similar to the substrates prior to growth, for AFM images and further details see [1].

X-ray diffraction (XRD) measurements were performed using a PANalytical X'pert PRO MRD with the line focus of a copper X-ray tube. As incident beam optics either a 4×Ge(220) monochromator (Kα_1-radiation) or a parabolic mirror (Kα-radiation) was used. For detection either a secondary monochromator with proportional counter (triple-axis) or the variable receiving slit of a PIXcel^{3D} array detector was used [1]. A careful analysis of 13 symmetric, skew-symmetric and asymmetric XRD peaks agrees

quite well with the continuum elastic strain theory of pseudomorphic distortion in corundum heterostructures by M. Grundmann [2].
Figure 9.6 shows reciprocal space maps (RSMs) around the symmetric (02.4) reflections, indicating the increasing splitting of substrate and film peaks with increasing Ga content x. For x = 0, no splitting was observed even in triple-axis XRD scans, indicating a perfect lattice match. Ref. [1] provides a detailed comparison on the experimental and theoretical splitting of film and substrate peaks for the 13 reflections, as well as the measured tilts of asymmetric film lattice planes. An even better overall agreement of experimental and theoretical peak splitting could be obtained using slightly modified c/a ratios, see the minor corrections of the order 10^{-4} in Table 2 of Ref. [1]. The standard deviations of the differences theory-experiment are considerably reduced by using these slightly corrected c/a ratios, indicating the very high sensitivity of the elastic theory [2] and the precision of the high-resolution XRD measurements [1].

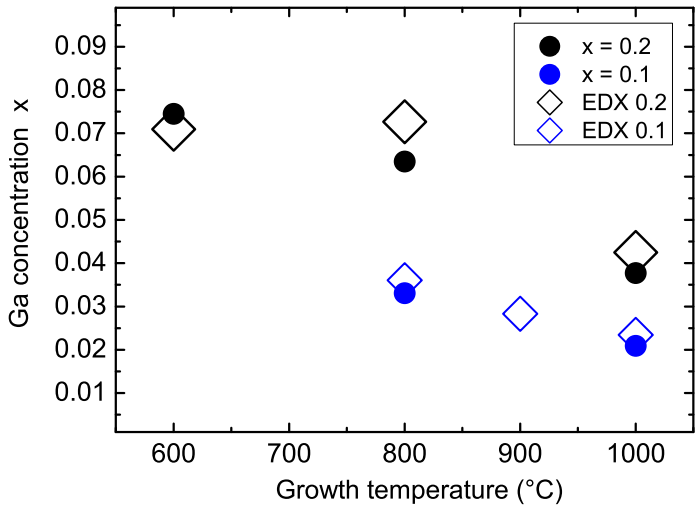

Figure 9.7: Ga-concentration x calculated from fits to experimental peak splitting *(circles)* and measured by EDX analysis *(diamonds)* in dependence of growth temperature, for films grown from PLD targets with Ga contents x = 0.1 *(blue)* and 0.2 *(black)*. Size of EDX symbols corresponds to their experimental uncertainty. Figure adopted from [1].

The Ga contents x obtained from best fits of the spacing of the (02.4), (04.8), and (00.6), (00.12) film and substrate XRD reflections is compared in Figure 9.7 with energy dispersive X-ray (EDX) analyses of the same samples. Taking into account the natural uncertainties of EDX, a reasonable agreement of theoretical and experimental Ga-contents of our epitaxial $(Al_{1-x}Ga_x)_2O_3$ films was obtained [1].

[1] M. Lorenz, S. Hohenberger, E. Rose, and M. Grundmann, Appl. Phys. Lett. **113**, 231902: 1-5 (2018)
[2] M. Grundmann, J. Appl. Phys. **124**, 185302: 1-10 (2018)

9.5 Properties of binary and ternary orthorhombic group-III sesquioxide thin films grown by pulsed laser deposition

The wide bandgap semiconductor gallium oxide has potential application in electronic high-power devices, because of its large breakdown field and high Baliga figure of merit [1]. Additional possible application fields are quantum well infrared photodetectors, UV-photodetectors, touch panel displays, or optical communication systems [2]. Ga_2O_3 can be stabilized in various polymorphs [3]. While the majority of publications focuses on the thermodynamically most stable β-phase, recently, the orthorhombic κ-phase gained interest due to its predicted large spontaneous polarization of 23 $\mu C/cm^2$ along the c-axis [4]. This would lead to a discontinuous change of the polarization at the interface of κ-Ga_2O_3 based, ternary heterostructures resulting in electron accumulation at the interface, which can be utilized to perform applications such as high-electron mobility transistors. Therefore, it is crucial to determine deposition conditions allowing the growth of binary as well as ternary layers with tailored material properties. In the following sections, we will discuss growth conditions and behavior of binary κ-Ga_2O_3 thin films grown by pulsed laser deposition (PLD) on different substrates [5]. Further, we discuss material properties of a κ-$(In_xGa_{1-x})_2O_3$ thin film grown with continuous composition spread [6] (CCS) by pulsed laser deposition on c-plane sapphire. Both, the binary and the ternary target were doped with tin to facilitate formation of the orthorhombic phase [7]. Resulting samples were investigated by means of X-ray diffraction (XRD), transmission, energy-dispersive X-ray spectroscopy (EDX), and atomic force microscopy (AFM).

9.5.1 Tin-assisted PLD-growth of binary κ-Ga_2O_3 thin films

M. Kneiß,[*] A. Hassa,[*] D. Splith,[*] C. Sturm,[*] H. von Wenckstern,[*] T. Schultz,[†] N. Koch,[†] M. Lorenz,[*] and M. Grundmann[*]

[*]Universität Leipzig, Felix-Bloch-Institut für Festkörperphysik
[†]Humboldt Universität zu Berlin, Institut für Physik

Kracht *et al.* [7] found that offering tin as as a catalyst during molecular beam epitaxy (MBE) of Ga_2O_3 is beneficial for stabilizing the κ-phase on c-plane sapphire. Similarly, for PLD grown thin films, Orita et al. [8] obtained thin films in the κ-phase under certain conditions by employing tin-doped targets. To shed a light on the growth mechanism of this phase in PLD and the determination of important material parameters, we performed an in-depth investigation on Ga_2O_3 thin films grown from tin-containing targets (Ga_2O_3 + 1 wt.% SnO_2) on various substrates such as c-sapphire, YSZ(111), STO(111), and MgO(111) [5]. Upon a variation of the oxygen partial pressure ($p(O_2)$) during the PLD process, we found that the orthorhombic κ-phase can be synthesized only for $p(O_2) \leq 0.016$ mbar, while for higher pressures the thin films crystallize in the thermodynamically stable monoclinic β-phase. Further, for a given $p(O_2)$ the critical pressure of 0.016 mbar, the κ-phase is only stabilized at growth temperatures above 500°C. Apparent is the significant increase in intensity and decrease of the broadening of the

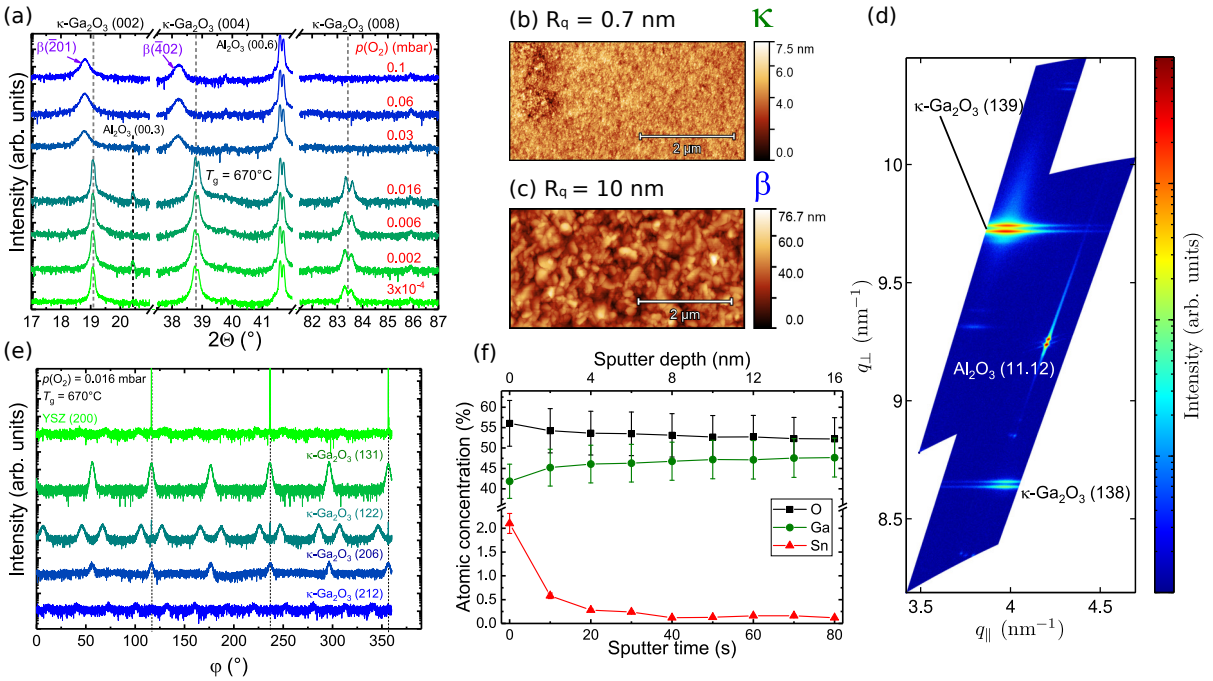

Figure 9.8: (a) XRD 2θ-ω scans of a series of Ga_2O_3 thin films deposited via PLD from a tin-doped target on c-sapphire substrates at various oxygen partial pressures $p(O_2)$ and a substrate temperature $T_g = 670°C$. (b) and (c): AFM images of Ga_2O_3 thin films in the (b) κ- and (c) β-phase. The thin films were deposited at nominally identical process parameters of $p(O_2) = 0.016$ mbar and $T_g = 670°C$ from a (b) tin-doped and (c) nominally undoped target. RMS roughness R_q as indicated. (d) Reciprocal space map of a κ-Ga_2O_3 thin film on c-sapphire around the asymmetric $Al_2O_3(11.12)$ reflection. (e) XRD ϕ scans of a κ-Ga_2O_3 thin film on YSZ(111) for several skew-symmetric substrate and film reflections as indicated. (f) Depth-resolved atomic concentrations of Ga, O and Sn for a κ-Ga_2O_3 thin film on c-sapphire determined from depth-resolved XPS measurements.

reflections in XRD 2θ-ω scans of the thin films in the κ-phase as compared to those in the β-phase, as shown in Fig. 9.8(a). At the same time, for identical process parameters, thin films grown from nominally undoped targets crystallize solely in the β-phase with much larger surface roughnesses, as revealed by AFM images in Fig. 9.8(b) and (c), emphasizing the superior surface quality of thin films in the κ-phase. Rocking curve measurements as well as reciprocal space maps (see e.g. Fig. 9.8(d)) proved once more the high crystalline quality of the κ-phase thin films. Lattice parameters determined from these measurements ($a = 5.053$ Å, $b = 8.701$ Å and $c = 9.265$ Å) are in good agreement to literature data [9]. We were further able to unambiguously prove the orthorhombic symmetry of the κ-phase as well as the epitaxial growth on all used substrates by XRD ϕ-scans of several skew-symmetric film and substrate reflections (see Fig. 9.8(e) for a thin film on YSZ(111)). The twelve-fold occurring (122) and (212) reflections are only expected in the orthorhombic system. Correspondingly, we found epitaxial growth of the thin films in three rotational domains rotated by 120° with respect to each other. The in-plane epitaxial relationships were determined as α-Al_2O_3 $\langle\bar{1}0.0\rangle\|\langle010\rangle$ κ-Ga_2O_3 and α-Al_2O_3 $\langle\bar{1}2.0\rangle\|\langle100\rangle$ κ-Ga_2O_3 for c-sapphire as well as cubic $\langle\bar{2}11\rangle\|\langle100\rangle$ κ-Ga_2O_3 and cubic $\langle0\bar{1}1\rangle\|\langle010\rangle$ κ-Ga_2O_3 for the cubic substrates. To further clarify the role of tin for the PLD growth of the κ-phase, depth-resolved X-ray photoelectron spectroscopy (XPS)

measurements were performed. The resulting atomic concentrations of the elemental species Ga, O and Sn are shown in dependence on the sputtering depth in Fig. 9.8(f). While almost no tin is incorporated in the bulk of the thin film, a clear enrichment of tin was observed towards the surface of the sample. We propose a liquid tin layer floating on top of the thin film during growth that enables the stabilization of the κ-phase in a vapor-liquid-solid process (surfactant-mediated epitaxy [10]). We could further confirm the transparency of our thin films up to the optical bandgap of the material of $\approx 4.9\,\mathrm{eV}$.
In summary, our κ-Ga_2O_3 layers are structurally and morphologically superior to thin films in the β-phase and represent an excellent basis for further research on the respective alloy systems and corresponding heterostructures for device applications. A detailed investigation by us on the PLD growth of binary κ-Ga_2O_3 can be found in Ref. 5.

9.5.2 Structural and optical investigations of κ-$(In_xGa_{1-x})_2O_3$ thin films

A. Hassa, M. Kneiß, D. Splith, C. Sturm, H. von Wenckstern, and M. Grundmann

A two inch in diameter thin film of κ-$(In_xGa_{1-x})_2O_3$ was prepared by PLD with CCS approach [6]. As ablation target we used two segments consisting of tin-doped gallium and indium oxides, respectively. The chemical cation composition in the film, depicted in Fig. 9.9(a), shows an In-content ranging between 1 at.% and 83.5 at.%. The cation distribution exhibits a non-linear behavior as visible in Fig. 9.9(b). For a z-position below 15 mm, the linescan shows a slight and for $z > 15\,\mathrm{mm}$ a rapid increase of x being connected to phase separation. To identify the different crystallographic phases, XRD measurements were performed. The results of 55 2θ-ω measurements acquired along the gradient are depicted in Fig. 9.9(c) and reveal three different phases, which can be assigned to the orthorhombic κ-Ga_2O_3 modification for $x \leq 0.35$, to hexagonal $InGaO_3$ (II) for $0.35 < x < 0.5$, and to the cubic bixbyite structure for $x \geq 0.5$. In the following we only will discuss the region with an In-content below 35 at.% assigned to the orthorhombic phase. The reflexes of the (001) orientation of κ-Ga_2O_3 and the reflexes of the (-201) orientation of β-Ga_2O_3 lie close to each other, but that of the κ-phase appear at slightly higher angles. In order to confirm that the thin film is indeed in the κ-phase, ϕ-scans were performed. Fig. 9.9(d) exhibits XRD ϕ-scans of skew-symmetric reflections corresponding to the (131), (122) and (206) lattice planes of the κ-phase. For the (131) and the (206) planes, six-fold reflections were observed with separations of 60°, which indicates epitaxial growth on the c-sapphire substrate. For the (122) lattice plane, twelve reflections occur corroborating the orthorhombic symmetry, because only in this structure twelve peaks are expected due to mirror planes. Fig. 9.9(e) shows the dependence of the c-lattice constant as well as the bandgap energy E_g and the growth rate r on the In-content. The c-lattice constant increases nearly linear with increasing x and can be described by $c = [\,(9.269 \pm 0.004) + (1.097 \pm 0.01) \cdot x\,]$ Å. Spectroscopic ellipsometry measurements were utilized to estimate E_g and the sample thickness d to calculate r ($= d/\,\mathrm{pulses}$), subsequently. The bandgap energy decreases with increasing x from 4.9 eV down to 4.3 eV for $0 \leq x \leq 0.35$. The growth rate shows different behavior for different x regimes. It starts for $x = 0.01$ at $\tau = 8.7\,\mathrm{pm/pulse}$ and

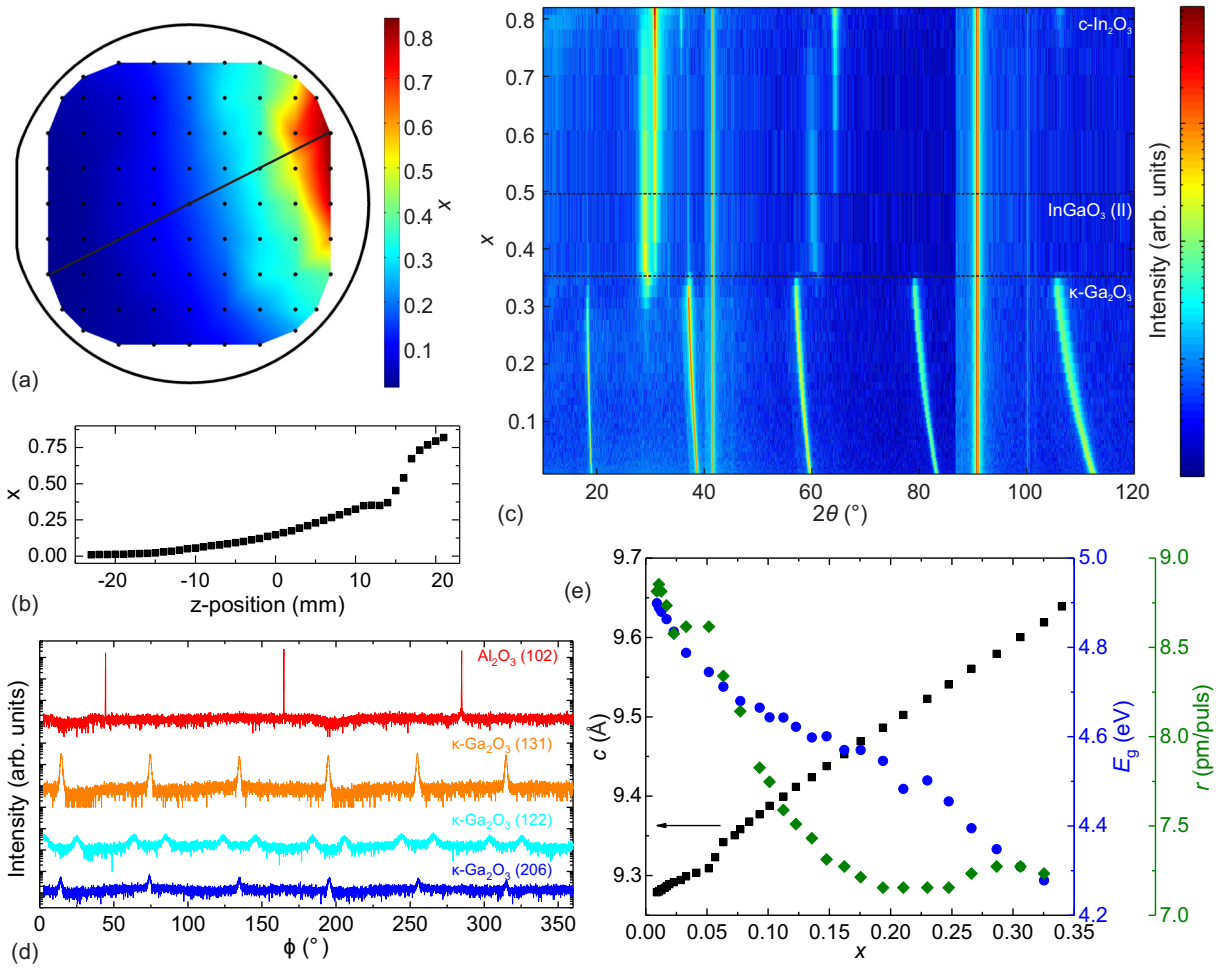

Figure 9.9: (a) False color representation of the In-content x of a $(In_xGa_{1-x})_2O_3$ thin film grown on a 2 inch in diameter c-plane sapphire substrate, (b) shows an EDX-linescan along the compositional gradient as indicated by the black line in (a). (c) False color plot of 55 XRD 2θ-ω measurements acquired along the gradient direction. (d) XRD ϕ-scans of a sample piece at $x \sim 0.01$. (e) The c-lattice constant determined from XRD patterns as well as the band gap E_g and growth rate r obtained from spectroscopic ellipsometry measurements as a function of the In-content x.

saturates around 7.2 pm/pulse for $x \geq 0.2$. Further informations can be found in more detail in Ref. 11.

[1] Higashiwaki *et al.*, Applied Physics Letters **100**, 013504 (2012)
[2] von Wenckstern, Adv. Electron. Mater **3**, 1600350 (2017)
[3] Roy *et al.*, Journal of the American Chemical Society **74**, 719–722 (1952)
[4] Maccioni *et al.*, Appl. Phys. Express **9**, 04102 (2016)
[5] Kneiß *et al.*, APL Materials **7**, 022516 (2019)
[6] von Wenckstern *et al.*, CrystEngComm **15**, 10020 (2013)
[7] Kracht *et al.*, Phys. Rev. Appl. **8**, 054002 (2017)
[8] Orita *et al.*, Thin Solid Films **411**, 134 (2002)
[9] Cora *et al.*, CrystEngComm **19**, 1509 (2017)
[10] Iwanari and Takayanagi, Jpn. J. Appl. Phys., Part 2 **30**, L1978 (1991)
[11] Hassa *et al.*, APL Materials **7**, 022525 (2019)

This work was supported by European Social Fund within the Young Investigator Group "Oxide Heterostructures" (SAB 100310460).

9.6 Investigation of cation vacancy concentrations in $(In_xGa_{1-x})_2O_3$ thin films by positron annihilation spectroscopy

V. Prozheeva,[*] H. von Wenckstern,[†] F. Toumisto,[*] M. Grundmann[†]

[*]Aalto University, Department of Applied Physics, Espoo, Finland
[†]Universität Leipzig, Felix-Bloch-Institut für Festkörperphysik

Various nominally undoped $(In_xGa_{1-x})_2O_3$ thin films with lateral variation of the alloy composition were grown on (00.1)Al_2O_3 and (100)MgO substrates by a continuous composition spread approach for pulsed-laser deposition [1]. Positron annihilation spectroscopy (PAS) in Doppler broadening mode was used to investigate the formation of cation vacancies as a function of the alloy composition [2]. Since In_2O_3 and Ga_2O_3 have different equilibrium crystal structure (cubic bixbyite for In_2O_3 and monoclinic beta-gallia structure for Ga_2O_3), the influence of alloying was studied for the cubic and the monoclinic modification.

In nominally undoped monoclinic samples ($x \leq 0,02$) on (00.1)Al_2O_3 the cation vacancy (V_M) concentration increases with increasing indium content as indicated by the increase of the S parameter depicted in fig. 9.10a). For binary Ga_2O_3 the density of V_M is estimated to $(2-4) \times 10^{16}\,cm^{-3}$. Binary Ga_2O_3 thin films grown by metal-organic vapor phase epitaxy have significantly larger gallium vacancy concentrations with values above $10^{17}\,cm^{-3}$ [3]. (S,W)-plots (not shown) reveal that the nature of these cation vacancies in our ternary layers corresponds to V_M in the monoclinic beta-gallia structure. For an indium content between 0.2 and 0.8 the cubic and the hexagonal $InGaO_3$ II modifications are observed besides the monoclinic phase. Here the type of the predominant cation vacancy changes to V_M in the cubic bixbyite lattice modification. For cubic $(In_xGa_{1-x})_2O_3$ on (00.1)Al_2O_3 the same type of cation vacancy is dominant even for Ga-rich samples, for which the composition dependence of the S-parameter is depicted in fig. 9.10b). The above findings and the larger value of the S-parameter in fig. 9.10b) demonstrate that the cation vacancy concentration in cubic $(In_xGa_{1-x})_2O_3$ PLD layers is higher than in monoclinic $(In_xGa_{1-x})_2O_3$ PLD thin films.

Monoclinic $(In_xGa_{1-x})_2O_3$ on (100)MgO substrate have significantly lower cation vacancy concentration than layers on (00.1)Al_2O_3. The vacancy concentration increases with increasing indium content. For $0.3 < x < 0.65$ samples on (100)MgO are X-ray amorphous, however, positron trapping at cation vacancies occurs and from (S,W)-plots (not shown) these vacancies correspond to V_{In} in cubic In_2O_3. The concentration of V_{In} is highest for $x = 0.5$ and decreases in a similar way for higher and lower In content. For $x > 0.65$ thin films have bixbyite crystal structure. Here, the cation vacancy concentration is above $10^{17}\,cm^{-3}$ and increases expectedly with increasing Ga admixture. Overall, the cation vacancy concentration in cubic $(In_xGa_{1-x})_2O_3$ is significantly lower than the free carrier density and hence it is not a relevant compensation center.

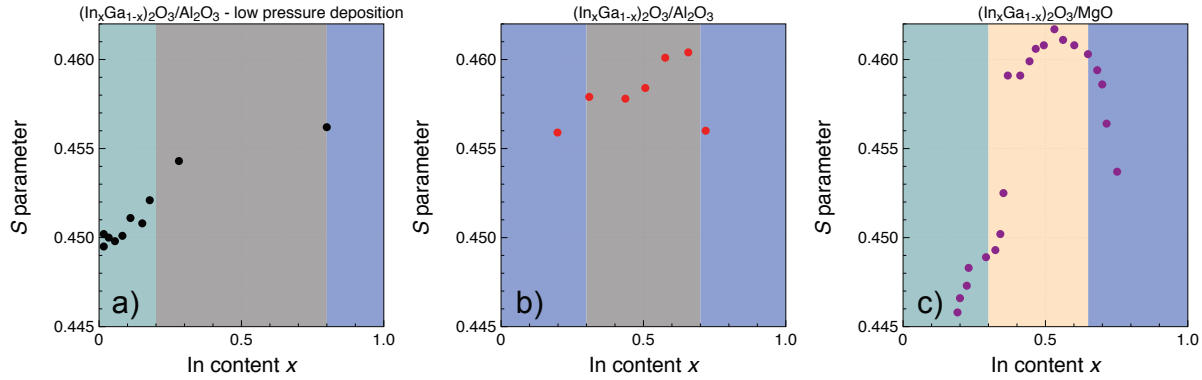

Figure 9.10: Dependence of he S-parameter on the indium content for $(In_xGa_{1-x})_2O_3$ thin films on a,b) (00.1)Al_2O_3 and c) (100) MgO substrate. Samples were grown at an oxygen partial pressure of a) 3×10^{-4} mbar and b,c) 8×10^{-2} mbar. The background color highlights samples with monoclinic (greenish), cubic (blueish), mixed (gray) or amorphous (orange) phase.

[1] H. von Wenckstern, Z. Zhang, F. Schmidt, J. Lenzner, H. Hochmuth, and M. Grundmann, CrystEngComm **15**, 10020 (2013).
[2] V. Prozheeva, R. Hölldobler, H. von Wenckstern, M. Grundmann, and F. Tuomisto, J. Appl. Phys. **123**, 125705 (2018).
[3] E. Korhonen, F. Tuomisto, D. Gogova, G. Wagner, M. Baldini, Z. Galazka, R. Schewski, and M. Albrecht, Appl. Phys. Lett. **106**, 242103 (2015).

9.7 Influence of oxygen deficiency on the rectifying behavior of transparent-semiconducting-oxide-metal interfaces

P. Schlupp,* S. Vogt,* T. Schultz,† H. vonWenckstern,* N. Koch,† M. Grundmann*

*Universität Leipzig, Felix-Bloch-Institut für Festkörperphysik
†Humboldt Universität zu Berlin, Institut für Physik

Conductive oxide materials were used for a long time mainly as transparent electrodes (e.g. In_2O_3 : Sn, ZnO:Ga) [1]. In recent years, also their semiconducting properties came into focus. ZnO, SnO_2, Ga_2O_3 and In_2O_3 as well as amorphous oxide materials like In-Ga-Zn-O or Zn-Sn-O are of interest because of various desired properties like transparency, high electron mobility or high breakdown fields [2–5]. For investigation as well as for applications development of technology allowing reproducible fabrication of highly rectifying diodes is crucial. Since oxide materials are mainly unipolar, rectifying contacts are realized by Schottky barrier diodes.

It is known, that the amount of oxygen in the material has a strong influence on the electrical and optical properties. Especially oxygen deficiency plays an important role on surface band bending and surface accumulation of electrons [6, 7]. The formation of oxygen vacancies near the surface strongly influences the performance of Schottky barrier diodes [8, 9].

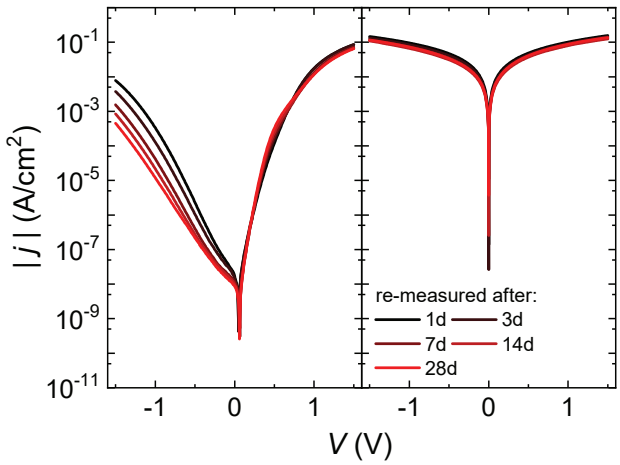

Figure 9.11: IV-characteristics of the ZTO/PtO_δ/Pt (left) and the ZTO/Pt (right) Schottky barrier diodes measured after times of fabrication as indicated.

To investigate the influence of oxygen on the formation and the stability of Schottky barrier diodes, current-voltage (IV) measurements and X-ray photoelectron spectroscopy (XPS) were applied to Pt-Schottky contacts on amorphous zinc tin oxide (ZTO) [10]. The ZTO thin films were fabricated by pulsed laser deposition and have an electron density of about 3×10^{17} cm^{-3} which was confirmed by Hall-effect measurement. Two types of Pt-contact were deposited as Schottky contacts: (i) sputtering in argon resulted in metallic Pt contacts and (ii) sputtering in oxygen capped by a Pt layer sputtered in argon resulted in PtO_δ contacts.

The IV-characteristics of the ZTO/PtO_δ/Pt (left) and the ZTO/Pt contacts (right) are depicted in figure 9.11. The ZTO/Pt contact does not show a rectifying behavior at all. Its IV-characteristics does not change within 28 days after the deposition of the contacts. In contrast, the ZTO/PtO_δ/Pt contact exhibits current rectification of about one order of magnitude at day 1, which increases to about two orders of magnitude at day 28. This change is mainly due to a decrease of the reverse current, the thin film resistance does not change. Therefore, we conclude that an interface effect is responsible for the change and oxygen may play a crucial role.

A piece of both samples, the ZTO/Pt as well as the ZTO/PtO_δ/Pt, was investigated by depth-resolved XPS. The contact material was removed stepwise by sputtering using argon with an acceleration voltage of 300 V. The elemental concentration of both samples is depicted in figure 9.12 starting at the Pt surface (low sputter times). The PtO_δ layer contains a large amount of oxygen. At the interface (reached after 275 s), the oxygen content increases. From the XPS signal it can be seen (not shown) that this increased oxygen amount is bound to the Sn atoms. At the interface of the ZTO/Pt contact a signal that can be assigned to PtO as well as an additional peak of the Sn in the vicinity of an oxygen vacancy was observed. Therefore we conclude, that in the ZTO/PtO_δ/Pt contact oxygen ions move from the oxygen reservoir within the PtO_δ layer into ZTO and saturate undercoordinated cations in the vicinity of the interface. The high electron density of the ZTO in the vicinity of the interface is lowered resulting in higher rectification of the Schottky barrier diode.

Using the Pt 4f peak, the $Pt(OH)_4$ and the PtO content were resolved for the

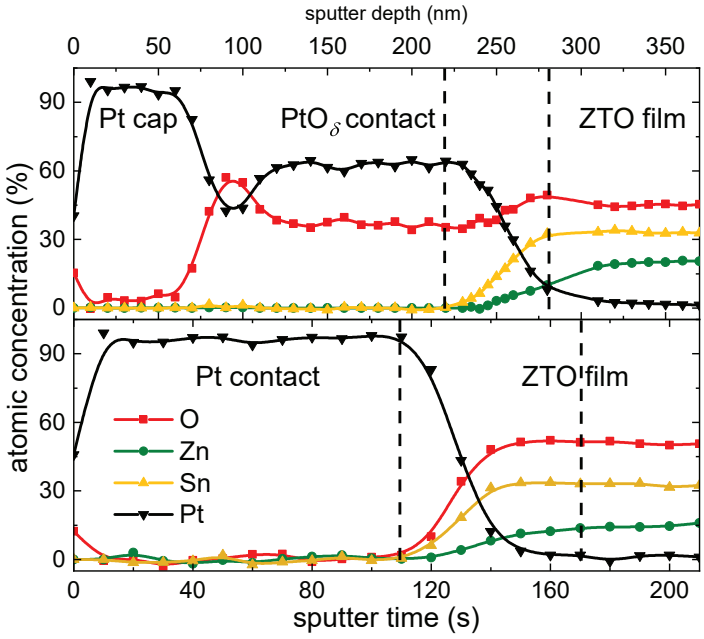

Figure 9.12: Elemental concentration in dependence of the depth of the ZTO/PtO$_\delta$/Pt (top) and the ZTO/Pt contacts (bottom).

ZTO/PtO$_\delta$/Pt. The intensity at day 1 and day 30 after fabrication of the contacts in dependence of the sputter depth is depicted in figure 9.13. The Pt(OH)$_4$ content in the sample did not change significantly in this time scale, however, a reduction towards the interface is visible. In contrast, the PtO content seems to decrease over time. Its content is reduced by about 50 %. From these results we conclude that the Pt(OH)$_4$ at the interface is completely reduced within the first 24 h resulting in improved diode characteristics compared to the metallic Pt contacts. The reduction of the PtO is much slower and the oxygen movement improves the diodes further over time decreasing the electron density at the interface-near ZTO. This leads to improved IV-characteristics which can be seen in figure 9.11.

The aging of the Schottky barrier diodes may be accelerated by the application of an external bias to the devices. This accelerates the movement of the oxygen ions into the ZTO. To prove this, a voltage of −1.5 V was repeatedly applied for 500 s to the diodes. A decrease of the reverse current is observed for the ZTO/PtO$_\delta$/Pt diode with increasing application time, whereas the ZTO/Pt diode remains unchanged. This mechanism is believed to be present also at other oxide-semiconductor-metal interfaces and our results provide a general methodology for achieving highly rectifying Schottky barrier diodes to these materials.

[1] K.L. Chopra, S. Major, D.K. Pandya: Thin Solid Films. **102**, 1-46 (1983)
[2] M. Grundmann, H. Frenzel, A. Lajn, M. Lorenz, F.-L. Schein, H. von Wenckstern: Physica Status Solidi A **207**, 1437-1449 (2010)
[3] H. von Wenckstern: Advanced Electronic Materials **3**, 1600350 (2017)
[4] T. Kamiya, K. Nomura, H. Hosono: Science and Technology of Advanced Materials **11**, 044305 (2010)

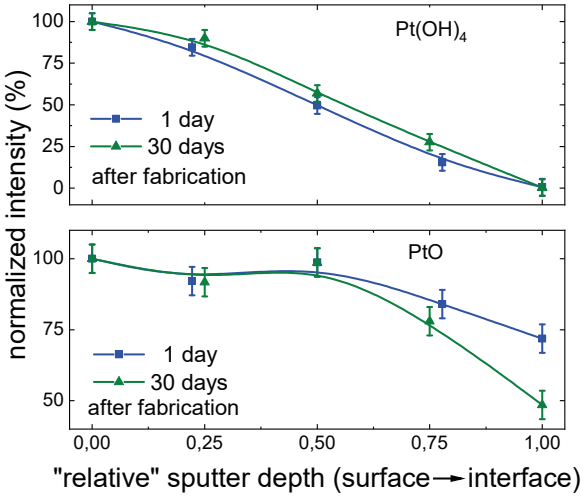

Figure 9.13: Change of the $Pt(OH)_4$ (top) and PtO (bottom) component of the Pt $4f$ peak for a ZTO/PtO_δ/Pt Schottky contact.

[5] H.Q. Chiang, J.F. Wagner, R.L. Hoffman, J. Jeong, D.A. Keszler: Applied Physics Letters **86**, 013503 (2005)
[6] T. Berthold, J. Rombach, T. Stauden, V. Polyakov, V. Cimalla, S. Krischok, O. Bierwagen, M. Himmerlich: Journal of Applied Physics **120**, 245301 (2016)
[7] B.J. Coppa, R.F. Davis, R.J. Nemanich: Applied Physics Letters **82**, 400 (2003)
[8] M.W. Allen, S.M. Durban: Applied Physics Letters **92**, 122110 (2008)
[9] S. Müller, H. von Wenckstern, F. Schmidt, D. Splith, R. Heinold, M. Allen, M. Grundmann: Journal of Applied Physics **116**, 194506 (2014)
[10] T. Schultz, S. Vogt, P. Schlupp, H. von Wenckstern, N. Koch, M. Grundmann: Physical Review Applied **9**, 064001 (2018)

9.8 MESFETs and inverters based on amorphous zinc-tin-oxide thin films prepared at room temperature

S. Vogt, H. von Wenckstern, M. Grundmann

Amorphous oxide semiconductors (AOSs) have great potential for future electronic applications due to low fabrication costs and their superior performance compared to amorphous Si [1]. A non-toxic and abundantly available compound belonging to the group of AOSs is zinc-tin-oxide (ZTO). The influence of the deposition method and conditions as well as the influence of the cation composition on the electrical properties of ZTO have been investigated [2–4]. Highly rectifying diodes based on amorphous ZTO have been reported for different gate contact materials such as metal oxides and *p*-type oxide semiconductors [6–10]. The first ZTO based metal-insulator field-effect transistor (MISFET) was presented by Chiang *et al.* in 2005 [11]. In 2016 the first metal-semiconductor field-effect transistor (MESFET) using silver oxide as gate material and amorphous ZTO as *n*-type channel was reported by Dang *et al.* [12].

However, the deposition process required elevated temperatures and an additional thermal annealing at 525°C to improve the device performance.

In this work we present amorphous ZTO based MESFETs fabricated at room temperature. The *n*-type ZTO channels were deposited by long throw magnetron sputtering [4]. It was previously found that an increase of the free carrier density towards the substrate inhibited the depletion of the ZTO channel for our ZTO layers. It was speculated that oxygen vacancies at the interface to the substrate may be the cause of the increasing free carrier density [13]. To prevent this effect, a novel sputtering process was implemented. The sputtering process was started in a gas mixture of 25 sccm oxygen and 30 sccm argon and subsequently, the oxygen content was continuously reduced to 0 sccm in 720 s. On top of this oxygen variation layer, a conductive channel was sputtered for a predefined time span under 30 sccm argon.

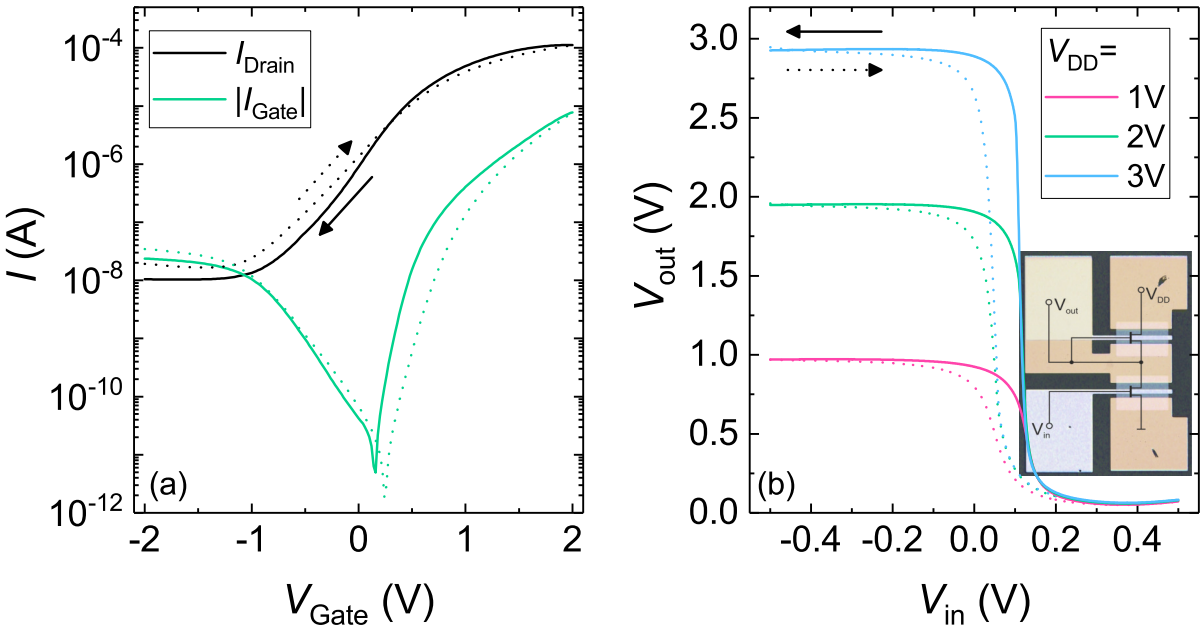

Figure 9.14: Transfer characteristics (a) of a MESFET based on amorphous zinc-tin-oxide and using platinum oxide as gate material and the voltage transfer characteristics (b) for an inverter based on such a MESFET.

The gate contacts of the MESFETs and the inverter were formed by reactively sputtered platinum covered by a metallic platinum layer [5]. The ohmic contacts were realized by sputtered gold. Three different ZTO layer thicknesses between 19 and 24 nm were investigated. A higher thin film thickness led to an increase of the free carrier density from 6×10^{17} to 2×10^{18} cm$^{-}3$ (always normalized to the entire ZTO layer thickness). In Figure 9.14 (a) the transfer characteristic for a MESFET with a ZTO layer thickness of 24 nm is depicted. A current on-to-off ratio of 1.1×10^4 with a threshold voltage of $V_T \approx 0$ V and a sub-threshold swing of 370 mV dec^{-1} were measured for this device. A maximum current on-to-off ratio of 1.8×10^6 was achieved for a ZTO layer thickness of 19 nm ($V_T \approx 0.5$ V). Thus a smaller ZTO layer thickness results in normally off devices. An improvement of the devices was observed for the application of a negative bias at the gate contact. It led to a reduction of the reverse gate leakage current and an

increasing steepness of the transfer characteristics.

To demonstrate a logic device based on these thin films, a 24 nm thick ZTO layer was used to fabricate inverters. The used layout and the resulting voltage transfer characteristic are shown in Figure 9.14 (b). The characteristics exhibit a hysteresis between forward and reverse voltage sweep direction, which is most likely due to a small change in the threshold voltage for these two sweep directions. An uncertainty level below 0.25 V and a peak gain magnitude as high as 110 for an operating voltage of V_{DD} = 3 V were obtained, which exceed previous reports on ZTO based inverters [14].

[1] H. Hosono *et al.*: J. Non-Cryst. Solids. **198-200**, 165 (1996)
[2] M. K. Jayaraj *et al.*: J. Vac. Sci. Technol. B **26**, 495 (2008)
[3] S. Bitter *et al.*: ACS Comb. Sci. **18**, 4, 188-194 (2016)
[4] H. Frenzel *et al.*: Physica Status Solidi (a) **212**, 7, 1482-1486 (2015)
[5] A. Lajn *et al.*: J. Vac. Sci. Technol. B **27**, 3, 1769 (2009)
[6] Y. Son *et al.*: ACS Appl. Mater. Interfaces **8**. 36, 23801-23809 (2016)
[7] S. Bitter *et al.*: ACS Appl. Mater. Interfaces **9**, 31, 26574-26581 (2017)
[8] P. Schlupp *et al.*: Adv. Electron. Mater. **1**, 1400023 (2015)
[9] P. Schlupp *et al.*: Physica Status Solidi (a) **214**, 10, 1700210 (2017)
[10] M. Grundmann *et al.*: J. Phys. D: Appl. Phys. **49**, 21, 213001 (2016)
[11] H. Chiang *et al.*: Appl. Phys. Letters **86**, 1, 013503 (2005)
[12] G. Dang *et al.*: Appl. Phys. Express **9**, 041101 (2016)
[13] T. Schultz *et al.*: Phys. Rev. Appl. **9**, 6, 064001 (2018)
[14] S. Tsai *et al.*: ECS J. Solid State Sci. Technol. **4**, 5, P176-P180 (2015)

9.9 Full-swing, high-gain inverters based on ZnSnO JFETs and MESFETs

O. Lahr, Z. Zhang, F. Grotjahn, P. Schlupp, S. Vogt, H. von Wenckstern, A. Thiede, M. Grundmann

Amorphous semiconducting oxides (AOS), consisting of heavy metal cations, exhibit remarkable transport properties despite their disordered structure [1]. The possibility of low-temperature deposition associated with their high transparency in the visible range enable the cost-efficient fabrication of transparent and even bendable circuits. One promising candidate for sustainable novel technology is the AOS zinc-tin-oxide (ZTO) for which first room-temperature (RT) fabricated metal-semiconductor field-effect transistors (MESFETs) and inverter structures have recently been reported by us [2].

Here, we present MESFETs and junction field-effect transistors (JFETs) as well as inverters using amorphous *n*-ZTO as channel material. The channels were deposited at RT by long-throw magnetron sputtering using a target with a 67 wt.% SnO_2 and 33 wt.% ZnO composition [3]. In case of MESFETs, reactively sputtered PtO_x with a Pt capping layer was used as gate material to reduce the free-carrier density close to the ZTO/PtO_x interface due to a saturation of under-coordinated cation bonds [4]. Additionally, a thin semi-insulating ZTO layer was primarily sputtered below the gate to further decrease

the leakage current through the gate diode [5]. For JFET-based devices a NiO gate contact was deposited on top of i-ZTO by pulsed laser deposition at RT and capped with a thin Au layer.

RT transfer characteristics of the best MESFET and JFET are depicted in Fig. 9.15 (a). Both devices exhibit a clear field-effect with on/off current ratios of about 8 orders of magnitude. The sub-threshold swing and maximum transconductance of the MESFET (JFET) are 242 (229) mV/dec and 236 (148) μS, respectively. Additionally, repeated measurements after a period of 200 days prove the long-term stability of the characterized devices concerning their electrical properties and performance. We investigated the cascading of MESFET- and JFET-based inverters using a FET logic (SDFL) implementing PtO_x/ZTO Schottky barrier diodes and NiO/ZTO pn-heterodiodes for level shifting, as depicted in Fig. 9.15. The corresponding voltage transfer characteristics of a MESFET-(JFET)-based inverter, as depicted in Fig. 9.16 (a), exhibit a maximum gain of 294 (347) and an uncertainty level as low as 0.27 (0.26) V (level shift not considered) at an operating voltage of $V_{DD} = 5$ V. In Fig. 9.16 (b) and (c) we depict the peak gain magnitude *pgm* and the uncertainty level V_{UC} for various operating voltages of inverters without level shifting diodes and for inverters with one or two level shifting diodes connected to the input. The uncertainty level is higher for inverters with level shift, however, a value of 380 mV is not exceeded for V_{DD} up to 5 V.

Amorphous ZTO-based inverter circuits reported here, comprising MESFETs and JFETs, were entirely fabricated at the lowest processing temperature and exhibit by far the highest gain despite operating at lowest supply voltages, compared to literature results on ZTO-based devices. In order to cascade such inverters, level shifting is necessary and was realized here by employing the SDFL approach. Our inverters exhibited stable *pgm* and V_{UC} values under operation with level shift making both FET types highly suited for realization of ring oscillators [6].

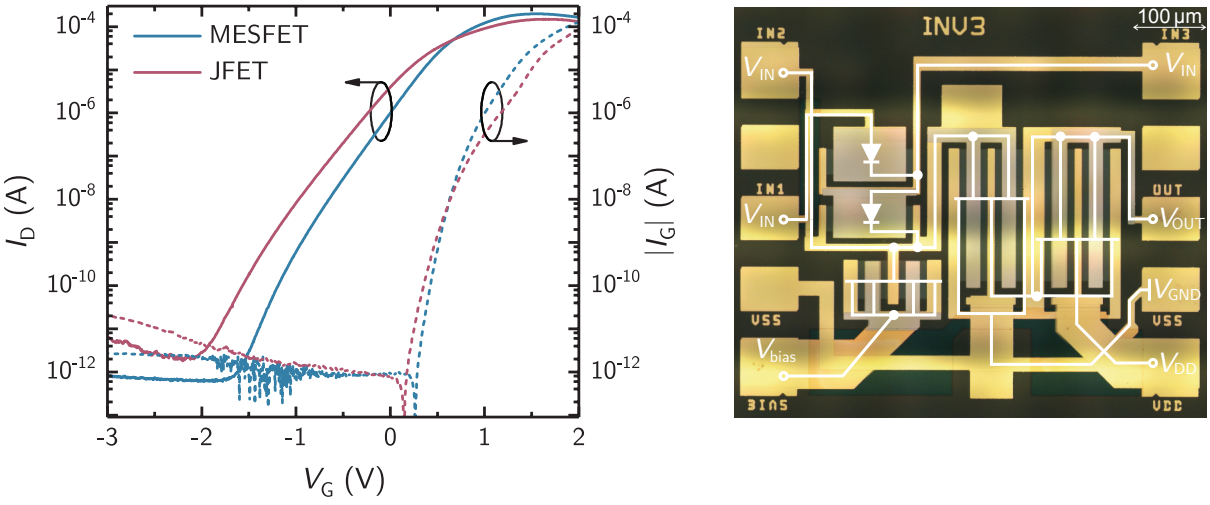

(a) (b)

Figure 9.15: (a) RT transfer characteristic of the best MESFET and JFET with corresponding source-gate characteristics for $V_D = 2$ V. (b) Microscopic image with overlayed circuit schematic of a SDFL inverter.

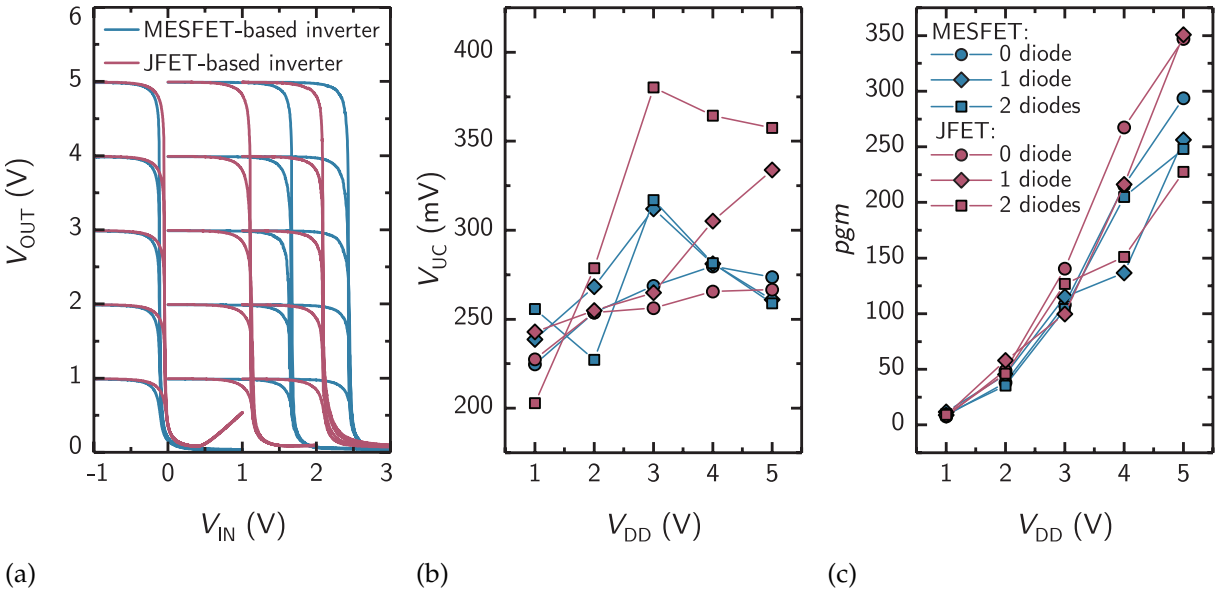

(a) (b) (c)

Figure 9.16: (a) Voltage transfer characteristics of ZTO-based SDFL inverters and dependence of (b) *pgm* and (c) V_{UC} on V_{DD} for no, one or two level shifting diodes.

[1] H. Hosono, Journal of Non-Crystalline Solids 351 (2006).
[2] S. Vogt *et al.*, Applied Physics Letters 113 (2018).
[3] H. Frenzel *et al.* Physica Status Solidi 212 (2015).
[4] T. Schultz *et al.*, Physical Review Applied 9 (2018).
[5] P. Schlupp *et al.*, Advanced Electronic Materials 1 (2015).
[6] F. Klüpfel *et al.*, Advanced Electronic Materials 2 (2016).

9.10 Properties of $In_2S_3/ZnCo_2O_4$ pin-heterostructures

T. Jawinski,* H. von Wenckstern,* L.A. Wägele,† R. Scheer,† M. Grundmann*

*Universität Leipzig, Felix-Bloch-Institut für Festkörperphysik
†Martin-Luther-Universität Halle-Wittenberg

Indium thiospinel semiconductors may potentially be used in intermediate band (IB) solar cells [1]. For that, transition metal ions have to substitute indium at octahedral lattice positions. For a sufficient transition metal concentration a delocalized defect band will form enabling transition from the valance band to the IB and from the IB to the conduction band leading to a substantial increase of the maximum efficiency of IB solar cells compared to conventional single junction solar cells [1]. So far, epitaxial growth of p-type In_2S_3 thin films was not reported. Hence, realization of pn-heterostructures has to be investigated for potential exploitation of In_2S_3 in IB solar cells. We have fabricated highly rectifying vertical heterostructures on undoped and vanadium-doped In_2S_3 [2]. All In_2S_3 layers were deposited by molecular beam epitaxy on AZO-layers. On top, thin films of $ZnCo_2O_4$ (ZCO) were grown by pulsed-laser deposition. The electrical

properties of the heterostructures were investigated by current-voltage measurements for temperatures between 100 and 300K. The reverse current of the diodes has an activation energy of about 1.6 eV for the undoped and 1.3 eV for the V-doped sample, respectively, and indicate defect assisted recombination as reverse current transport process.

Room temperature current-density–voltage characteristics of AZO/ZCO/In_2S_3:V pn-diodes are depicted in figure 9.17 for various vanadium doping concentration. A current rectification of more than six orders of magnitude is achieved for diodes comprising nominally undoped In_2S_3 layers. The incorporation of vanadium leads to a slightly reduced (increased) forward (reverse) current and with that lower current rectification, however, the electrical properties of these diodes are sufficient for photo-voltaic activity. For both type of diodes an open-circuit voltage and a short-circuit current of 300 mV and 0.29 mA/cm^2 were determined upon illumination with an AM1.5 spectra (100 mW/cm^2).

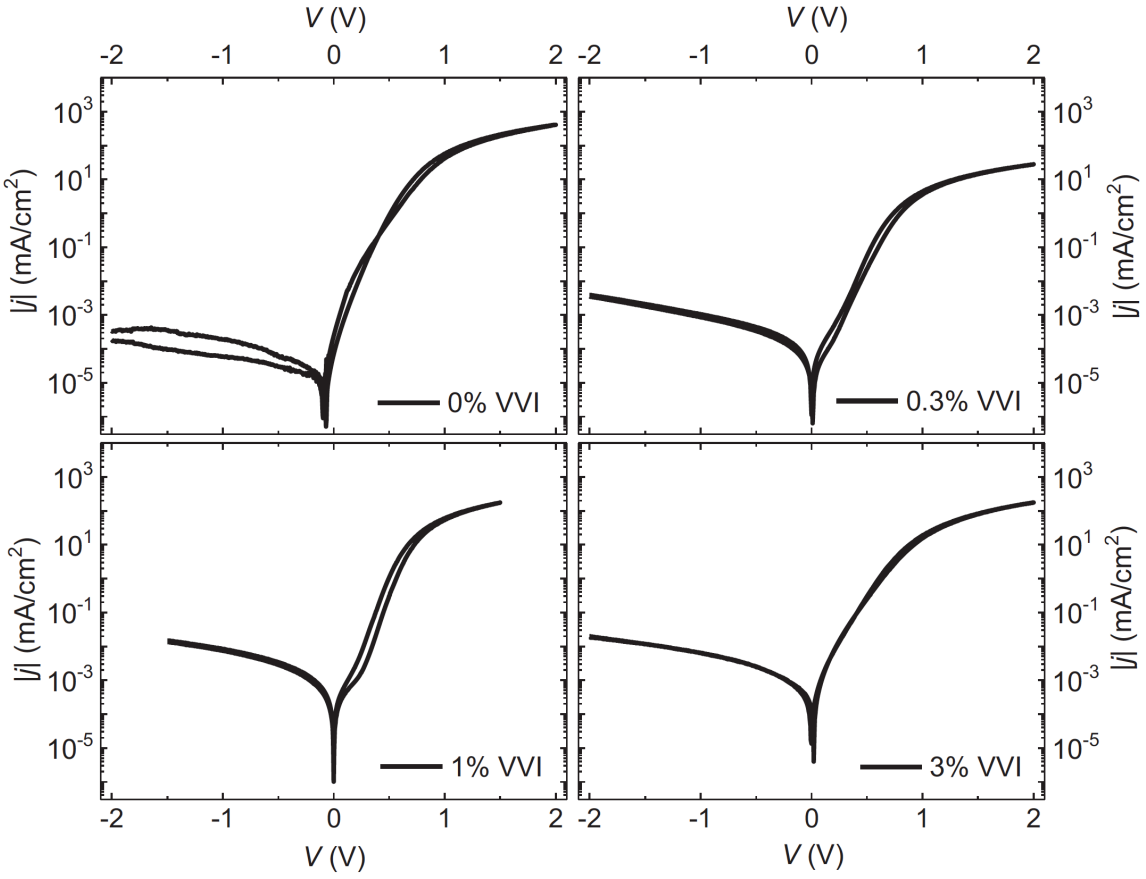

Figure 9.17: Room temperature current-density–voltage characteristics of representative AZO/In_2S_3:V/ZCO-diodes with varying V/(V+In)-ratios. The oxygen partial pressure during deposition was 0.03 mbar.

[1] P. Palacios, I. Aguilera, K. Sánchez, J. C. Conesa, and P. Wahnón, Phys. Rev. Lett. **101**, 046403 (2008).

[2] T. Jawinski, L. A. Wägele, R. Scheer, M. Grundmann, and H. von Wenckstern, physica status solidi (a), **215**, 1700827 (2018).

9.11 Negative-U properties of the deep level E3 in ZnO

R. Pickenhain,[*] H. von Wenckstern,[*] M. Schmidt,[†] A. Pöppl,[*] G. Benndorf,[*] R. Böttcher,[*] M. Grundmann[*]

[*]Universität Leipzig, Felix-Bloch-Institut für Festkörperphysik
[†]Helmholtz-Zentrum für Umweltforschung, Leipzig

A common electronic defect in the wide bandgap semiconductor zinc oxide (ZnO) is the so-called E3 defect having one transition level about 300 meV below the conduction band minimum. E3 has been found in material of various source including bulk single crystals and heteroepitaxial thin films [1]. Despite numerous experimental and theoretical studies, the microscopic origin of the E3 defect is not resolved, conclusively. We comprehensively investigated properties of the E3 defect by temperature-dependent capacitance measurements, deep-level transient spectroscopy (DLTS), electron paramagnetic resonance, temperature-dependent photo luminescence (PL) measurements and optical DLTS (ODLTS).

The capacitance, DLTS and ODLTS measurements reveal that E3 can capture up to two electrons; the capture of the first occurs very quickly, an energetic barrier of about 100 meV exists for the capture of the second electron. The capture of the second electron leads to strong lattice relaxation. In a thermal emission process these two electrons are emitted simultaneously, implying that the E3 defect is a negative-U center. We determined the photoionization cross-sections for the three possible transitions $\epsilon(+2/+1)$, $\epsilon(+1/0)$ and $\epsilon(+2/0)$. If thermal emission is suppressed optical excitation with energy between 550 meV and 1 eV will induce the optical emission of both electrons into the conduction band. Photon energies above 1 eV will excite a single electron into the conduction band and reconfigure the level into the meta-stable singly occupied state that would correspond to V_{O}^{+}. Further, we have demonstrated, that E3 is involved in a radiative recombination that can be excited with sub-bandgap energy photons and that has its maximum intensity at about 2.1 eV. By temperature dependent measurements we demonstrated, that this transition can only be excited for temperatures at which the E3 defect is not occupied by electrons. If this is the case, we only observed the commonly reported defect band emission. Next, the samples were investigated by electron paramagnetic resonance (EPR) measurements as a function of temperature and optical excitation energy. We found that numerous properties of the E3 defect, determined by DLTS, ODLTS and PL, and the oxygen vacancy, investigated by the EPR experiments, are similar. These include temperature range in which E3 $\epsilon(+2/+1)$ transition level or V_{O}^{+} is observable, temperature dependence of E3-related emission band and EPR V_{O}^{+} intensity, excitation energy dependence of photo cross-section of the E3 $\epsilon(+2/+1)$ transition and EPR V_{O}^{+} line amplitude being depicted in fig. 9.18. These similarities suggest that the nature of the E3 defect is the oxygen vacancy.

[1] R. Pickenhain, M. Schmidt, H. von Wenckstern, G. Benndorf, A. Pöppl, R. Böttcher, and M. Grundmann, phys. stat. sol. (b), **255**, 1700670 (2018).

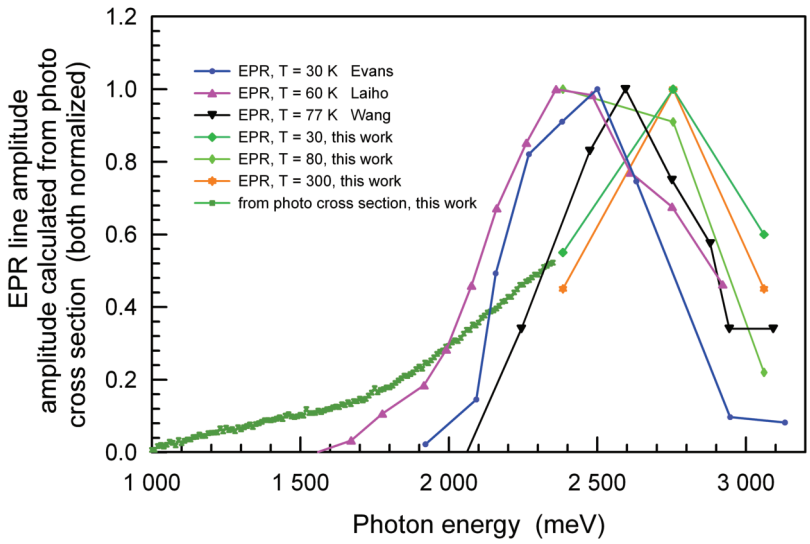

Figure 9.18: Collection of available literature data on the the dependence of the V_O^+ EPR signal strength on incident photon energy, our own EPR results and the photo ionization cross-section of the E3 $\epsilon(+2/+1)$ transition level calculated from ODLTS data.

9.12 Magnetoelectric coupling in $BaTiO_3$-$BiFeO_3$ multilayers – an interface effect?

S. Hohenberger, J. Jochum*, K. Temst*, M. Grundmann, M. Lorenz

*Institute for Nuclear and Radiation Physics, KU Leuven, Belgium

Composite multiferroic heterostrctures, consisting of ferroelectric and (anti-) ferromagnetic materials, promise to play a central role in the utilization of the magnetoelectric (ME) effect in e.g. data storage and magnetic sensing applications [1]. A particularly successful approach has been the combination of the only known single-phase ME multiferroic $BiFeO_3$ (BFO) [2] with the archetypal ferroelectric $BaTiO_3$ (BTO) in epitaxial multilayer thin films [3–6]. Up to a tenfold increase of the ME coupling coefficient α_{ME} relative to the single layer value for BFO of 6 $Vcm^{-1}Oe^{-1}$ [2] was reported.
Our previous work [3] suggests a significant influence of the thickness of either the BFO layer, or the double layer thickness d_{dl} of BTO and BFO together, on the magnitude of ME coupling in these multilayers. This calls into question the results reported in [4] and [5], which compared samples deposited at various oxygen pressures and concluded a dependency on p_{O_2}. A closer look at the investigated samples reveals that the laser pulse numbers for the films deposited at varied p_{O_2} were kept constant, leading to different double layer thicknesses, as the deposition rates strongly depend on the background gas pressure. For example the 0.01 mbar and 0.25 mbar samples in [5] have respective

double layer thicknesses of 38.6 nm and 13.8 nm, with α_{ME} values of 13.4 $Vcm^{-1}Oe^{-1}$ and 49.7 $Vcm^{-1}Oe^{-1}$. A TEM investigation revealed a higher level of microstrain in the low-α_{ME} sample, which was attributed to increased oxygen deficiency due to lower p_{O_2}. In an effort to re-evaluate and distinguish the influences of oxygen partial pressure, double-layer thickness, and BTO-to-BFO thickness ratio, three sample series were grown by pulsed laser deposition on Nb-doped $SrTiO_3$ under closely controlled deposition conditions. The first series of multilayer samples was created with p_{O_2} ranging from 0.01 mbar to 0.25 mbar and tightly controlled d_{dl} of 20.0 ± 0.2 nm. For the second series, a constant 1:1 BTO:BFO ratio was maintained while varying d_{dl} from 4.6 ± 0.2 nm to 20.1 ± 1.0 nm. For the last series, d_{BTO} and d_BFO were varied from 2 nm to 18 nm, while keeping a constant d_{dl} of 19.7 ± 0.3 nm. The substrate temperature was maintained at 680 C and p_{O_2} was 0.25 mbar for the ratio- and d_{dl}-series.
Fig. 9.19 a)-c) shows the measurement values of α_{ME} at 300 K in 0 T H_{DC} obtained via the dynamical method in 10 Oe H_{AC} for the respective sample series, as measured at the KU Leuven in Belgium. In [4] a monotonic decline of α_{ME} with decreasing p_{O_2} was apparent. However, the measurements presented in Fig. 9.19 a) show an initial decline of α_{ME} from 0.25 mbar to 0.1 mbar, which is reverted toward lower p_{O_2}. The value of α_{ME} for 0.01 mbar is even slightly larger than for 0.25 mbar, reaching 110 $Vcm^{-1}Oe^{-1}$. The explicit variation of d_{dl} reveals a monotonous dependency of α_{ME} on d_{dl}, see Fig. 9.19 b). The absolute as-measured ME voltage U_{ME} is similar for all five presented samples with 35.3 ± 1.9 mV, which results in a thickness-normalized α_{ME}-value of 480 $Vcm^{-1}Oe^{-1}$ for the d_{dl} = 4.6 nm sample and a $\propto 1/x$ dependency of α_{ME} on d_{dl}. Hence, the reported dependence of α_{ME} on p_{O_2} [4, 5] must be regarded in part as a result of the varying d_{dl}. The variation of BTO-BFO thickness ratios from 1:9 to 9:1 in series of multilayers with d_{dl} = 19.7 ± 0.3 nm, as presented in Fig. 9.19 c) has no substantial effect on α_{ME}. Across the ratio series, U_{ME} values vary only slightly around 35.1 ± 0.6 mV and the resulting α_{ME} values around 110 ± 3 $Vcm^{-1}Oe^{-1}$. In strain-coupled ME heterostructures consisting of piezoelectric and magnetostrictive materials, the dependency of α_{ME} on the volume fraction of the piezoelectric phase typically resembles an inverted bell curve [7], much unlike the plateau-behavior presented in Fig. 9.19 c). The variation of α_{ME} reported in [3] and shown in Fig. 9.19 b) can be said to depend on the total d_dl, and not just the individual BFO-layer thickness.

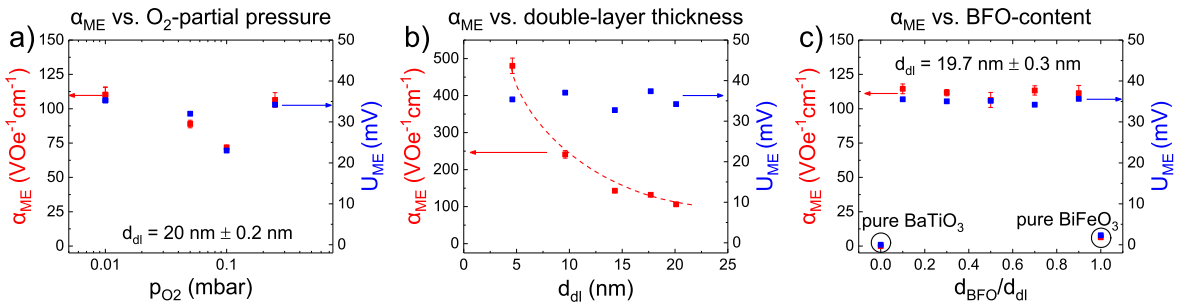

Figure 9.19: Magnetoelectric voltage (blue) and thickness-normalized magnetoelectric coupling coefficient (red) for multilayers under variation of a) oxygen pressure p_{O_2}, b) double-layer-thickness d_{dl}, and c) BTO-BFO ratio.

These measurements combined suggest that the true origin of the greatly enhanced ME coupling in the presented BTO-BFO multilayers does not lie strictly in mechanical coupling and microstrain distribution, but is rather to be considered an interface effect.

Various heterostructures have been reported where interface effects, rather than strain mediate the ME coupling. In $BaTiO_3/La_{2/3}Sr_{1/3}MnO_3$ heterostructures, e.g., orbital reconstruction was identified as the source of ME coupling [8]. The possibility of a thickness-dependent crossover from strain- to charge-mediated ME coupling was reported for $La_{0.7}Sr_{0.3}MnO_3/PbZr_{0.2}Ti_{0.8}O_3$ [9]. The occurrence of a similar effect could explain the observed non-dependency of the ME voltage on d_{dl} and the BTO-BFO ratio. This could also explain the scaling of α_{ME} with the number of double layers of BTO-BFO reported in [6], which showed a linear increase of α_{ME} from $16.1 \pm 3\,\mathrm{Vcm^{-1}Oe^{-1}}$ to $27.6 \pm 3\,\mathrm{Vcm^{-1}Oe^{-1}}$ for 2 to 20 double layers of $\propto 22\,\mathrm{nm}$ thickness.

[1] J. Ma *et al.*, *Adv. Mater.* **23**, 1062 (2011)
[2] J. Wang *et al.*, *Science*, **299** (5613), 1719-1722 (2003)
[3] S. Hohenberger *et al.*, *J. Phys. D: Appl. Phys.* **51**, 184002 (2018)
[4] M. Lorenz *et al.*, *Appl. Phys. Lett.* **106**, 012905 (2015)
[5] M. Lorenz *et al.*, *Adv. Mater. Interfaces*, 1500822 (2016)
[6] V. Lazenka *et al.*, *Appl. Phys. Lett.* **110**, 092902 (2017)
[7] M. I. Bichurin *et al.*, *Phys. Rev. B* **68**, 05402 (2003)
[8] B. Cui *et al.*, *Adv. Mater.* **27**, 6651 (2015)
[9] S. Spurgeon *et al.*, *ACS Nano* **8** (1), 894 (2014)

9.13 Femtosecond time-resolved spectroscopic ellipsometry

O. Herrfurth, L. Trefflich, M. Rebarz*, S. Espinoza*, T. Pflug†, M. Olbrich†, J.A. Leveillee‡, A. Schleife‡, M. Grundmann, A. Horn†, J. Andreasson*§, R. Schmidt-Grund

*ELI Beamlines, Institute of Physics, Czech Academy of Science, Prague, Czech Republic
†Laserinstitut Hochschule Mittweida,Schillerstr. 10, 09648 Mittweida, Germany
‡Department of Materials Science and Engineering, University of Illinois at Urbana-Champaign, Urbana, USA
§Condensed Matter Physics, Department of Physics, Chalmers University of Technology, Gothenburg, Sweden

9.13.1 Transient birefringence and dichroism in *m*-ZnO

The recently established collaboration between ELI Beamlines (Czech Republic) and Universität Leipzig led to the development of a set-up for pump-probe femtosecond time-resolved spectroscopic ellipsometry (tSE). It enables ellipsometric measurements with very high time resolution (200 fs) in a broad observable spectral range (1.8 eV to 3.6 eV). First experiment were conducted on 30 nm thin *c*-plane oriented chemZnO film on an amorphous glass substrate grown by pulsed laser deposition [1]. In this work, the dielectric function (DF) was modelled as isotropic because the experimental set-up

is mostly sensitive to the DF tensor component perpendicular to the crystal's optic axis such that the optical anisotropy of ZnO is neglected. In subsequent experiments, the full DF tensor was obtained from measurements parallel and perpendicular to the crystal's optic axis on an *m*-plane oriented ZnO thin film grown by molecular beam epitaxy. The estimated UV-pump induced density of electron-hole pairs is $2 \times 10^{19}\mathrm{cm}^{-3}$. As a result, we observe transient birefringence and dichroism (Fig. 9.20) upon UV-pumping in the visible spectral range that is transparent under equilibrium conditions. The film becomes dichroic for a few ps in the spectral range below 2.0 eV and reveals an additional pseudo-isotropic point where $n_e = n_o$ but $\kappa_e \neq \kappa_o$. Comparison to the ZnO bandstructure and first-principles dielectric-function calculations provide evidence for inter-valence-band transitions of hot charge carriers near the *M* point in the Brillouin zone. The dipole transitions are governed by selection rules for light polarized perpendicular or parallel to the material's optic axis which can cause the transient optical anisotropy.

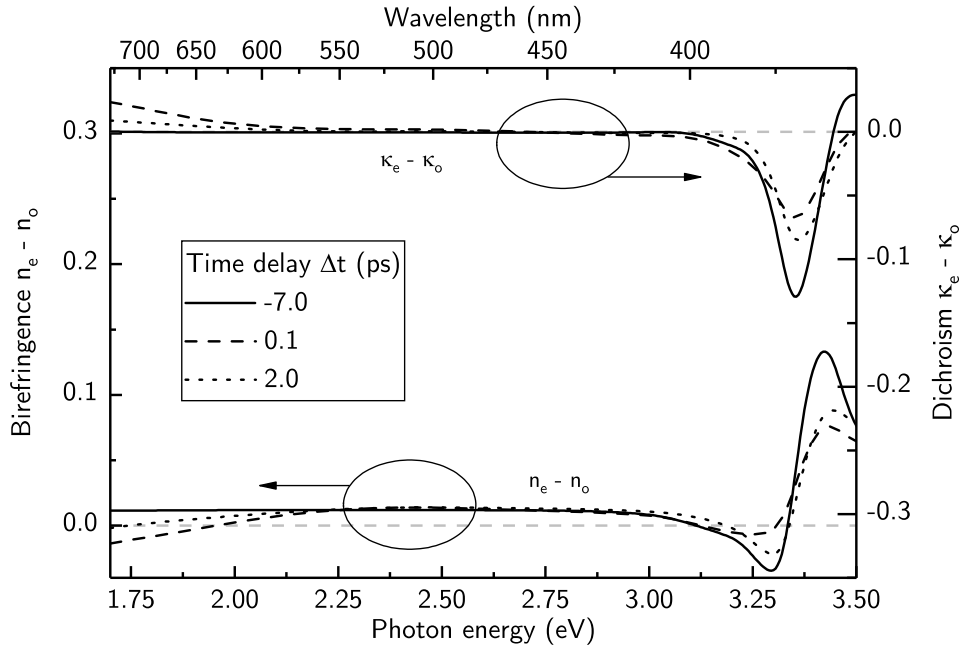

Figure 9.20: Transient optical anisotropy shown as birefringence $n_e - n_o$ and dichroism $\kappa_e - \kappa_o$ for selected pump-probe time delays Δt.

9.13.2 Comparison of the dielectric function with existing models for highly excited ZnO and conventional transient spectroscopy

In comparison to ellipsometry, conventional reflectance and transmittance measurements lack any phase information of the electromagnetic waves interacting with the sample. This is usually compensated for by before-hand assumptions on the physical processes that, however, can lead to incorrect conclusions. Reflectance and transmittance spectra can be reconstructed from the knowledge of the DF. We generate reflectance spectra based on the DF obtained by tSE and compare them to theoretical values of Versteegh et al. [2] which were refined by Wille et al. [3]. The underlying DF of Wille et al. allows to explain gain and lasing mechanisms in ZnO micro- and nanowires [4].

Both theoretical approaches are based on a solution of the Bethe-Salpeter equation [5] for a simplified ZnO-like bulk system. The reflectance spectra are exemplary for various different pump-probe reflectance studies on ZnO [6–9].

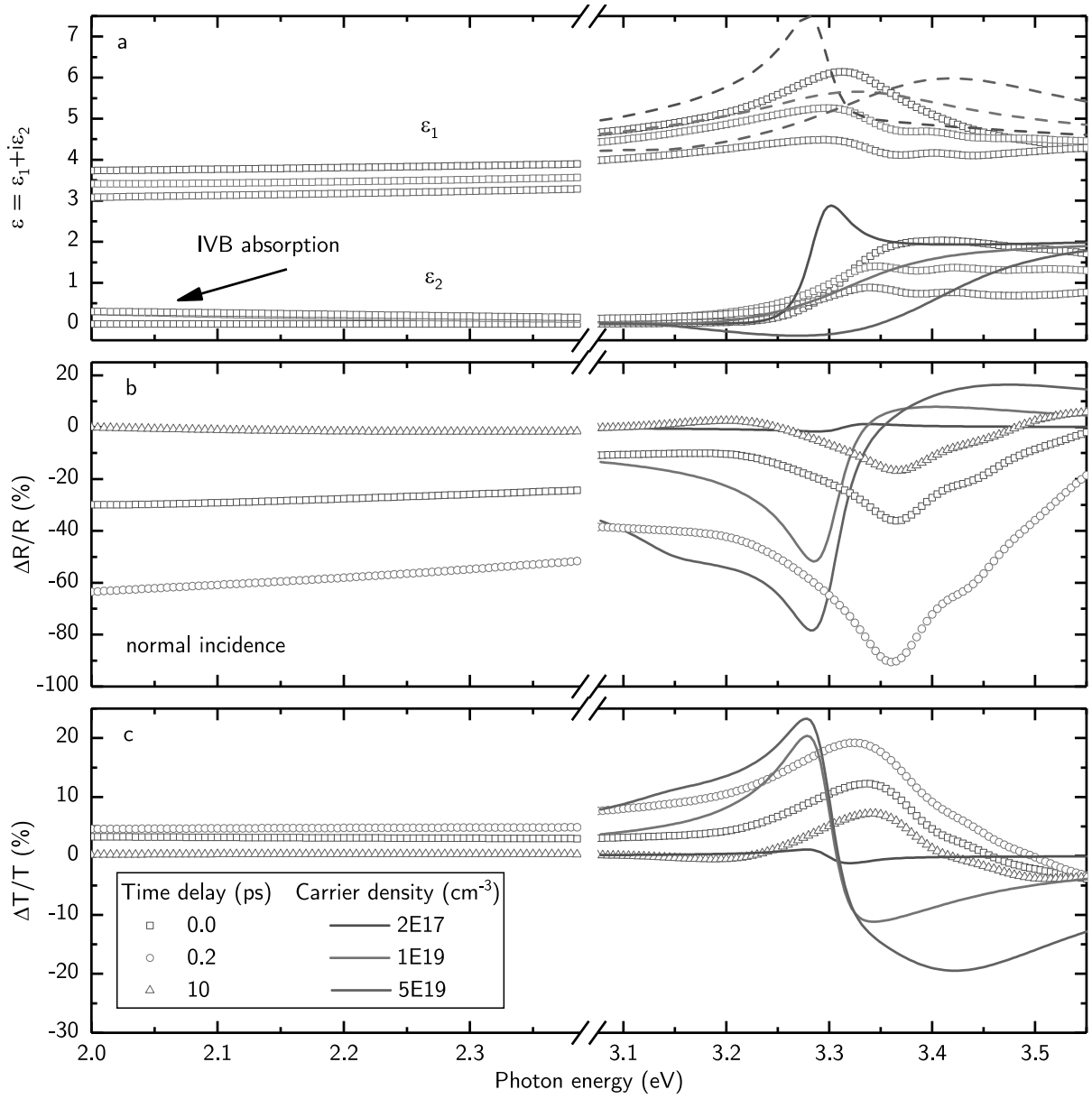

Figure 9.21: a DF of highly excited ZnO. Symbols represent the spectra obtained in this work at three different delays after photo-excitation. Lines show the expected spectra according to the model of Wille et al. for three different charge-carrier densities. **b** Computed transient reflectance and **c**: transmittance difference spectra at normal incidence for a 30 nm thin ZnO film on fused silica substrate according to the DFs in **a**. Note that although IVB absorption sets in, transmittance at lower energies increases upon pumping while reflectance decreases. This is caused by the lowered refractive index.

Symbols in Fig. 9.21 show the DF as obtained in this work at selected pump-probe time delays; lines represent theoretical curves according to Wille et al. for various carrier densities. Both studies find a decrease in the real and the imaginary part of the DF with increasing carrier density. The model of Wille et al. is about 100 meV blueshifted

and predicts $\varepsilon_2 < 0$ which can lead to optical gain and lasing. This is not observed in our experiment due to the reflection geometry. Optical gain can only occur due to stimulated emission involving photons of equal wavevector (magnitude and direction). So-called gain spectroscopy was only reported in transmission geometry. Furthermore, it is seen that the theoretical curve of Wille et al. is not able to explain the features related to exciton-phonon complexes at 3.4 eV since electron-phonon interaction is neglected in the model. In the spectral range far below the band gap which is not covered by Wille et al., we find increased absorption which is related to the IVB absorption. The relative difference spectra of transmittance (panel b in Fig. 9.21) and reflectance (panel c) are computed for a structure consisting of 30 nm *c*-plane oriented ZnO on a glass substrate which is equivalent to the sample studied in this work. Reflection from the substrate backside is ignored. Changes around the absorption edge of ZnO are of the same order of magnitude for both using the DF from theoretical model (lines) and applying the DF obtained in this work. Surprisingly, in the spectral range of the IVB aborption the transmittance is increased although absorption appears. It is clear that the increased transmittance is related to decreased reflectance caused by the decrease in ε_1 and hence refractive index. This is in accordance with the Kramers-Kronig relations and is related to both, the occurring inter-valence-band absorption as well as the absorption bleaching at the absorption edge. We would like to emphasize here that interpretation of the conventional reflectance or transmittance changes can lead to erroneous conclusions about their physical origin because effects caused by changes in the real and imaginary part of the DF cannot be separated. Assuming a non-varying refractive index is insufficient and retrieval by exploiting the Kramers-Kronig relations is usually hampered by the limited spectral range.

9.13.3 Spatially and time-resolved single-wavelength pump-probe ellipsometry on a *c*-ZnO thin film

Additional information on the transient physical processes in highly excited semiconductors can be obtained by performing time-resolved ellipsometry with spatial resolution [10, 11]. To this aim, joint experiments with the Laserinstitut Mittweida were conducted [11]. We report on spatially and time-resolved pump-probe ellipsometry measurements performed on the same c-plane oriented ZnO thin film as in reference [1] using ultrafast single-wavelength probe radiation ranging from the near-IR to visible spectral range with a time resolution of approximately 50 fs. The ellipsometer is built in PSC_RA configuration which is favourable compared to the PC_RSA configuration [10] due to the non-moving spot of the probe beam. The imaging optics enables a magnification of factor 20 and the spatial resolution (<1 μm) is limited by the respective probe wavelength and the pixel size of the CCD detector. The thickness of the ZnO film is in the order of the optical penetration depth of the applied pump radiation (266 nm wavelength) whereby homogeneous optical excitation by single-photon absorption can be assumed throughout the entire film thickness. The fluence of the pump radiation is well below the ablation threshold and the induced charge carrier density is estimated to be approximately $1 \times 10^{20}\,\mathrm{cm}^{-3}$. The ellipsometric angles Ψ and Δ (Fig. 9.22) are obtained by numerical evaluation of reflectance-difference images for each measured angle of the compensator.
Therewith, the transient wavelength-by-wavelength dielectric function (DF) is calcu-

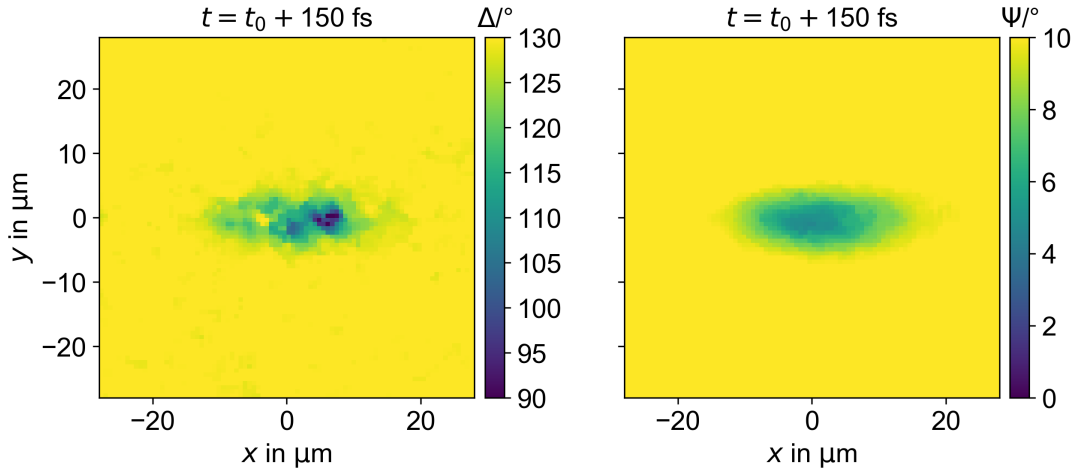

Figure 9.22: Spatially resolved ellipsometric angles Ψ and Δ obtained by pump-probe ellipsometry at time delay 150 fs and probe wavelength 515 nm. The dark area in the center corresponds to the spot of the pump laser.

lated via the transfer-matrix algorithm. We find a transient increase of the imaginary part of the DF simultaneous to a drop of the real part. This effect may be attributed to electronic transitions between different valence bands being possible as optically excited holes scatter to the edges of the Brillouin zone.

[1] S. Richter, *et al.*: arXiv:http://arxiv.org/abs/1902.05832v1 (2019)
[2] M. A. M. Versteegh, *et al.*: Phys. Rev. B **84** (2011) doi:10.1103/physrevb.84.035207
[3] M. Wille, *et al.*: Nanotechnology **27**, 225702 (2016) doi:10.1088/0957-4484/27/22/225702
[4] M. Wille, *et al.*: Appl. Phys. Lett. **109**, 061102 (2016) doi:10.1063/1.4960660
[5] H. Haug, S. W. Koch: *Quantum Theory of the Optical and Electronic Properties of Semiconductors* (WORLD SCIENTIFIC, 1990) doi:10.1142/0936
[6] T. Shih, *et al.*: Appl. Phys. A **96**, 363 (2009) doi:10.1007/s00339-009-5196-0
[7] C. J. Cook, *et al.*: in *Oxide-based Materials and Devices*, edited by F. H. Teherani, *et al.*. (SPIE, 2010) doi:10.1117/12.845636
[8] T. Shih, *et al.*: J. Appl. Phys. **109**, 043504 (2011) doi:10.1063/1.3549614
[9] P.-C. Ou, *et al.*: Appl. Phys. B **106**, 399 (2011) doi:10.1007/s00340-011-4706-x
[10] J. Csontos, *et al.*: Appl. Surface Science **421**, 325 (2017) doi:10.1016/j.apsusc.2017.03.186
[11] T. Pflug, *et al.*: Appl. Phys. A **124**, 116 (2018) doi:10.1007/s00339-018-1550-4

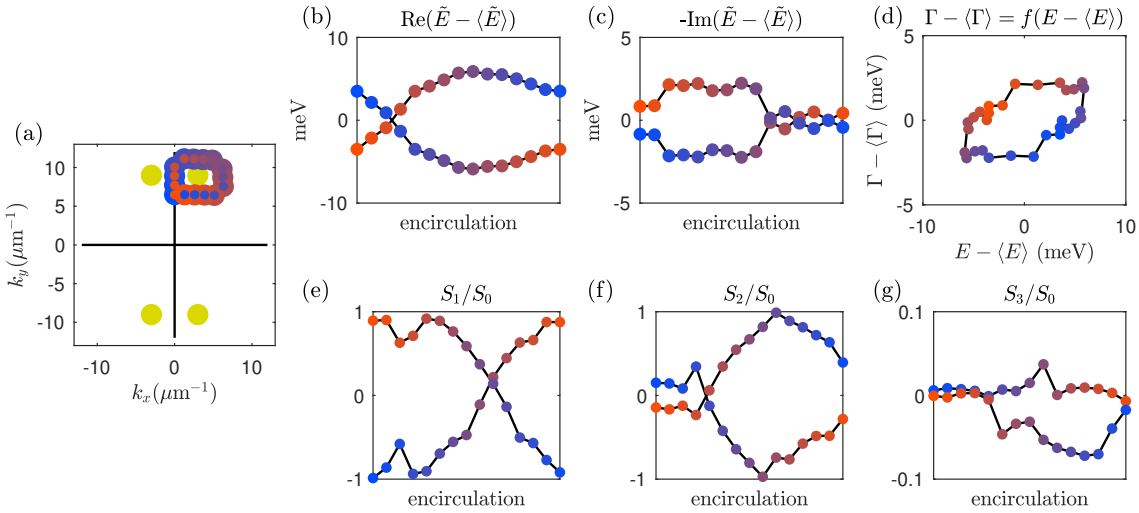

Figure 9.23: Overview of the trajectory corresponding to a clockwise encirclement of a Voigt exceptional point. (a): trajectory in the momentum space ($k_{||}$), (b): mode energy and (c): broadening along the path. Encircling once flips one mode to the other. (d): mode broadening as a function of mode energy along the path. (e,f,g): Stokes parameter spectra of the modes from the amplitudes of the Lorentz oscillators along the trajectory.

9.14 Voigt exceptional-points in an anisotropic ZnO-based planar microcavity: square-root topology and polarization vortices

S. Richter, H.-G. Zirnstein*, E. Krüger, J. Zúñiga-Pérez†, C. Deparis†, L. Trefflich, C. Sturm, B. Rosenow*, M. Grundmann, R. Schmidt-Grund

*Universität Leipzig, Institut für Theoretische Physik, Brüderstr. 16, 04103 Leipzig, Germany
†Université Côte d'Azur, CRHEA-CNRS, rue Bernard Gregóry, 06560 Valbonne, France

Exceptional points (EP) that represent topological charges, are of great interest in the recent research of topological non-trivial photonic systems. A particular class of such exceptional points are Voigt points [1], which represent the propagation directions in anisotropic crystals along which optical modes degenerate, leading to a single circularly polarized eigenmode. However, the presence of such EPs is not limited to bulk single crystals and can occur in a variety of systems described by non-Hermitian Hamiltonians, as e.g. planar microcavities with broken cylindrical symmetry [2], which allows to exploit a special kind of exceptional points, associated to propagation of circularly polarized light along specific directions, in widespread optoelectronic devices (e.g. VCSELs). The various design degrees of freedom of such microcavities render them an ideal model systems and allow to circumvent the limitations caused by the difficulties of modifying material absorption by counting on the dissipation by photon loss, instead. Thus, the occurence and direction of such exceptional points can be controlled by the geometrical microcavity design.

Here we report on dielectric, anisotropic optical microcavities, based on nonpolar m-plane oriented ZnO that implements a non-Hermitian system and mimicks the

behaviour of natural Voigt points in anisotropic bulk crystals. The bottom distributed Bragg reflector (DBR), consisting of 16 pairs ZnO and $Mg_{0.29}Zn_{0.71}O$, as well as the cavity layer were fabricated by means of molecular beam epitaxy using m-plane oriented ZnO substrates [3], such that all ZnO and $Mg_{0.29}Zn_{0.71}O$ layers are m-plane oriented. The top-DBR was prepared non-epitaxially by pulsed laser deposition and consists of 6 pairs of Al_2O_3 and YSZ (Y-stabilized ZrO_2). The cavity layer thickness is tuned to 9/8 of the central wavelength of the DBR ($\approx$ 400 nm) and corresponds to a cavity photon mode energy of about 3 eV, such that the structure is working in the transparent spectral range of all used materials.

Polarization-resolved reflection experiments depending on the angle of incidence and sample azimuth angle were used to map the momentum space of the radiative modes. The achieved Stokes parameter spectra $\vec{S}(E)$ have been modeled simultaneously in a spectral range of 100 meV around the cavity modes, using Lorentzian peaks to describe the mode energy and broadening. The experimental positions of exhibited exceptional points, which can be identified as degeneracies of the complex mode energy, are reproduced by our theoretical calculations. The square-root topology of the mode energy surface around the Voigt exceptional points was proved by encircling such a point in the momentum space. As can be seen in Fig. 9.23 one roundtrip in momentum space yields a continuous exchange of the two modes, i.e. the energetically higher (and spectrally narrower) mode becomes the energetically lower (and broader) one and vice versa. Indeed only encircling the Voigt point twice restores the initial situation, as observed in the first experimental demonstration of exceptional points in a microwave cavity [4], proving that the observed Voigt points are indeed exceptional points.

[1] W. Voigt: The London, Edinburgh, and Dublin Philosophical Magazine and Journal of Science **4**, 19 (1902)
doi:10.1080/14786440209462820
[2] S. Richter *et al.*: Phys. Rev. A **95**, 023836 (2017)
doi:10.1103/PhysRevA.95.023836
[3] J. Zúñiga-Pérez *et al.*: Appl. Phys. Lett. **108**, 251904 (2016)
doi:10.1063/1.4954796
[4] C. Dembowski *et al.*: Phys. Rev. Lett. **86**, 787 (2001)
doi:10.1103/PhysRevLett.86.787

9.15 Structural and optical properties of carbon nanodot based planar microcavities

L. Trefflich, F. Dissinger*, C. Sturm, S.R. Waldvogel*, M. Grundmann, R. Schmidt-Grund

*Institute for Organic Chemistry, Johannes Gutenberg Universität Mainz, 55128 Mainz

Carbon nanodots (cdots) are discrete quasispherical nanoparticles with diameters below 10 nm [1]. They can be synthesized from many carbon sources like tea, gras, coffee, and citric acid [1]. They are very eco-friendly and biocompatible [2] and show some interesting properties like photocatalysis [3] and a strong, tunable photoluminescence [4]. This has led to a number of interesting applications like chemical sensing[5] and the use as acitve laser material [6]. Our goal is to incorporate carbon nanodots in a

verticle planar microcavity for LED and laser applications. In a verticle microcavity, the cavity layer has to fullfill the condition $n(\lambda) \cdot d = \lambda/2$, with the wavelength-dependent refractive index $n(\lambda)$, the layer thickness d and the design-wavelength λ. For a cdot emission wavelength of around 400 nm and a typical refractive index of gelatin of around 1.5 (at 400 nm) we find a minimum cavity thickness in the range of 130 nm. This is much larger than the cdot itself. Therefor, we need to incorporate them into a matrix which thickness we can control. A suitable cavity material has to fullfill a couple more conditions. The material has to be transparent, in order to avoid reabsorption of the cdot luminescence. Furthermore, the material should be ecofriendly and show no photoluminescence itself. We decided on commercial gelatin as a cavity material. In the first section of this work we report about the stuctural properties of the microcavities. In the second section we investigate the optical properties using angularly resolved microreflectivitiy measurements as well as microphotolumincescence spectroscopy.

9.15.1 Sample Fabrication and Structural Properties

The microcavity consists of two distributed bragg reflectors (DBR) and a cavity layer inbetween. The bottom DBR is made of 12 layer pairs YSZ and Al_2O_3 grown by pulsed laser deposition [7]. For the cavity layer we solved 10 mg cdots in ethanol using a ultrasonic cleaner and filtered the solution with a filter with 200 nm pore size. We than mixed 0.2 ml of this ethanol-cdot-solution with 1 ml liquid gelatin at 45°C. This mixture was then spincoated on the bottom DBR at 180 RPS for 3 min resulting in a layer thickness of around 600 nm. The top DBR was grown on top of that, again with pulsed laser depositon at room temperature. It has only 10 layerpairs, which gives a slightly lower reflectivity and helps to guide the light out of the upper side of the microcavity. Figure 9.24(a) shows an optical image of the whole sample. Large scale inhomogenities are easily visible due to a not fully optimized spin coating process. A scanning transmission electron microscope (STEM) image of a focussed ion beam (FIB) cut cross-section (figure 9.24(b)) shows a good homogeneity of the DBRs with smooth interfaces and a homogeneous cavity layer on the scale of a few micrometers.

9.15.2 Optical properties

Angularly resolved reflectivity measurements (spot size 5 μm) were used to determine the quality of the microcavity (figure 9.25(a)). The quadratic angular dispersion of the cavity mode is clearly visible. The energy of the cavity modes shifts from 3.00 eV at normal incidence to 3.06 eV for incidence angles of ±20° respectively. The qualtiy factor of the cavity mode decreases with increasing incidence angles, visible by the increasing linewidth of the mode. Therefor, the smallest linewidth is achieved at normal incidence. A linescan at normal incidence is shown in figure 9.25(b). The stop band of the resonator begins at 3.26 eV and ends at 2.64 eV. By fitting a Lorentzian model to the data, the energy of the cavitymode was determined to 3.00 eV with a linewidth 4.3 meV. We can therefore calculate the qualityfactor at normal incidence to 702 indicating a good quality resonator structure when investigated with a microspot.

Microphotoluminescence spectroscopy (excitation with Coherent Mira HP, 360nm, 200fs, 3MHz) shows strong photoluminescence in the energy range of the cavity mode (figure 9.26(a)). Because of the integration over all incidence angles between ±20° we

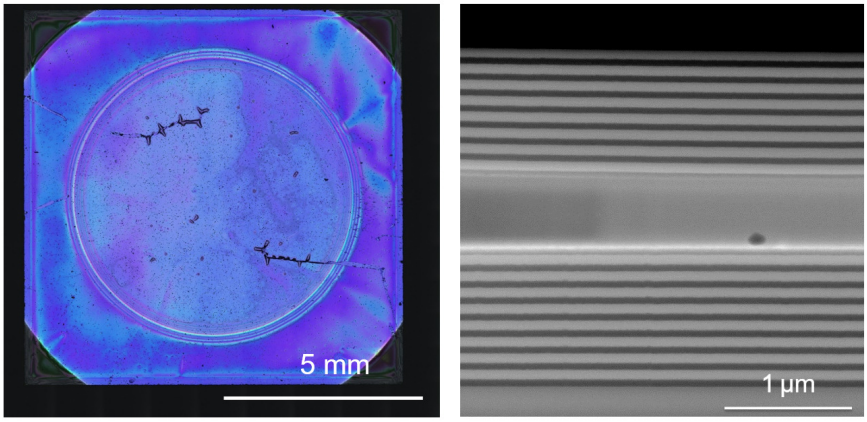

Figure 9.24: (a) Laser scanning microscope image of a carbon nanodot based planar microcavity. Millimeter scale inhomogeneities due to a not yet fully optimized spincoating process are visible. The top DBR has a smaller diameter to allow measurments of the cavity layer itself. (b) STEM image of a FIB lamella cut through the microcavity. The c-sapphire substrate, the bottom DBR, the gelatin cdot cavity mode as well as the top DBR are clearly visible. The cavity layer is homogeneous on the micrometer scale.

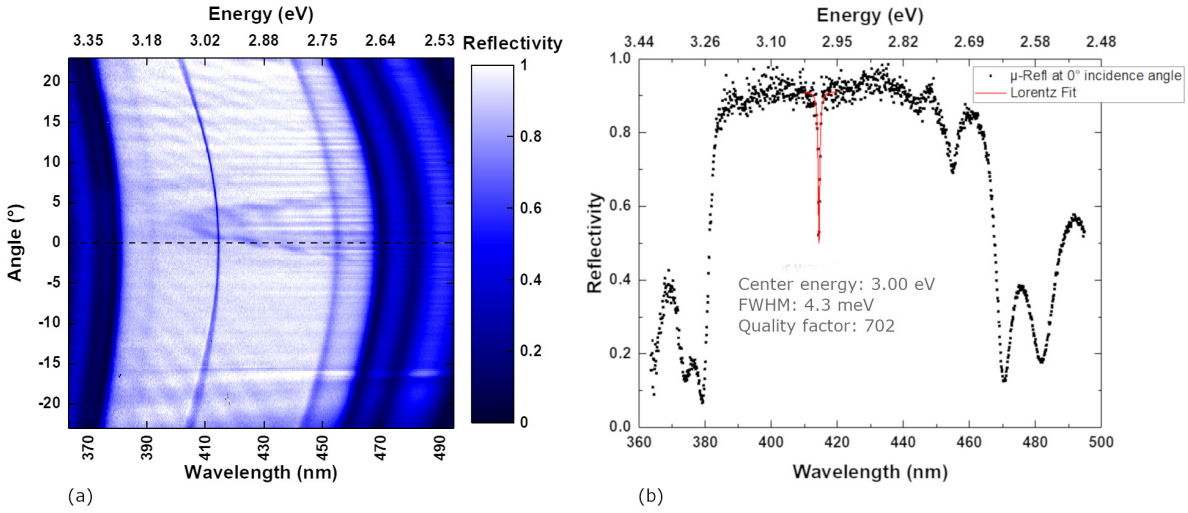

Figure 9.25: (a) Angularly resolved reflectivity measurement of the carbon nanodot based planar microcavity. The stopband of the microcavity (white area) and the cavity mode at 3.00 eV at normal incidence are visible. The cavity mode shows a quadratic angular dispersion, as expected. (b) Linescan of (a) for normal incidence (dashed line). A Lorentzian fit of the cavitymode gives an energy of 3.00 eV with a linewidth of 4.3 meV. That results in a quality factor of 702.

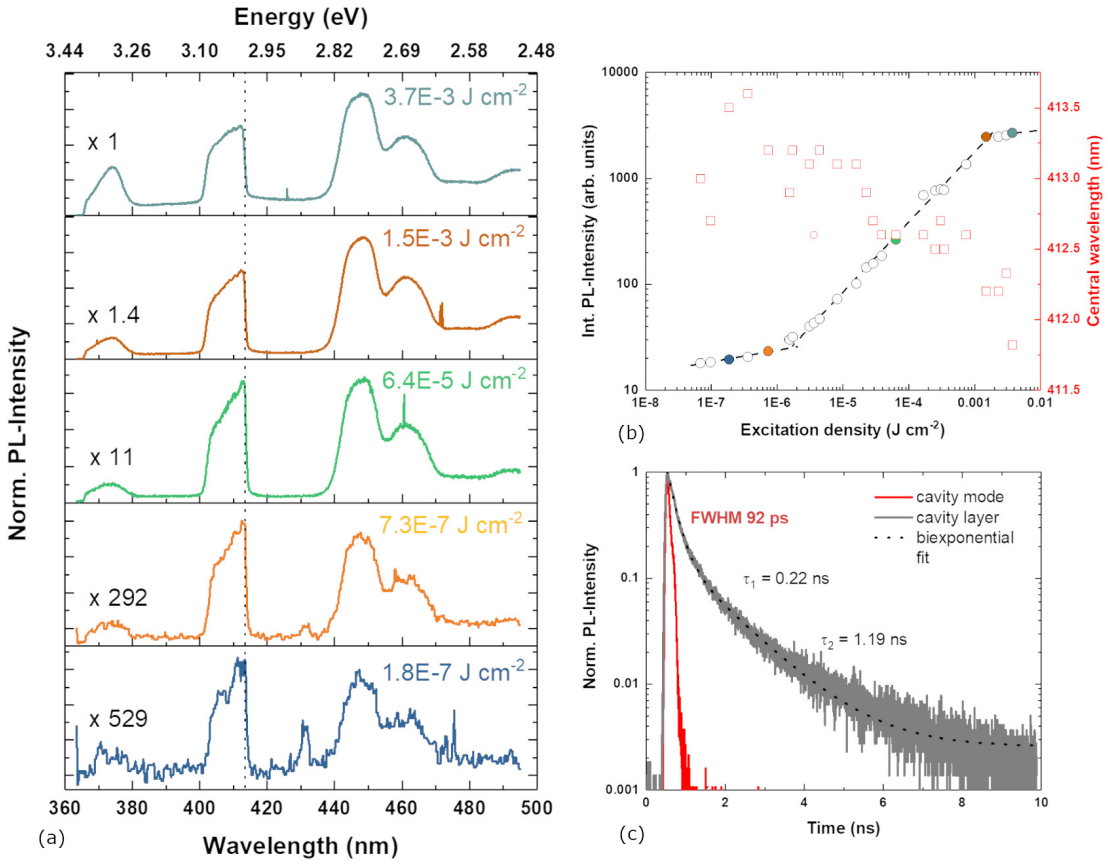

Figure 9.26: (a)Angularly integrated photoluminescence spectra of the carbon nanodot based microcavity for excitation densities from 1.8×10^{-7} Jcm^{-2}to 3.7×10^{-3} Jcm^{-2}. (b) The input-output characteristic of the device shows a slight s-curve with sublinear slope indicating only spontaneous emission. The damage threshold is reached for excitation densities higher than 1.5×10^{-3} Jcm^{-2}. The central wavelength of the cavity mode shows a slight shift towards shorter wavelengths. (c) The TCSPC measurements show a biexponential decay of the luminescence of the cavity mode with time constants of 0.2 ns and 1.2 ns. The luminecence of the cavity mode decays with a timeconstant of 90 ps. This is a clear sign for amplification of the cdot luminescence in the device.

see a broadened, asymmetric cavity mode. For increasing excitation densities we see a s-curved shape of the input-output charcteristic (figure 9.26(b)). Howhever, the slope is always lower than a linear increase, indicating only spontaneous emission with high losses from the sample. For excitation densities larger than 1 mJ we find a saturation behaviour because we are reaching the damage threshold of the carbon nanoparticles. The cavity mode shows a slight shift towards shorter wavelengths.To compensate for the increasing thermal losses at higher excitation intensities, the cavity mode shifts towards higher energies. Timeresolved measurements using a time-correlated single photon counting (TCSPC) setup show a biexponential decay for the luminescence of the cavity layer itself with time constants of 0.2 ns and 1.2 ns respectively. However, the luminescence of the cavity mode decreases with a time constant of 90 ps, which is roughly the time resolution of the setup. We can therefore conclude that there is amplification of the cdot emission through the cavity mode.

[1] P. Roy *et al.*: Mater Today **8**, 18 (2015)
doi:10.1016/j.mattod.2015.04.005
[2] J.C.G.E. da Silva *et al.*: Trends Anal Chem **8**, 30 (2011)
doi:10.1016/j.trac.2011.04.009
[3] L. Cao *et al.*: J Am Chem Soc **13**, 133 (2011)
doi:10.1021/ja200804h
[4] Y. Sun *et al.*: J Am Chem Soc **24**, 128 (2006)
doi:10.1021/ja062677d
[5] Y. Dong *et al.*: Anal Chem **14**, 84 (2012)
doi:10.1021/ac3012126
[6] W.Zhang *et al.*: Nanoscale **9**, 5957 (2017)
doi:10.1039/c7nr01101f
[7] H. Hilmer *et al.*: AIP Conf Proc **1199**, 151 (2010)
doi:10.1063/1.3295340

9.16 Spectroscopic determination of cation distribution in ferrimagnetic spinel ferrite thin films

V. Zviagin, P. Huth [*], M. Bonholzer [†], C. Sturm, J. Lenzner, A. Setzer, R. Denecke [*], P. Esquinazi, M. Grundmann, R. Schmidt-Grund.

[*]Universtät Leipzig, Wilhelm-Ostwald-Institut für Physikalische und Theoretische Chemie, Linnéstr. 2, Germany.
[†]now at: Max-Planck-Institut für Extraterrestrische Physik, Giessenbachstr. 1, D-85748 Garching, Germany.

Remarkable capabilities of complex oxides are realized by the virtue of versatile ion arrangement within the crystallographic lattice. Particularly, transition metal oxides, MFe_2O_4 ($M = Fe^{2+}, Zn^{2+}$), exhibit a diversity of cation configurations, making them uniquely suitable for a vast scope of applications. As the inverse spinel configuration ($Fe^{2+}Fe^{3+}_2O_4$) is modified to a normal ($Zn^{2+}Fe^{3+}_2O_4$) by Zn substitution, the magnetic and electric properties of magnetite, a half-metallic ferromagnet, can be tuned to a ferrimagnetic semiconductor or to that of franklinite, a superparamagnetic insulator. Additionally, remarkable optoelectronic tunability, high thermal and chemical stability enables photoanode application of $ZnFe_2O_4$ for solar water oxidation[1]. $ZnFe_2O_4$ is considered to be antiferromagnetic with a Néel temperature of 10 K. It crystallizes in a normal spinel structure, where Zn^{2+} and Fe^{3+} cations occupy tetrahedral (Td) and octahedral (Oh) lattice site, respectively. The rise in conductivity in the insulating $ZnFe_2O_4$ with the decrease in deposition pressure has been related to the increase in Fe^{2+} concentration, due to intrinsic defects[2]. Theoretical works have shown that oxygen vacancies and tetrahedrally coordinated Fe^{3+} cations alter magnetic interactions, giving rise to spontaneous magnetization at room temperature[3]. Furthermore, the formation of macroscopic defects, which show strong dependence on the substrate as well as the deposition temperature and atmosphere, result in an inhomogeneous cation configuration distribution within the thin film. Efforts to precisely determine the distribution of atomic species still remain technically challenging, and the mechanisms, responsible for

the strong magnetic response in $ZnFe_2O_4$, are yet to be fully understood. The Zn^{2+} and Fe^{2+} cations preferentially occupy the Td- and Oh-sites, respectively, whereas the Fe^{3+} has no preference and could be distributed over both sites. Therefore, depending on the amount of disorder and inversion within the normal spinel structure, the formula for possible cation distribution can be given by $[(Zn^{2+}Fe^{3+}]_{Td}[Zn^{2+}Fe^{3+}Fe^{2+}]_{Oh}O_4^{2-}$.

Spectroscopic ellipsometry, in a wide spectral range $(0.5-8.5)$ eV, was applied in order to probe the bulk cationic configuration in relation to the magnetic response, measured by superconducting quantum interference device (SQUID) and vibrating sample magnetometer (VSM). The dielectric function was approximated by a parametric model, consisting of Lorentzian, Gaussian and Critical Point Model functions, positioned at energies that correspond to electronic transitions. The model dielectric function (MDF) spectra was found to be dominated by transitions between d orbitals of Fe^{2+} ($\leq$1 eV), and transitions from O2p to Fe as well as Zn3d and 4s orbitals ($\geq$1 eV). Structural defects in the normal spinel, such as tetrahedral Fe^{3+} and octahedral Fe^{2+}, were evident from the strength of electronic transitions in the MDF spectra and showed a strong dependence on the substrate temperature and oxygen pressure, respectively. The transition involving Fe^{3+}_{Td} at 3.5 eV showed a strong magneto-optical response, determined by magneto-optical Kerr effect spectroscopy (MOKE)[4]. The presence of Fe^{3+} cations located on tetrahedrally coordinated lattice sites is due to the inversion mechanism, where the Zn^{2+} moves to octahedral and Fe^{3+} moves to tetrahedral lattice site, or to Fe^{3+} occupying nominally unoccupied tetrahedral lattice site. This would result in the antiferromagnetic oxygen mediated super-exchange (SE) interaction between Fe^{3+}_{Td} and Fe^{3+}_{Oh} to dominate over the ferromagnetic SE interaction between Fe^{3+}_{Oh} and Fe^{3+}_{Oh}. Therefore, the increase of the Fe^{3+}_{Td} cation transition strength in the MDF was directly correlated to the increase in magnetization saturation and remanence measured at 5 K with decreasing deposition temperature from 600 ℃ to 400 ℃[4]. Furthermore, the theoretical approximation of individual cation contribution to the X-ray photoelectron spectroscopy (XPS) Fe2p and 3p core level surface spectra allowed determination of Fe site occupation as well as an estimation of the relative concentration of individual cation.

$ZnFe_2O_4$ thin films were fabricated on $SrTiO_3$ substrates by pulsed laser deposition at 300 ℃ and at low (LPZFO) and high (HPZFO) oxygen partial pressures. The difference in the low energy features of the MDF is due to the presence of Fe^{2+}, as a likely result of oxygen vacancy formation in the LPZFO film, (Fig. 9.27(a)). The LPZFO and HPZFO films were subsequently annealed in oxygen and argon atmospheres, respectively, at temperatures varying from $(250-375)$ ℃. The sample surface was found to become smooth and roughen after annealing in oxygen and argon environment, respectively. Annealing the films at 250 ℃ induces a small change in room temperature magnetization saturation which could be attributed to change in cation distribution in the surface layer. A significant change to the MDF line-shape, after annealing the films at higher temperatures, is coincident with the decrease in the magnetic response, (Fig. 9.27(b)). This behavior can be explained by a cation redistribution mechanism, as the disordered spinel tends to a more stable, normal configuration. This is evident by a decrease (increase) in the peak involving tetrahedrally (octahedrally) coordinated Fe^{3+} cations in the MDF spectra.

The surface and bulk cation configuration was investigated as a function of Zn concentration in the $Zn_xFe_{3-x}O_4$ thin films with x varying from $(0-1.26)$. The clear dis-

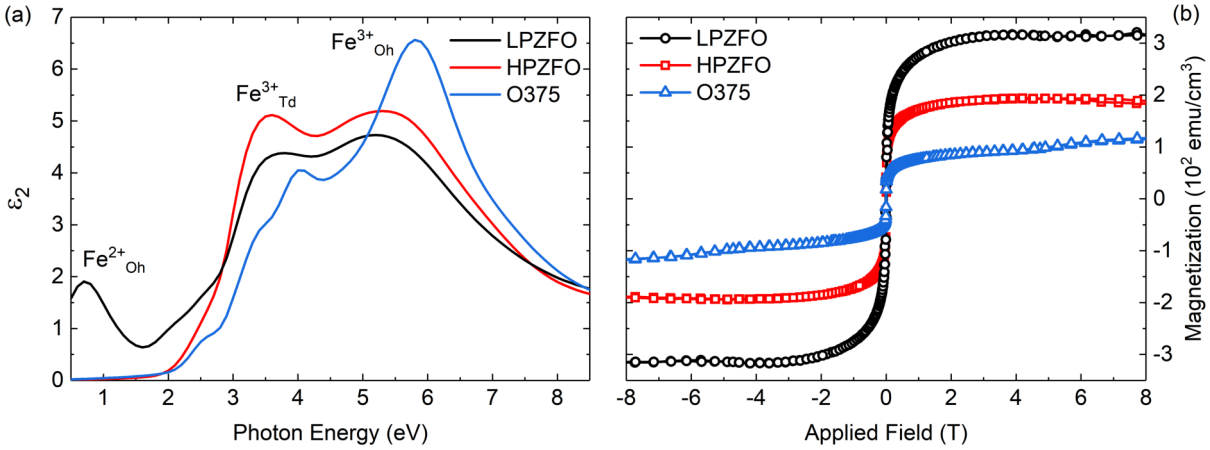

Figure 9.27: (a) Model dielectric function (ϵ_2), determined from spectroscopic ellipsometry for the $ZnFe_2O_4$ films grown at low (LPZFO) and high (HPZFO) oxygen pressure as well as annealed at 375 ℃ in oxygen atmosphere (O375). The distinct features result from transitions involving Fe cations on octahedral (Oh) and tetrahedral (Td) lattice sites. (b) Room temperature magnetization as a function of applied magnetic field for the respective films from (a).

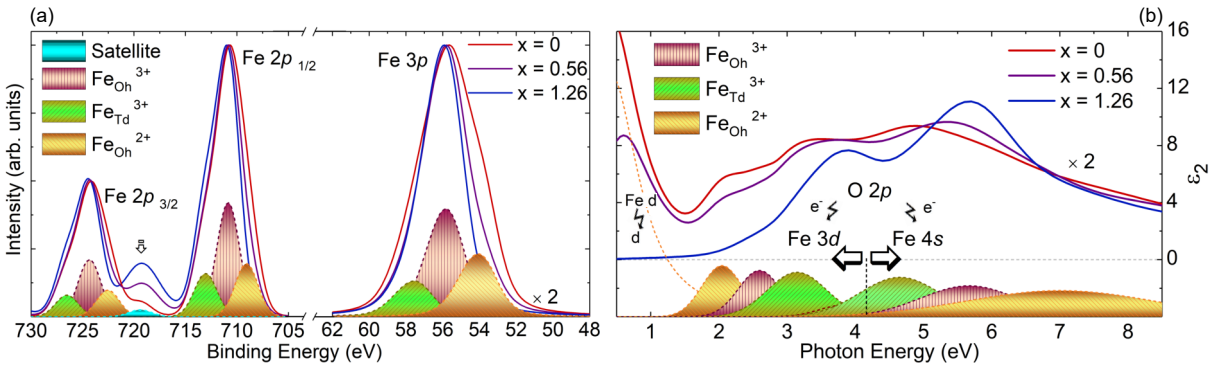

Figure 9.28: (a) Model approximation to the measured surface Fe2p and 3p XPS core level spectra without the Shirley background and (b) the bulk MDF for the x = 0, 0.56 and 1.56 thin films. XPS intensity of the resulting fit and ϵ_2 approximation line-shapes are multiplied by a factor of two for clarity. The individual Fe cation contribution to the modeled spectra for chemical composition determination are indicated by the shaded areas. The satellite contribution between the XPS Fe2p$_{3/2}$ and 2p$_{1/2}$ core levels is indicated by an arrow.

tinction in the XPS spectra with increase in Zn concentration is evident by the decrease of the low energy shoulder in both Fe2p and 3p core levels as well as the increase in the satellite peak at 719 eV, (Fig. 9.28(a)). The contribution of the MDF transitions involving Fe^{2+} cations decreases at a nearly linear rate as the Zn concentration increases, (Fig. 9.28(b)). This is due to the preservation of charge neutrality as Zn^{2+} replaces the Fe^{3+} on tetrahedral lattice sites. The surface morphology of the x = 0 film was found to be dominated by large grain-like structures, which are likely due to the formation of antiphase boundaries. The homogeneous film formation in the x = 0.87 film is in coincidence with a uniform cation distribution (Fig. 9.29), smooth surface morphology and Bloch law behavior of the magnetization as a function of temperature. It was determined that the bulk (surface) of spinel ferrite film in its predominantly inverse configuration (x ≤ 0.56), would be primarily occupied by Fe^{3+}_{Td} (Fe^{3+}_{Oh}), while that of

a normal spinel ((x ≥ 0.87)) would be occupied by Fe^{3+}_{Oh} (Fe^{3+}_{Td}), (Fig. 9.29). While the former results in a diminishing ferrimagnetic order in inverse spinel magnetite, the latter mechanism could be responsible for the strong magnetic response in the disordered $ZnFe_2O_4$ thin film.

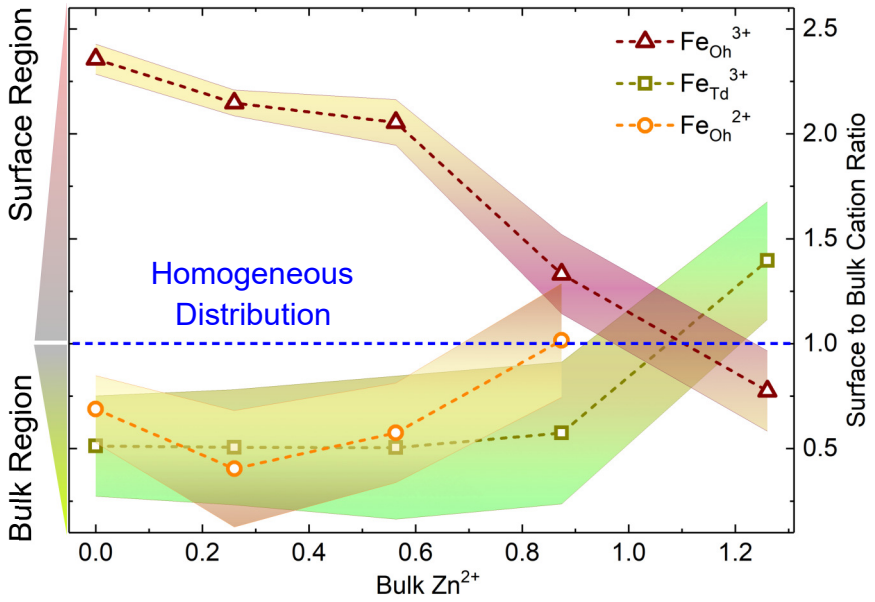

Figure 9.29: Relative surface to bulk cation concentration Fe ratio as a function of Zn^{2+}. The horizontal dashed line represents the ratio value for homogeneous distribution. The errors are indicated by the shaded regions.

[1] N. Guijarro *et al.*: Sustainable Energy Fuels **2**, 103 (2018) doi:10.1039/C7SE00448F
[2] K. Brachwitz *et al.*: Appl. Phys. Lett. **102**, 172104 (2013) doi:10.1063/1.4803475
[3] C. R. Torres *et al.*: Phys. Rev. B **89**, 104411 (2014) doi:10.1103/PhysRevB.89.104411
[4] V. Zviagin *et al.*: Phys. Status Solidi **253**, 429 (2016) doi:10.1002/pssb.201552361
[5] V. Zviagin *et al.*: Appl. Phys. Lett. **108**, 13 (2016) doi:10.1063/1.4944898

9.17 Temperature dependence of the dielectric function of thin film CuI in the spectral range (0.6 - 8.3) eV

E. Krüger, V. Zviagin, C. Yang, C. Sturm, R. Schmidt-Grund, M. Grundmann

γ -CuI is a wide band gap p-type semiconductor with a high exciton binding energy [1], high hole mobility [2] and the best known thermoelectric properties in comparison with other transparent p-type thermoelectric materials [3], and thus a promising material for transparent optoelectronic and thermoelectric devices. Although CuI thin films

can be easily prepared at room temperature [4] and were already successfully applied in e.g. transparent p-n-heterojunctions [5], there have been a lack of detailed investigation of the optical properties, escpecially of the temperature dependent dielectric function in a wide spectral range, which is crucial for understanding the nature of the underlying transitions in the electronic structure, so far.

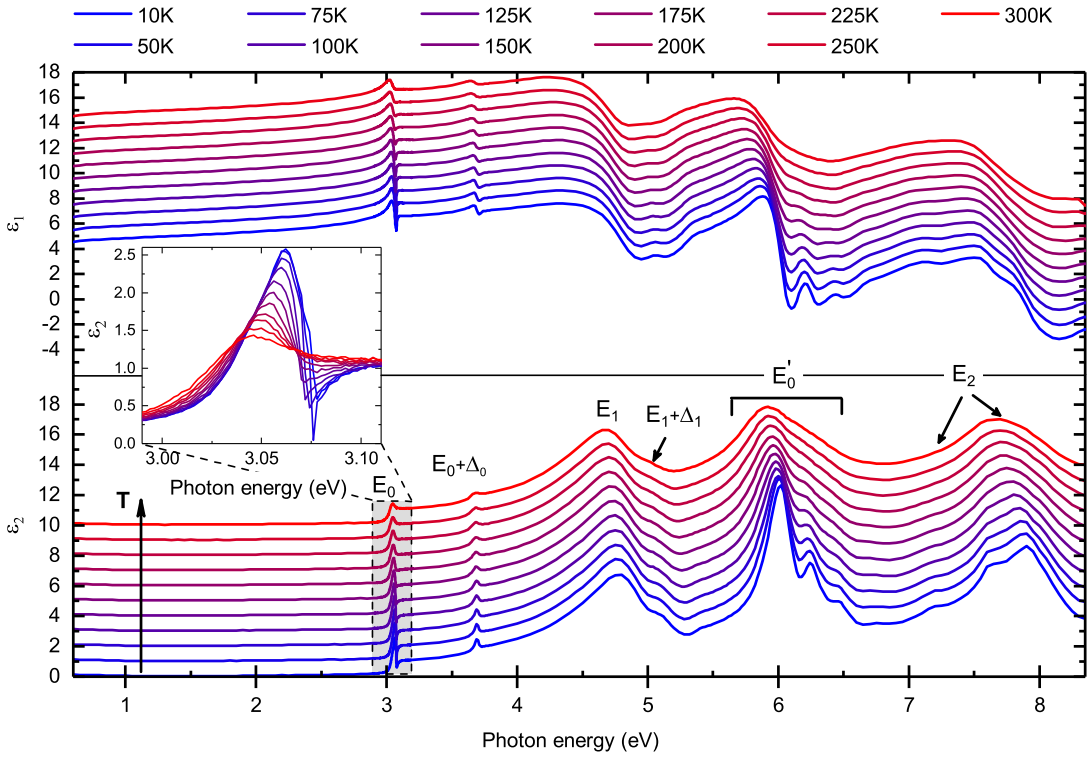

Figure 9.30: Spectra of the real (ε_1) and imaginary (ε_2) part of the dielectric function of the CuI thin film as a function of temperature. The spectra are shifted vertically by one against each other for better clarity. The inset shows ε_2 near the excitonic resonance E_0 (shaded area).

Thus, we determined the dielectric function of high quality γ-CuI thin film by means of spectroscopic ellipsometry in the spectral range from 0.6 eV up to 8.3 eV for temperatures from 10 K to 300 K [6]. In order to improve the crystalline quality as well as the surface morphology, which is favorable for reliable ellipsometry investigations, CuI thin films with different thicknesses in the range (30 – 150) nm were deposited on Al_2O_3 substrates at 360 ℃ and the film, exhibiting the best structural properties, was used for the temperature dependent ellipsometric measurements. Further ellipsometric measurements on similar thin films at room temperature were performed to verify, that the achieved results are specific for CuI thin films. The dielectric function was determined numerically by a Kramers-Kronig consistent point-by-point regression analysis of the experimental data using the Levenberg-Marquardt algorithm and the transition energies were estimated from the zero crossing of the first-derivative spectra $d\varepsilon_2/dE$, which were smoothed using Savitzky-Golay-Filter [7] after the numerical differentiation.

As can be seen in Fig.9.30 the investigated thin film is almost fully transparent in the spectral range (1 – 3) eV. For photon energies above 3 eV the dielectric function is dominated by various peak structures, which are attributed to electronic transitions at different symmetry points in the Brillouin zone and are labelled as E_0 (3.1 eV, $E_0+\Delta_0$ (3.7 eV),

E_1 (4.7 eV), $E_1+\Delta_1$ (5.1 eV), E_0 (6 eV), and E_2 (7.6 eV), in accordance with the nomenclature introduced by Cardona [8]. The observed split-off energies of 630 meV at the Γ -point and approximately 330 meV at the L-point coincide with recent band structure calculations [9]. In the investigated temperature range the change of the observed features is dominated by red shift of the transition peak energies as well as strong broadening with increasing temperature, related to thermal lattice expansion and increasing electron-phonon interaction with increasing temperature. Thus, the temperature dependence of the observed transition energies can be described by a Bose-Einstein model, presented by Viña *et al*. [10], and thus the electron-phonon coupling strength as well as the average phonon energy can be deduced. The determined temperature dependent energy shift of the transitions at the Γ -point ($E_0, E_0 + \Delta_0$) yields a coupling strength of about $\alpha = 0.08$ meV/K, indicating weak electron-phonon coupling and an average phonon energy of 16 meV, which agrees with the LO-phonon energy in CuI. For high energy transitions ($E_1, E_1 + \Delta_1, E_0'$) the coupling constant was determined to be about 0.4 meV/K indicating a stronger electron-phonon coupling to phonons with an average energy of approximately 7 meV.

[1] T. Sauder *et al.*: Phys. Lett. A **101**, 55 (1984)
doi:10.1016/0375-9601(84)90092-6
[2] D. Chen *et al.*: Crystal Growth & Design **10**, 2057 (2010)
doi:10.1021/cg100270d
[3] C. Yang *et al.*: Nat. Commun. **8**, 16076 (2017)
doi:10.1088/1361-648X/aa9e2a
[4] M. Grundmann *et al.*: Phys. Status Solidi A **210** 1671 (2013)
doi:https://doi.org/10.1002/pssa.201329349
[5] C. Yang *et al.*: Sci. Rep. **6**, 21937 (2016)
doi:10.1021/ac60214a047
[6] E. Krüger *et al.*: Appl. Phys. Lett. **113**, 172102 (2018)
doi:10.1063/1.5051963
[7] A. Savitzky and M. J. E. Golay: Analytical Chemistry **36**, 1627 (1964)
doi:10.1021/ac60214a047
[8] M. Cardona: Phys. Rev. **129**, 69 (1963)
doi:10.1103/PhysRev.129.69
[9] Y. Li *et al.*: Phys. Rev. Mater. **2**, 035003 (2018)
doi:10.1103/PhysRevMaterials.2.035003
[10] L. Viña *et al.*: Phys. Rev. B **30**, 1979 (1984)
doi:10.1103/PhysRevB.30.1979

9.18 Applicability of the constitutive equations for optical active materials

C. Sturm, V. Zviagin, M. Grundmann

Optical activity is an intrinsic material property leading to a circular birefringence and dichroism. Typically, the optical activity is determined by transmission spectroscopy, which limits these investigations to the transparent spectral region. However,

due to the boundary condition the change of the polarization state of the transmitted wave, caused by the optical activity, affects also the polarization of the reflected wave. This allows to determine the optical activity by ellipsometry as it was recently demonstrated on $AgGaS_2$ [2]. The optical response of such materials cannot be described by the dielectric function only and the constitutive equations have to be extended by the pseudo gyration tensor. Typically, three different approaches are proposed [1], namely the so-called Fedorov-Condon, Landau and Drude-Berreman approach. Although it was already shown that only the Fedorov-Condon approach does not lead to a violation of the conservation of the energy at the interface, all three approaches are still used in the literature for the analysis of optically active materials (cf. [3, 4]).

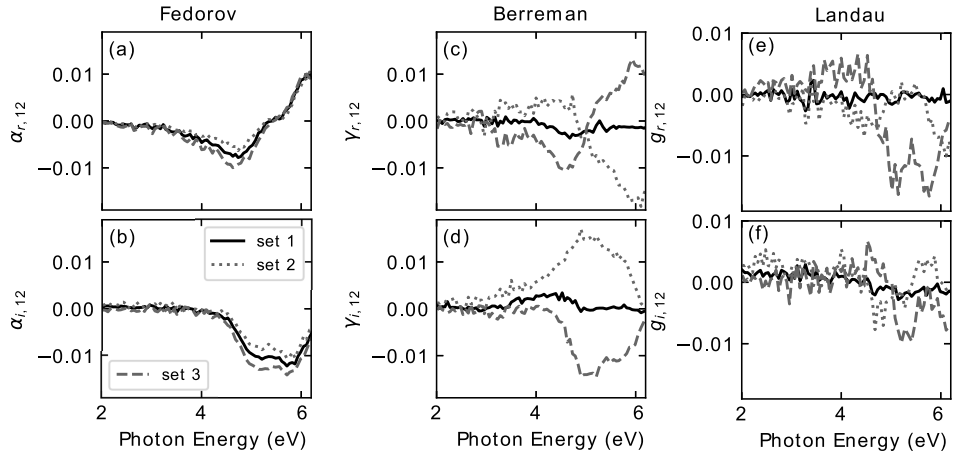

Figure 9.31: Determined gyration tensor by using the Fedorov (a,b), Berreman (c,d) and Landau approach (e,f) for the constitutive equations by taking into account different sets of crystallographic orientations

We investigated the impact of the choice of the constitutive equation on the optical properties. In doing so, we analyzed the optical response of potassium titanyl phosphate ($KTiOPO_4$, KTP), determined by spectroscopic ellipsometry for the different approaches of constitutive equations. Since KTP has an orthorhombic crystal structure and thus it is optically biaxial, for the determination of the optical properties by means of ellipsometry the optical response for different crystallographic orientations with respect to the laboratory system have to be measured and analyzed simultaneously. In order to investigate the validity of the different approaches, we analyzed three different sets of crystallographic orientations. Whereas the determined dielectric function for the different constitutive equations and crystallographic orientation yield similar results, the magnitude of the gyration tensor depends strongly on the choice of the constitutive equation [5]. In the case of the Fedorov-Condon approach, the gyration tensor is well pronounced in the absorption spectral range and reaches values up to ±0.01. This is in contrast to the Landau and Drude-Berreman approach where the gyration tensor is negligible in the entire spectral range or rather only pronounced at an energy of about 4 eV (Fig. 9.31). Furthermore, we found that only in the case of the Fedorov-Condon approach, the determined gyration tensor does not depend on the crystallographic orientations which were taken into account. This finding can be explained by the fact, that the Fedorov-Condon approach consists of a symmetric set of constitutive equation where the impact of the optical activity on the magnetic field and flux density is directly

taken into account whereas in the case of a non-symmetric set of constitutive equation, as given by the Landau and Drude-Berreman approach, this impact is described indirectly [5]. Thus, only a symmetric set of the constitutive equations as proposed by the Fedorov-Condon approach allows the unique determination of the pseudo gyration tensor.

[1] A. F. Konstantinova *et al.:* Crystallogr. Rep. **47**, 815, (2002) doi:10.1134/1.1509398
[2] O. Arteaga, Opt. Lett. **40**, 4277 (2015) doi:10.1364/OL.40.004277
[3] Y. Sah and J. G. Krishna: J. Opt. Soc. Am. A **18**, 1388 (2001) doi:10.1364/JOSAA.18.001388
[4] V. M. Agranovich and V. Ginzburg, *Crystal Optics with Spatial Dispersion, and Excitons* (Springer Science & Business Media, 2013)
[5] C. Sturm *et al*: Opt. Lett. **44**, 1351 (2019) doi:10.1364/OL.44.001351

9.19 Observation of the unpolarized Brewster point in the sky

M. Scholz*, O. Herrfurth, L. Trefflich, S. Richter, M. Grundmann, R. Schmidt-Grund

*Gymnasium Engelsdorf, Arthur-Winkler-Str. 6, 04319 Leipzig, Germany

Sunlight is mostly linearly polarized due to scattering from molecules in the atmosphere. The physical origin is Rayleigh scattering on molecular dipoles. It is interesting that multiple Rayleigh scattering processes lead to linearly polarized light with its polarization perpendicular to that of single Rayleigh scattering and the superposition of both results in the appearance of four unpolarized points in the sky [1, 2]. During a two-weeks pupil internship in 2016, a wide-angle map of the polarization pattern of the sky was measured and the Babinet point was observed above the sun as seen from the observer [3]. An improved set-up was build during a second internship in July 2018. The commercial digital camera was replaced by a very sensitive CCD camera equipped with a camera objective (±15° field of view). Thereby, the observable field of view is is smaller compared to the first experiment but the angular resolution increased. Employing a metal interference filter for 515 ± 12 nm wavelength further improves the resolution such that the unpolarized points in the sky are not smeared out by different spectral contributions. Polarization resolution was realized with a commercial "circular polarization filter", i.e a quarter-wave plate attached to linear polarizer. On Friday 13th July 2018 13:31, the unpolarized point below the sun and just above the horizon was observed as demonstrated by the vortex of the polarization orientation in Fig. 9.32. This point is called "Brewster point" and it is hidden below the horizon most of the time because of the low declination of the sun. The declination was 62.2° at this time such that the Brewster point was just high enough to be observed. The polarization pattern is smeared out and the degree of polarization is far below one due to the depolarizing contributions of clouds and haze in the sky, which were not even visible to the bare eye but only could manifest themselves by depolarization.

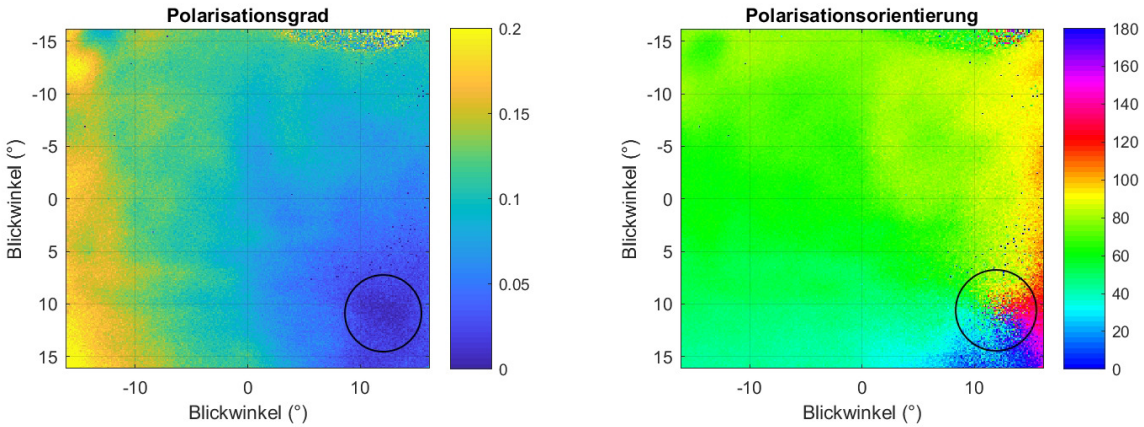

Figure 9.32: Degree of polarization (left) and orientation (right) of the polarized light (wavelength 515 ± 12 nm) observed in the sky above Leipzig (51°20′N 12°23′E) at the 13th July 2018, 13:31 just above the horizon. The declination of the sun was 62.2°. The vortex in the polarization orientation corresponds to the unpolarized Brewster point.

[1] S. Chandrasekhar: *Radiative transfer*, International series of monographs on physics (Clarendon Press, Oxford, 1950)
https://katalog.ub.uni-leipzig.de/Record/0001022152
[2] G. Horváth, *et al.*: Appl. Optics **41**, 543 (2002)
doi:10.1364/ao.41.000543
[3] M. Scholz et al.: *Polarization patterns of the sky*, in *Report Halbleiterphysik/Semiconductor Physics 2016*
http://research.uni-leipzig.de/hlp/publications/HLP-Report-2016.pdf

9.20 Funding

Polarisationswechselwirkung in Laser-MBE Wurtzit-Perowskit-Heterostrukturen
Prof. Dr. M. Lorenz
SFB 762/3, TP A2 within SFB 762 *Funktionalität Oxidischer Grenzflächen*

Optische Untersuchungen zu magneto-elektro-optischen Wechselwirkungen in ihrer Dynamik in oxidischen Heterostrukturen
Dr. R. Schmidt-Grund
SFB 762/3, TP B03 within SFB 762 *Funktionalität Oxidischer Grenzflächen*

Lateraler Transport in oxidischen Feldeffekt-Strukturen
Dr. H. von Wenckstern, Prof. Dr. M. Grundmann
SFB 762/3, TP B04 within SFB 762 *Funktionalität Oxidischer Grenzflächen*

Spinabhängiges Tunneln in oxidischen Heterostrukturen
Prof. Dr. M. Grundmann, Prof. Dr. B. Rosenow
SFB 762/3, TP B06 within SFB 762 *Funktionalität Oxidischer Grenzflächen*

Quantum Gases and Liquids in Semiconductor Rods conformally coated with Bragg Mirrors

Dr. R. Schmidt-Grund, Prof. Dr. M. Grundmann
DFG SCHM 2710/2-2, TP P1 within FOR 1616 *Dynamics and Interactions of Semiconductor Nanowires for Optoelectronics*

Flexible analoge und digitale Grundschaltungen in amorphen Metalloxiden
Prof. Dr. M. Grundmann
DFG GR 1011/31-1, within SPP *High Frequency Flexible Bendable Electronics for Wireless Communication Systems (FFLexCom)*

Raman-Streuung in anisotropen Kristallen
Prof. Dr. M. Grundmann
GR 1011/33-1

Topologische Effekte in optisch-anisotropen Mikrokavitäten
Dr. R. Schmidt-Grund
DFG SCHM 2710/3-1

Wurtzitische Zink-basierte Oxynitride als vielversprechende photovoltaische Absorber: Epitaxie, Bandstruktur-Anpassung und Heterostrukturen
Dr. C. Yang
YA 511/1-1

Zink-Magnesium Oxinitride
Prof. Dr. M. Grundmann
GR 1011/36-1

LOMID - Large cost-effective OLED microdisplays and their applications
Prof. Dr. M. Grundmann, Dr. H. von Wenckstern
European Union, Horizon 2020 644101

COSIMA - Combinatorisches Oxide-Screening für Materialien und Anwendungen
Prof. Dr. M. Grundmann
Europäischer Fonds für regionale Entwicklung (EFRE)
100282338 and 100315366

Nachwuchsforschergruppe - Oxid-Heterostrukturen: Anwendungen in Bauelementen
Prof. Dr. M. Grundmann
Europäische Sozialfonds (ESF)
100310460

9.21 Organizational Duties

M. Grundmann

- Director of the Felix Bloch Institute for Solid State Physics
- Sprecher der Graduiertenschule "Leipzig School of Natural Sciences - Building with Molecules and Nano-objects" (BuildMoNa), http://www.buildmona.de/
- Stellvertretender Sprecher des Sonderforschungsbereiches "Funktionalität Oxidischer Grenzflächen" (SFB762), http://www.physik.uni-halle.de/sfb762/

- Stellvertretender Sprecher der Forschergruppe FOR 1616, http://www.for1616.uni-jena.de/
- Sprecher der Fächerübergreifenden Arbeitsgemeinschaft Halbleiterforschung Leipzig (FAHL), https://home.uni-leipzig.de/fahl/
- Mitglied des wissenschaftlichen Beirats des Leibniz-Instituts für Oberflächenmodifizierung e. V., Leipzig (IOM)
- Member Editorial Board: Physica Status Solidi (a), (b), RRL, MDPI nanomaterials
- Member International Advisory Board: Advanced Electronic Materials
- Project Reviewer: Deutsche Forschungsgemeinschaft (DFG), Alexander von Humboldt-Stiftung (AvH), Schweizerischer Nationalfonds zur Förderung der wissenschaftlichen Forschung (FNSNF), Fonds zur Förderung der Wissenschaften (FWF), EU, Österreichische Forschungsförderungsgesellschaft mbH (FFG), Agence Nationale de la Recherche (ANR, France)
- Referee: Applied Physics Letters, Electronics Letters, Journal of Applied Physics, Nature, Physica E, Physical Review B., Physical Review Letters, Physica Status Solidi, Advanced Materials, u.a.

M. Lorenz

- Member Editorial Board: Journal of Physics D: Applied Physics (IOP, Bristol, U.K.)
- Project Reviewer: Deutsche Forschungsgemeinschaft (DFG), Dutch Research Council NWO (Niederlande), Alexander von Humboldt Stiftung, Public Authority of Applied Education and Training (PAAET) – College of Technological Studies (Kuwait)
- Referee: ACS Applied Materials Interfaces, ACS Applied Nano Materials, Applied Physics Letters, Applied Surface Sciences, Applied Physics A, Crystal Growth and Design, CrystEngComm, Dalton Transactions, IEEE Transact. Magnetics, Journal of Alloys and Compounds, Journal of Physics D: Applied Physics, Journal of Applied Physics, Journal of Materials Research, Journal: Optics and Laser Technology, Journal of Magnetism and Magnetic Materials, Materials Science in Semiconductor Processing, Materials Horizons, Thin Solid Films

R. Schmidt-Grund

- Extended board member of German Association on Ellipsometry (Arbeitskreis Ellipsometrie – Paul Drude e.V.)
- Project Reviewer: Deutsche Forschungsgemeinschaft (DFG), US Department of Energy, Österreichische Akademie der Wissenschaften, German-Israeli Foundation for Scientific Research and Development
- Referee: Scientific journals (ACS, AIP, APS, DPG, Elsevier, IOP, MRS, Nature Publ. Group, OSA, PIER,Wiley)

C. Sturm

- Referee: Applied Optics, Applied Physic Letters

H. von Wenckstern

- Project Reviewer: Deutsche Forschungsgemeinschaft, U.S. Department of Energy – Office of Science, National Research Fondation RSA
- Associate Editor: Journal of Electronic Materials
- Referee: ACS Materials and Interfaces, Advanced Functional Materials, Annalen der Physik, Applied Physical Letters, APL Materials, Electronic Device Letters, Journal

of Applied Physics, Material Science in Semiconductor Processing, Physica Status Solidi, Scientific Reports, Solid State Electronics, Superlattices and Microstructures, Thin Solid Films, u.a.

C. Yang

- Referee: Materials Horizons, Applied Physics Letters, Physical Review Applied, Nanoscale, Advanced Materials Interfaces

9.22 External Cooperations

Academic

- Leibniz-Institut für Oberflächenmodifizierung e. V., Leipzig, Germany
  Prof. Dr. A. Anders, Prof. Dr. S. Mayr, Dr. C. Bundesmann, Dr. A. Lotnyk
- Universität Leipzig, Fakultät für Chemie und Mineralogie, Germany
  Prof. Dr. H. Krautscheid, Prof. Dr. R. Denecke, Porf. Dr. O. Oeckler, Dr. S. Blaurock
- Universität Halle-Wittenberg, Germany
  Prof. Dr. I. Mertig, Prof. Dr. S.G. Ebbinghaus, Prof. Dr. W. Hergert, Prof. Dr. R. Scheer
- Fraunhofer-Institut für Mikrostruktur von Werkstoffen und Systemen IMWS, Halle (Saale), Germany
  Prof. Dr. T. Höche, Dr. C. Patzig, Dr. S. Selle
- Forschungszentrum Dresden-Rossendorf, Germany
  Dr. S. Zhou
- Technische Universität Berlin, Germany
  Prof. Dr. A. Hoffmann
- Humboldt-Universität zu Berlin, Germany
  Prof. Dr. N. Koch
- Leibniz-Institut für Festkörperelektronik – Paul Drude (PDI), Berlin, Germany
  Dr. O. Bierwagen
- Universität Magdeburg, Germany
  Porf. Dr. A. Dadgar, Dr. J. Bläsing
- Universität Jena, Germany
  Prof. Dr. C. Ronning, Prof. Dr. S. Botti
- University of Canterbury, Christchurch, New Zealand
  Prof. Dr. M. Allen
- Centre de Recherche sur l' Hétéro-Epitaxie et ses Applications (CNRS-CRHEA), Valbonne, France
  Dr. J. Zúñiga-Pérez, Dr. Guy Feuillet
- Western Michigan University, USA
  Prof. Dr. S. M. Durbin
- The Ohio State University, USA
  Prof. Dr. L. Brillson
- Katholieke Universiteit Leuven, Belgium
  Dr. V. Lazenka, Prof. Dr. K. Temst
- University of Oslo, Norway
  Prof. Dr. L. Vines

Industry

- Freiberger Compound Materials GmbH, Freiberg, Germany
  Dr. G. Leibiger

9.23 Publications

Journals

A. Bouvet-Marchand, A. Graillot, J. Volk, R. Dauksevicius, C. Sturm, E. Saoutieff, A. Viana, B. Christian, V. Lebedev, J. Radó, I.E. Lukács, M. Grundmann, D. Grosso, C. Loubat: *Design of UV-Crosslinked Polymeric Thin Layers for Encapsulation of Piezoelectric ZnO Nanowires for Pressure-Based Fingerprint Sensors*, J. Mat. Chem. C **6**(3), 605-613 (2018)

K. Brachwitz, T. Böntgen, J. Lenzner, K. Ghosh, M. Lorenz, M. Grundmann: *Evolution of magnetization in epitaxial $Zn_{1-x}Fe_xO_z$ thin films (0 = x = 0.66) grown by pulsed laser deposition*, J. Phys. D: Appl. Phys. **51**(24), 245003:1-7 (2018)

L.J. Brillson, G.M. Foster, J. Cox, W.T. Ruane, A.B. Jarjour, H. Gao, H. von Wenckstern, M. Grundmann, B. Wang, D.C. Look, A. Hyland, M.W. Allen: *Defect Characterization, Imaging, and Control in Wide-Bandgap Semiconductors and Devices*, J. Electr. Mat. **47**(9), 4980-4986 (2018)

J.W. Cox, G.M. Foster, A. Jarjour, H. von Wenckstern, M. Grundmann, L.J. Brillson: *Defect Manipulation to Control ZnO Micro-/Nanowire - Metal Contacts*, Nano Lett. **18**(11), 6974-6980 (2018)

H. Gao, S. Muralidharan, N. Pronin, M.R. Karim, S.M. White, T. Asel, G. Foster, S. Krishnamoorthy, S. Rajan, L.R. Cao, M. Higashiwaki, H. von Wenckstern, M. Grundmann, H. Zhao, D.C. Look, L.J. Brillson: *Optical signatures of deep level defects in Ga_2O_3*, Appl. Phys. Lett. **112**(24), 242102:1-5 (2018)

M. Grundmann: *Elastic Theory of Pseudomorphic Monoclinic and Rhombohedral Heterostructures*, J. Appl. Phys. **124**(18), 185302:1-10 (2018)

M. Grundmann: *Monolithic Forward-looking Photodetector for Use as Ultra-Compact Wavemeter with Wide Spectral Range*, phys. stat. sol. (a) **215**(24), 1800651:1-5 (2018)

M. Grundmann: *Report of The Physics Institutes of Universität Leipzig 2017*, Universität Leipzig, M. Grundmann, ed. (2018)

M. Grundmann: *Report Halbleiterphysik/Semiconductor Physics 2017*, Universität Leipzig, M. Grundmann, ed. (2018)

S. Hohenberger, V. Lazenka, K. Temst, C. Patzig, S. Selle, T. Höche, M. Grundmann, M. Lorenz: *Effect of double layer thickness on magnetoelectric coupling in multiferroic $BaTiO_3$-$Bi_0.95Gd_0.05FeO_3$ multilayers*, J. Phys. D: Appl. Phys. **51**(18), 184002:1-9 (2018)

A. Jarjour, J.W. Cox, W.T. Ruane, H. von Wenckstern, M. Grundmann, L.J. Brillson: *Single Metal Ohmic and Rectifying Contacts to ZnO Nanowires: A Defect Based Approach*, Ann. Phys. **530**(2), 1700335:1-6 (2018)

T. Jawinski, L.A. Wägele, R. Scheer, M. Grundmann, H. von Wenckstern: *Properties of In_2S_3-based pin-heterojunctions*, phys. stat. sol. (a) **215**(11), 1700827:1-6 (2018)

J.K. Jochum, M. Lorenz, H.P. Gunnlaugsson, C. Patzig, T. Höche, M. Grundmann, A. Vantomme, K. Temst, M.J. Van Bael, V. Lazenka: *Impact of magnetization and hyperfine field distribution on high magnetoelectric coupling strength in $BaTiO_3$-$BiFeO_3$ multilayers*, Nanoscale **10**(12), 5574-5580 (2018)

M. Kneiß, P. Storm, G. Benndorf, M. Grundmann, H. von Wenckstern: *Combinatorial material science and strain engineering enabled by pulsed laser deposition using radially segmented targets*, ACS Comb. Sci. **20**, 643-652 (2018)

M. Kneiß, C. Yang, J. Barzola-Quiquia, G. Benndorf, H. von Wenckstern, P. Esquinazi, M. Lorenz, M. Grundmann: *Suppression of grain boundary scattering in p-type transparent γ-CuI thin films due to interface tunneling currents*, Adv. Mater. Interf. **5**(6), 1701411:1-12 (2018)

E. Krüger, V. Zviagin, C. Yang, C. Sturm, R. Schmidt-Grund, M. Grundmann: *Temperature dependence of the dielectric function of thin film CuI in the spectral range (0.6-8.3) eV*, Appl. Phys. Lett. **113**(17), 172102:1-5 (2018)

C. Laube, J. Hellweg, C. Sturm, J. Griebel, M. Grundmann, A. Kahnt, B. Abel: *Photo-Induced-Heating of Graphitised Nanodiamonds monitored by the Raman-Diamond-Peak*, J. Phys. Chem. C **122**, 25685-25691 (2018)

M. Lorenz, S. Hohenberger, E. Rose, M. Grundmann: *Atomically stepped, pseudomorphic, corundum-phase $(Al_{1-x}Ga_x)_2O_3$ thin films ($0 = x < 0.08$) grown on R-plane sapphire*, Appl. Phys. Lett. **113**(23), 231902:1-5 (2018) (Editor's pick)

M. Lorenz:*Pulsed Laser Deposition*, chapter 5, File No. eap810 in Encyclopedia of Applied Physics (Wiley VCH, Weinheim) accepted May 2018, currently in production

T. Meister, F. Ellinger, J.W. Bartha, M. Berroth, J. Burghartz, M. Claus, L. Frey, A. Gagliardi, M. Grundmann, J. Hesselbarth, H. Klauk, K. Leo, P. Lugli, S. Mannsfeld, Y. Manoli, R. Negra, D. Neumaier, U. Pfeiffer, T. Riedl, S. Scheinert, U. Scherf, A. Thiede, G. Troester, M. Vossiek, R. Weigel, C. Wenger, G. Alavi, M. Becherer, C.A. Chavarin, M. Darwish, M. Ellinger, C.-Y. Fan, M. Fritsch, F. Grotjahn, M. Gunia, K. Haase, P. Hillger, K. Ishida, M. Jank, S. Knobelspies, M. Kuhl, G. Lupina, S.M. Naghadeh, N. Münzenrieder, S. Özbek, M. Rasteh, G.A. Salvatore, D. Schrüfer, C. Strobel, M. Theisen, C. Tückmantel, H. von Wenckstern, Z. Wang, Z. Zhang: *Program FFlexCom – High Frequency Flexible Bendable Electronics for Wireless Communication Systems*, 2017 IEEE International Conference on Microwaves, Antennas, Communications and Electronic Systems (COMCAS), p. 1-4 (2018)

T. Michalsky, M. Wille, M. Grundmann, R. Schmidt-Grund: *Tunable and switchable lasing in a ZnO microwire cavity at room temperature*, J. Phys. D: Appl. Phys. **51**(42), 425305:1-6 (2018)

T. Michalsky, M. Wille, M. Grundmann, R. Schmidt-Grund: *Spatiotemporal evolution of coherent polariton modes in ZnO microwire cavities*, Nano Lett. **18**(11), 6820-6825 (2018)

T. Michalsky, M. Wille, E. Krüger, C. Sturm, M. Grundmann, R. Schmidt-Grund: *Coherent polariton states and lasing in ZnO nano- and microstructures*, IEEE Photonics Society Summer Topical Meeting Series, p. 171-172 (2018), ISBN 978-1-5386-4076-0

H. Modarresi, E. Menéndez, V.V. Lazenka, N. Pavlovic, M. Bisht, M. Lorenz, C. Petermann, M. Grundmann, A. Hardy, M.K. Van Bael, M.J. Van Bael, A. Vantomme, K. Temst: *Morphology-induced spin frustration in granular $BiFeO_3$ thin films: Origin of the magnetic vertical shift*, Appl. Phys. Lett. **113**(14), 142402:1-5 (2018)

R. Pickenhain, M. Schmidt, H. von Wenckstern, G. Benndorf, A. Pöppl, R. Böttcher, M. Grundmann: *Negative U Properties of the Deep Level E3 in ZnO*, phys. stat. sol. (b) **255**, 1700670:1-16 (2018)

V. Prozheeva, R. Hölldobler, H. von Wenckstern, M. Grundmann, F. Tuomisto: *Effects of alloy composition and Si-doping on vacancy defect formation in $(In_xGa_{1-x})_2O_3$ thin films*, J. Appl. Phys. **123**(12), 125705:1-6 (2018)

S. Prucnal, Y. Berencén, M. Wang, J. Grenzer, M. Voelskow, R. Hübner, Y. Yamamoto, A. Scheit, F. Bärwolf, V. Zviagin, R. Schmidt-Grund, M. Grundmann, J. Zuk, M. Turek, A. Drozdziel, K. Pyszniak, R. Kudrawiec, M.P. Polak, L. Rebohle, W. Skorupa, M. Helm, S. Zhou: *Strain and band gap engineering in GeSn alloys via P doping*, Phys. Rev. Appl. **10**(6), 064055:1-11 (2018)

S. Richter, J Zúñiga-Pérez, C. Deparis, L. Trefflich, H.-G. Zirnstein, T. Michalsky, C. Sturm, B. Rosenow, M. Grundmann, R. Schmidt-Grund: *Exceptional Points in the Dispersion of Optically Anisotropic Planar Microcavities*, IEEE Photonics Society Summer Topical Meeting Series, p. 195-196 (2018), ISBN 978-1-5386-4076-0

T. Schulz, S. Bitter, P. Schlupp, H. von Wenckstern, N. Koch, M. Grundmann: *The influence of oxygen deficiency on the rectifying behavior of transparent semiconducting oxide-metal interfaces* , Phys. Rev. Appl. **9**, 064001:1-8 (2018) (Editor's suggestion)

D. Splith, S. Müller, H. von Wenckstern, M. Grundmann: *Modeling of Schottky barrier diode characteristics on heteroepitaxial β-gallium oxide thin films*, Proc. SPIE **10533**, 105330C:1-8 (2018), David J. Rogers, David C. Look, Ferechteh H. Teherani, eds.

S. Vogt, H. von Wenckstern, M. Grundmann: *MESFETs and inverters based on amorphous zinc-tin-oxide thin films prepared at room temperature*, Appl. Phys. Lett. **113**(13), 133501:1-5 (2018)

Talks

S. Espinoza, M. Rebarz, S. Richter, O. Herrfurth, M. Kloz, R. Schmidt-Grund, J. Andreasson, S. Zollner: *Phase-Filling Singularities in Femtosecond Transient Dielectric Spectra of Germanium*, DPG spring meeting, Berlin, Germany, March 2018

M. Grundmann: *Neues zur Kristalloptik bei Dissipation: Singuläre Achsen und Topologie Exzeptioneller Punkte*, Sächsische Akademie der Wissenschaften zu Leipzig, Plenarvortrag, Leipzig, Germany, June 2018 (invited)

M. Grundmann: *Birefringence in the Absorption Regime: Singular Optic Axes and Exceptional Points*, International and dissemination workshop of the Research Unit FOR1616, Weimar, Germany, September 2018 (invited)

M. Grundmann: *Birefringence Effects in Transparent Conductive Materials or Singular and Topological Optical States*, 7th International Symposium on Transparent Conductive Materials (TCM-7), Chania, Crete, Greece, October 2018 (invited)

M. Grundmann, C. Yang, E. Rose, M. Kneiß, P. Schlupp, Z. Zhang, H. von Wenckstern, M. Lorenz: *Towards High Performance p-Type Transparent Conductors and Semiconductors with Copper Iodide*, 7th International Symposium on Transparent Conductive Materials (TCM-7), Chania, Crete, Greece, October 2018

O. Herrfurth, S. Richter, M. Rebarz, S. Espinoza, J. Zúñiga-P'erez, A. Schleife, J. Leveilee, S. Zollner, J. Andreasson, M. Grundmann, R. Schmidt-Grund: *Transient birefringence and dichroism of a m-ZnO film studied by tSE*, 3rd ELIps Workshop, Dolní Brezany, Czech Republic, October 2018 (invited)

S. Hohenberger, J. Jochum, K. Temst, M. Lorenz, M. Grundmann: *Thickness dependent magnetoelectric coupling in $BaTiO_3$-$BiFeO_3$ multilayers*, E-MRS Fall Meeting, Warsaw, Poland, September 2018

M. Kneiß, P. Storm, G. Benndorf, H. von Wenckstern, M. Grundmann: *A pulsed laser deposition technique for continuous variation of alloy composition in growth direction: Demonstration on the transparent $Mg_xZn_{1-x}O$ alloy system*, Annual BuildMoNa Conference 2018, Leipzig, Germany, March 2018

M. Kneiß, P. Storm, G. Benndorf, H. von Wenckstern, M. Grundmann: *A pulsed laser deposition technique to control the composition of ternary thin films in growth direction demonstrated on the $Mg_xZn_{1-x}O$ alloy*, DPG Spring Meeting 2018, Berlin, Germany, March 2018

M. Kneiß, P. Storm, G. Benndorf, H. von Wenckstern, M. Grundmann: *A pulsed laser deposition technique for continuous variation of alloy composition in growth direction: Demonstration on the transparent $Mg_xZn_{1-x}O$ alloy system*, Electronic Materials Conference 2018, Santa Barbara, California, USA, June 2018

M. Kneiß, A. Hassa, D. Splith, H. von Wenckstern, M. Grundmann: *PLD-growth of ternary β-$(Al_xGa_{1-x})_2O_3$ thin films with $x \leq 0.28$ using a single elliptically-segmented target*, E-MRS Fall Meeting 2018, Warsaw, Poland, September 2018

E. Krüger, V. Zviagin, C. Yang, R. Schmidt-Grund, M. Grundmann: *Temperature dependent dielectric function of CuI*, DPG spring meeting, Berlin, Germany, March 2018

E. Krüger, V. Zviagin, C. Yang, R. Schmidt-Grund, M. Grundmann: *Temperature dependent dielectric function of CuI thin films*, 10th Workshop Ellipsometry, Chemnitz, Germany, March 2018

M. Lorenz: *Pulsed Laser Deposition of functional oxides for electronic applications*, Technische Hochschule Deggendorf, AG Prof. Benstetter, Deggendorf, Germany, April 2018

M. Lorenz, V. Lazenka, S. Hohenberger, C. Patzig, S. Selle, D. Hirsch, T. Höche, K. Temst, M. Grundmann: *Origin of high magnetoelectric coupling in multiferroic Bi(Gd)FeO_3-$BaTiO_3$ superlattices: Chemical interface features by TOF-SIMS and STEM-EDX*, 14th International Ceramic Congress at CIMTEC 2018, Perugia, Italy, June 2018

M. Lorenz, V. Lazenka: *Magnetoelectric coupling in multiferroic epitaxial $BiFeO_3$-$BaTiO_3$ thin film composites*, Qufu Normal University, Qufu, China, September 2018

T. Michalsky, M. Wille, E. Krüger, C. Sturm, M. Grundmann, R. Schmidt-Grund: *Coherent polariton states and lasing in ZnO nano- and microstructures*, IEEE Photonics Society Summer Topical Meeting, Waikoloa, Hawaii, USA, July 2018

S. Richter, O. Herrfurth, S. Espinoza, M. Rebarz, M. Kloz, J. Andreasson, M. Grundmann, R. Schmidt-Grund: *Time-resolved spectroscopic ellipsometry with sub-ps resolution*, DPG spring meeting, Berlin, Germany, March 2018

S. Richter, O. Herrfurth, S.J. Espinoza Herrera, M. Rebarz, M. Grundmann, S. Zollner, J. Andreasson, R. Schmidt-Grund: *fs-time-resolved spectroscopic ellipsometry*, 10th Workshop Ellipsometry, Chemnitz, Germany, March 2018 (Winner of the Paul Drude Medal 2018)

S. Richter, J. Zúñiga-Pérez, C. Deparis, L. Trefflich, H.-G. Zirnstein, T. Michalsky, C. Sturm, B. Rosenow, M. Grundmann, R. Schmidt-Grund: *Exceptional Points in the Dispersion of Optically Anisotropic Planar Microcavities*, IEEE Photonics Society Summer Topical Meeting, Waikoloa, Hawaii, USA, July 2018

S. Richter, S. Espinoza, M. Rebarz, J. Andreasson, O. Herrfurth, R. Schmidt-Grund, S. Zollner: *Time-resolved VIS-UV spectroscopic ellipsometry at ELI Beamlines*, 3rd ELIps Workshop, Dolní Brezany, Czech Republic, October 2018 (invited)

P. Schlupp, S. Bitter, H. von Wenckstern, M. Grundmann: *Room temperature fabricated junction field-effect transistors and inverters on rigid and flexible substrates*, DPG spring meeting, Berlin, Germany, March 2018

R. Schmidt-Grund,T. Michalsky, M. Wille, E. Krüger, R. Buschlinger, C. Sturm, H. Franke, U. Peschel, M. Grundmann: *Coherent polariton modes and lasing in ZnO nano- and microstructures*, 34th International Conference on the Physics of Semiconductors, ICPS2018, Montpellier, France, July/August 2018

R. Schmidt-Grund, C. Sturm, C. Kranert, J. Furthmüller, F. Bechstedt, D. Fritsch, M. Grundmann: *Dielectric Function Tensor of Anisotropic Crystals*, 3rd ELIps Workshop, Dolní Brezany, Czech Republic, October 2018 (invited)

R. Schmidt-Grund: *Some Examples for Ellipsometry in Leipzig: Electronic and Magnetic Properties, Dynamics and Low-Symmetry Materials*, Colloquium, Department of Physics, New Mexico State University, Las Cruces, NM, USA, July 2018 (invited)

R. Schmidt-Grund: *Dynamics of hot charge carriers and phonons as well as lasing in ZnO*, Colloquium, Koszalin University of Technology, Koszalin, Poland, October 2018 (invited)

D. Splith, H. von Wenckstern, M. Grundmann: *Schottky diodes on gallium-oxide and indium-oxide thin-films: optimization of the sample structure and modeling of the IV characteristics*, SPIE Photonics West, San Francisco, USA, January 2018

C. Sturm, A. Werner, V. Zviagin, D. Splith, H. von Wenckstern, M. Lorenz, J. Lenzner, R. Schmidt-Grund, M. Grundmann: *Dielectric function of epsilon-(In,Ga)$_2O_3$ thin films*, 10th Workshop Ellipsometry, Chemnitz, Germany, March 2018

C. Sturm: *Crystal optics and tensor properties of low symmetry crystals*, EPIOPTICS-15, Erice, Italy, July 2018 (invited)

C. Sturm, A. Werner, V. Zviagin, D. Splith, H. von Wenckstern, M. Lorenz, J. Lenzner, R. Schmidt-Grund, M. Grundmann: *Dielectric function and Raman tensor of epsilon-(In,Ga)$_2O_3$ thin films*, 34th International Conference on the Physics of Semiconductors, ICPS2018, Montpellier, France, July/August 2018 (invited)

C. Sturm, V. Zviagin, M. Grundmann: *Determination of the pseudo-gyration tensor of KTP by ellipsometry*, 2nd International Workshop on Biophotonics and Optical Angular Momentum, Palaiseau, France, October 2018

C. Sturm: *Crystal optics and tensor properties of low symmetry crystals*, Fakultätsseminar (Universität Linz), Linz, Austria, May 2018 (invited)

C. Sturm: *Crystal optics and tensor properties of low symmetry crystals*, Gruppenseminar (Prof. Wiersig), Magdeburg, Germany, December 2018 (invited)

H. von Wenckstern, A. Werner, M. Kneiß, D. Splith, F. Storm, M. Grundmann: *Properties of ternary, kappa-phase group-III sesquioxides*, 2nd Annual GraFOx Meeting, Humboldt-Universität zu Berlin, Berlin, Germany, July 2018

H. von Wenckstern: *Exploration of ternary semiconducting oxides by compositional screening*, E-MRS Fall Meeting, Warsaw, Poland, September 2018

C. Yang: *ZnGaON project - Wurtzite zinc-based oxynitrides as promising photovoltaic absorbers*, Kick-Off Meeting ZONE, Valbonne, France, April 2018

C. Yang, M. Kneiß, P. Schlupp, Z. Zhang, H. von Wenckstern, M. Lorenz, M. Grundmann: *Copper Iodide, a High-Performance p-Type Wide Bandgap Semiconductor*, 34th International Conference on the Physics of Semiconductors (ICPS), Montpellier, France, July 2018

M. Zapf, R. Röder, K. Winkler, L. Kaden, J. Greil, M. Wille, M. Grundmann, R. Schmidt-Grund, A. Lugstein, C. Ronning: *Dynamical Tuning of Nanowire Laser Spectra*, DPG spring meeting, Berlin, Germany, March 2018

V. Zviagin, P. Huth, C. Sturm, J. Lenzner, A. Setzer, R. Denecke, P. Esquinazi, M. Grundmann, R. Schmidt-Grund: *Cationic Configuration in Relation to Magnetic Properties of PLD Grown Spinel Ferrite Thin Films*, Collaborative Research Centre SFB 762: Functionality of Oxide Interfaces International Workshop, Frauenchiemsee, Germany, February/March 2018

V. Zviagin, Y. Kumar, C. Sturm, I. Lorite, P. Esquinazi, M. Grundmann, R. Schmidt-Grund: *The Influence of Crystallographic Order on Ferrimagnetic Response of Spinel $ZnFe_2O_4$ Thin Films*, DPG spring meeting, Berlin, Germany, March 2018

V. Zviagin, P. Huth, C. Sturm, M. Bonholzer, J. Lenzner, A. Setzer, R. Denecke, P. Esquinazi, M. Grundmann, R. Schmidt-Grund: *Spectroscopic investigation of cation configuration state of Spinel Ferrite thin films*, 10th Workshop Ellipsometry, Chemnitz, Germany, March 2018

Posters

K. Dorywalski, M. Grundmann, R. Schmidt-Grund: *Hybrid GA-gradient method for thin films ellipsometric data evolution*, 10th Workshop Ellipsometry, Chemnitz, Germany, March 2018

S. Espinoza, S. Zollner, S. Richter, M. Rebarz, O. Herrfurth, R. Schmidt-Grund, J. Andreasson: *Phase-filling singularities in femtosecond transient dielectric spectra of Germanium*, International Science@FELs Conference, Stockholm, Sweden, June 2018

O. Herrfurth, S. Richter, M. Rebarz, M. Kloz, S. Espinoza, J. Andreasson, M. Grundmann, R. Schmidt-Grund: *Time-resolved dielectric function tensor of m-plane ZnO studied by femtosecond spectroscopic ellipsometry*, DPG spring meeting, Berlin, Germany, March 2018

O. Herrfurth, S. Richter, S.J. Espinoza Herrera, M. Rebarz, M. Grundmann, S. Zollner, J. Andreasson, R. Schmidt-Grund: *Pitfalls of time-resolved spectroscopic ellipsometry*, 10th Workshop Ellipsometry, Chemnitz, Germany, March 2018

O. Herrfurth, S. Richter, S. Espinoza, M. Rebarz, M. Kloz, J. Andreasson, M. Grundmann, R. Schmidt-Grund: *Charge carrier dynamics of ZnO structures studied with femtosecond-time-resolved spectroscopic ellipsometry*, 34th International Conference on the Physics of Semiconductors, ICPS2018, Montpellier, France, July/August 2018

F. Jung, S. Ellis, C. Sturm, R. Schmidt-Grund, M. Lorenz, M. Grundmann, C. Patzig, S. Selle, T. Höche: *Optical and structural properties of PLD-grown TiN single layers and TiN/MgO superlattices on MgO(100) substrates*, DPG spring meeting, Berlin, Germany, March 2018

M. Kneiß, A. Hassa, D. Splith, C. Sturm, H. von Wenckstern, T. Schultz, N. Koch, M. Lorenz, M. Grundmann: *PLD-growth of epitaxial κ-Ga_2O_3 thin films on different substrates*, E-MRS Fall Meeting 2018, Warsaw, Poland, September 2018

E. Krüger, M. Wille, S. Blaurock, V. Zviagin, R. Deichsel, G. Benndorf, V. Gottschalch, H. Krautscheid, R. Schmidt-Grund, M. Grundmann: *Optical properties of highly excited CuI based microwire cavities*, DPG spring meeting, Berlin, Germany, March 2018

E. Krüger, V. Zviagin, C. Yang, R. Schmidt-Grund, M. Grundmann: *Temperature dependent dielectric function of CuI*, 34th International Conference on the Physics of Semiconductors, ICPS2018, Montpellier, France, July/August 2018

E. Krüger, M. Wille, S. Blaurock, V. Zviagin, R. Deichsel, G. Benndorf, L. Trefflich, V. Gottschalch, H. Krautscheid, R. Schmidt-Grund, M. Grundmann: *Lasing in CuI microwires*, 34th International Conference on the Physics of Semiconductors, ICPS2018, Montpellier, France, July/August 2018

E. Krüger, V. Zviagin, C. Yang, R. Schmidt-Grund, M. Grundmann: *Temperature dependent dielectric function of CuI*, 3rd ELIps Workshop, Dolní Brezany, Czech Republic, October 2018

O. Lahr, S. Vogt, Z. Zhang, H. von Wenckstern, M. Grundmann: *Devices and integrated circuits based on amorphous zinc-tin-oxide*, DPG spring meeting, Berlin, Germany, March 2018

M. Grundmann, S. Hohenberger, M. Lorenz: *Pseudomorphic Strain in Monoclinic and Rhombohedral Heterostructures*, 34th International Conference on the Physics of Semiconductors, ICPS2018, Montpellier, France, July/August 2018

T. Michalsky, M. Wille, E. Krüger, M. Grundmann, R. Schmidt-Grund: *Dynamics of coherent polariton modes and tunable lasing in ZnO microwire cavities at room temperature*, International Conference on Superlattices, Nanostructures and Nanodevices, Madrid, Spain, July 2018

A. Reinhardt, H. von Wenckstern, M. Grundmann: *Electrical properties of unipolar devices based on amorphous zinc oxynitride*, DPG spring meeting, Berlin, Germany, March 2018

S. Richter, J. Zúñiga-Pérez, C. Deparis, L. Trefflich, H.-G. Zirnstein, T. Michalsky, C. Sturm, B. Rosenow, M. Grundmann, R. Schmidt-Grund: *Exceptional Points in the Dispersion of Optically Anisotropic Planar Microcavities*, International Conference on Superlattices, Nanostructures and Nanodevices, Madrid, Spain, July 2018

S. Richter, S. Espinoza, M. Rebarz, O. Herrfurth, M. Kloz, M. Rübhausen, M. Grundmann, R. Schmidt-Grund, S. Zollner, J. Andreasson: *Fs-time-resolved ellipsometry to study the dynamics in the electronic density of states*, 34th International Conference on the Physics of Semiconductors, ICPS2018, Montpellier, France, July/August 2018

S. Richter, J. Zúñiga-Pérez, C. Deparis, L. Trefflich, H.G. Zirnstein, C. Sturm, B. Rosenow, M. Grundmann, R. Schmidt-Grund: *Exceptional points in planar semiconductor-microcavities of optically anisotropic media*, 34th International Conference on the Physics of Semiconductors, ICPS2018, Montpellier, France, July/August 2018

D. Splith, S. Lanzinger, S. Müller, C. Sturm, H. von Wenckstern, M. Grundmann: *Influence of Ga incorporation into bixbyite In_2O_3 thin films on the performance of Schottky barrier diodes thereon*, DPG spring meeting, Berlin, Germany, March 2018

C. Sturm, M. Grundmann: *Dielectric Function and Singular Optic Axes of KTP*, 10th Workshop Ellipsometry, Chemnitz, Germany, March 2018

C. Sturm, M. Grundmann: *Dielectric Function and Singular Optic Axes of KTP*, 34th International Conference on the Physics of Semiconductors, ICPS2018, Montpellier, France, July/August 2018

L. Trefflich, F. Dissinger, M. Kakei, C. Sturm, S.R. Waldvogel, M. Grundmann, R. Schmidt-Grund: *Optical properties of carbon nanodots as active material in planar microcavities*, DPG spring meeting, Berlin, Germany, March 2018

L. Trefflich, F. Dissinger, C. Sturm, S.R. Waldvogel, M. Grundmann, R. Schmidt-Grund: *Carbon nanodot based planar microcavities*, International and dissemination work shop of the research unit FOR1616, Weimar, Germany, September 2018

A. Werner, H. von Wenckstern, M. Grundmann: *Investigations of Ge-doped (Al,Ga)$_2$O$_3$ thin films*, DPG spring meeting, Berlin, Germany, March 2018

A. Werner, R. Hoelldobler, V. Prozheeva, D. Splith, C. Sturm, H. von Wenckstern, M. Grundmann: *Occurence of the ϵ-phase in (In$_x$Ga$_{1-x}$)2O3 and (Ga$_x$Al$_{1-x}$)$_2$O$_3$ thin films*, DPG spring meeting, Berlin, Germany, March 2018

A. Werner, H. von Wenckstern, M. Grundmann: *Influence of growth conditions on deposition of $\beta-$ and ϵ-phase (Al,Ga)$_2$O$_3$ thin films grown by PLD on sapphire substrates*, Annual BuildMoNa Conference, Leipzig, Germany, March 2018

V. Zviagin, P. Huth, C. Sturm, J. Lenzner, A. Setzer, R. Denecke, P. Esquinazi, M. Grundmann, Rüdiger Schmidt-Grund: *Optical and Magnetic Properties of PLD Grown Spinel Ferrite Thin Films in Relation to their Cation Configuration*, Collaborative Research Centre SFB 762: Functionality of Oxide Interfaces, International Workshop, Frauenchiemsee, Germany, February/March 2018

V. Zviagin, P. Huth, C. Sturm, D. Spemann, S. Mändl, J. Lenzner, A. Setzer, J. Meijer, R. Denecke, P. Esquinazi, M. Grundmann, R. Schmidt-Grund: *Optical and Magnetic Properties of Spinel Type Ferrites in Relation to their Crystallographic Order*, DPG spring meeting, Berlin, Germany, March 2018

V. Zviagin, P. Huth, C. Sturm, J. Lenzner, A. Setzer, R. Denecke, P. Esquinazi, M. Grundmann, R. Schmidt-Grund: *Spinel Ferrite Bulk and Surface Cation and Defect Contribution to the Ferrimagnetic Response*, International Conference on Magnetism, San Francisco, USA, July 2018

V. Zviagin, P. Huth, C. Sturm, J. Lenzner, A. Setzer, R. Denecke, P. Esquinazi, M. Grundmann, R. Schmidt-Grund: *Bulk and Surface Cation Configuration Investigation of PLD Grown Spinel Ferrites in Relation to the Magnetic Response*, 34th International Conference on the Physics of Semiconductors, ICPS2018, Montpellier, France, July/August 2018

V. Zviagin, P. Huth, C. Sturm, J. Lenzner, A. Setzer, R. Denecke, P. Esquinazi, M. Grundmannm, R. Schmidt-Grund: *Spinel Ferrite Bulk and Surface Cation and Defect Contribution to the Ferrimagnetic Response*, 3rd ELIps Workshop, Dolní Brezany, Czech Republic, October 2018

9.24 Graduations

Doctorate

- Robert Karsthof
  NiO/ZnO-Heteroübergänge: Charakterisierung des elektrischen Transports und Realisierung transparenter aktiver Bauelemente
  February 2018

- Tom Michalsky
  Propagating exciton-polariton states in one- and two-dimensional ZnO-based cavity systems
  April 2018
- Marcus Purfürst
  Influence of Soot on the Transport Mechanisms inside the Filter Wall of SCR-Coated Diesel Particulate Filters
  April 2018
- Anna Reinhardt
  Amorphes Zinkoxinitrid - Untersuchung einer vielversprechenden Alternative zu amorphen Oxidhalbleitern
  January 2018
- Steffen Richter
  Optically aniostropic planar microcavities
  January 2018
- Peter Schlupp
  Funktionelle amorphe Dünnschichten: Bauelemente auf Basis von Zink-Zinn-Oxid
  February 2018
- Peter Schwinkendorf
  Magnetoelektrische Kopplung in $BaTiO_3$- und $BiFeO_3$-Kompositschichten und Leitfähigkeitsphänomene in Sr_2FeMoO_6-Dünnschichten
  April 2018
- Alexander Shkurmanov
  ZnO-based nanostructures by PLD: growth mechanism, doping and geometry
  April 2018
- Marcel Wille
  ZnO- und CuI-Nano- und Mikrostrukturen: Laseremission und Komplexer Brechungsindex
  February 2018

Master

- Rafael Deichsel
  Untersuchung von Kupferiodid-Kristallen mittels Photolumineszenz
  January 2018
- Rebecca Sabine Hölldobler
  Eigenschaften von $(GaIn)_2O_3$ Dünnfilmen
  March 2018
- Florian Jung
  Optical and structural properties of TiN/MgO superlatties
  October 2018
- Evgeny Krüger
  Optische Eigenschaften von CuI-Dünnschichten und -Mikrodrähten
  May 2018

- Steffen Lanzinger
  Untersuchung von Schottkydioden auf kubischem (Ju,Ga)$_2O_3$
  March 2018

Bachelor

- Philipp Bischoff
  Herstellung und elektrische Charakterisierung von ZTO-basierten MESFETs
  January 2018
- Misuki Kakei
  The determination of the suitability of the gelatine as cavity material for planar microcavity
  October 2018
- Sandra Montag
  Modification of transparent NiO/ZnO-heterojunctions by gradual substitution with MgO
  October 2018
- Andreas Müller
  Untersuchung der optischen Phonenmoden von epsilon-Galliumoxid
  October 2018
- Sophie Müller
  Herstellung und Charakterisierung von Molybdäntrioxid-Mikroflakes
  February 2018

9.25 Guests

- Dr.-Ing. Krzysztof Grzegorz Dorywalski
  Politechnika Koszalinska, Koszalin, Poland
  October 2017 – June 2018
- Michitaka Fukumoto
  Japan Society for the Promotion of Science: Overseas Challenge Program for Young Researchers
  April 2018 – March 2019
- Dr. Wenlei Yu
  Wenzhou Medical University, Zhejiang, PR China
  August 2018 – July 2019

10

Superconductivity and Magnetism

10.1 Introduction

The main interests of the group at the division are phenomena related to superconductivity and magnetism in solids. In the last few years the research activities in superconductivity have been mainly concentrated in searching for its existence in graphite, especially at graphite interfaces between Bernal-like crystalline regions. This research issue started in our division in Leipzig in the year 2000 and became supporting experimental evidence quite recently, indicating the existence of superconductivity at temperatures above 100 K. Future work will be concentrated in the localization of the superconducting phases and the increase of the superconducting yield.

Our division was the first to show that atomic lattice defects can produce magnetic order in graphite without the need of magnetic ions. This phenomenon is known nowadays as Defect-Induced Magnetism and it is found in a broad spectrum of different materials. We are involved in a collaborative research project with the aim of triggering this phenomenon in nominally non-magnetic oxides, via vacancies and/or hydrogen doping. Further research topic is the study of the electrical and magnetic properties of oxide multilayers of thickness of a few unit cells, especially the investigation of topological signatures in the Hall effect of $SrRuO_3$-based heterostructures.

Pablo Esquinazi

10.2 Local Magnetic Measurements of Trapped Flux Through a Permanent Current Path in Graphite

M. Stiller*, P. Esquinazi*, J. Barzola-Quiquia*, C.E. Precker*

*Division of Superconductivity and Magnetism, Felix-Bloch-Institut für Festkörperphysik, Leipzig University, 04103 Leipzig, Germany

Temperature- and field-dependent measurements of the electrical resistance of different natural graphite samples suggest the existence of superconductivity at room temperature in some regions of the samples. To verify whether dissipationless electrical currents are responsible for the trapped magnetic flux inferred from electrical resistance measurements, we localized them using magnetic force microscopy on a natural graphite

sample in remanent state after applying a magnetic field. The obtained evidence indicates that at room temperature a permanent current flows at the border of the trapped flux region. The current path vanishes at the same transition temperature $T_c \approx 370$ K as the one obtained from electrical resistance measurements on the same sample. This sudden decrease in the phase is different from what is expected for a ferromagnetic material. Time-dependent measurements of the signal show the typical behavior of flux creep of a permanent current flowing in a superconductor. The overall results support the existence of room-temperature superconductivity at certain regions in the graphite structure and indicate that magnetic force microscopy is suitable to localize them. Magnetic coupling is excluded as origin of the observed phase signal.

10.3 Influence of Interfaces on the Transport Properties of Graphite revealed by Nanometer Thickness Reduction

M. Zoraghi[*] [†], J. Barzola-Quiquia[*], M. Stiller[*], P. Esquinazi[*], I. Estrela-Lopis[‡]

[*]Division of Superconductivity and Magnetism, Felix-Bloch-Institut für Festkörperphysik, Leipzig University, 04103 Leipzig, Germany

[†]Current address: Department of Neurophysics, Max Planck Institute for Human Cognitive and Brain Sciences, 04103 Leipzig, Germany.

[‡]Institute of Medical Physics and Biophysics, University of Leipzig, 04107 Leipzig, Germany

We investigated the influence of thickness reduction on the transport properties of graphite microflakes. Using oxygen plasma etching we decreased the thickness of highly oriented pyrolytic graphite (HOPG) microflakes from $\approx$ 100 nm to $\approx$ 20 nm systematically. Keeping current and voltage electrodes intact, the electrical resistance $R(T)$, the magnetoresistance (MR) and Raman spectra were measured in every individual sample and after each etching step of a few nm. The results show that $R(T)$ and MR can increase or decrease with the sample thickness in a non-systematic way. The results indicate that HOPG samples are inhomogeneous materials, in agreement with scanning transmission electron microscopy images and X-ray diffraction data. Our results further indicate that the quantum oscillations in the MR are not an intrinsic property of the ideal graphite structure but their origin is related to internal conducting interfaces.

10.4 Magnetotransport properties of microstructured $AlCu_2Mn$ Heusler alloy thin films in the amorphous and crystalline phase

J. Barzola-Quiquia[*], M. Stiller[*], P. Esquinazi[*], J. Quispe-Marcatoma[†], P. Häussler[‡]

[*]Division of Superconductivity and Magnetism, Felix-Bloch-Institut für Festkörperphysik, Leipzig University, 04103 Leipzig, Germany

[†]Facultad de Ciencias Físicas, Universidad Nacional Mayor de San Marcos,
14-0149 Lima 14, Peru
[‡]Division of Thin Films Physics, Institute of Physics, Chemnitz University of Technology,
09107 Chemnitz, Germany

We have studied the resistance, magnetoresistance and Hall effect of $AlCu_2Mn$ Heusler alloy thin films prepared by flash evaporation on substrates cooled at ^{4}He liquid temperature. The as-prepared samples were amorphous and were annealed stepwise to induce the transformation to the crystalline phase. The amorphous phase is metastable up to above room temperature and the transition to the crystalline phase was observed by means of resistance measurements. Using transmission electron microscopy, we have determined the structure factor $S(K)$ and the pair correlation function $g(r)$, both results indicate that amorphous $AlCu_2Mn$ is an electronic stabilized phase. The X-ray diffraction of the crystallized film shows peaks corresponding to the well ordered $L2_1$ phase. The resistance shows a negative temperature coefficient in both phases. The magnetoresistance (MR) is negative in both phases, yet larger in the crystalline state compared to the amorphous one. The magnetic properties were studied further by anomalous Hall effect measurements, which were present in both phases. In the amorphous state, the anomalous Hall effect disappears at temperatures below 175 K and is present up to above room temperature in the case of crystalline $AlCu_2Mn$.

10.5 Diamagnetism of Bulk Graphite Revised

B. Semenenko[*], P.D. Esquinazi[*]

[*]Division of Superconductivity and Magnetism, Felix-Bloch-Institut für Festkörperphysik,
Leipzig University, 04103 Leipzig, Germany

Recently published structural analysis and galvanomagnetic studies of a large number of different bulk and mesoscopic graphite samples of high quality and purity reveal that the common picture assuming graphite samples as a semimetal with a homogeneous carrier density of conduction electrons is misleading. These new studies indicate that the main electrical conduction path occurs within 2D interfaces embedded in semiconducting Bernal and/or rhombohedral stacking regions. This new knowledge incites us to revise experimentally and theoretically the diamagnetism of graphite samples. We found that the c-axis susceptibility of highly pure oriented graphite samples is not really constant, but can vary several tens of percent for bulk samples with thickness $t \gtrsim 30$ μm, whereas by a much larger factor for samples with a smaller thickness. The observed decrease of the susceptibility with sample thickness qualitatively resembles the one reported for the electrical conductivity and indicates that the main part of the c-axis diamagnetic signal is not intrinsic to the ideal graphite structure, but it is due to the highly conducting 2D interfaces. The interpretation of the main diamagnetic signal of graphite agrees with the reported description of its galvanomagnetic properties and provides a hint to understand some magnetic peculiarities of thin graphite samples.

10.6 Hall Effect of Asymmetric $La_{0.7}Sr_{0.3}MnO_3/SrTiO_3/SrRuO_3$ and $La_{0.7}Sr_{0.3}MnO_3/BaTiO_3/SrRuO_3$ Superlattices

M. Ziese*, I. Lindfors-Vrejoiu†

*Division of Superconductivity and Magnetism, Felix-Bloch-Institut für Festkörperphysik, Leipzig University, 04103 Leipzig, Germany

†II. Physikalisches Institut, Universität zu Köln, D-50937 Köln, Germany

The Hall resistivity and magnetization of high quality asymmetric $La_{0.7}Sr_{0.3}MnO_3/SrTiO_3/SrRuO_3$ and $La_{0.7}Sr_{0.3}MnO_3/BaTiO_3/SrRuO_3$ superlattices were investigated. The superlattices were fabricated by pulsed laser deposition. A high resolution scanning transmission electron microscopy image is shown in Fig. 10.1(a). The Hall resistivity hysteresis curves have a complex magnetic field dependence in an intermediate temperature regime that is not reflected in the global magnetization, see Fig. 10.1(b). This arises either from the formation of complex magnetization textures that lead to the appearance of a topological Hall effect or from the shift of the Weyl nodes in $SrRuO_3$ by the coupling to the adjacent $La_{0.7}Sr_{0.3}MnO_3$ magnetization.

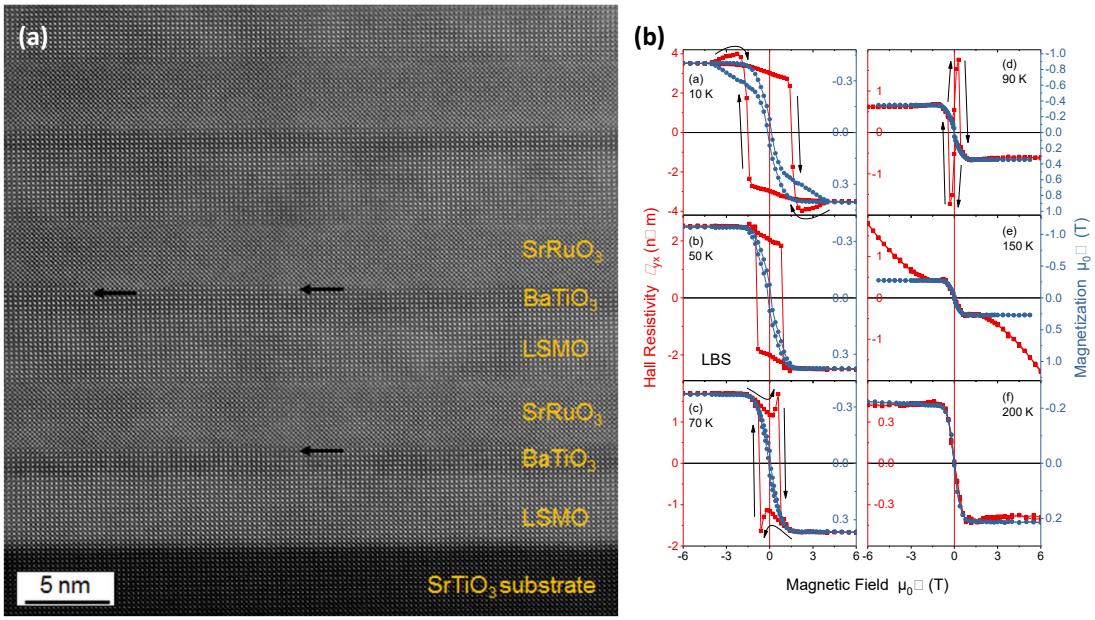

Figure 10.1: (a) High resolution scanning transmission electron microscopy image of a $La_{0.7}Sr_{0.3}MnO_3/BaTiO_3/SrRuO_3$ superlattice. (b) Anomalous Hall effect (left axis) and magnetization (right axis) of the superlattice shown in (a).

10.7 Funding

Defect-induced Magnetism in Oxides
Prof. Dr. Pablo Esquinazi
DFG SFB 762/3, B1

Magnetic and electric properties of ultrathin oxide films
Prof. Dr. Pablo Esquinazi and Prof. Dr. Michael Ziese
DFG SFB 762/3, B5

Controlled creation of defect-induced magnetism (DIM) in graphite- and diamond-based films
Prof. Dr. Pablo Esquinazi
DFG-ES86/29-1

10.8 Organizational Duties

P. Esquinazi

- Project Reviewer: Deutsche Forschungsgemeinschaft (DFG), National Science Foundation (USA), German-Israeli Foundation (GIF), Israel Science Foundation, Department of Energy (Washington), DAAD
- Referee: Phys. Rev. Lett, Phys. Rev. B., Appl. Phys. Lett., Chem. Phys. Lett., Nature Physics, Nature Materials, Physica C, Phys. Lett. A, phys. stat. sol., J. Low Temp. Phys., Carbon, J. Chem. Phys., Eur. J. Phys. B, J. Magn. Magn. Mater.

M. Ziese

- Head of the General Physics Laboratory
- Dean of Studies
- Referee: Phys. Rev. Lett., Phys. Rev. B., Adv. Mater., Appl. Phys. A, Current Nanoscience, Eur. Phys. J. B, IEEE Trans. Magn., J. Phys.: Condens. Matter, J. Phys. D: Appl. Phys., J. Alloys Comp., J. Appl. Phys., J. Am. Ceram. Soc., J. Magn. Magn. Mater., J. Mater. Research, J. Mater. Science, Materials Science and Engineering B, Nanotechnology, phys. stat. sol., Thin Solid Films

W. Böhlmann

- Referee: J. Physical Chemistry, J. of American Chemical Society, Microporous and Mesoporous Materials

10.9 External Cooperations

Academic

- State University of Campinas, Campinas, Brazil
  Prof. Dr. Yakov Kopelevich
- Universität zu Köln, Cologne, Germany
  Dr. Ionela Vrejoiu

- Martin-Luther Universität Halle-Wittenberg, Halle, Germany
  Prof. Ingrid Mertig
- Martin-Luther Universität Halle-Wittenberg, Halle, Germany
  Prof. Wolfram Hergert
- Martin-Luther Universität Halle-Wittenberg, Halle, Germany
  Dr. Angelika Chassé
- Martin-Luther Universität Halle-Wittenberg, Halle, Germany
  Dr. Manfred Dubiel
- Stanford Synchrotron Radiation Laboratory, USA
  Dr. Hendrik Ohldag
- Laboratorio de Física de Sistemas Pequeños y Nanotecnologíia, Consejo Superior de Investigaciones Científicas, Madrid, Spain
  Prof. N. García (Madrid)
- Forschungszentrum Dresden-Rossendorf e.V., Institut für Ionenstrahlphysik und Materialforschung, Germany
  Dr. W. Anwand
- Forschungszentrum Dresden-Rossendorf e.V., Institut für Ionenstrahlphysik und Materialforschung, Germany
  Dr. G. Brauer
- Tucuman University, Argentina
  Prof. S. P. de Heluani
- University of La Plata, Argentina
  Dr. C. E. Rodriguez Torres
- Universidad Autónoma de Madrid, Spain
  Prof. Dr. Miguel Angel Ramos
- Bar Ilan University, Israel
  Dr. G. D. Nessim

10.10 Publications

Journals

J. Barzola-Quiquia, M. Stiller, P.D. Esquinazi, J. Quispe-Marcatoma, P. Häussler: *Magnetotransport properties of microstructured $AlCu_2Mn$ Heusler alloy thin films in the amorphous and crystalline phase*, J. Magn. Magn. Mater. **456**, 281 (2018)

P. Esquinazi: *Topological Matter and Flat Bands (TMFB)*, J. Low Temp. Phys. **191**, 1 (2018)

C. Hanisch, F. Hofmann, M. Ziese: *Linear momentum, angular momentum and energy in the linear collision between two balls*, Eur. J. Phys. **39**, 015003 (2018)

C. Hanisch, F. Hofmann, M. Ziese: *Impuls-, Drehimpuls- und Energieerhaltung beim eindimensionalen Stoß zweier Kugeln: Impressionen aus dem Praktikumsalltag*, PhyDid-A **17**, 13 (2018)

M. Kneiß, Ch. Yang, J. Barzola-Quiquia, G. Benndorf, H. von Wenckstern, P. Esquinazi, M. Lorenz, M. Grundmann: *Suppression of Grain Boundary Scattering in Multifunctional p-Type Transparent γ-CuI Thin Films due to Interface Tunneling Currents*, Adv. Mater. Interfaces **5**, 1701411 (2018)

K.L. Salcedo Rodríguez, G. Bridoux, S.P. de Heluani, G.A. Pasquevich, P.D. Esquinazi, C.E. Rodríguez Torres: *Influence of substrate effects in magnetic and transport properties of magnesium ferrite thin films*, J. Magn. Magn. Mater. **469**, 643 (2019)

B. Semenenko, P.D. Esquinazi: *Diamagnetism of Bulk Graphite Revised*, Magnetochemistry **4**, 52 (2018)

M. Stiller, P. Esquinazi, J. Barzola-Quiquia, C. E. Precker: *Local Magnetic Measurements of Trapped Flux Through a Permanent Current Path in Graphite*, J. Low Temp. Phys. **191**, 105 (2018)

M. Ziese, I. Lindfors-Vrejoiu: *Hall effect of asymmetric $La_{0.7}Sr_{0.3}MnO_3/SrTiO_3/SrRuO_3$ and $La_{0.7}Sr_{0.3}MnO_3/BaTiO_3/SrRuO_3$ superlattices*, J. Appl. Phys. **124**, 163905 (2018)

M. Zoraghi, J. Barzola-Quiquia, M. Stiller, P.D. Esquinazi, I. Estrela-Lopis: *Influence of interfaces on the transport properties of graphite revealed by nanometer thickness reduction*, Carbon **139**, 1074 (2018)

L. Wysocki, R. Mirzaaghayev, M. Ziese, L. Yang, J. Schöpf, R.B. Versteeg, A. Bliesener, J. Engelmayer, A. Kovács, L. Jin, F. Gunkel, R. Dittmann, P.H.M. van Loosdrecht, I. Lindfors-Vrejoiu: *Magnetic coupling of ferromagnetic $SrRuO_3$ epitaxial layers separated by ultrathin non-magnetic $SrZrO_3/SrIrO_3$*, Appl. Phys. Lett. **113**, 192402 (2018)

10.11 Graduations

Doctorate

- M. Sc. Francis Bern
  Electric and Magnetic Coupling Phenomena at Oxide Interfaces
  May 2018

Master

- B. Sc. Tiago Rafael Silva Cordeiro
  Transport properties of bilayer graphene
  February 2018
- B. Sc. Lukas Botsch
  Probing the spin-orbit coupling induced spin texture of the ZnO[1010] *surface by photogalvanic spectroscopy*
  October 2018

Bachelor

- cand. B. Sc. Devesh Jawla
  Investigation of granular superconductivity in natural graphite under a magnetic force microscope
  March 2018
- cand. B. Sc. Anthony Chukwunonso Ogbuehi
  Influence of contact barrier on the transport properties of micro structured ZnO thin films
  March 2018
- cand. B. Sc. Laetitia Paula Bettmann
  Analysis of quantum oscillations generated at interfaces in different graphite samples
  October 2018
- cand. B. Sc. Ratna Bamadur Bista
  Effect of hydrogen and lithium on the transport properties of Zinc oxide microwires and single crystals
  November 2018

10.12 Guests

- Prof. Dr. Ana Melva Champi Farfán
  Universidade Federal do ABC, Santo André, São Paulo/Brazil
  September 2017 – August 2018
- Dr. Mihai V. Putz
  West University of Timisoara / Romania
  March 2018
- Dr. Dagmar Franziska Weickert
  National High Magnetic Field Laboratory, Los Alamos / USA
  June 2018
- Prof. Dr. Paula Gabriela Bercoff
  Universidad Nacional de Córdoba, Instituto de Fisica Enrique Gaviola / Argentinien
  September 2018 - November 2018

11

Applied Magnetic Resonance

11.1 Introduction

Nuclear magnetic resonance is a very diverse and powerful experimental technique to address a wide spectrum of different phenomena. It finds numerous applications for understanding various dynamic processes in soft- to hard matter on the time scale from nanoseconds to seconds. The particular focuses of the Applied Magnetic Resonance Division include the applications of (i) the pulsed field gradient technique of NMR to assess molecular translation motion in complex materials in a broad range of thermodynamic conditions and of (ii) the solid-state NMR to probe different physico-chemical material properties. Besides NMR, close collaboration between the division and the Max-Planck Institute for Brain Sciences ensures synergistic research on the interface between conventional materials-related NMR and magnetic resonance imaging in biological matter.

Prof. Dr. Rustem Valiullin

11.2 Revealing the Transient Concentration of CO_2 in a Mixed-Matrix Membrane by IR Microimaging and Molecular Modleing

S. Hwang, R. Semino[*], B. Seoane[†], M. Zahan, C. Chmelik, R. Valiullin, M. Bertmer, J. Haase, F. Kapteijn[†], J. Gascon[†], G. Maurin[*], J. Kärger

[*]Université de Montpellier, Institut Charles Gerhardt Montpellier, Place Eugène Bataillon, 34095 Montpellier Cedex 5, France

[†]Delft University of Technology, Catalysis Engineering, ChemE Department, Van der Maasweg 9, 2629 HZ Delft, The Netherlands

Through IR microimaging the spatially and temporally resolved development of the CO_2 concentration in a ZIF-8@6FDA-DAM mixed matrix membrane (MMM) was visualized during transient adsorption, see Fig. 11.1. By recording the evolution of the CO_2 concentration, it is observed that the CO_2 molecules propagate from the ZIF-8

filler, which acts as a transport 'highway', towards the surrounding polymer. A high-CO_2-concentration layer is formed at the MOF/polymer interface, which becomes more pronounced at higher CO_2 gas pressures. A microscopic explanation of the origins of this phenomenon is suggested by means of molecular modeling. By applying a computational methodology combining quantum and force-field based calculations, the formation of microvoids at the MOF/polymer interface is predicted. Grand canonical Monte Carlo simulations further demonstrate that CO_2 tends to preferentially reside in these microvoids, which is expected to facilitate CO_2 accumulation at the interface.

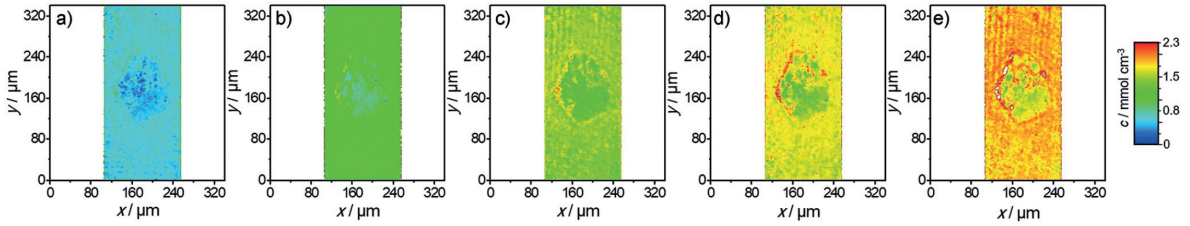

Figure 11.1: Images of CO_2 concentration in the MMM at different pressures: a) 200 mbar, b) 400 mbar, c) 600 mbar, d) 800 mbar, e) 1000 mbar of CO_2 at 308 K.

11.3 $LiSr_2SiO_4H$, an Air-Stable Hydride as Host for Eu(II) Luminescence

F. Gehlhaar*, R. Finger*, N. Zapp*, M. Bertmer, H. Kohlmann*

*Inorganic Chemistry, Leipzig University, Leipzig, Germany

$LiSr_2SiO_4H$ is synthesized by solid-state reaction of LiH and α- Sr_2SiO_4. It crystallizes in space group $P2_1/m$ (a = 658.63(4) pm, b = 542.36(3) pm, c = 695.01(4) pm, β = 112.5637(9)°) as proven by X-ray and neutron diffraction, is isotypic to $LiSr_2SiO_4F$, and exhibits isolated SiO_4 tetrahedra. Hydride anions are located in Li_2Sr_4 octahedra, which share faces to form columns, with H-H distances of 271.18(2) pm. NMR (Fig. 11.2, IR, and Raman spectroscopy, d. measurements, elemental anal., and theor. calcns. confirm these results. Despite its hydridic nature, it is stable in air up to 550 K. When doped with europium, it emits bright yellow-green light with an intensity max. at 560 nm for $LiSr_{1.98}Eu_{0.02}SiO_4H$. Even after treatment in water for several hours, the solid shows luminescence. The broad emission peak is attributed to the allowed $4f^65d \rightarrow 4f^7$ transition of divalent europium. $LiSr_2SiO_4H$ is the first silicate hydride, a class of compds. that might have potential as host for luminescent materials.

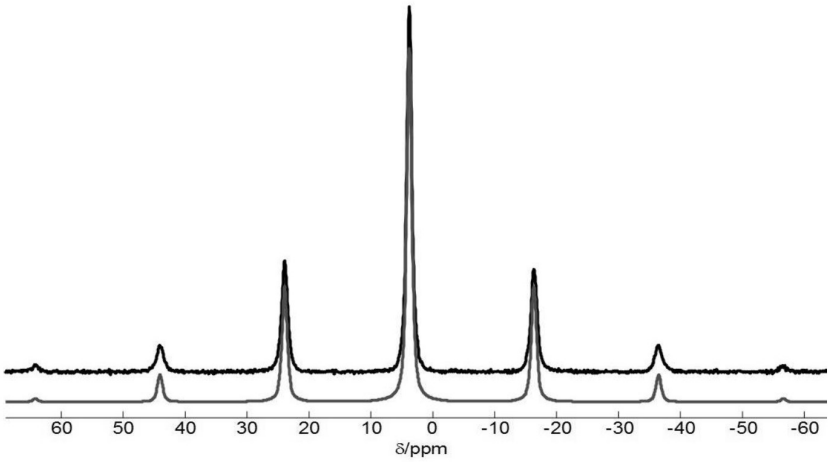

Figure 11.2: ^{2}H MAS spectrum of $LiSr_2SiO_4D$ (black). Below in grey is the calculated spectrum taking into account dipolar coupling to the closest lithium and deuterium atoms.

11.4 Water transport in periodic mesoporous organosilica materials

J.B. Mietner*, M. Fröba*, R. Valiullin

*Institute of Inorganic and Applied Chemistry, University of Hamburg, Hamburg

Water transport in periodic mesoporous organosilicas (PMO) was studied using pulsed field gradient (PFG) NMR. A series of isogeometric PMO materials with different chemical compositions of the pore walls were investigated and compared to a purely siliceous MCM-41 material with an identical pore size. The long-range water diffusivities measured were found to be largely controlled by the macroscopic textural properties of the materials, namely by the particle geometry and a degree of the particle agglomeration, and by thermodynamic conditions under which the experiments were performed. It is shown that their combined effect caused water molecules either to propagate predominantly along the capillary-condensed water domains or to frequently alternate their trajectories between these domains and the water phase in the inter-particle space. Because the transport rates in these two regimes differ substantially, it is suggested that, by a purposeful choice of the PMO composition, both the long-range transport rate and the chemical functionality can deliberately be tuned.

11.5 Superficial white matter imaging: Contrast mechanisms and U-fiber mapping

E. Kirilina*,†, S. Helbling*, M. Morawski‡, K. Pine*, K. Reimann‡, S. Jankuhn§, J. Dinse*, A. Deistung¶, J.R. Reichenbach¶, R. Trampel*, S. Geyer*, L. Müller‖, N. Jakubowski‖, T. Arendt‡, P.-L. Bazin*, N. Weiskopf*

*Department of Neurophysics, Max Planck Institute for Human Cognitive and Brain Sciences
†Center for Cognitive Neuroscience Berlin, Free University Berlin

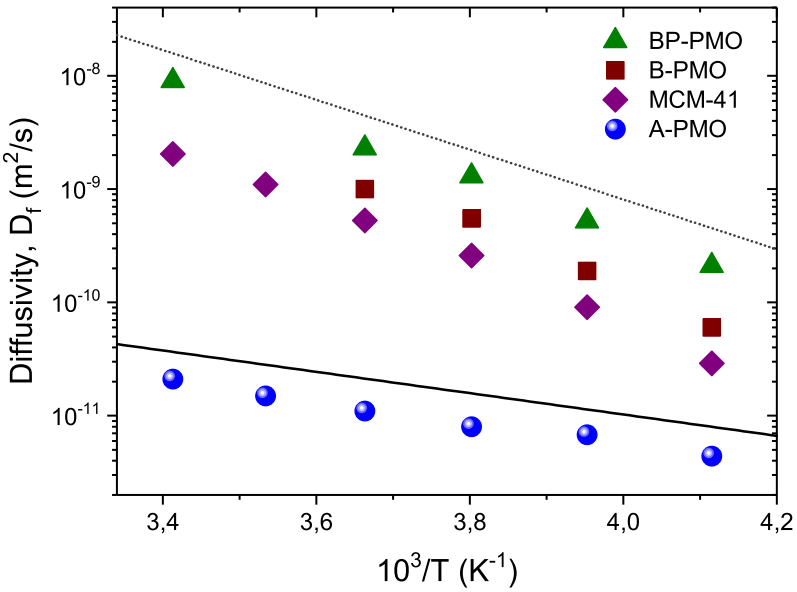

Figure 11.3: Arrhenius plot of the average water diffusivities in the mesopore channels of different PMO materials.

‡Paul Flechsig Institute for Brain Research, Leipzig University
§Department of Solid State Physics, Faculty of Physics and Earth Sciences, Leipzig University
¶Medical Physics Group, Institute of Diagnostic and Interventional Radiology, Jena University Hospital - Friedrich Schiller University Jena
‖Federal Institute for Materials Research and Testing, Berlin

Superficial white matter (SWM) is the thin layer of white matter just below the cortical sheet containing short association fibers or U-fibers, intestinal neurons and glia. These region hosts the majority of white matter connections and crucially support cortico-cortical connectivity. However, SWM is poorly characterized in humans due to the lack of reliable non-invasive imaging methods. Here we propose ultra-high resolution magnetic resonance imaging (MRI), measuring transverse relaxation rates (R2, R2*) and magnetic susceptibility for the non-invasive characterization of SWM. We used a combination of ultra high resolution in vivo and post mortem quantitative MRI, iron histology and tissue iron extraction to characterize the contrast mechanisms in SWM. We found that the SWM exhibits an MRI contrast distinct from both gray and deep white matter, driven by the high iron content in the oligodendrocytes and myelin sheaths. We developed and validated a specific SWM contrast model using cellular-resolution iron maps and fundamental relaxation theory and applied it to map iron deposits in SWM across the brain. We demonstrated that iron content in SWM strongly vary across the brain with sharp boarders between cortical areas with different cytoarchtecture. Enhanced iron deposits were observed in U-fiber-rich frontal, temporal and parietal association areas potentially reflecting higher fiber density or late myelination in these areas. Our approach paves the way for further studies of SWM distribution, and inter-individual differences in this region critical for cortico-cortical connectivity.

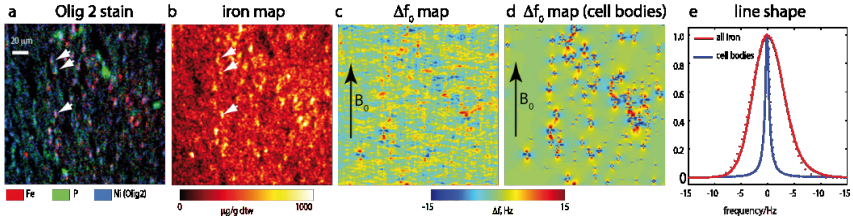

Figure 11.4: Biophysical modeling of MRI contrast informed by ion beam microscopy (a,b) Oligodendrocytes in SWM visualized by PIXE elemental maps of phosphor (green), iron (red) and nickel (Ni-enhanced Olig2 stain for oligodendrocyte nuclei). Quantitative map of iron concentration obtained on a 12 μm thick slice in SWM with PIXE. Position of 200 $\times$ 200 μm^2 field of view in the brain slice is indicated on Fig. 3a; (c,d) Simulated map of microscopic distortion of magnetic field resulting from the iron distribution shown in (b). (e) Shapes of water MR line shape resulting from magnetic field distribution (c) and (d) predicting MRI parameters in SWM.

11.6 Funding

Structure and Transport Characterization of Hierarchical Porous Solids
Prof. Dr. Rustem Valiullin
DFG, VA 463/6-1

Freezing and melting transitions in mesoporous solids: From fundamental understanding to advanced characterization using thermoporometry
Prof. Dr. Rustem Valiullin, Proff. Dr. Dirk Enke
DFG, VA 463/7-1

MOFs as carrier for nitric oxide delivery in biological systems - microscopic fundamentals of adsoprtion and controlled release studied by infrared and electron and nuclear spin resonance spectroscopy
PD Dr. Marko Bertmer, Prof. Dr. Andreas Pöppl, Prof. Dr. Martin Hartmann, Prof. Dr. Michael Fröba
DFG, BE 2434/4-2, PO 426/8-2

Charakterisierung der [2+2]-Photodimerisierung von photoaktiven Substanzen auf der Basis von Zimtsäure eingebaut in Polymeren oder in supramolekularen Strukturen mit Festkörper-NMR-Spektroskopie
PD Dr. Marko Bertmer
DFG, BE 2434/2-3

11.7 Organizational Duties

Prof. Dr. Nikolaus Weiskopf

- Member of the UK Biobank Imaging Extension External Advisory Board
- Member Scientific Council, Leibniz Institute for Neurobiology, Magdeburg, Germany
- Member of Committee of Directors, Centre of Magnetic Resonance at the University of Leipzig, Germany
- Associate Editor Frontiers in Brain Imaging Methods

- Editor Neurons, Behavior, Data Analysis and Theory
- Reviewing of grant applications for the Wellcome Trust (UK), Medical Research Council (MRC, UK), Federal Ministry of Education and Research (BMBF, Germany), Helmholtz Association of German Research Centres, German Research Council (DFG, Germany), Swiss National Science Foundation, Wings for Life (Austria), University of Freiburg (Germany), The German Israeli Foundation for Scientific Research and Development (GIF, Israel), Agence Nationale de la Recherche (France), Israel Science Foundation (ISF), Fonds de la Recherche Scientifique (FNRS) (Belgium)
- Referee: Science, Mag. Reson. Med., Neuroimage, Physical Review Letters, Human Brain Mapping, IEEE Trans. Medical Imaging, IEEE Trans. Biomed. Eng., MAGMA, Brain Structure and Function, JMRI, Trends in Cognitive Sciences, Journal of Neurophysiology, Journal of Neuroscience, Current Biology, eLife

Prof. Dr. Rustem Valiullin

- Member of the German Physical Society
- Scientific Advisory Board of the AMPERe Bologna Conference Magnetic Resonance in Porous Media
- Editorial Boards Diffusion Fundamentals, Dataset Papers in Physical Chemistry
- Referee: Physical Review, RSC, ACS, Elsevier

PD Dr. Marko Bertmer

- Referee: Angewandte Chemie, Chemistry of Materials, Journal of Physical Chemistry, Solid State Nuclear Magnetic Resonance, Microporous and Mesoporous Materials

11.8 External Cooperations

Academic

- University of Massachusetts, MA, USA
  Prof. P. Monson
- University of Giessen, Germany
  Prof. A. Bunde
- Washington University, Department of Chemistry, St. Louis, MO, USA
  Sophia E. Hayes
- Universität Koblenz-Landau, Abteilung Chemie, Landau, Germany
  Prof. Dr. Gabriele Schaumann
- Universität Erlangen-Nürnberg, Erlangen Catalysis Resource Center - ECRC, Erlangen, Germany
  Prof. Dr. Martin Hartmann

Industry

- BASF, Ludwigshafen, Germany
  E. Thompson

11.9 Publications

Journals

F. Gehlhaar, R. Finger, N. Zapp, M. Bertmer, H. Kohlmann: *$LiSr_2SiO_4H$, an Air-Stable Hydride as Host for Eu(II) Luminescence* Inorg. Chem. 57 (2018) 11851-11854

S. Hwang, R. Semino, B. Seoane, M. Zahan, C. Chmelik, R. Valiullin, M. Bertmer, J. Haase, F. Kapteijn, J. Gascon, G. Maurin, J. Kärger: *Revealing the Transient Concentration of CO_2 in a Mixed-Matrix Membrane by IR Microimaging and Molecular Modeling*, Angew. Chem. Int. Ed. 57 (2018) 5156-5160

A. H. Khan, B. Barth, M. Hartmann, J. Haase, M. Bertmer: *Nitric oxide adsorption in MIL-100(Al) MOF studied by solid-state NMR* J. Phys. Chem. C 122 (2018) 12723-12730

S. Matsia, O. Tsave, A. Hatzidimitriou, C. Gabriel, M. Bertmer, A. Salifoglu: *A Systematic Synthetic Study of Aqueous Chemistry of Binary Boron-Hydroxycarboxylic Acid Systems: Boron Structural Speciation Correlation to the Biotoxicity Profile*, Eur. J. Inorg. Chem. 2018 (2018) 1284-1301

B.J. Mietner, M. Fröba, R. Valiullin: *Water Transport in Periodic Mesoporous Organosilica Materials*, J. Phys. Chem. C 122 (2018) 12673-12680

M. Simenas, M. Ptak, A.H. Khan, L. Dagys, V. Balevicius, M. Bertmer, G. Völkel, M. Maczka, A. Pöppl, J. Banys: *Spectroscopic Study of $[(CH_3)_2NH_2][Zn(HCOO)_3]$ Hybrid Perovskite Containing Different Nitrogen Isotopes*, J. Phys. Chem. C 122 (2018) 10284-10292

Talks

R. Valiullin: *Cooperativity effects in phase transitions for fluids in mesoporous solids*, Bologna Conference Magnetic Resonance in Porous Media, Gainesville, USA, February 2018

R. Valiullin: *Phase transitions in geometrically disordered mesoporous solids*, Chatacterisation of Porous Materials, Boyton Beach, USA, May 2018

R. Valiullin: *Phase equilibria and molecular transport in mesoporous solids*, Schlumberger Doll Research, Boston, USA, May 2018

R. Valiullin: *Phase equilibria and molecular transport in mesoporous solids*, FGMR Meeting 2018, Leipzig, Germany, September 2018

R. Valiullin: *Phase equilibria and molecular transport in mesoporous solids*, 11th Seminar Porous Glasses, Wroclaw, Poland, September 2018

Posters

M. Bertmer: *Nitric Oxide Adsorption in Two Types of Metal-Organic Frameworks (MOFs) - Chemisorption as NONOates Besides Physisorption*, Rocky Mountain Conference on Magnetic Resonance, Snowbird, UT, USA, July 2018

H.R.N.B. Enninful: *Solid-Liquid Equilibria in Small-Pore Disordered Porous Glasses*, CRYSPOM VI Workshop, Hamburg, Germany, September 2018

11.10 Graduations

Doctorate

- Daniel Schneider
  Fluid behavior in porous solids: Microscopic insight by lattice models
  October 2018

III

Institute for Theoretical Physics

12

Computational Quantum Field Theory

12.1 Introduction

The Computational Physics Group performs basic research into classical and quantum statistical physics with special emphasis on phase transitions and critical phenomena. In the centre of interest are the physics of spin glasses, diluted magnets and other materials with quenched, random disorder, soft condensed matter physics with a focus on fluctuating paths and interfaces, biologically motivated problems such as polymer collapse/folding, adsorption and aggregation as well as related properties of proteins, and the intriguing physics of low-dimensional quantum spin systems.

The methodology is a combination of numerical and analytical techniques. The numerical tools are mainly Monte Carlo (MC) and Molecular Dynamics (MD) computer simulations, chain-growth algorithms, and exact enumeration techniques. The computational approach to theoretical physics is expected to gain more and more importance with the future advances of massively parallel computer technologies, and is likely to become the third cornerstone of physics besides experiment and analytical theory as sketched in Fig. 12.1. Already now it often helps to bridge the gap between experiments and the often necessarily approximate calculations in analytic approaches. To achieve the desired high efficiency of the numerical studies we develop new algorithms and, to guarantee the flexibility required by basic research, all computer codes are implemented by ourselves. The technical tools are Fortran, C, C++, and Python programs running under Unix or Linux operating systems and computer algebra using Maple or Mathematica. The software is developed and tested at the Institute on a cluster of PCs and workstations, where also most of the numerical analyses are performed. Currently we are also exploring the possibilities of the rapidly developing graphics card computing, that is computer simulations on general purpose graphics processing units (GPGPUs) with a very large number of cores. High-performance simulations requiring vast amounts of computer time are carried out at the Institute on quite powerful compute servers, at the parallel computers of the Saxon computing centre in Dresden, and, upon successful grant application, at the national supercomputing centres in Jülich, Stuttgart and München on parallel high-capability computers. This hierarchy of various platforms gives good training and qualification opportunities for the students, which offers promising job perspectives in many different fields for their future careers.

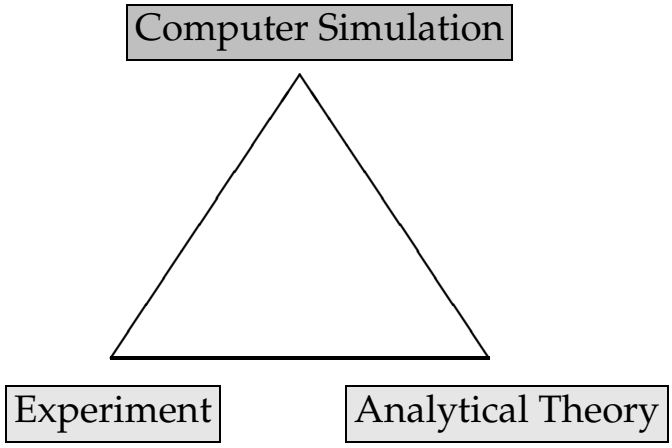

Figure 12.1: Sketch of the "triangular" relationship between experiment, analytical theory and computer simulation.

Our research activities are closely integrated into the Graduate School "BuildMoNa": Leipzig School of Natural Sciences – *Building with Molecules and Nano-objects*, the International Max Planck Research School (IMPRS) *Mathematics in the Sciences*, and the International Doctoral College *Statistical Physics of Complex Systems* with Université de Lorraine in Nancy, France, supported by the Deutsch-Französische Hochschule (DFH-UFA). In the second funding period 2011–2013, Coventry University in England has been integrated as an associated partner, and in the third funding period 2014–2016, also the National Academy of Sciences of Ukraine in Lviv has joined as another associated partner institution, offering our PhD students now several interesting options for secondments. For instance, in 2014, one PhD student started a "co-tutelle de thèse" jointly supervised with a colleague from Coventry University. Currently the DFH-UFA Doctoral College under the acronym "$\mathbb{L}^4$" is in its fourth funding period 2017–2020. The three Graduate Schools are all "Classes" of the Research Academy Leipzig (RALeipzig), providing the organizational frame for hosting visiting students and senior scientists, offering language courses, organizing childcare and for many other practical matters.

At a more post-graduate level our research projects are embedded into the Sonderforschungsbereich/Transregio SFB/TRR 102 *Polymers under Multiple Constraints: Restricted and Controlled Molecular Order and Mobility* together with Halle University. Our group also actively contributes to two of the top level research areas ("Profillinien") and the Centre for Theoretical Sciences (NTZ) of the University. Beside "BuildMoNa" the latter structures are particularly instrumental for our cooperations with research groups in experimental physics and biochemistry on the one hand and with mathematics and computer science on the other.

On an international scale, our research projects are carried out in a wide net of collaborations which are currently mainly funded by the Deutsch-Französische Hochschule (DFH-UFA) through the Doctoral College "$\mathbb{L}^4$" and the EU IRSES Network DIONICOS: *Dynamics of and in Complex Systems*, a consortium of 6 European and 12 non-European partners, including sites in Austria, England, France and Germany as well as in Armenia, Russia, Ukraine, India, the United States and Venezuela. Fur-

ther close contacts and collaborations are established with research groups in Armenia, Austria, China, France, Great Britain, India, Israel, Italy, Japan, Poland, Russia, Spain, Sweden, Taiwan, Turkey, Ukraine, and the United States. These contacts are refreshed and furthered through topical Workshops, Advanced Training Modules and Tutorials, and our International Workshop series *CompPhys: New Developments in Computational Physics*, taking annually place at the end of November just before the first advent weekend.

Wolfhard Janke

12.2 Monte Carlo simulations of poly(3-hexylthiophene) (P3HT): Comparison of three coarse-grained models

J. Gross, M. Ivanov, N. Oberthür, F. Müller, W. Janke

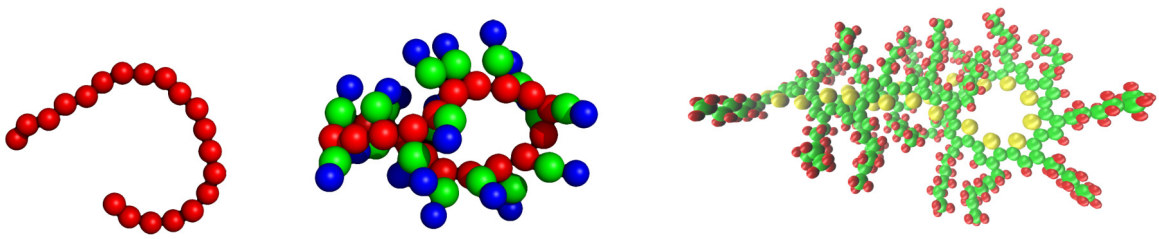

(a) (b) (c)

Figure 12.2: Hairpin conformations of poly(3-hexylthiophene) for a degree of polymerization $DP_n = 20$ in three different models. (a) One-particle coarse-grained model (one bead per monomer), (b) three-particle coarse-grained model, and (c) fully atomistic model.

Regioregular poly(3-hexylthiophene) (P3HT) is a very interesting conjugated polymer due to its electronic and optical properties [1]. One of its applications is the use as semiconducting layer in organic photovoltaics [2]. Studies of P3HT on the microscopic level are of great importance for a fundamental understanding of the tuneability of electronic properties and their dependence on external constraints, e.g., the adsorption on electrode surfaces. Hence a number of experimental studies addressed for example the influence of structure formation by polymer self-assembly on ideal surfaces on the electronic properties of oligo- and polythiophenes [3]. Due to the complexity of these macromolecules many of the experimental findings have not been supported with simulations so far, which in contrast is well-established for studies of small organic molecules. Our previous study [4] reported on an collaborative effort within the DFG SFB/TRR 102 project to combine the experimental observation of polymer chain conformations adsorbed on a metal surface with Monte Carlo simulations of a coarse-grained P3HT model developed by Huang *et al.* [5]. Based on our previous work on a three beads per monomer coarse-grained model, we expanded our studies in two directions. We focused our interest on the polymer itself and, firstly, investigated an

even coarser model with one bead per monomer [6] using Monte Carlo simulations. Secondly, we simulated a fully atomistic representation of P3HT using molecular dynamics. The different levels of resolution are illustrated in Fig. 12.2. We pursue these two routes to gauge the level of detail that is necessary to reproduce experimental findings more accurately. Another interest is the development of our own simplified model by systematically performing the coarse-graining procedure ourselves. For this we looked at the iterative Boltzmann inversion method [7]. A comparative analysis of all three models regarding structural observables, but also the computational effort is discussed in Ref. [8]. Recently we extended our simulations with the three-particle coarse-grained P3HT model to the case where the polymers are entirely adsorbed on a two-dimensional substrate with a striped pattern, modeling for instance the modulation pattern of a surface-reconstructed Au(001) gold substrate [9]. Our results show that the shape of the stripe pattern has a substantial effect on the obtained conformations of the polymer and can be tailored to promote either more stretched out or more compact configurations. In the compact phases we observe different structural motifs, such as hairpins, double-hairpins, and interlocking "zipper" states, cf. Fig. 12.3.

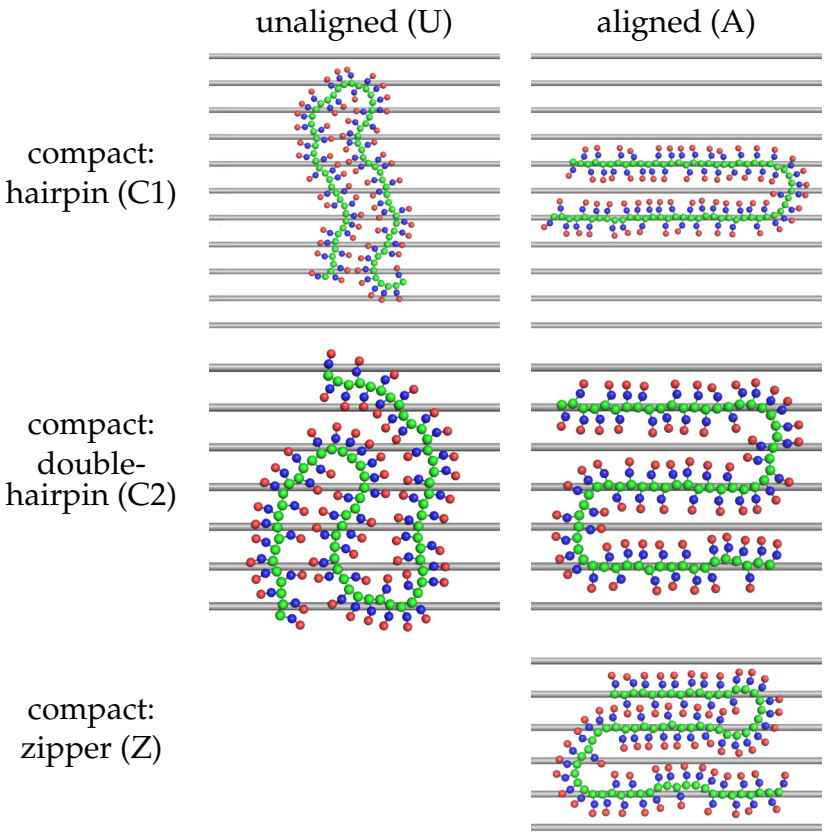

Figure 12.3: Snapshots of coarse-grained P3HT polymers of length $N = 65$ in different structural phases on a modulated surface with stripe-distance parameter $m = 3.5$, resembling the modulation pattern of a surface-reconstructed Au(001) gold substrate.

[1] X. Bai, S. Holdcroft: Macromolecules **26**, 4457 (1993); Z. Bao et al.: Appl. Phys. Lett. **69**, 4108 (1996); M.R. Andersson et al.: J. Mater. Chem. **9**, 1933 (1999); B.W. Boudouris et al.: Macromolecules **44**, 6653 (2011)

[2] J.M. Frost et al.: Nano Letters **6**, 1674 (2006); M. Campoy-Quiles et al.: Nat. Mater. **7**, 158 (2008); A.M. Ballantyne et al.: Adv. Funct. Mater. **18**, 2373 (2008)
[3] Z.Y. Yang et al.: ACS Nano **2**, 743 (2008); Y.F. Liu et al.: Nanoscale **5**, 7936 (2013)
[4] S. Förster et al.: J. Chem. Phys. **141**, 164701 (2014)
[5] D.M. Huang et al.: J. Chem. Theory Comput. **6**, 526 (2010)
[6] C.K. Lee et al.: Energy Environ. Sci. **4**, 4124 (2011)
[7] D. Reith et al.: J. Comput. Phys. **24**, 1624 (2003); Macromolecules **36**, 5406 (2003)
[8] J. Gross et al.: J. Phys.: Conf. Ser. **750**, 012009 (2016); Eur. Phys. J. – Special Topics **226**, 667 (2017)
[9] N. Oberthür et al.: J. Chem. Phys. **149**, 144903 (2018)

12.3 Adsorption of semiflexible polymers

K.S. Austin, J. Zierenberg*, W. Janke

*Max Planck Institute for Dynamics and Self-Organization, Am Fassberg 17, 37077 Göttingen, Germany

The conformational properties of a semiflexible polymer in the vicinity of an attractive surface is of relevance for a wide range of applications from material design to catalysis to DNA sequencing through nanopores. If the polymer adsorbs, which is not always desired in applications, there may occur different structural conformations. Often, the discussion of semiflexible polymer adsorption considers polymers under good solvent conditions with purely *repulsive* monomer-monomer interactions [1, 2]. Finite-size scaling analyses of computer simulation data show that the adsorption transition temperature increases linearly with persistence length for stiff polymers as predicted [2]. This may be expected to be maintained under poor solvent conditions. However, additional short-range *attractive* monomer-monomer interactions will lead to a rich conformational phase space as a result of the competition of polymer stretching and collapse close to an attractive surface.

In general, there has been an extensive theoretical and numerical effort towards the study of flexible polymers near attractive surfaces. Under poor solvent conditions, the final adsorbed states range from partially adsorbed to fully flat conformations, demonstrated for an entire class of flexible polymers [3]. Similar observations were made for the adsorption of specific lattice proteins [4]. If the surface shows complex attractive motifs, one observes in addition pattern recognition effects [4, 5].

Semiflexible, *self-attractive* polymers undergoing a collapse transition exhibit a rich variety of structural phases already in the case of an isolated chain [6, 7]. These include collapsed, toroidal, hairpin, and knotted conformations, partially depending on the geometric and energetic constraints of the model. This plays a crucial role for practical purposes, since semiflexibility is a common property of biopolymers such as DNA. The question arises how semiflexibility influences the structural and thermal adsorption properties of dilute self-attractive polymers. A detailed study of the interplay of (effective) polymer stiffness and surface adsorption for the full range of self-attracting polymer models was so far lacking and in Ref. [8] we intended to fill this gap.

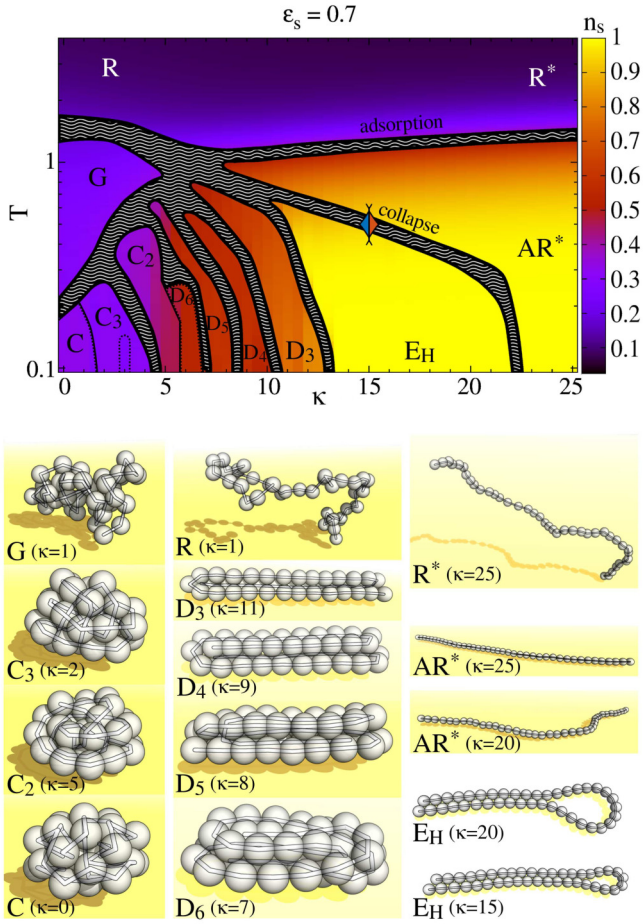

Figure 12.4: Structural phase diagram for a semiflexible polymer of length $N = 40$ grafted to a weakly attractive surface ($\epsilon_s = 0.7$). The background color encodes the average fraction of surface contacts $n_s = N_s/N$. Dotted lines indicate that signals are found only in a small subset of observables. Representative conformations from the respective conformational regimes are shown below. They comprise globule-like (G), compact (C), and random coil-like (R) conformations, as well as folded bundles (D_m), desorbed and adsorbed weakly bent rods (R* and AR*, respectively), and hairpins (E_H). The (blue-red) rhombus at $\kappa \approx 15$ marks the crossover from a second-order-like to a first-order-like collapse transition.

This study comprises sophisticated Monte Carlo computer simulations of a linear homopolymer consisting of $N = 40$ monomers connected by anharmonic springs fluctuating around an "equilibrium" bond length r_0. We consider the cases of a completely free polymer and a polymer grafted to a non-interacting as well as an attractive substrate (i.e., the first monomer remains at a fixed location on the surface). Our polymer description is intended to model a full class of (grafted) semiflexible polymers in a range of solvent conditions. The resulting coarse-grained model incorporates four energy terms: bond-vibrational energy, non-neighboring 12-6 Lennard-Jones interactions, bending energy parametrized by the bending stifness κ, and 9-3 Lennard-Jones surface interaction parametrized by the interaction strength ε_s. As a typical example of our results, Fig. 12.4 shows the κ-T phase diagram for a weakly attractive surface with $\varepsilon_s = 0.7$. For a recent overview see Ref. [9].

[1] T. Sintes et al.: Macromolecules **34**, 1352 (2001)
[2] H.-P. Hsu, K. Binder: Macromolecules **46**, 2496 (2013)
[3] J. Luettmer-Strathmann et al.: J. Chem. Phys. **128**, 064903 (2008); M. Möddel et al.: Phys. Chem. Chem. Phys. **12**, 11548 (2010)
[4] A.D. Swetnam, M.P. Allen: Phys. Chem. Chem. Phys. **11**, 2046 (2009); Phys. Rev. E **85**, 062901 (2012)
[5] M. Möddel et al.: Phys. Rev. Lett. **112**, 148303 (2014)
[6] D.T. Seaton et al.: Phys. Rev. Lett. **110**, 028103 (2013)
[7] M. Marenz, W. Janke: Phys. Rev. Lett. **116**, 128301 (2016)
[8] K.S. Austin et al.: Macromolecules **50**, 4054 (2017)
[9] W. Janke: *Generalized ensemble computer simulations of macromolecules*, invited Ising Lecture Notes 2016, in *Order, Disorder and Criticality: Advanced Problems of Phase Transition Theory*, Vol. 5, ed. Y. Holovatch (World Scientific, Singapore, 2018), pp. 173–225

12.4 Computer simulations of semiflexible polymers in disordered environments

J. Bock, W. Janke

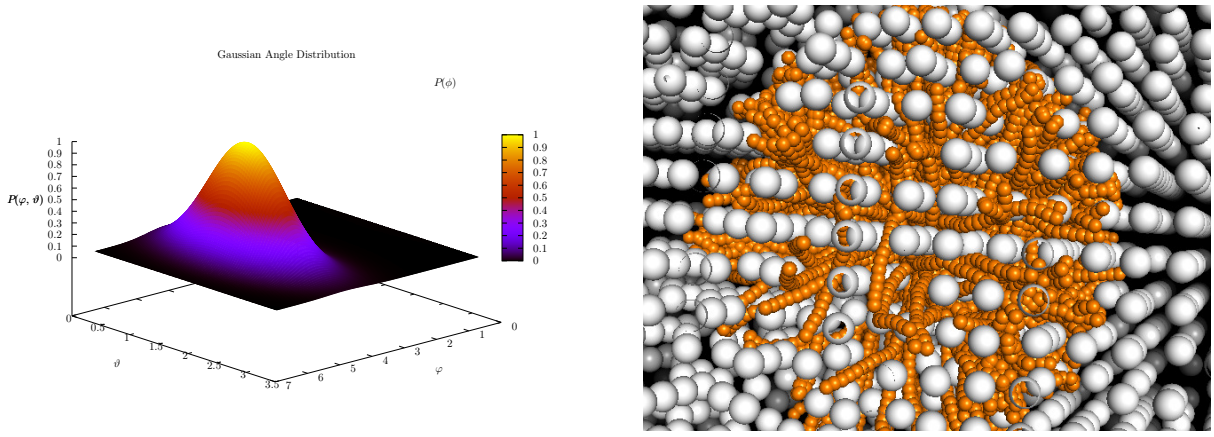

(a) Weighting histogram (b) Semiflexible polymer in 3D disorder

Figure 12.5: (a) Histogram used for the guiding field in 3D and (b) an examplary configuration of a polymer with $N = 30$ and $\xi = 1$.

Single-molecule experiments have established the wormlike chain (WLC) as a standard model for semiflexible polymers [1]. Exploiting the analogy of the WLC with a one-dimensional Heisenberg ferromagnet, it can be shown that the equilibrium tangent-tangent correlation function decays exponentially. The decay rate defines the thermal persistence length l_p. When the same polymer is embedded in a quenched, disordered environment in three dimensions, this property may change quantitatively or even qualitatively. We addressed this problem by performing extensive numerical simulations of

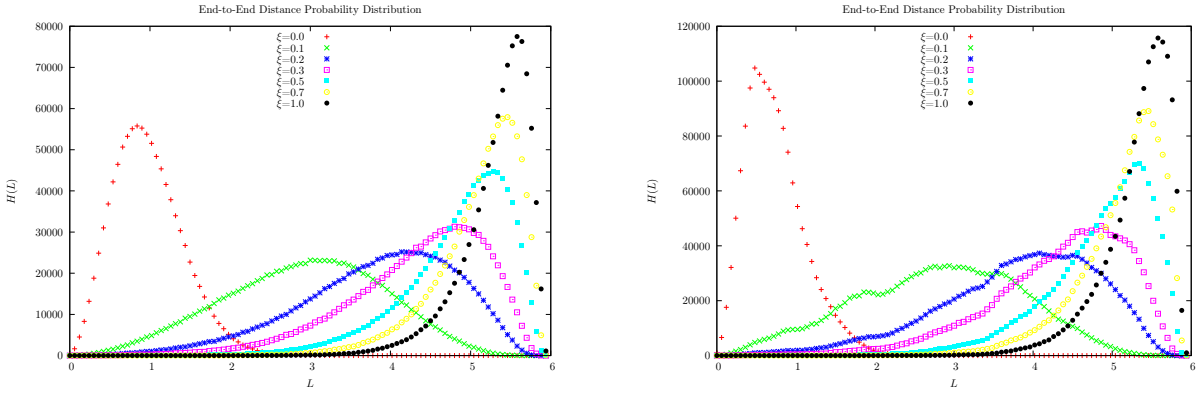

(a) Free polymers (b) Polymers in disorder

Figure 12.6: End-to-end distance distributions for (a) free polymers and (b) polymers in gaseous disorder, both in 3D.

semiflexible polymers in a simple lattice disorder and in a gaseous disorder constructed by microcanonical Lennard-Jones gas simulation which represents the disordered environment. Further plans are to simulate the polymers in algebraically correlated disorder. Only the space between the spheres is accessible to the polymer. The extreme strength and density of the environmental constraints are a great challenge to conventional Monte Carlo simulation schemes, which we found hard to overcome even with a sophisticated multicanonical histogram reweighting procedure [2]. We have therefore adopted a breadth-first chain-growth algorithm [3] that resolves this difficulty by circumventing energy barriers instead of trying to cross them [2, 4], see examples in Fig. 12.5. Therefore the already existing procedures were expanded to the third dimension to investigate the behaviour of the tangent-tangent correlation length, the mean square end-to-end distance and the end-to-end probability distribution function, see Fig. 12.6. A difference in behaviour is clear and the task now is to check wether the differences scale similarly as in two dimensions, where the disorder renormalization is stated to be [5]:

$$\frac{1}{l_p^*} = \frac{1}{l_p} + \frac{1}{l_p^D},$$

with l_p^* the renormalized persistence length, l_p the persistence length given as simulation parameter and l_p^D the measured disorder persistence length.

[1] O. Otto et al.: Nat. Commun. **4**, 1780 (2013)
[2] S. Schöbl et al.: Phys. Rev. E **84**, 051805 (2011)
[3] T. Garel, H. Orland: J. Phys. A: Math. Gen. **23**, L621 (1999)
[4] S. Schöbl et al.: J. Phys. A: Math. Theor. **45**, 475002 (2012)
[5] S. Schöbl et al.: Phys. Rev. Lett. **113**, 238302 (2014)

12.5 From particle condensation to polymer aggregation

J. Zierenberg*, P. Schierz, W. Janke

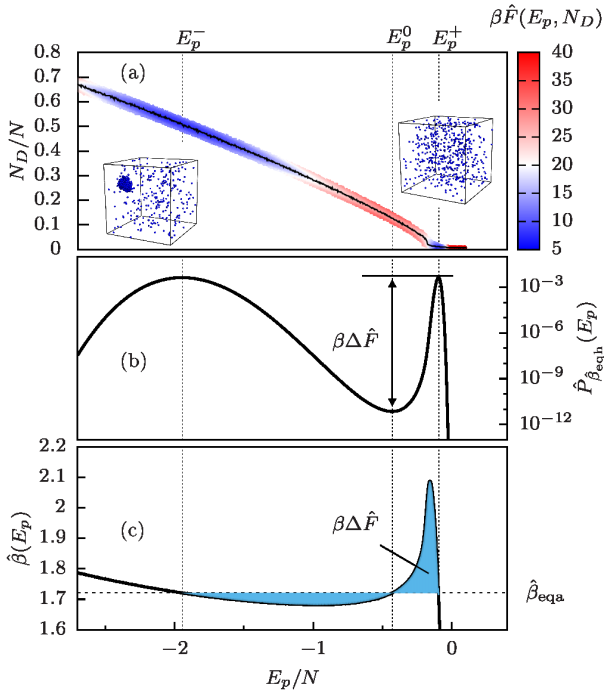

Figure 12.7: (a) Illustration of the free-energy landscape $\beta\hat{F}(E_p, N_D)$ (color map) as a function of potential energy E_p and droplet size N_D for $N = 512$ Lennard-Jones particles. The minimal free-energy path (black solid line) connects a droplet ($E_p \approx E_p^-$) and a gaseous ($E_p \approx E_p^+$) phase, visualized by the snapshots at $E_p^\pm$. The projection onto the reaction-coordinate E_p yields the canonical potential-energy probability distribution $\hat{P}_\beta(E_p)$, where the free-energy barrier $\beta\Delta\hat{F}$ is encoded in the ratio between maximum and minimum at $\hat{\beta}_{\rm eqh}$. (c) Equivalently, $\beta\Delta\hat{F}$ is the (equal) area size enclosed between the microcanonical inverse temperature $\hat{\beta}(E_p)$ and the accordingly defined transition temperature $\hat{\beta}_{\rm eqa}$, where $\hat{\beta}_{\rm eqa} = \hat{\beta}_{\rm eqh} = 1.72099(3)$.

*Max Planck Institute for Dynamics and Self-Organization, Am Fassberg 17, 37077 Göttingen, Germany

A common approach to study nucleation rates is the estimation of free-energy barriers. This usually requires knowledge about the shape of the forming droplet, a task that becomes notoriously difficult in macromolecular setups starting with a proper definition of the cluster boundary or a proper ensemble choice. Here, we demonstrate that a shape-free determination of temperature-driven cluster formation is directly accessible in the canonical ensemble for particle as well as polymer systems. Combined with rigorous results on canonical equilibrium droplet formation, this allows for a well-defined finite-size scaling analysis of the effective interfacial free energy at fixed density as illustrated in Fig. 12.7. We first verified the theoretical predictions for the formation of a liquid droplet in a supersaturated particle gas by (parallelized) generalized-ensemble Monte Carlo simulations [1–3] of a Lennard-Jones system [4, 5]. Going one step further, we then generalized this approach to the aggregation process in a dilute polymer solution [5], cf. Fig. 12.8. Our results suggest an analogy between particle condensation and polymer aggregation, when the macromolecules are interpreted as extended particles.

Because the standard approach in Monte Carlo simulations is to work in the conformational ensemble governed by potential energy only, we show that excluding the

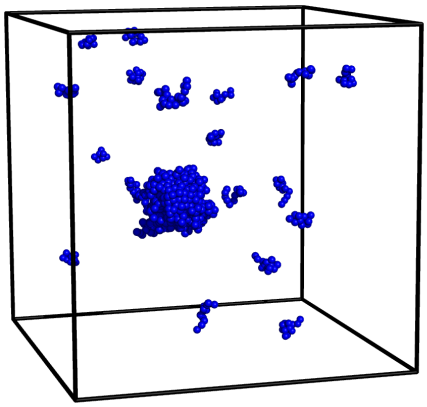

Figure 12.8: Illustration of an aggregate of polymers in a dilute solution ($N = 64$ bead-spring polymers with 13 monomers each; monomer density $\rho = 10^{-2}$). The snapshot stems from the droplet phase ($E_p \approx E_p^-$).

kinetic energy from the partition function leads to finite-size differences in the free energy compared to the full ensemble [6–9] but retains intensive parameters in the thermodynamic limit [5]. Our study of nucleation rates at fixed density corresponds to a heating-cooling framework where simulation and experiment may meet at the nanometer scale.

[1] B.A. Berg, T. Neuhaus: Phys. Lett. B **267**, 249 (1991); Phys. Rev. Lett. **68**, 9 (1992)
[2] W. Janke: Int. J. Mod. Phys. C **03**, 1137 (1992); Physica A **254**, 164 (1998)
[3] J. Zierenberg et al.: Comput. Phys. Commun. **184**, 1155 (2013)
[4] J. Zierenberg, W. Janke: Phys. Rev. E **92**, 012134 (2015); in *Computer Simulation Studies in Condensed-Matter Physics XXIX*, eds. D.P. Landau, H.-B. Schüttler, S. Lewis, M. Bachmann, J. Phys.: Conf. Ser. **750**, 012017 (2016)
[5] J. Zierenberg et al.: Nat. Commun. **8**, 14546 (2017)
[6] P. Schierz et al.: Phys. Rev. E **94**, 021301(R) (2016)
[7] W. Janke et al.: in *Computer Simulation Studies in Condensed-Matter Physics XXX*, eds. D.P. Landau, M. Bachmann, S.P. Lewis, and H.-B. Schüttler, J. Phys.: Conf. Ser. **921**, 012018 (2017)
[8] W. Janke: *Generalized ensemble computer simulations of macromolecules*, invited Ising Lecture Notes 2016, in *Order, Disorder and Criticality: Advanced Problems of Phase Transition Theory*, Vol. 5, ed. Y. Holovatch (World Scientific, Singapore, 2018), pp. 173–225
[9] W. Janke, J. Zierenberg: *From particle condensation to polymer aggregation*, invited Plenary Talk, International Conference *Computer Simulations in Physics and beyond (CSP2017)*, Moscow, Russia, J. Phys.: Conf. Ser. **955**, 012003 (2018)

12.6 Droplet condensation of 2D Lennard-Jones particles

F.P. Spitzner, J. Zierenberg*, W. Janke

*Max Planck Institute for Dynamics and Self-Organization, Am Fassberg 17, 37077 Göttingen, Germany

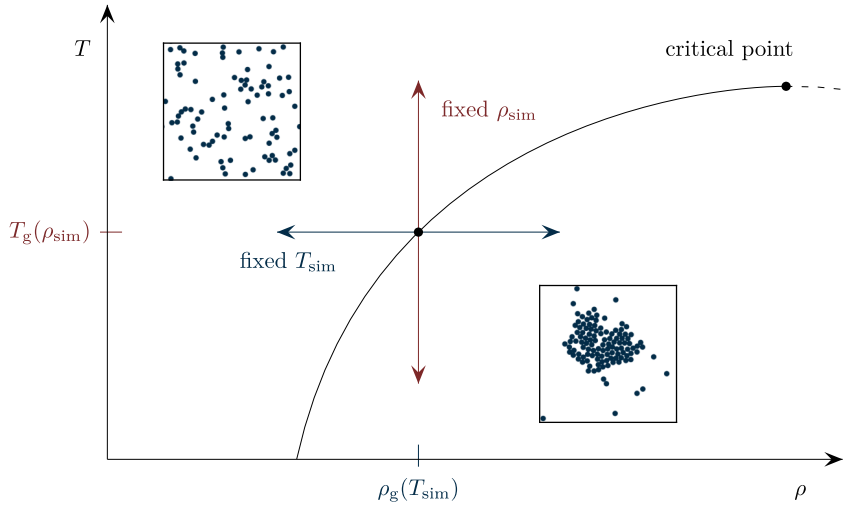

Figure 12.9: Sketch of the transition between the pure gas phase and the mixed phase of a liquid droplet surrounded by vapour. Below the critical point, the black infinite-size transition line can be crossed in either one of two orthogonal directions: The blue horizontal arrow depicts the fixed-temperature approach in which density serves as the control parameter, where $\rho_{\mathrm{g}}(T_{\mathrm{sim}})$ is the infinite-size transition density. Alternatively, the red vertical arrow depicts the fixed-density approach in which temperature serves as the control parameter and $T_{\mathrm{g}}(\rho_{\mathrm{sim}})$ is the infinite-size transition temperature.

The formation and dissolution of a droplet is an important mechanism related to various nucleation phenomena [1, 2]. Here, we address the droplet formation-dissolution transition in a two-dimensional Lennard-Jones gas to demonstrate a consistent finite-size scaling approach from two perspectives using orthogonal control parameters [3, 4], see Fig. 12.9. For the canonical ensemble, this means that we fix the temperature while varying the density and vice versa. An example for the resulting grand canonical probability distribution $P(\rho)$ iat fixed temperature is shown in Fig. 12.10. Using specialised parallel multicanonical methods for both cases, we confirm analytical predictions at fixed temperature (rigorously only proven for lattice systems [5–8]) and corresponding scaling predictions from expansions at fixed density [3]. Importantly, our methodological approach provides us with reference quantities from the grand canonical ensemble that enter the analytical predictions [9]. Our orthogonal finite-size scaling setup can be exploited for theoretical and experimental investigations of general nucleation phenomena – if one identifies the corresponding reference ensemble and adapts the theory accordingly [4]. In this case, our numerical approach can be readily translated to the corresponding ensembles and thereby proves very useful for numerical studies of equilibrium cluster formation, in general.

[1] D.M. Herlach et al.: J. Chem. Phys. **145**, 211703 (2016)

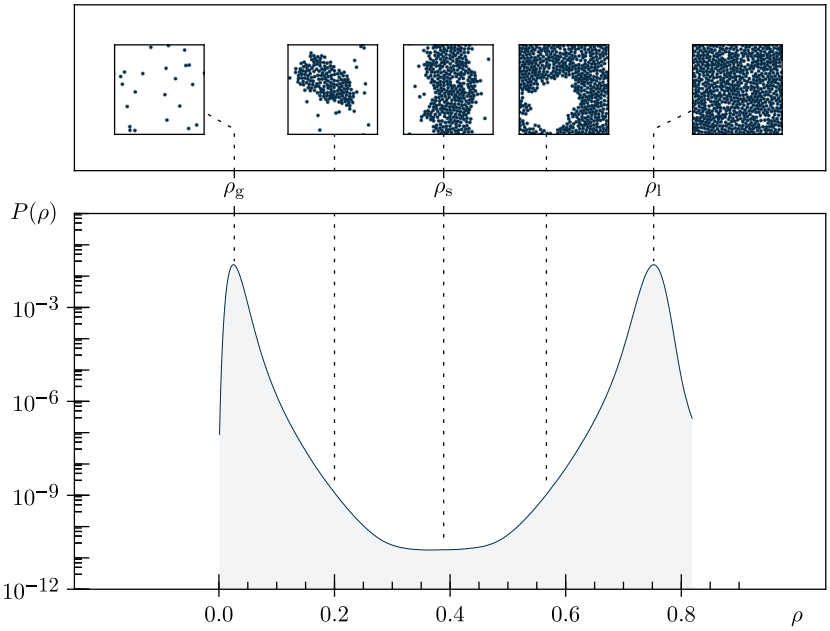

Figure 12.10: Grand canonical probability distribution $P(\rho)$ for a system of linear size $L = 30$ at temperature $T = 0.4$ and equal-height chemical potential $\mu \approx -1.6518$. $P(\rho)$ shows peaks at the densities corresponding to the gas (ρ_g) and the liquid (ρ_l) phase. In between a suppressed plateau developed around the density where a stripe occurs (ρ_s). On the top representative snapshots are shown for the whole density region over which the gas-liquid transition takes place.

[2] K. Binder, P. Virnau: J. Chem. Phys. **145**, 211701 (2016)
[3] J. Zierenberg, W. Janke: Phys. Rev. E **92**, 012134 (2015)
[4] J. Zierenberg et al.: Nat. Commun. **8**, 14546 (2017)
[5] M. Biskup et al.: Europhys. Lett. 60, 21 (2002)
[6] T. Neuhaus, J. S. Hager: J. Stat. Phys. **113**, 47 (2003)
[7] K. Binder: Physica A **319**, 99 (2003)
[8] A. Nußbaumer et al.: Europhys. Lett. **75**, 716 (2006); Phys. Rev. E **77**, 041109 (2008)
[9] F.P. Spitzner et al.: SciPost **5**, 062 (2018)

12.7 Effect of temperature on the scaling laws governing the kinetics of collapse of a homopolymer

S. Majumder, J. Zierenberg*, W. Janke

*Max Planck Institute for Dynamics and Self-Organization, Am Fassberg 17, 37077 Göttingen, Germany

The collapse transition of a polymer upon transfer from a good solvent (high temperature) to a poor solvent (low temperature) bears significant connection to the folding process of a proteins and other biomolecules. Thus understanding the kinetics of a homopolymer in that respect may provide useful primary information on the underlying

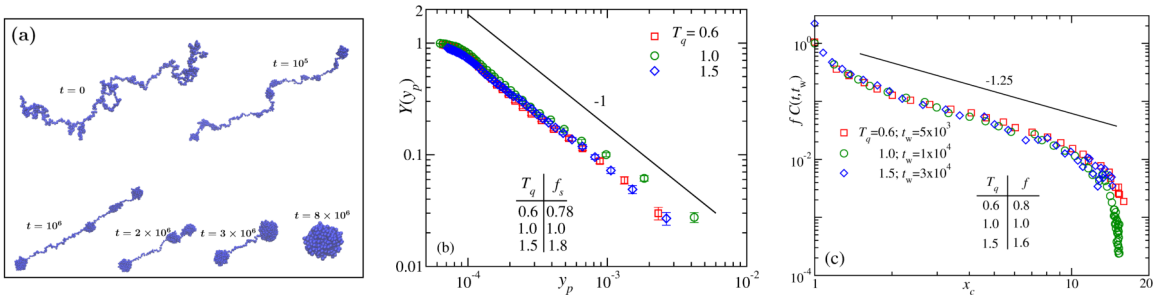

Figure 12.11: (a) Snapshots [1] showing the sequence of events occurring during the collapse of a polymer upon being quenched from an expanded state (at high temperature) into the globular phase (at low temperatures). (b) Universal finite-size scaling function $Y(y_p)$ with a non-universal metric factor f_s in the scaling variable y_p describing the scaling in the cluster growth during the collapse [2]. (c) Temperature-independent scaling plot for the aging and related dynamical scaling, probed by the behavior of a suitable density-density autocorrelation function $C(t, t_w)$ against $x_c = C_s(t)/C_s(t_w)$, the ratio of cluster sizes $C_s(t)$ at the observation time t and the waiting time t_w [2].

mechanism of more realistic problems [1, 2]. On the other hand, if one considers the usual "pear-necklace" like picture of the collpase [3] as shown in Fig. 15.2(a), it also resembles coarsening phenomena popular in spin and particle systems [4]. Over the last two years we have been exploiting this connection to understand the kinetics of collapse of a homopolymer [5, 6].

In this work, from the state of the art Monte Carlo simulations of an off-lattice polymer model, we understand the effect of the quench temperature (T_q) on the various scaling laws related to the collapse viz., scaling of the cluster growth and the dynamical scaling related to the aging. Our results in conjunction with the nonequilibrium finite-size scaling analysis [7] show that the cluster growth is rather universal in nature and can be described by a universal finite-size scaling function with a non-universal metric factor that depends on the amplitudes of the growth [2], see Fig. 15.2(b). This observation has recently been confirmed in a related lattice model for the polymer [8]. For a direct comparison of the lattice and off-lattice formulations, see Ref. [9]. Furthermore, the scaling related to the aging (which is probed by a suitable two-time density-density autocorrelation function) is also found to be independent of the quench temperature T_q, shown in Fig. 15.2(c).

[1] S. Majumder, W. Janke: J. Phys.: Conf. Ser. **750**, 012020 (2016)
[2] S. Majumder et al.: Soft Matter **13**, 1276 (2017)
[3] A. Halperin, P. Goldbart: Phys. Rev. E **61**, 565 (2000)
[4] A.J. Bray: Adv. Phys. **51**, 481 (2002)
[5] S. Majumder, W. Janke: Europhys. Lett. **110**, 58001 (2015)
[6] S. Majumder, W. Janke: Phys. Rev. E **93**, 032506 (2016)
[7] S. Majumder, S.K. Das: Phys. Rev. E **81**, 050102(R) (2010); Phys. Rev. E **84**, 021110 (2011)
[8] H. Christiansen et al.: J. Chem. Phys. **147**, 094902 (2017)
[9] S. Majumder et al.: J. Phys.: Conf. Ser. **955**, 012008 (2018)

12.8 Coarsening and aging of lattice polymers: Influence of bond fluctuations

H. Christiansen, S. Majumder, W. Janke

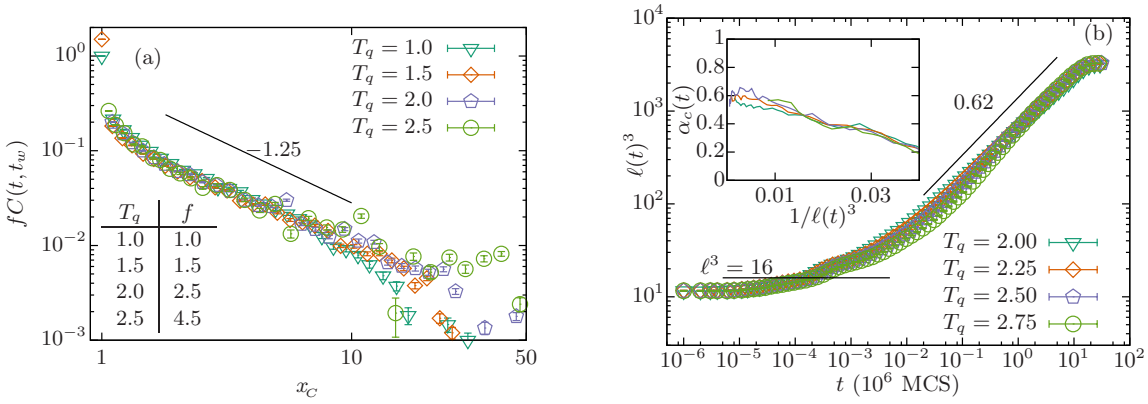

Figure 12.12: (a) The two-time correlation function $C(t, t_w)$ against the ratio of length-scales $x_C = \ell(t)/\ell(t_w)$ for the model with fixed bonds and different quench-temperatures T_q. In (b) the growth of the length-scales for the model with flexible bonds is shown for different T_q. Here the growth is independent of T_q and follows a power law with exponent $\alpha = 0.62(5)$.

The nonequilibrium properties of homopolymer collapse were investigated using Monte Carlo simulations of the interacting self-avoiding walk on a simple cubic lattice (with lattice-spacing 1) using fixed bond lengths 1 and flexible bond lengths; 1, $\sqrt{2}$, and $\sqrt{3}$ [1]. The phenomenological picture of pearl necklace polymer collapse [2] was observed, in which a polymer, when transferred from a good solvent ($T_h > T_\theta$) to a bad solvent ($T_q < T_\theta$), undergoes a collapse transition from an expanded coil by forming clusters at locally higher densities which then subsequently coalesce with each other until only a single globular cluster is left. The aging exponent $\lambda \approx 1.25$ was found to be independent of the bond conditions and the same as in the off-lattice exponent [3] [see Fig. 12.12(a) for the model with fixed bonds at different quench temperatures T_q]. For the model with flexible bonds, the power-law growth exponent of the clusters of monomers was likewise observed to be independent of temperature $\alpha = 0.62(5)$ [see Fig. 12.12(b)], while the same exponent was found to be dependent on the temperature in the fixed bond model. In the off-lattice model on the other hand, $\alpha = 1$ was found [4]. The discrepency in the exponent α is attributed to the constraints introduced by the lattice structure. For a recent review, see Ref. [5].

[1] H. Christiansen et al.: J. Chem. Phys. **147**, 094902 (2017)
[2] A. Halperin, P. M. Goldbart: Phys. Rev. E **61**, 565 (2000)
[3] S. Majumder, W. Janke: Phys. Rev. E **93**, 032506 (2016)
[4] S. Majumder, W. Janke: Europhys. Lett. **110**, 58001 (2015)
[5] Majumder et al.: *Understanding nonequilibrium scaling laws governing collapse of a polymer*, Leipzig preprint (September 2019)

12.9 Scaling laws during collapse of a homopolymer: Lattice versus off-lattice

S. Majumder, H. Christiansen, W. Janke

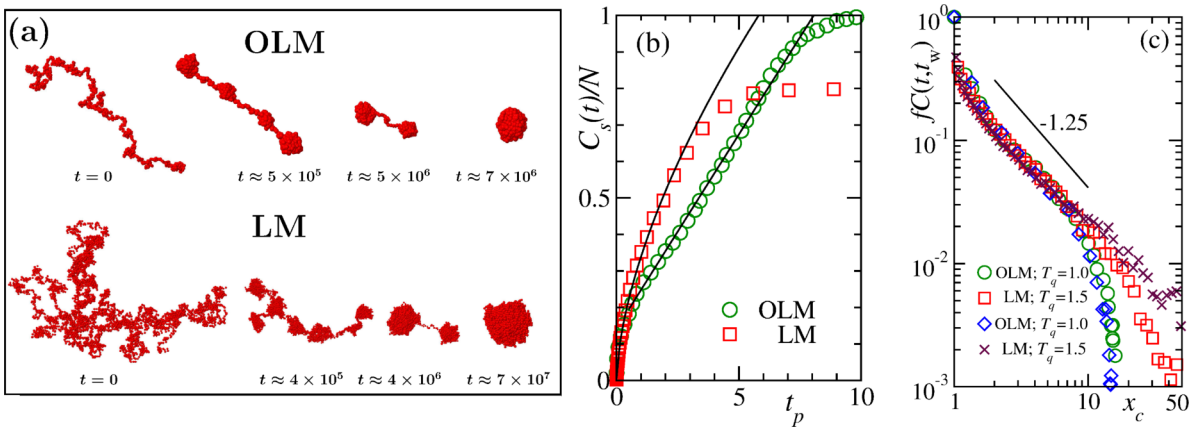

Figure 12.13: (a) Time evolution snapshots of the collapse of a homopolymer, after being quenched from an extended coil phase to a temperature, $T_q = 1$ for OLM, and $T_q = 2.5$ for LM, in the globular phase.(b) Plots of the average cluster size $C_s(t)/N$ as function of time for the two models. To make both the data visible on the same plot, we divide the time axis by a factor m to obtain $t_p = t/m$, where $m = 1 \times 10^6$ and 3.5×10^6, respectively, for OLM and LM. The solid lines there are fits to the form $C_s(t) = C_0 + At^{\alpha_c}$ with $\alpha_c = 0.98$ for OLM and $\alpha_c = 0.62$ for LM. (c) Plot showing that universal aging scaling at different T_q for the two models can be described by a single master-curve behavior. The solid line here also corresponds to $C(t, t_w) = A_C x_c^{-\lambda_C}$ with $\lambda_C = 1.25$. Note that $C(t, t_w)$ is multiplied by a factor f to make them collapse onto the same curve. For OLM $t_w = 10^4$ whereas for LM $t_w = 10^3$.

The pathways of collapse of a homopolymer, upon a transfer from a good to a poor solvent, bears resemblance to coarsening processes. Simulation results in this context can be explained by the phenomenonlogical "pearl-necklace" picture of Halperin and Goldbart (HG) [1]. Recently we have shown via Monte Carlo simulations of both a lattice model (LM) and an off-lattice model (OLM) polymer that this nonequilibrium evolution dynamics is also a scaling phenomenon [2]. In this work we compared the results obtained from the LM and OLM, in particular the scaling of the cluster growth [3] and the aging scaling [4] probed by the two-time density-density autocorrelation function.

For the OLM, we opt for the bead-spring model of a flexible homopolymer in $d = 3$ dimensions where bonds between successive monomers are maintained via the standard finitely extensible non-linear elastic (FENE) potential

$$E_{\mathrm{FENE}}(r_{ii+1}) = -\frac{KR^2}{2} \ln\left[1 - \left(\frac{r_{ii+1} - r_0}{R}\right)^2\right], \tag{12.1}$$

with $K = 40$, $r_0 = 0.7$ and $R = 0.3$. The nonbonded interaction energy is modeled by $E_{\mathrm{nb}}(r_{ij}) = E_{\mathrm{LJ}}(\min(r_{ij}, r_c)) - E_{\mathrm{LJ}}(r_c)$, where

$$E_{\mathrm{LJ}}(r) = 4\epsilon\left[\left(\frac{\sigma}{r}\right)^{12} - \left(\frac{\sigma}{r}\right)^{6}\right] \tag{12.2}$$

is the standard Lennard-Jones (LJ) potential with $\sigma = r_0/2^{1/6}$ as the diameter of the monomers, ϵ (= 1) as the interaction strength and $r_c = 2.5\sigma$ as the cut-off radius.

For LM, we consider [5] a variant of the interactive self-avoiding walk on a simple-cubic lattice, where each lattice site can be occupied by a single monomer. The energy is given by

$$E_{\mathrm{LM}} = -\frac{1}{2}\sum_{i\neq j,j\pm 1} w(r_{ij}), \quad \text{where} \quad w(r_{ij}) = \begin{cases} J & r_{ij} = 1 \\ 0 & \text{else} \end{cases}. \tag{12.3}$$

In Eq. (12.3), r_{ij} is the Euclidean distance between two nonbonded monomers i and j, $w(r_{ij})$ is an interaction parameter that considers only nearest neighbors, and J(= 1) is the interaction strength. We allow a fluctuation in the bond length by considering diagonal bonds, i.e., the possible bond lengths are 1, $\sqrt{2}$, and $\sqrt{3}$.

Phenomenonlogically both LM and OLM show intermediate structures consistent with the "pear-necklace" picture of HG [Fig. 12.13(a)]. However, the cluster-growth scaling in LM and OLM are different. While the OLM yields a linear growth ($\alpha_c \approx 1$), in the LM the growth is slower ($\alpha_c \approx 0.62$) [Fig. 12.13(b)], which could be attributed to the topological constraints one experiences in a lattice model. On the other hand, surprisingly, both the models show evidence of simple aging scaling having the same autocorrelation exponent $\lambda_C \approx 1.25$ [Fig. 12.13(c)], thus implying that the aging scaling is rather universal. This allowed us to demonstrate that scaling of the autocorrelation functions for the two models can be described by a single master curve. For a more detailed discussion, see the recent review in Ref. [6]

[1] A. Halperin, P. M. Goldbart: Phys. Rev. E **61**, 565 (2000)
[2] S. Majumder et al.: J. Phys.: Conf. Ser. **955**, 012008 (2018)
[3] S. Majumder, W. Janke: Europhys. Lett. **110**, 58001 (2015)
[4] S. Majumder, W. Janke: Phys. Rev. E **93**, 032506 (2016)
[5] H. Christiansen et al.: J. Chem. Phys. **147**, 094902 (2017)
[6] Majumder et al.: *Understanding nonequilibrium scaling laws governing collapse of a polymer*, Leipzig preprint (September 2019)

12.10 Dynamics of collapse of a flexible polymer with Vicsek-like active beads

S. Paul, S. Majumder, S.K. Das*, W. Janke

*Theoretical Sciences Unit, Jawaharlal Nehru Centre for Advanced Scientific Research, Jakkur P.O., Bangalore 560064, India

A polymer undergoes a collapse transition when it is quenched from a high-temperature extended coil state (or in good solvent) to a temperature lower (or in poor solvent) than its θ-transition value, for which the equilibrium phase is a globular one. Though various aspects of equilibrium and nonequilibrium dynamics of such transition for the case of a passive polymer is reasonably well understood [1, 2], studies with active polymers are relatively new [3, 4]. Studying the motion of a single flexible polymer in

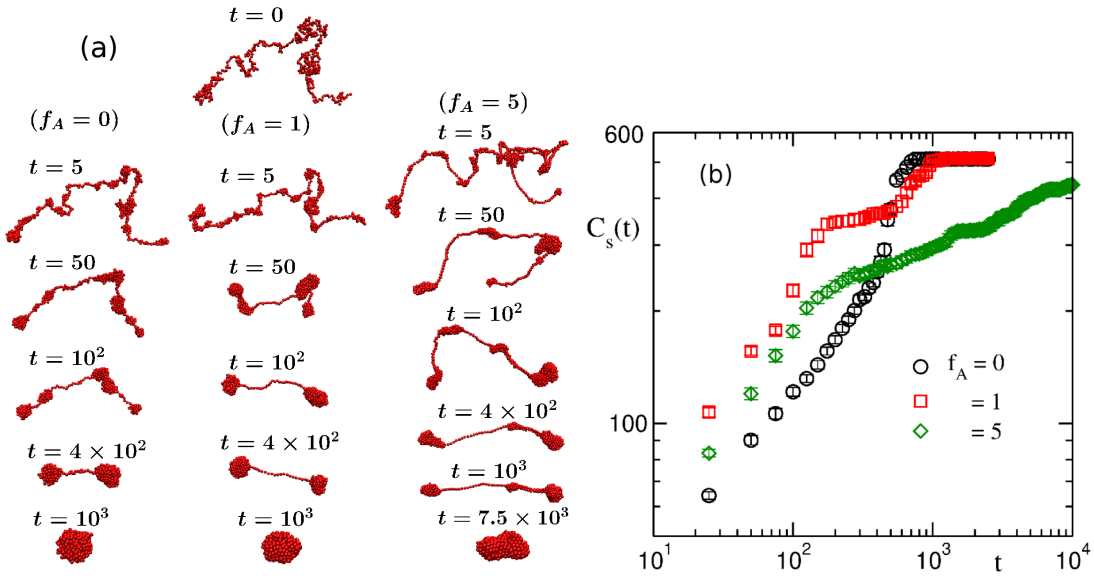

Figure 12.14: (a) Time evolution snapshots of the events occurring during the collapse transition of a polymer with $N_b = 512$ beads when quenched from an extended coil state into the globular phase at low temperature. $f_A = 0$ stands for the passive case, while $f_A = 1$ and 5 corresponds to the case of the active polymer. (b) Average size of clusters as a function of time for the three cases.

presence of controlled active forces is necessary in case of drug delivery, directed self assembly, etc. Experimental realizations of such a system are given by linking artificially synthesized colloidal particles that show controlled motion and enhanced diffusion [5]. Here we have modeled each bead as an active element for which we applied Vicsek-like alignment interaction rules [6]. Our main aim is to look at the nonequilibrium dynamics, such as, relaxation time of collapse, cluster growth, etc. by tuning the activity and to compare them with the case of a passive polymer.

Here we consider a flexible bead-spring model of a polymer chain with N_b beads, determining the degree of polymerization [1]. The equation of motion of each bead is solved via molecular dynamics simulation using the Langevin equation, in which the quenching temperature has been chosen as $T = 0.5$. The interaction potentials acting among the beads consist of two terms. The non-bonded interaction is the standard LJ potential and the bonded interaction between two monomers is the FENE potential. As we have applied Vicsek-like alignment interaction rule [6], the velocity of each bead gets modified by the average direction of its neighbors present within a cut-off distance r_c, for which we choose $r_c = 2.5\sigma$, where σ is the diameter of each bead. Following Ref. [7], the active force $\vec{f_i}$ for the i'th bead can be written as,

$$\vec{f_i} = f_A \vec{D}_n \,, \tag{12.4}$$

where f_A determines the strength of the active force and $\vec{D}_n$ is the average direction determined by the neighbors.

In Fig. 12.14(a) we present comparative snapshots for a chain with $N_b = 512$ beads during the collapse of the polymer for the passive case as well for two different values of the active force. Whereas the intermediate snapshots look quite different in the higher

activity case ($f_A = 5$) than in the passive or $f_A = 1$ case, the final state is in all cases a globular phase. However, for $f_A = 0,1$ the polymer evolves to a rather compact spherical globule, while for $f_A = 5$ it remains in a slightly elongated or sausage-like globular phase. And the time scale required to reach the final state is much higher for $f_A = 5$ than in the other two cases. The run time for $f_A = 5$ is up to $t = 10^4$ measured in units of LJ time scale. Though the preferred final phase is a globular one because of the presence of an attractive potential among the beads, a few realizations still remain in a dumbbell phase for $f_A = 5$. The persistance of this dumbbell phase for $f_A = 5$ increases with the value of N_b as well. To make a quantitative comparison, here in Fig. 12.14(b) we plot the average cluster size $C_s(t)$ of the clusters as a function of time for all the three cases. We see that for the active cases, though initially the growth amplitude is higher than in the passive case suggesting a faster initialization of the coarsening process, at later time $C_s(t)$ crosses over to a lower amplitude as well as a smaller exponent for the growth. This lowering of the exponent for the active case compared to the passive one is more prominent for $f_A = 5$. We will investigate these issues in more detail.

[1] S. Majumder, W. Janke: Europhys. Lett. **110**, 58001 (2015)
[2] A. Halperin, P. Goldbart: Phys. Rev. E **61**, 565 (2000)
[3] R.E. Isele-Holder et al.: Soft Matter **11**, 7181 (2015)
[4] V. Bianco et al.: Phys. Rev. Lett. **121**, 217802 (2018)
[5] B. Biswas et al.: ACS Nano **11**, 10025 (2017)
[6] T. Vicsek et al.: Phys. Rev. Lett. **75**, 1226 (1995)
[7] S.K. Das: J. Chem. Phys. **146**, 044902 (2017)

12.11 Explicit solvent model for polymer dynamics using Lowe-Andersen approach

S. Majumder, H. Christiansen, W. Janke

Dynamics of a polymer chain in a dilute solution, although being extensively studied, is still a topic of utmost importance. In particular, this topic serves as a benchmark for establishing a coarse-grained or mesoscopic approach to understand more realistic problems on larger time and length scales. The dynamics of a single chain, generally, is characterized by the self-diffusion coefficient D which scales with chain length N as $D \sim N^{-x}$. In absence of hydrodynamic effects, one has $x = 1$, whereas in presence of hydrodynamic effects, one expects $x = 3/5$. The former is referred to as Rouse scaling [1] and the latter as Zimm scaling [2].

In this work [3] we construct an explicit solvent model for a polymer by considering a bead-spring model of a flexible homopolymer in three spatial dimensions. The bonds between successive monomers are maintained via the standard finitely extensible non-linear elastic (FENE) potential

$$E_{\mathrm{FENE}}(r_{ii+1}) = -\frac{K}{2}R^2 \ln\left[1 - \left(\frac{r_{ii+1} - r_0}{R}\right)^2\right], \tag{12.5}$$

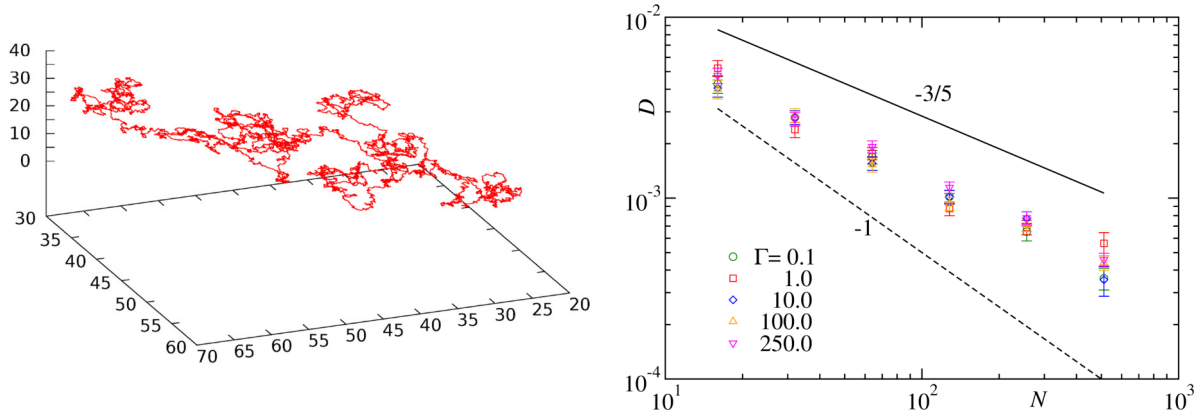

Figure 12.15: Left panel: The trajectory of the center of mass of a polymer of length $N = 512$, over a time period of 200τ in equilibrium at $T = 1.0$. Right panel: Dependence of the self-diffusion coefficient D on the chain length N of a polymer for different solvents with a collision frequency Γ as indicated. The solid and dashed lines represent the Zimm ($D \sim N^{-3/5}$) and Rouse scaling ($D \sim N^{-1}$), respectively.

with $K = 40$, $r_0 = 0.7$ and $R = 0.3$. The monomers and the solvent molecules both are considered to be spherical beads of mass $m = 1$ and diameter σ. All nonbonded interactions are modeled by

$$E_{\rm nb}(r_{ij}) = E_{\rm LJ}\left[\min(r_{ij}, r_c)\right] - E_{\rm LJ}(r_c)\ , \tag{12.6}$$

where $E_{\rm LJ}(r)$ is the standard Lennard-Jones (LJ) potential given as

$$E_{\rm LJ}(r) = 4\epsilon\left[\left(\frac{\sigma}{r}\right)^{12} - \left(\frac{\sigma}{r}\right)^{6}\right] \tag{12.7}$$

with $\sigma = r_0/2^{1/6}$ as the diameter of the beads, $\epsilon(= 1)$ as the interaction strength and $r_c = 2^{1/6}\sigma$ as cut-off radius that ensures a purely repulsive interaction.

We simulate our system via molecular dynamics (MD) simulations at constant temperature using the Lowe-Andersen (LA) thermostat **[?**]. In this approach, one updates the position $\vec{r}_i$ and velocity $\vec{v}_i$ of the i-th bead using Newton's equations as follows,

$$\frac{d\vec{r}_i}{dt} = \vec{v}_i, \quad \frac{d\vec{v}_i}{dt} = \vec{f}_i\ , \tag{12.8}$$

where $\vec{f}_i$ is the conservative force (originating from the bonded and nonbonded interactions) acting on the bead. For controlling the temperature with the LA thermostat, one considers a pair of particles within a certain distance R_T [4]. Then, with a probability $\Delta t\Gamma$, a bath collision is executed, after which the pair gets a new relative velocity from the Maxwellian distribution. Here, Δt is the width of the time step chosen for the updates in Eq. (12.8) and Γ determines the collision frequency. By varying R_T and Γ, one can effectively control the frictional drag or in other words the solvent viscosity. The exchange of relative velocities with the bath is only done on its component parallel to the line joining the centers of the pair of particles, thus conserving the angular

momentum. Additionally, the new velocities are distributed to the chosen pair in such a way that the linear momentum is also conserved.

Via the scaling of the radius of gyration R_g with the chain length N as $R_g \sim N^{3/5}$ we confirm that our approach yields the known static critical exponent. The method conserves both the linear and angular momenta locally, thereby preserving the hydrodynamics. Thus the scaling of the self-diffusion coefficient D with chain length N (shown in the right panel of Fig. 12.15) indicates a much faster dynamics than the Rouse dynamics, and in fact is pretty consistent with Zimm scaling $D \sim N^{-3/5}$ valid in the presence of hydrodynamic effects.

[1] P.E. Rouse: J. Chem. Phys. **21**, 1272 (1953)
[2] B.H. Zimm: J. Chem. Phys. **24**, 269 (1956)
[3] S. Majumder et al.: J. Phys.: Conf. Ser. **1163**, 012072 (2019)
[4] C.P. Lowe: Europhys. Lett. **47**, 145 (1999)

12.12 Kinetics of the collapse of polyglycine in water

S. Majumder, U.H.E. Hansmann*, W. Janke

*Department of Chemistry and Biochemistry, University of Oklahoma, Norman, Oklahoma 73019, USA

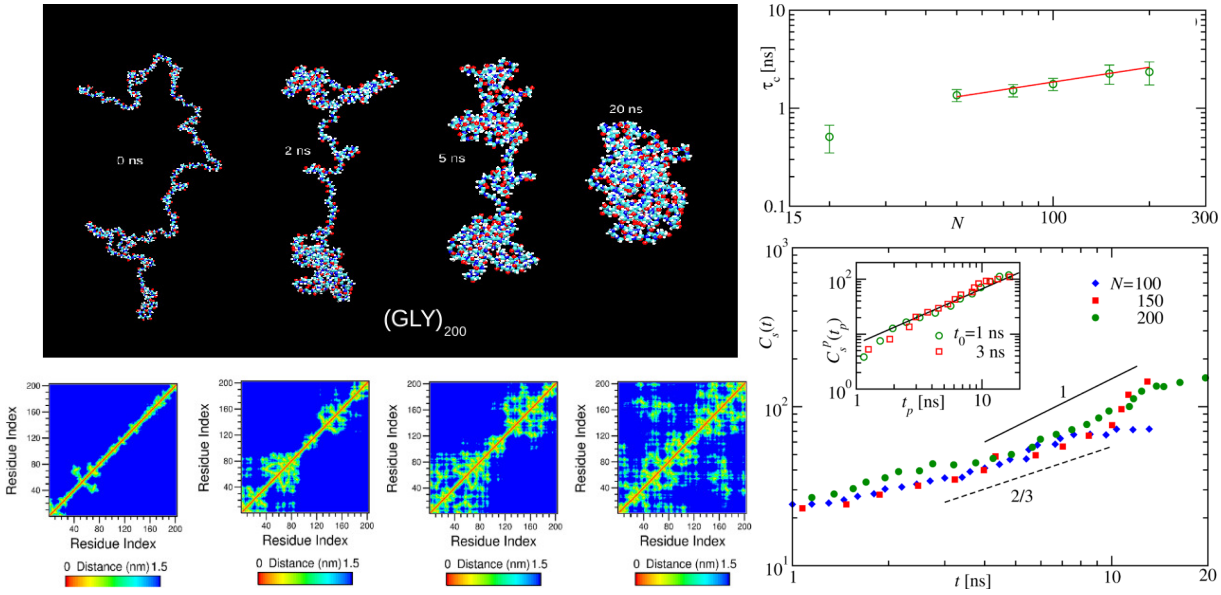

Figure 12.16: Left panel: Snapshots showing the sequence of events during the collapse of polyglycine with 200 residues. Below each snapshot the corresponding contact maps are also shown revealing the pearl-necklace formation more clearly. Right panel: The upper plot shows the scaling of the collapse time τ_c with respect to the chain length. The solid line demonstrates the consistency of the data with power-law scaling with an exponent $z = 0.5$. The lower plot shows the scaling associated with the cluster coarsening from pearl-necklace to globule.

The collapse of homopolymers was first described by de Gennes' seminal "sausage" model [1], but today the phenomenological "pearl-necklace" picture by Halperin and

Goldbart [2] is more commonly used, both for flexible and semiflexible polymer models. In this picture the collapse begins with nucleation of small local clusters (of monomers) leading to formation of an interconnected chain of (pseudo-)stable clusters, i.e., the "pearl-necklace" intermediate. These clusters grow by eating up the un-clustered monomers from the chain and subsequently coalesce, leading eventually to a single cluster. Finally, monomers within this final cluster rearrange to form a compact globule.

Of central interest in this context is the scaling of the collapse time τ_c with the degree of polymerization N (the number of monomers). While scaling of the form

$$\tau_c \sim N^z, \tag{12.9}$$

where z is the dynamic exponent, has been firmly established, there is no consensus on the value of z. Molecular dynamics (MD) simulations provide much smaller values ($z \approx 1$) than Monte Carlo (MC) simulations ($z \approx 2$). This difference is often explained with the presence of hydrodynamics in the MD simulations, but a value $z \approx 1$ has been reported recently also for MC simulations [3]. The "pearl-necklace" stage or the cluster-growth kinetics can be understood by monitoring the time (t) dependence of the mean cluster size $C_s(t)$, the relevant length scale. By drawing analogy with coarsening ferromagnets, it has been shown that scaling of the form

$$C_s(t) \sim t^{\alpha_c} \tag{12.10}$$

with growth exponent $\alpha_c \approx 1$ holds for flexible homopolymers [3, 4].

In this work [5] we investigated the nonequilibrium pathways by which the biological homopolymer polyglycine [$(\mathrm{Gly})_N$] collapses in water with the aim of exploring the above mentioned scaling laws. For short chains, the pathway has few noticeable features and is driven by the competition between the hydration of the peptide, opposing the collapse, and the intra-peptide attractions, favoring the collapse [6]. For chains with $N > 20$, the importance of hydration effects decreases, and the kinetics of hydrogen bonds indicates that van der Waals interactions of the backbone dominate [6] and drive the collapse. The nonequilibrium intermediates seen during the collapse exhibit local ordering or clustering that is analogous to the phenomenological "pearl-necklace" picture [cf. Fig. 12.16 (left)], known to be valid for the earlier studied coarse-grained homopolymer models [2]. Using the contact probability of the Cα-atoms in the backbone, we extract a relevant dynamic length scale, i.e., cluster size, that as in simple homopolymer models grows linearly with time [3].

Especially intriguing is that the scaling of the collapse time with length of the chain indicates a faster dynamics, with a critical exponent $z = 0.5$ [cf. Fig. 12.16 (upper right)] instead of $z = 1$ that was seen in earlier homopolymer collapse studies which considered simplified models describing non-hydrogen-bonded polymers such as polyethylene and polystyrene. The smaller exponent found in this study may be connected with a mechanism that allows in amino acid based polymers a more rapid collapse than seen in non-biological homopolymers such as poly(N-isoporpylacrylamide) and polystyrene, where collapse times of $\approx$ 300 ms up to $\approx$ 350 s have been reported. We conjecture that the smaller exponent z is characteristic for collapse transitions in amino acid based polymers where the presence of intra-chain hydrogen bonding immediately seeds (transient) local ordering, while in non-hydrogen-bonded polymers such local ordering only happens as a consequence of diffusive motion.

The scaling of the cluster growth during the collapse is shown in Fig. 12.16 (lower right). The solid and the dashed lines represent power-law behavior, $C_s(t) \sim t^{\alpha_c}$, with $\alpha_c = 1$ and $2/3$, respectively. In the inset, two different choices for a crossover time t_0 are taken into account by plotting $C_s^p(t) \equiv C_s(t) - C_s(t)_0$ vs. $t_p = t - t_0$. Here the solid line indicates a power-law behavior with exponent $\alpha_c = 1$.

[1] P.-G. de Gennes: J. Phys. Lett. **46**, 639 (1985)
[2] A. Halperin, P. Goldbart: Phys. Rev. E **61**, 565 (2000)
[3] S. Majumder et al.: Soft Matter **13**, 1276 (2017)
[4] S. Majumder, W. Janke: Europhys. Lett. **110**, 58001 (2015)
[5] S. Majumder et al.: Macromolecules **52**, 5491 (2019)
[6] D. Asthagiri et al.: J. Phys. Chem. B **121**, 8078 (2017)

12.13 Universal finite-size scaling for kinetics of phase separation in multicomponent mixtures

S. Majumder, S.K. Das*, W. Janke

*Theoretical Sciences Unit, Jawaharlal Nehru Centre for Advanced Scientific Research, Jakkur P.O., Bangalore 560064, India

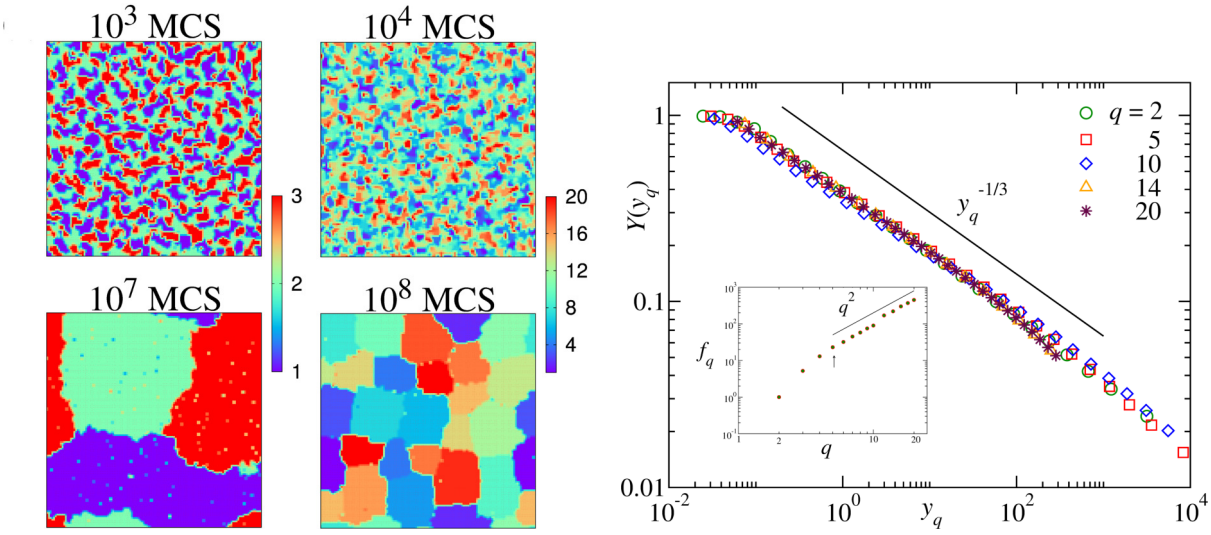

Figure 12.17: Left panel: Typical snapshots at two different times demonstrating the domain growth during phase separation in the q-state Potts model, for two different q. Results were obtained via Monte Carlo simulations mimiking diffusive dynamics. Right panel: The main frame illustrates the universality of the finite-size scaling function $Y(y_q)$ with a nonuniversal metric factor f_q in the scaling variable y_q, for different q. The inset shows the dependence of the metric factor f_q on q.

In this work [1] we have presented results for the kinetics of phase separation in multicomponent solid mixtures in space dimension $d = 2$, via Monte Carlo simulations

of the q-state conserved Potts model that has the Hamiltonian [2]

$$H = -J \sum_{\langle ij \rangle} \delta_{\sigma_i,\sigma_j}; \quad \sigma_i = 1, 2, \ldots, q; \quad J > 0 \,. \tag{12.11}$$

The primary interest in our work was to quantify the domain-growth kinetics. We achieve this via the application of appropriate finite-size scaling analyses [3–5]. Like in critical phenomena [6], this technique allows one to obtain a precise estimation of the growth exponent α, without using very large systems. We observe that finite-size effects are weak, as in the Ising model [3, 4]. By considering an initial domain length [3] in the scaling ansatz, we show that one obtains the Lifshitz-Slyozov growth, for all q, from rather early time, like in the Ising case.

Intriguingly, we find that the growth for different q can be described by a universal finite-size scaling function $Y(y_q)$, with a nonuniversal q-dependent metric factor f_q in the scaling variable y_q, arising from the amplitude of growth. This is illustrated in the main frame of the right panel of Fig. 12.17. Similarly, for a range of quench depth, viz. $T \in [0.5T_c, 0.8T_c]$, we show that the growth follows Lifshitz-Slyozov law, irrespective of the temperature, for all q. This also can be described by a similar common finite-size scaling function. Another important fact we observed is the crossover in the behaviour of f_q as a function of q [7]. Surprisingly, this crossover happens at $q = 5$ where the nature of phase transition changes from second order to first order [2].

[1] S. Majumder et al.: Phys. Rev. E **98**, 042142 (2018)
[2] F.Y. Wu: Rev. Mod. Phys. **54**, 235 (1982)
[3] S. Majumder, S.K. Das: Phys. Rev. E **81**, 050102(R) (2010)
[4] S.K. Das et al.: Europhys. Lett. **97**, 66006 (2012)
[5] S. Majumder et al.: Soft Matter **13**, 1276 (2017)
[6] M.E. Fisher: *The theory of critical point singularities*, in *Critical Phenomena*, Proc. 51st Enrico Fermi Summer School, Varenna, Italy, edited by M.S. Green (Academic Press, London, 1971), p. 1
[7] W. Janke et al.: Submitted to J. Phys.: Conf. Ser. (2018)

12.14 Phase-ordering kinetics of the long-range Ising model

H. Christiansen, S. Majumder, W. Janke

The nonequilibrium properties of the long-range Ising model with Hamiltonian

$$\mathcal{H} = -\sum_i \sum_{j<i} J(r_{ij}) s_i s_j, \text{ with } J(r_{ij}) = \frac{1}{r_{ij}^{d+\sigma}} \tag{12.12}$$

are investigated. We vary the exponent σ, which controls the decay of the potential $J(r_{ij})$ between spins s_i and s_j at distance r_{ij}. In Fig. 12.18(a) we show snapshots of this system for some of those σ and for two different times. The ordering of structured regions is clearly visible, where obviously the amplitude of growth depends on σ. However, this does not tell us something about the underlying law of growth. To quantify this, we investigate the characteristic length $\ell(t)$, which we extract from the decay of the

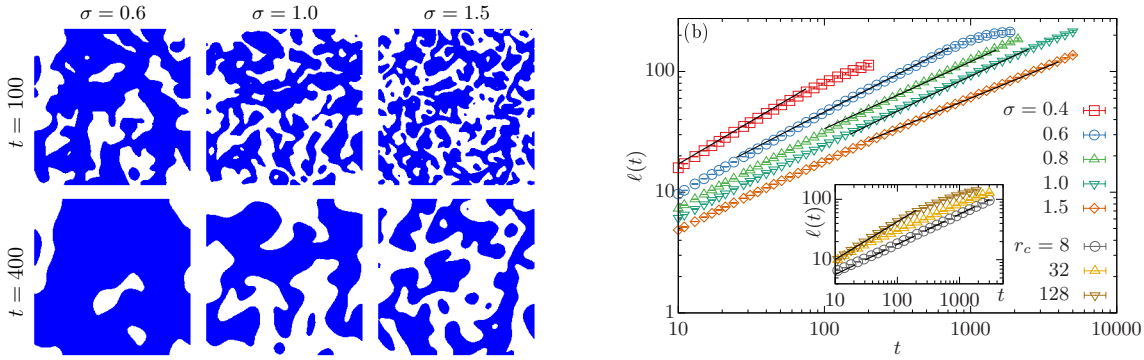

Figure 12.18: (a) Snapshots of the coarsening in the two-dimensional Ising model with long-range interactions with different $\sigma = 0.6$, 1.0, and 1.5 for the two times $t = 100$ and 400. Only spins pointing up are marked blue. (b) Length scale $\ell(t)$ for different σ, where the solid lines correspond to the prediction (12.13). The inset shows the influence of a finite cut-off on the growth of length scale.

equal-time two-point spin-spin autocorrelation function. For this model, there exists a prediction [3], reading

$$\ell(t) \propto t^{\alpha} = \begin{cases} t^{\frac{1}{1+\sigma}} & \sigma < 1 \\ (t \ln t)^{\frac{1}{2}} & \sigma = 1 \\ t^{\frac{1}{2}} & \sigma > 1 \end{cases} . \tag{12.13}$$

A previous publication observed $\ell(t) \propto t^{1/2}$ independent of σ, however, using a cut-off in the potential $J(r_{i,j})$ [4]. In the inset of Fig. 12.18(b) we show the influence of the cut-off for $\ell(t)$ with $\sigma = 0.6$ and observe that one indeed finds the exponent 1/2 for small cut-offs, whereas prediction (12.13) is confirmed for a sufficiently large cut-off. In the main plot of Fig. 12.18(b) we demonstrate for the first time that indeed (12.13) holds for all σ investigated when no cut-off is used.

[1] H. Christiansen et al.: Phys. Rev. E **99**, 011301(R) (2019)
[2] W. Janke et al.: J. Phys.: Conf. Ser. **1163**, 012002 (2019)
[3] A.J. Bray, A.D. Rutenberg: Phys. Rev. E **49**, R27(R) (1994)
[4] J. Gundh et al.: PloS One **10**, e0141463 (2015)

12.15 Percolation on square lattices with long-range correlated defects

J. Zierenberg*, N. Fricke, M. Marenz, F.P. Spitzner, V. Blavatska†, W. Janke

*Max Planck Institute for Dynamics and Self-Organization, Am Fassberg 17, 37077 Göttingen, Germany

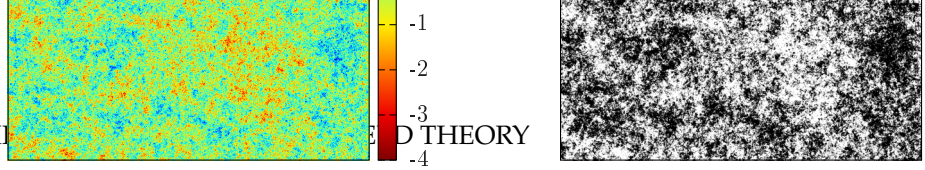

Figure 12.19: Correlated continuous variables on a $2^{11} \times 2^{11}$ lattice for (left figure) correlation strength $a = 0.5$ and (right figure) corresponding discrete lattice at the percolation threshold with defects shown in black.

Institute for Condensed Matter Physics of the National Academy of Sciences of Ukraine, 79011 Lviv, Ukraine

Structural obstacles (impurities) play an important role for a wide range of physical processes as most substrates and surfaces in nature are rough and inhomogeneous [1]. For example, the properties of magnetic crystals are often altered by the presence of extended defects in the form of linear dislocations or regions of different phases. Another important class of such disordered media are porous materials, which often exhibit large spatial inhomogeneities of a fractal nature. Such fractal disorder affects a medium's conductivity, and diffusive transport can become anomalous [2] This aspect is relevant, for instance, for the recovery of oil through porous rocks [3], for the dynamics of fluids in disordered media [4], or for our understanding of transport processes in biological cells [5].

In nature, inhomogeneities are often not distributed completely at random but tend to be correlated over large distances. To understand the impact of this, it is useful to consider the limiting case where correlations asymptotically decay by a power law rather than exponentially with distance:

$$C(r) \sim |r|^{-a} \tag{12.14}$$

where a is the correlation parameter. If a is smaller than the spatial dimension D, the correlations are considered long-range or "infinite." An illustration of such power-law correlations for continuous and discrete site variables on a square lattice is shown in Fig. 12.19.

In this project we studied long-range power-law correlated disorder on square and cubic lattices [6, 7]. In particular, we obtained high-precision results for the percolation thresholds and the fractal dimension of the largest clusters as a function of correlation parameter a. The correlations are generated using a discrete version of the Fourier filtering method [8]. We consider two different metrics to set the length scales over which the correlations decay, showing that the percolation thresholds are highly sensitive to such system details. By contrast, we verify that the fractal dimension d_f is a universal quantity and unaffected by the choice of metric. We also show that for weak correlations, its value coincides with that for the uncorrelated system. In two dimensions we observe a clear increase of the fractal dimension with increasing correlation strength, approaching $d_f \to 2$. The onset of this change, however, does not seem to be determined by the extended Harris criterion.

As a follow-up project that heavily relies on these results, we are currently studying the site-disordered Ising model on three-dimensional lattices with long-range correlated defects [9].

[1] D. Avnir et al.: Nature (London) **308**, 261 (1984)
[2] J.-P. Bouchaud, A. Georges: Phys. Rep. **195**, 127 (1990); I. Goychuk et al.: Phys. Rev. E **96**, 052134 (2017)
[3] M. Sahimi: *Flow and Transport in Porous Media and Fractured Rock* (VCH, Weinheim, 1995)
[4] M. Spanner et al.: Phys. Rev. Lett. **116**, 060601 (2016)
[5] F. Höfling, T. Franosch: Rep. Prog. Phys. **76**, 046602 (2013)

[6] N. Fricke et al.: Condens. Matter Phys. **20**, 13004 (2017)
[7] J. Zierenberg et al.: Phys. Rev. E **96**, 062125 (2017)
[8] H.A. Makse et al.: Phys. Rev. E **53**, 5445 (1996)
[9] S. Kamin, W. Janke: *Critical exponent ν of the Ising model in three dimensions with long-range correlated site-disorder*, Leipzig preprint (September 2019)

12.16 Monte Carlo study of the Ising model in three dimensions with long-range correlated disorder

S. Kazmin, W. Janke

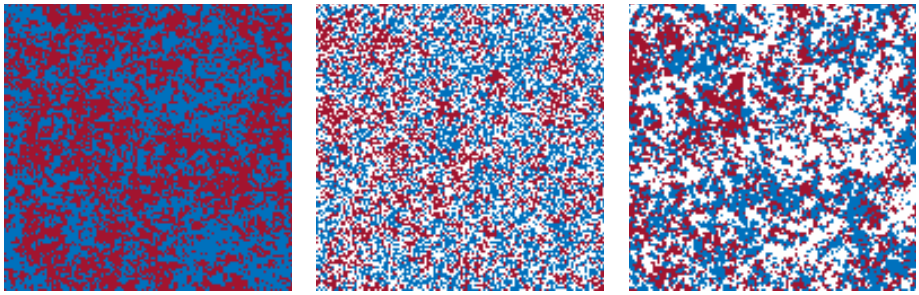

(a) $p_d = 0, a = \infty$ (b) $p_d = 0.4, a = \infty$ (c) $p_d = 0.4, a = 1.5$

Figure 12.20: Slices of a three-dimensional Ising model with linear lattice extension $L = 128$ at critical temperatures for different defect concentrations and correlation exponents. White dots represent the defects $\eta = 0$, blue and red the spin states $s = \pm 1$.

The aim of this work is to study the critical behaviour of the Ising model with long-range correlated disorder on the lattice with Monte Carlo simulation techniques. In nature the disorder often does come with a certain structure and not at random. We want to mimic this by introducing spatially correlated defects on the lattice. We use the Fourier method for the generation of the correlation between the defects as introduced by Makse et al. [1] and modified by Zierenberg et al. [2]. The main goal is to obtain the critical exponents in dependence of the disorder concentration and correlation strength as well as to analyze other aspects of the phase transition from paramagnetic to ferromagnetic state.

The Ising model with site disorder on a lattice is described by the Hamiltonian

$$\mathcal{H} = -J \sum_{\langle xy \rangle} \eta_x \eta_y s_x s_y - h \sum_x \eta_x s_x \,, \tag{12.15}$$

where J is the coupling constant, $s_x = \pm 1$ is a spin at site x, $\langle \cdot \rangle$ stands for next-neighbour indices, h is the external magnetic field and $\eta_x = 1$ when the site is occupied by a spin or $\eta_x = 0$ if it is a defect (vacant site). We can recover the pure Ising model by setting $\eta_x = 1$ for each site x on the lattice. In one disorder realization the defects can be placed randomly and uniformly in which case we speak about the uncorrelated disorder. In

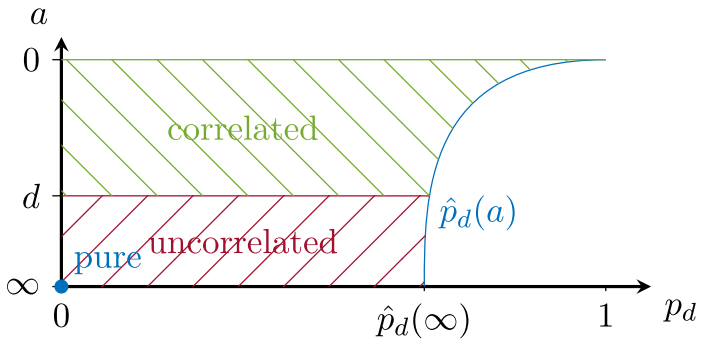

Figure 12.21: Universality classes of the three-dimensional Ising model for different disorder concentrations p_d and correlation exponents a. The curve $\hat{p}_d(a) = 1 - \hat{p}(a)$ is the percolation threshold below which the system has the probability 1 to have an infinite cluster of spins for $L \to \infty$ and therefore the Ising model is well defined. As can be seen qualitatively and was studied in [2] one can add more defects without destroying the infinite cluster when the defects are correlated.

the case of correlated disorder we place them randomly but in such a way that they obey the spatial correlation decay of the form

$$\langle \eta_x \eta_y \rangle \propto \frac{1}{d(x,y)^a} \,, \tag{12.16}$$

where d is the distance between two sites and a is the so-called correlation decay exponent. Formally, $a = \infty$ corresponds to the uncorrelated case. Finally, the mean concentration of the defects over a number of realizations is denoted by p_d. In Fig. 12.20 one can see the influence of the disorder correlation.

The universality class of the three-dimensional Ising model is expected to be different for the pure system, the uncorrelated disorder system according to the Harris criterion [3] and the correlated disorder system for $a \leq d = 3$ (strong correlation) according to the extended Harris criterion [4]. The situation is sketched in Fig. 12.21.

Before dealing with the critical exponents we must determine the critical temperatures at which the transition happens for various disorder concentrations p_d and various correlation exponents a. We performed Monte Carlo Simulations on lattices with maximal linear extent of $L = 64$ at different temperatures and obtained the critical temperatures from the intersections of the Binder cumulant observables $U_2 = 1 - \langle |m|^2 \rangle / (3\langle m \rangle^2)$ for different L. This method is commonly used and is explained in, e. g., Ref. [5]. Results are shown in Fig. 12.22, where the precise critical temperature is taken from Ref. [6]. The critical temperature decays with larger defect concentration and is expected to go to zero as p_d approaches the percolation threshold. On the other hand for stronger correlation of the defects (smaller a) the temperature increases at each concentration p_d.

The simulation at critical temperatures and the observation of the critical exponents is ongoing research. In particular, we want to apply the histogram reweighting technique [7] to the observables of interest. While the overall program is clear, there are various subtle aspects like different competing length scales which render the problem less trivial than may be thought at first glance.

[1] H. Makse et al.: Chaos, Solitons & Fractals **6**, 295 (1995); Phys. Rev. E **53**, 5445 (1996)
[2] J. Zierenberg et al.: Phys. Rev. E **96**, 062125 (2017)

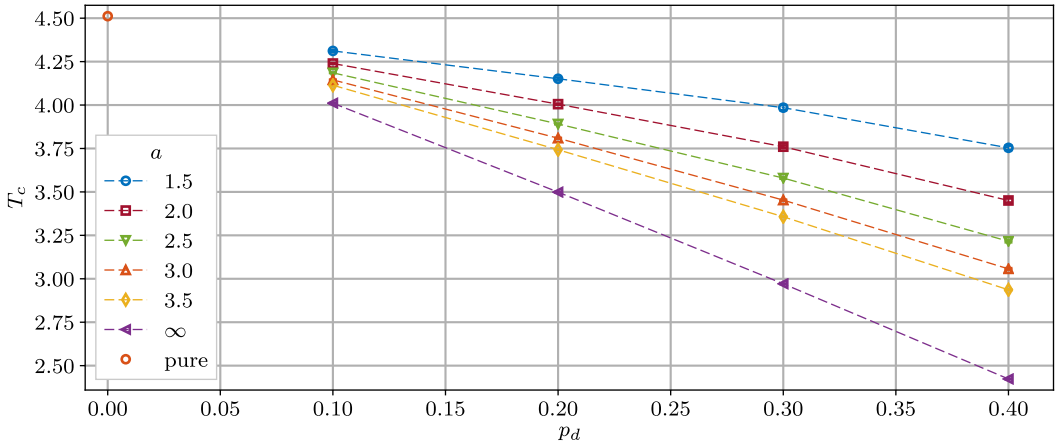

Figure 12.22: Critical temperatures T_c of the three-dimensional Ising model with disorder for different disorder concentrations p_d and different correlation exponents a. The value for the pure Ising model is taken from [6].

[3] A.B. Harris: J. Phys. C: Solid State Phys. **7**, 1671 (1974)
[4] A. Weinrib, B.I. Halperin: Phys. Rev. B **27**, 413 (1983)
[5] W. Janke: *Monte Carlo simulations in statistical physics – From basic principles to advanced applications*, in *Order, Disorder and Criticality: Advanced Problems of Phase Transition Theory*, ed. Y. Holovatch (World Scientific, Singapore, 2012)
[6] A.M. Ferrenberg et al.: Phys. Rev. E **97**, 043301 (2018)
[7] A.M. Ferrenberg, R.H. Swendsen: Phys. Rev. Lett. **63**, 1195 (1989)

12.17 Distribution of local minima for the Edwards-Anderson spin-glass model

S. Schnabel, W. Janke

In statistical physics the term "complex behavior" is usually used to characterize systems that posses a rough free-energy landscape with many metastable states. This can be the result of competing interactions on different scales like in the case of protein folding or it may arise from quenched disorder as for spin glasses. A conceptually simple model for such a system is the Edwards-Anderson spin-glass model [1], whose Hamiltonian is given by

$$\mathcal{H} = \sum_{\langle ij \rangle} J_{ij} S_i S_j,$$

where the spins sit on the sites of a cubic lattice, can take two values $S_i \in \{-1, 1\}$, and adjacent spins interact via normally distributed random couplings J_{ij}. Since these interactions can be either ferromagnetic (positive) or antiferromagnetic (negative), there is no trivial order established at low temperatures. Instead, many very different pure states might coexist, each one of them corresponding to a minimum in free energy.

Albeit not identical, minima of the energy, i.e. spin configurations that are stable against single spin flips are closely related to these pure states. It is thought that

minima in energy form the end-points of hierarchical tree-like structures with branches corresponding to different pure states. Understanding their properties might, therefore, improve our understanding of the behavior of the system. However, they have proven to be a very demanding subject of inquiry.

We have developed an advanced Monte Carlo method that in its basic form allows to sample the local energy minima with uniform distribution, i.e., each minimum configuration is occupied with equal probability. This is achieved by establishing within the simulation the combination of a spin configuration together with a random minimization thereof. I.e., the repeated flipping of spins with positive energy until a local minimum is reached. If one now alters the spin configuration and the parameters of the minimization in a suitable way it is possible to ensure that all local minima are equally likely found this way. This corresponds to 'simple sampling' in the space of local minima. It is also possible to perform 'importance sampling' by including suitable weight functions. We can for instance sample a canonical distribution of local minima in energy by including the Boltzmann weight.

A basic application of this method is the measurement of the distribution of the energy minima. Since existing algorithms are unable to perform such a task, there is no numerical data for comparison. However, we can use our results to test analytical approximations [2] that are based on the expansion of meanfield solutions. We found that there are considerable deviations (Fig. 12.23) [3]. In fact, the distributions much more closely – although not entirely – resemble Gaussian distributions.

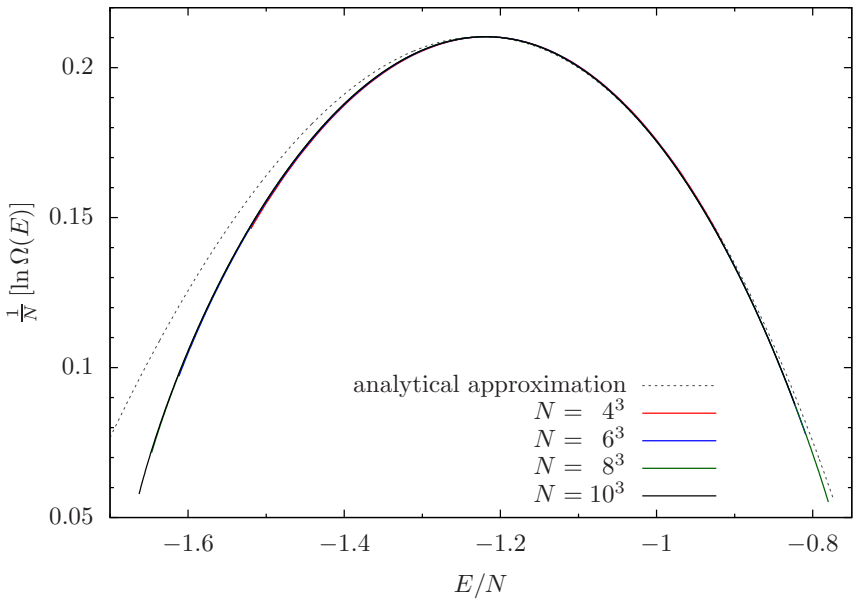

Figure 12.23: The distribution of local minima for different system sizes and the analytical approximation.

[1] S.F. Edwards, P.W. Anderson: J. Phys. F **5**, 965 (1975)
[2] A.J. Bray, M.A. Moore: J. Phys. C **14**, 1313 (1981)
[3] S. Schnabel, W. Janke: Phys. Rev. B **97**, 174204 (2018)

12.18 Spin glasses with variable frustration

R. Kumar, M. Weigel*, W. Janke

*Applied Mathematics Research Centre, Coventry University, England, UK

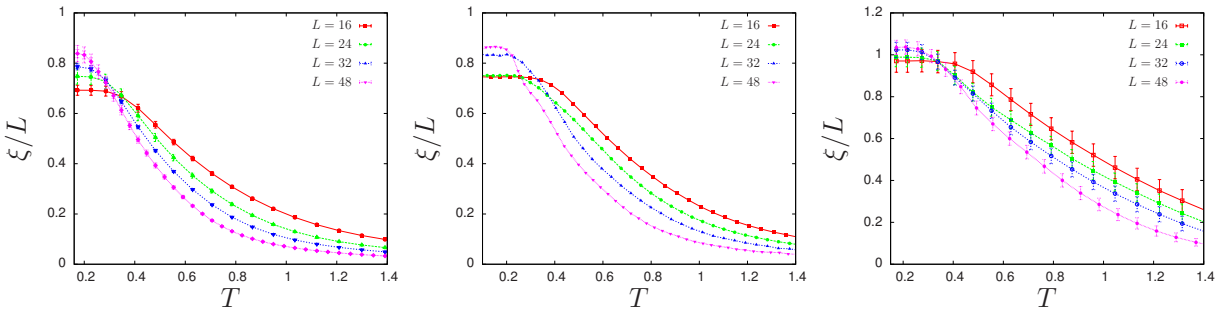

Figure 12.24: Correlation length as a function of temperature for (a) stochastically frustrated system, (b) a system with 46% frustration, and (c) a system with 20% frustration.

Together with randomness, frustration is believed to be a crucial prerequisite for the occurrence of glassy behaviour in spin systems. The degree of frustration is normally the result of a chosen distribution of exchange couplings in combination with the structure of the lattice under consideration. Here, however, we discuss a process for tuning the frustration content of the Edwards-Anderson model on arbitrary lattices. With the help of extensive parallel-tempering Monte Carlo simulations we study such systems on the square lattice and compare the outcomes to the predictions of a recent study employing the Migdal-Kadanoff real-space renormalization procedure [1]. We use a cluster algorithm proposed in [2] in order to reduce the equilibration time. The phase transition studies are done by looking at the divergence of the correlation length, see Fig. 12.24. The results are benchmarked by comparing to the stochastic case described in [3]. We also study the freezing temperature of such a system and observe a different behaviour compared to the stochastically frustrated case. Studies on larger system sizes are very crucial to confirm these differences.

We find that the divergence of the correlation length occurs at non-zero finite temperature for the 2D Ising spin glass. This gives hints of a phase transition, but such transitions have to be studied carefully in order to fully understand the phases [4].

[1] E. Ilker, A.N. Berker: Phys. Rev. E **89**, 042139 (2014)
[2] J. Houdayer: Eur. Phys. J. B **22**, 479 (2001)
[3] H.G. Katzgraber, L.W. Lee: Phys. Rev. B **71**, 134404 (2005)
[4] A. Hartmann: Phys. Rev. B **67**, 214404 (2003)

12.19 Random field q-state Potts model: Ground states and low-energy excitations

R. Kumar*, M. Kumar†‡, M. Weigel§, V. Banerjee‡, S. Puri†, W. Janke

*Doctoral College for the Statistical Physics of Complex Systems, Leipzig-Lorraine-Lviv-Coventry ($\mathbb{L}^4$)
†School of Physical Sciences, Jawaharlal Nehru University, New Delhi – 110067, India
‡Department of Physics, Indian Institute of Technology, Hauz Khas, New Delhi – 110016, India
§Applied Mathematics Research Centre, Coventry University, England, UK

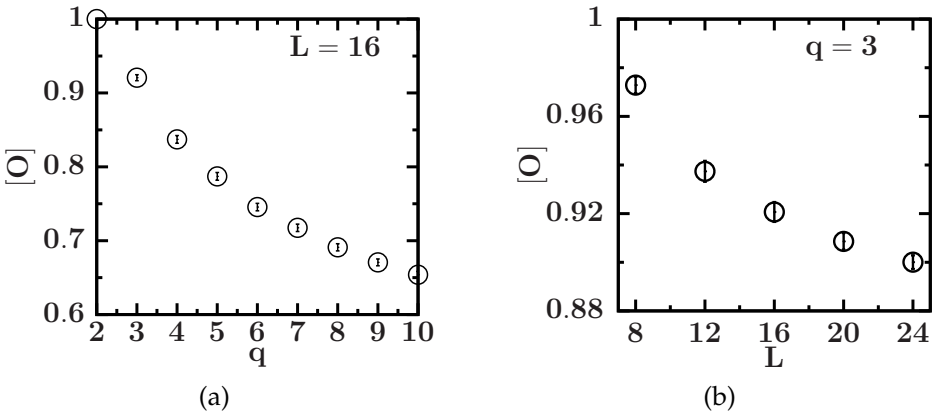

Figure 12.25: Overlap between the lowest states found by graph-cut methods (GCM) and the putative ground state (a) as a function of the number of Potts states q and (b) as a function of system size L.

While the ground-state (GS) problem for the random-field Ising model is polynomial and can be solved by using a number of well-known algorithms for maximum flow [1–4], the analogue random-field q-state Potts model with $q \geq 3$ corresponds to a multi-terminal flow problem that is known to be NP hard. Hence an efficient exact algorithm is extremely unlikely to exist [5]. Still, it is possible to employ an embedding of binary degrees of freedom into the Potts spins to use graph-cut methods (GCMs) to solve the corresponding ground-state problem approximately with polynomial methods. It is shown in this project [6] that this works relatively well. We compare results produced by this heuristic algorithm to energy minima found by an appropriately tuned parallel tempering method that is configured to find ground states for the considered system sizes with high probability. The method based on graph cuts finds the same states in a fraction of the time. The new method is used for a first exploratory study of the random-field Potts model in $d = 2, 3$.

We observe that the probability of finding a ground state decreases exponentially with q for GCM, but for parallel tempering this decay is linear [Fig. 12.25(a)]. Hence, GCM is more suitable for lower q studies. We also find that the lower energies found by GCM are very close to the ground state and the excess energy is very small. The probability of finding the ground state falls exponentially with the system size, whereas for GCM it falls linearly [Fig. 12.25(b)]. Therefore, GCM is better suited for studying larger system sizes. This is one very good feature of GCM as for the smaller system sizes we have larger finite-size effects. The overlap between the states found by GCM and the ground state is observed to be very large. Hence, we conclude that GCM produces the approximate GS which can be treated as an exact GS for sufficiently small q ($q = 3, 4$) for studying the critical behaviour and ground-state morphologies.

[1] G.P. Shrivastav et al.: Europhys. Lett. **96**, 36003 (2011)
[2] G.P. Shrivastav et al.: Phys. Rev. E **90**, 032140 (2014)
[3] G.P. Shrivastav et al.: Eur. Phys. J. E **37**, 98 (2014)
[4] V. Banerjee et al.: Ind. J. Phys. **88**, 1005 (2014)
[5] J.C. Angles d'Auriac et al.: J. Physique Lett. **46**, L173 (1985)
[6] M. Kumar et al.: Phys. Rev. E **97**, 053307 (2018)

12.20 Effects of the low-temperature phase degeneracy of the fcc Ising antiferromagnet on its finite-size scaling behavior

R. Stübel, W. Janke

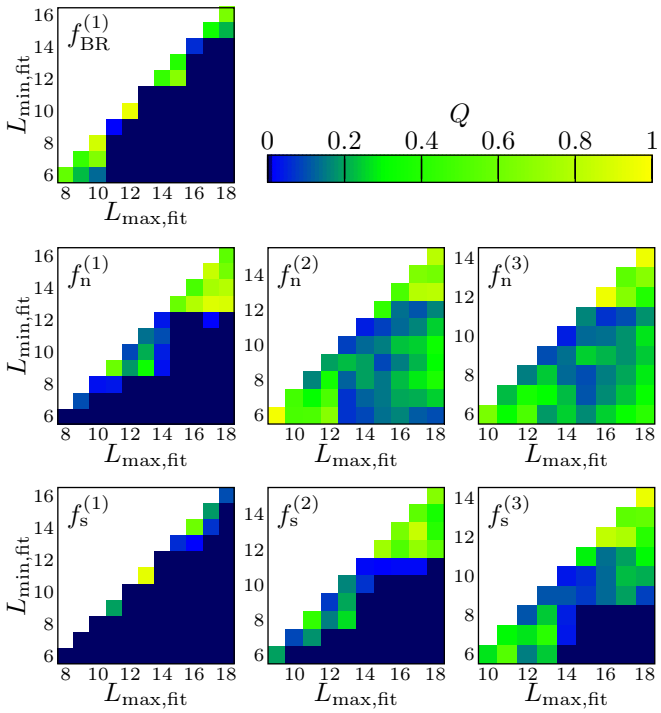

Figure 12.26: Quality of fit parameter $Q \in [0,1]$ for the fits of $\beta_{\mathrm{eqw}}(L)$ with the different fit functions. Here, the lattice size range $[L_{\mathrm{min,fit}}, L_{\mathrm{max,fit}}]$, over which the fit is performed, is varied. The color-value-key of Q is shown above.

The ordering of the Ising antiferromagnet on a face-centered cubic (fcc) lattice presents a long-standing problem which has received extensive attention since the 1930s. An important motivation for research on this model is the interest in frustrated magnetism in general which mainly prompted the later publications on this model. The model is well known to exhibit a macroscopic (exponential in the system size L) ground-state degeneracy. With increasing temperature, this degeneracy is expected to be lifted and the model undergoes a first-order phase transition. For a model with an exponential

degeneracy in the *whole* low-temperature phase, it was recently found that the finite-size scaling behaviour is governed by leading correction terms $\sim L^{-2}$ instead of $\sim L^{-3}$ as usual [1, 2]. To test the conjecture that such a transmuted behaviour may effectively persist also for the fcc antiferromagnet up to some crossover system size, we have performed multicanonical Monte Carlo simulations [3, 4] in a parallelized implementation [5] for lattices of linear size $L \leq 18$ with periodic boundary conditions and determined various inverse pseudo phase-transition temperatures, as well as the extremal values of the specific heat and the energetic Binder parameter.

Via least-squares fits [6], the regarded inverse pseudo phase-transition temperatures were fitted with the fit functions

$$f_{\mathrm{n}}^{(o)}(L) = k_0 + \frac{k_1}{L^2} + \frac{k_2}{L^3} + \frac{k_3}{L^4}, \tag{12.17}$$

$$f_{\mathrm{s}}^{(o)}(L) = k_0 + \frac{k_1}{L^3} + \frac{k_2}{L^6} + \frac{k_3}{L^9}, \tag{12.18}$$

where $f_{\mathrm{n}}^{(o)}$ corresponds to the non-standard scaling and $f_{\mathrm{s}}^{(o)}$ represents the standard ansatz, and $o = 1, 2, 3$ denotes the order of the fit function. We also compared with the ansatz

$$f_{\mathrm{BR}}^{(1)}(L) = \left(k_0 + \frac{k_1}{L}\right)^{-1} \tag{12.19}$$

which Beath and Ryan [7] employed, however, without a theoretical justification.

The results for the fits of $\beta_{\mathrm{eqw}}(L)$ are shown in Fig. 12.26 by means of the quality of fit parameter Q. The corresponding heat maps for $\beta_{c_{\max}}(L)$, $\beta_{B_{\min}}(L)$ and $\beta_{\mathrm{eqh}}(L)$ look very similar and hence are not depicted here. One can see that up to the first order, the ansatz $f_{\mathrm{BR}}^{(1)}$ of Beath and Ryan [7] is slightly better than the standard ansatz $f_{\mathrm{s}}^{(1)}$ but clearly not as good as the non-standard ansatz $f_{\mathrm{n}}^{(1)}$. Taking into account also the second order, the non-standard ansatz $f_{\mathrm{n}}^{(2)}$ yields good fits for all ranges $[L_{\min,\mathrm{fit}}, L_{\max,\mathrm{fit}}]$ of fitted lattice sizes L. Of course, also the results of the standard ansatz $f_{\mathrm{s}}^{(o)}$ improve with increasing order o, but they stay behind the non-standard ansatz $f_{\mathrm{n}}^{(o)}$ in any case. This leads to the conclusion that up to the largest simulated lattice size $L = 18$, the non-standard ansatz fits best [8]. A crossover between the different ansatzes is not observable in the range of the simulated lattice sizes. However, it cannot be excluded that such a crossover might occur for larger lattice sizes $L > 18$.

[1] M. Mueller et al.: Phys. Rev. Lett. **112**, 200601 (2014)
[2] M. Mueller et al.: Nucl. Phys. B **888**, 214 (2014)
[3] B.A. Berg, T. Neuhaus: Phys. Lett. B **267**, 249 (1991); Phys. Rev. Lett. **68**, 9 (1992)
[4] W. Janke: Int. J. Mod. Phys. C **03**, 1137 (1992)
[5] J. Zierenberg et al.: Comput. Phys. Commun. **184**, 1155 (2013)
[6] P. Young: *Everything You Wanted to Know About Data Analysis and Fitting but Were Afraid to Ask* (Springer, Heidelberg, 2015) (see also arXiv:1210.3781)
[7] A.D. Beath, D.H. Ryan: Phys. Rev. B **73**, 174416 (2006)
[8] R. Stübel, W. Janke: Phys. Rev. B **98**, 174413 (2018)

12.21 The two-dimensional Blume-Capel model: Scaling and universality

N.G. Fytas*, J. Zierenberg†, P.E. Theodorakis‡, M. Weigel*, W. Janke, A. Malakis§

*Applied Mathematics Research Centre, Coventry University, England, UK
†Max Planck Institute for Dynamics and Self-Organization, Am Fassberg 17, 37077 Göttingen, Germany
‡Institute of Physics, Polish Academy of Sciences, Al. Lotników 32/46, 02-668 Warsaw, Poland
§Department of Physics, University of Athens, Greece

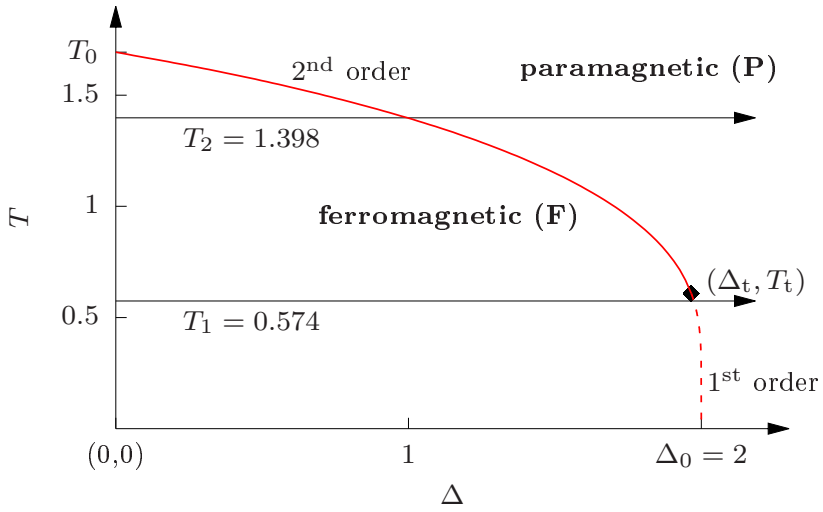

Figure 12.27: Phase diagram of the pure two-dimensional Blume-Capel model, showing the ferromagnetic (F) and paramagnetic (P) phases that are separated by a continuous transition for small (solid line) and a first-order transition for large (dotted line). The line segments meet at a tricritical point, as indicated by the black diamond. The horizontal arrows indicate the paths of crossing the phase boundary implemented in the simulations of the present work.

The Blume-Capel model [1, 2] is a perfect test model for studies of phase transitions. We consider this spin-one Ising model in a crystal field on a square lattice in two dimension (2D), described by the Hamiltonian

$$\mathcal{H} = -\sum_{\langle ij \rangle} J_{ij}\sigma_i\sigma_j + \Delta \sum_i \sigma_i^2 = E_J + \Delta E_\Delta \,, \tag{12.20}$$

where the spin variables $\sigma_x \in \{-1, 0, +1\}$ and the couplings are $J_{ij} \equiv J$ in the pure model or drawn randomly from a bimodal distribution

$$\mathcal{P}(J_{xy}) = \frac{1}{2}\left[\delta(J_{xy} - J_1) + \delta(J_{xy} - J_2)\right] \tag{12.21}$$

in the disordered model, where we choose $J_1 + J_2 = 2$ and $J_1 > J_2 > 0$, so that $r = J_2/J_1$ defines the disorder strength (for $r = 1$ one recovers the pure model). We investigated the behaviour in the vicinity of the first-order and second-order regimes of the

ferromagnet-paramagnet phase boundary, respectively [3], see the phase diagram for the pure model in Fig. 12.27. To achieve high-precision results, we utilized a combination of (i) a parallel version of the multicanonical algorithm and (ii) a hybrid updating scheme combining Metropolis and generalized Wolff cluster moves. These techniques are combined to study for the first time the correlation length ξ of the model, using its scaling with system size L in the regime of second-order transitions to illustrate universality through the observed identity of the limiting value of ξ/L with the exactly known result for the Ising universality class.

In contrast to most previous work, we focused on crossing the phase boundary at constant temperature by varying the crystal field Δ [4]. Employing a multicanonical scheme in Δ allowed us to get results as continuous functions of Δ and to overcome the free-energy barrier in the first-order regime of the transitions. A finite-size scaling analysis based on a specific-heat-like quantity and the magnetic susceptibility provided us with precise estimates for the transition points in both regimes of the phase diagram that compare very well to the most accurate estimates of the current literature. In the first-order regime, we found a somewhat surprising $1/L$ correction in the scaling of the conventionally defined magnetic susceptibility χ. As it turns out, this is due to the explicit symmetry breaking by using the absolute value of the magnetisation (i.e., $|M|$ instead of M) in the definition of χ. For a modified symmetry breaking prescription that leaves the disordered peak invariant, this correction disappears. It would be interesting to see whether similar corrections are found in other systems with first-order transitions, such as the Potts model.

More recently we extended this study by considering the effect of the quenched disorder in the exchange couplings J_{ij} [5]. We find that the first-order transition for large crystal-field coupling is softened to become continuous, with a divergent correlation length. An analysis of the scaling of the correlation length as well as the susceptibility and specific heat reveals that this transition belongs to the Ising universality class with additional logarithmic corrections which are also observed for the Ising model itself if coupled to weak disorder. While the leading scaling behavior of the disordered system is thus identical in the second-order and first-order segments of the phase diagram of the pure model, the finite-size scaling in the ex-first-order regime turns out to be strongly affected by transient effects with a crossover length scale $L^* \approx 32$ for the chosen parameters [5].

[1] M. Blume: Phys. Rev. **141**, 517 (1966)
[2] H.W. Capel: Physica (Utr.) **32**, 966 (1966)
[3] J. Zierenberg et al.: Eur. Phys. J. – Special Topics **226**, 789 (2017)
[4] J. Zierenberg et al.: Phys. Rev. E **91**, 032126 (2015)
[5] N.G. Fytas et al.: Phys. Rev. E **97**, 040102(R) (2018)

12.22 Simulation of self-avoiding walks and polymers in continuum by means of binary trees

S. Schnabel, W. Janke

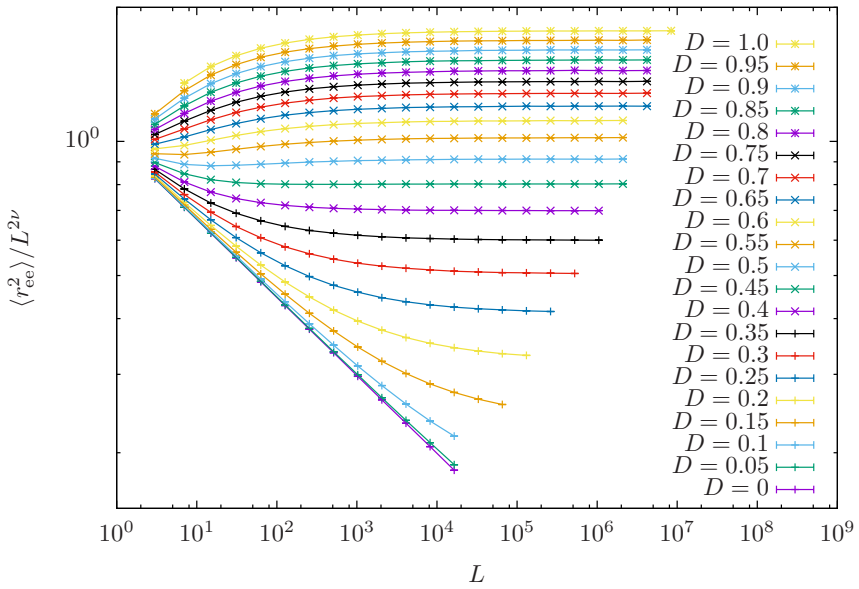

Figure 12.28: Rescaled quadratic end-to-end distance r_{ee} of the hard-sphere polymer as a function of length L for different sphere diameters D. The crossover from the random walk ($D = 0$) to the self-avoiding walk is apparent.

A few years ago Nathan Clisby has introduced a novel technique [1] for the simulation of self-avoiding walks on lattice geometries. These systems serve as simple models for polymers with excluded-volume interaction and allow for the investigation of the related scaling behaviour. With the new method walks are stored as binary trees where the leaves correspond to individual occupied lattice sites and any internal node contains collective geometric information of the subtree to which it is root in form of a box (in case of a simple-cubic lattice) that contains all derived monomers. This allows one to test for non-intersection of large parts of the walk very efficiently using nodes high up in the tree which represent many occupied lattice sites. Lower nodes representing few sites in more detail are only accessed if necessary. It was possible to determine the 3d Flory exponent with great accuracy, $\nu = 0.587\,597\,0(4)$ [2], with the new method.

Our first goal is to apply this method to the slightly more realistic hard-sphere polymer model, also known as continuum self-avoiding walks. A set of monomers $\mathbf{x}_i$ that are connected by bonds of fixed length $|\mathbf{x}_i - \mathbf{x}_{i+1}| = 1$ and represent hard spheres of diameter D: $|\mathbf{x}_i - \mathbf{x}_j| \geq D$. Otherwise the chain is fully flexible. The adaptation of the binary-tree method to the latter system is straightforward. The boxes are replaced by spheres and transformations are generalized. Now it is easily possible to simulate systems with many million monomers. In Fig. 12.28 we show the dependence of the end-to-end distance as a function of the polymer length divided by the asymptotic scaling law. The crossover from a behaviour akin to a random walk (where $\nu = 1/2$) for small chains and small diameters to the self-avoiding walk (horizontal in Fig. 12.28) can be observed. It becomes apparent that for $D \approx 0.45$ the corrections to scaling become very small and asymptotic behaviour is already realized for comparatively short chains.

[1] N. Clisby: J. Stat. Phys. **140**, 349 (2010)
[2] N. Clisby, B. Dünweg: Phys. Rev. E **94**, 052102 (2016)
[3] S. Schnabel, W. Janke: Preprint arXiv:1904.11191

12.23 Non-flat histogram techniques for spin glasses

F. Müller, S. Schnabel, W. Janke

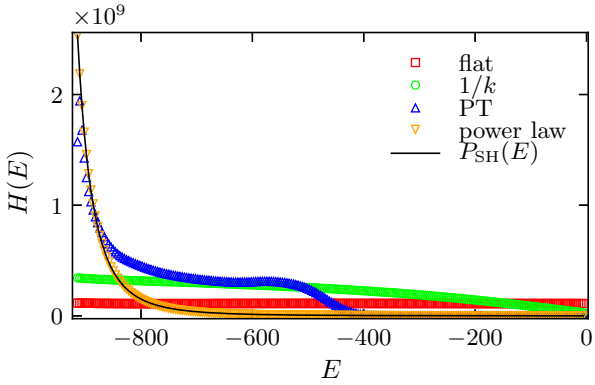

Figure 12.29: Histograms of the simulation with the different methods together with the prescribed power-law shape $P_{\mathrm{SH}}(E)$.

We took into consideration the three-dimensional bimodal Edwards-Anderson (EA) spin-glass model [1]. Spin glasses are difficult to simulate with conventional simulation methods and their investigation requires calculating disorder averages over a sufficiently large set of samples. Each sample has its own characteristics and it is known that finding the ground state of hard samples, i.e., solving the underlying optimization problem of that sample, is NP-hard.

There are existing methods such as the multicanonical (MUCA) method [2, 3], the $1/k$ ensemble [4] and parallel tempering (PT) [5] which have already been applied to the three-dimensional EA model. Especially also their performance in terms of the ability to solve the underlying optimization problem has been investigated. We looked at the round-trip times in energy which are defined as the average time which a simulation takes to reach the ground state and travel back to high energies. The ability of finding the ground state strongly influences the round-trip times of the respective method.

In addition to the above mentioned methods we modified the MUCA approach from sampling a flat distribution in energy to sampling a power-law shaped distribution in energy with a parametric form of the distribution of the form

$$P_{\mathrm{SH}}(E, \Delta E, \alpha) = \left(\frac{E}{\Delta E - E_g} + 1 \right)^{\alpha} , \tag{12.22}$$

where $\Delta E = 96$ is the position of the pole of the power law relative to the ground-state energy E_g and $\alpha = -3.6$ is the exponent [6]. In Fig. 12.29 the outcoming histograms of one sample with linear lattice size $L = 8$ are plotted. The figure shows clearly that the effort of the simulation is concentrated towards the ground-state region for all methods but the traditional MUCA. The power-law MUCA and PT have similar distributions of sampled states which increase drastically towards the ground-state energy.

Table 1 shows the comparison of the mean round-trip times for the three different methods. The mean round-trip times of the power-law MUCA improve significantly compared to the traditional MUCA and also compared to the other methods.

Table 12.1: Ratios of the population mean and the quantile mean of round-trip times of the flat MUCA and parallel-tempering methods with respect to the power-law MUCA method.

	flat MUCA		parallel tempering	
L	r_{pop}	$r_{\epsilon=10^{-4}}$	r_{pop}	$r_{\epsilon=10^{-4}}$
3	$1.16^{+0.02}_{-0.02}$	$1.17^{+0.04}_{-0.04}$	$1.64^{+0.03}_{-0.03}$	$1.64^{+0.04}_{-0.04}$
4	$1.62^{+0.05}_{-0.05}$	$1.66^{+0.09}_{-0.08}$	$1.17^{+0.04}_{-0.04}$	$1.22^{+0.07}_{-0.07}$
5	$2.3^{+0.2}_{-0.2}$	$2.34^{+0.3}_{-0.3}$	$1.14^{+0.05}_{-0.05}$	$1.14^{+0.1}_{-0.09}$
6	$3.8^{+0.6}_{-0.5}$	$3.5^{+0.7}_{-0.6}$	$2.8^{+0.4}_{-0.4}$	$3.3^{+0.8}_{-0.6}$
8	13^{+12}_{-7}	$15^{+25}_{-10.0}$	3^{+3}_{-2}	3^{+6}_{-2}

[1] S.F. Edwards, P.W. Anderson: J. Phys. F **5**, 965 (1975)
[2] B.A. Berg, T. Neuhaus: Phys. Lett. B **267**, 249 (1991); Phys. Rev. Lett. **68**, 9 (1992)
[3] W. Janke: Int. J. Mod. Phys. C **03**, 1137 (1992)
[4] B. Hesselbo, R.B. Stinchcombe: Phys. Rev. Lett. **74**, 2151 (1995)
[5] K. Hukushima, K. Nemoto: J. Phys. Soc. Jpn. **65**, 1604 (1996)
[6] F. Müller et al.: *Non-flat histogram techniques for spin glasses*, Leipzig preprint (June 2019)

12.24 Population annealing: A massively parallel computer simulation scheme

M. Weigel[*], L.Yu. Barash[†‡], M. Borovský[§], L.N. Shchur[†‡¶], W. Janke

[*]Applied Mathematics Research Centre, Coventry University, England, UK
[†]Landau Institute for Theoretical Physics, 142432 Chernogolovka, Russia
[‡]Science Center in Chernogolovka, 142432 Chernogolovka, Russia
[§]P.J. Šafárik University, Park Angelinum 9, 040 01 Košice, Slovak Republic
[¶]National Research University Higher School of Economics, 101000 Moscow, Russia

The generic technique for Monte Carlo simulations in statistical physics is importance sampling via a suitably constructed Markov chain [1]. While such approaches are quite successful, they are not particularly well suited for parallelization as the chain dynamics is sequential, and if replicated chains are used to increase statistics each of them relaxes into equilibrium with an intrinsic time constant that cannot be reduced by parallel work. Population annealing is a sequential Monte Carlo method that simulates an ensemble of system replica under a cooling protocol as sketched in Fig. 12.30. This method was first suggested in 2001 by Iba [2] and later on discussed in more detail by Hukushima and Iba [3] as a method to tackle potentially difficult sampling problems, but with no particular view to a parallel implementation. More recently, Machta [4] used a variant that avoids the recording of weight functions through population control in every step. This is the variant we adapted in our own implementation.

The population element makes this method naturally well suited for massively parallel simulations, and both the bias in estimated quantities and the statistical errors

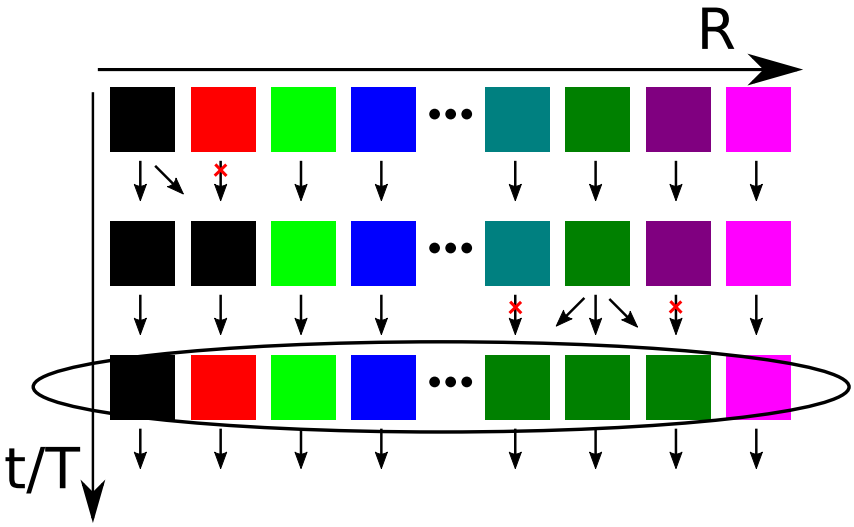

Figure 12.30: Schematic illustration of the population annealing method: R replica of the system are cooled down in discrete temperature steps. At each temperature T the current configurations at the next higher temperature are resampled according to their Boltzmann weights. This amounts to deleting some of them (e.g., the red one in the upper row) and replicating others one, two or more times (e.g., the dark green one in the second row). This new population is then further evolved in "time" t by any valid update procedure at this temperature.

can be systematically reduced by increasing the population size. To demonstrate this, we developed an implementation of population annealing on graphics processing units (GPUs) [5] and benchmarked its behaviour for different systems undergoing continuous and first-order phase transitions [6, 7]. For a recent overview, see Ref. [8].

[1] D.P. Landau, K. Binder: *A Guide to Monte Carlo Simulations in Statistical Physics*, 4th ed. (Cambridge University Press, Cambridge, 2015)
[2] Y. Iba: Trans. Jpn. Soc. Artif. Intell. **16**, 279 (2001)
[3] K. Hukushima, Y. Iba: AIP Conf. Proc. **690**, 200 (2003)
[4] J. Machta: Phys. Rev. E **82**, 026704 (2010)
[5] L.Yu. Barash et al.: Comput. Phys. Commun. **220**, 341 (2017)
[6] L.Yu. Barash et al.: Eur. Phys. J. – Special Topics **226**, 595 (2017)
[7] M. Weigel et al.: in *Computer Simulation Studies in Condensed-Matter Physics XXX*, eds. D.P. Landau, M. Bachmann, S.P. Lewis, H.-B. Schüttler, Phys.: Conf. Ser. **921**, 012017 (2017)
[8] L. Shchur et al.: Communications in Computer and Information Science (CCIS) **965**, 354 (2019)

12.25 Accelerating molecular dynamics with population annealing

H. Christiansen, M. Weigel*, W. Janke

*Applied Mathematics Research Centre, Coventry University, England, UK

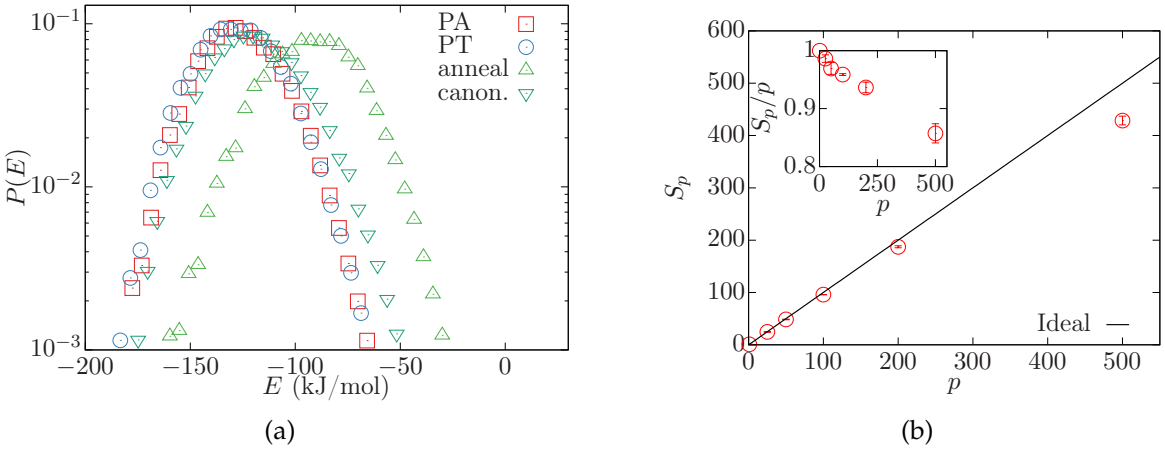

Figure 12.31: (a) Energy histogram for Met-enkephalin at the lowest temperature (T = 200 K) considered for the different methods. (b) Speedup S_p and, in the inset, efficiency S_p/p for different number of CPU cores p.

Systems having a rugged free-energy landscape cannot be simulated using naive canonical (NVT) simulations, because they get trapped in local minima. Therefore, one uses so-called generalized ensemble methods to overcome those barriers. In Molecular Dynamics, one mostly uses Parallel Tempering [1], which is easy to parallelize. However, this method can only effectively use a limited number of CPU cores. In this work, we adapt Population Annealing [2, 3] to Molecular Dynamics simulations. This method has the advantage that it scales to effectively "arbitrary" number of CPU cores while having comparable performance to Parallel Tempering when using the same computational resources. For a broad range of systems, this opens the door to the world of highly efficient computer simulations on petaflop supercomputers of the present and the exaflop machines of the future. To demonstrate this advantage, we have investigated the penta-peptide Met-enkephalin [4, 5], a system commonly used to probe the performance of novel simulation methods. In Fig. 12.31(a) we show the energy histogram for the lowest temperature considered at T = 200 K, where the free-energy barriers are most prominent. Both Population Annealing (PA) and Parallel Tempering (PT) produce energy histograms that are compatible with each other, whereas a single canonical simulation leads to a shifted histogram. Here "anneal" corresponds to an ensemble of independent Simulated Annealing runs. The excellent scaling with the number of CPU cores p is presented in Fig. 12.31(b), where we show the speedup S_p for up to p = 500 CPU cores. In the inset, the efficiency S_p/p is shown, indicating a parallel performance of clearly above 80% in this case.

[1] K. Hukushima, K. Nemoto: J. Phys. Soc. Jpn. **65**, 1604 (1996)
[2] Y. Iba: Trans. Jpn. Soc. Artif. Intell. **16**, 279 (2001)
[3] K. Hukushima, Y. Iba: AIP Conf. Proc. **690**, 200 (2003)
[4] H. Christiansen et al.: Phys. Rev. Lett. **122**, 060602 (2019)
[5] H. Christiansen et al.: J. Phys.: Conf. Ser. **1163**, 012074 (2019)

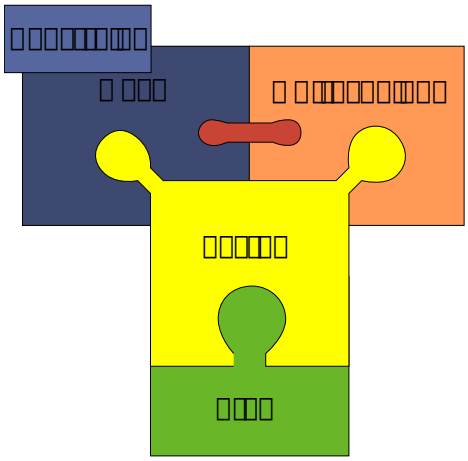

Figure 12.32: The 5 basic building blocks.

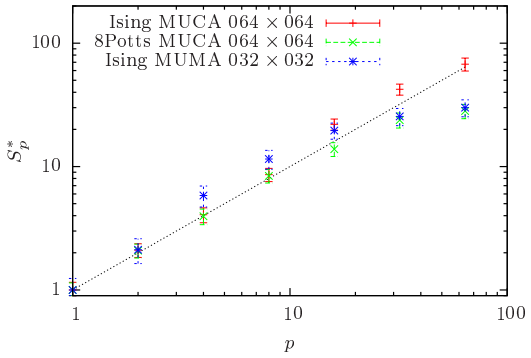

Figure 12.33: Scaling properties of the parallel multicanonical algorithm as a function of the number of processors p.

12.26 Framework for programming Monte Carlo simulations (βMC)

M. Marenz, J. Zierenberg*, W. Janke

*Max Planck Institute for Dynamics and Self-Organization, Am Fassberg 17, 37077 Göttingen, Germany

Monte Carlo (MC) computer simulations are a very powerful tool for investigating and understanding the thermodynamic behavior of a wide variety of physical systems. These systems range from such simple ones like the Ising or Blume-Capel spin models to complex ones like semiflexible polymers confined in a sphere or proteins interacting with surfaces. In contrast to Molecular Dynamics (MD) simulations, the other important class of algorithm to simulate microscopic systems, MC simulations are not suitable to investigate dynamical properties. On the other hand, the ability of modern MC methods to explore effectively the phase space of physical systems, especially those with a phase transition, makes them a very powerful and indispensable tool.

Another difference to MD simulations is the lack of a widely used program package for generic MC simulations. One reason for this lack is the versatility of modern MC algorithms – there are various different algorithm and many different possibilities to adjust a MC simulation to a specific problem. This was the starting point for the development of our framework for advanced MC algorithms. The aim of the framework is to enable the programmer to implement specific simulations in an easy and efficient way, without the need to implement all the tricky details for every new problem. The framework is implemented in the C++ programming language and is designed such that it separates basics parts of a MC algorithm in separate building blocks. These building blocks can be used by the programmer to implement a specific simulation.

There are 5 basic building blocks as illustrated in Fig. 12.32: The first one is the "system", which defines the Hamiltonian and the structure of the physical system. This means that the "system" building block encapsulates the energy calculation and the structure of the considered physical problem. For off-lattice system this block contains a smaller subpart, the "atom" block, which encodes the geometry of the system

(e.g., boundary conditions). As systems we have implemented so far different kinds of coarse-grained homopolymers, the Lennard-Jones gas, the TIP4P water model, lattice polymers and the Potts model in different dimensions. On top of the "system" are the last two other building blocks, the "move" and the "MC technique". A "move" defines a single update proposal, propagating the system from the current state to the next one. Additionally a "constraint" can be added to every "move" in order to simulate efficiently systems with geometrical confinements. The "MC technique" implements the Monte Carlo algorithm itself. At the moment we have implemented various algorithms such as Metropolis MC, parallel tempering, multicanonical MC, multimagnetic MC and the Wang-Landau MC algorithm. One of the most advanced MC algorithms we have implemented is a parallel version of the multicanonical algorithm [1, 2], see Fig. 12.33.

The boundaries between these blocks are well defined, so that one can easily exchange one of them. For example one can use two different algorithm to simulate a specific system without implementing a completely new program. The framework is already in practical use for different studies, for example the investigation of the influence of bending stiffness on a coarse-grained homopolymer, the influence of a spherical confinement to pseudo-phase transitions of homopolymers, and the study of polymer aggregation of several polymers for a large set of parameters (temperature, bending stiffness). Thus, the framework is very useful and has led already to several publications [3–9].

[1] J. Zierenberg et al.: Comput. Phys. Commun. **184**, 1155 (2013)
[2] J. Gross et al.: Comput. Phys. Commun. **224**, 387 (2018)
[3] J. Zierenberg et al.: J. Chem. Phys. **141**, 114908 (2014)
[4] J. Zierenberg, W. Janke: Europhys. Lett. **109**, 28002 (2015)
[5] J. Zierenberg at al: Phys. Rev. E **91**, 032126 (2015)
[6] M. Marenz, W. Janke: Phys. Rev. Lett. **116**, 128301 (2016)
[7] J. Zierenberg et al: Polymers **8**, 333 (2016)
[8] J. Zierenberg et al.: Nat. Commun. **8**, 14546 (2017)
[9] N.G. Fytas et al.: Phys. Rev. E **97**, 040102(R) (2018)

12.27 Funding

Sonderforschungsbereich/Transregio SFB/TRR 102 *Polymers under Multiple Constraints: Restricted and Controlled Molecular Order and Mobility*
W. Janke (Principal Investigator, project B04)
Deutsche Forschungsgemeinschaft (DFG)

Free-Energy Landscapes of Semiflexible Theta-Polymer Aggregation with and without External Force
W. Janke
Deutsche Forschungsgemeinschaft (DFG), Grant No. JA 483/31-1

Stable Knotted Phases in Semiflexible Polymers
W. Janke
Deutsche Forschungsgemeinschaft (DFG), Grant No. JA 483/33-1

Marie Curie IRSES Network *DIONICOS: Dynamics of and in Complex Systems*
W. Janke (Principal Investigator, Head of Leipzig node)
European Union (EU), Contract No. PIRSES-GA-2013-612707

COST Action CA17139: EUTOPIA – *European Topology Interdisciplinary Action*
W. Janke (Principal Investigator)

Doctoral College *Statistical Physics of Complex Systems* ($\mathbb{L}^4$)
W. Janke (with B. Berche, Nancy)
Deutsch-Französisches Doktorandenkollegium (DFDK) with "Co-tutelle de Thèse", jointly with Université de Lorraine, Nancy, France, and Coventry University, UK, and National Academy of Sciences of Ukraine, Lviv, Ukraine, as associated partners
Deutsch-Französische Hochschule (DFH-UFA), Grant No. CDFA-02-07

Graduate School *"BuildMoNa": Leipzig School of Natural Sciences – Building with Molecules and Nano-objects*
W. Janke (Principal Investigator)

International Max Planck Research School (IMPRS) *Mathematics in the Sciences*
W. Janke (Scientific Member)
Max Planck Society and Klaus Tschira Foundation

Free-Energy Landscapes of Semiflexible Polymer Aggregation
W. Janke, J. Zierenberg
NIC Jülich (computer time grant for "JURECA"), Grant No. HLZ24

12.28 Organizational Duties

Wolfhard Janke

- *Adjunct Professor* of The University of Georgia, Athens, Georgia, USA
- *International Visiting Professor* of Coventry University, England, UK
- Director, Institute for Theoretical Physics (ITP), Universität Leipzig
- Director, Naturwissenschaftlich-Theoretisches Zentrum (NTZ), Universität Leipzig
- Member of Department Council ("Fakultätsrat"), Faculty for Physics and Earth Sciences, Universität Leipzig
- Member of the Steering Committee ("Direktorium") of the Graduate Centre *Mathematics/Computer Science and Natural Sciences*, Research Academy Leipzig
- Principal Investigator of the Graduate School "BuildMoNa"
- Scientific Member of the International Max Planck Research School (IMPRS) *Mathematics in the Sciences*
- Principal Investigator of the DFG Sonderforschungsbereich/Transregio SFB/TRR 102 *Polymers under Multiple Constraints: Restricted and Controlled Molecular Order and Mobility*
- Principal Investigator of "Profillinie" *Complex Matter*, Universität Leipzig
- Principal Investigator of "Profillinie" *Mathematical and Computational Sciences*, Universität Leipzig

- Spokesperson of the German-French Graduate College *Statistical Physics of Complex Systems* with Nancy (France), and associated partners in Coventry (England, UK) and Lviv (Ukraine), of the Deutsch-Französische Hochschule (DFH-UFA)
- External Member of the Jagiellonian University Graduate School *International Ph.D. Studies in Physics of Complex Systems*, Krakow, Poland
- Permanent Member of the International Advisory Board for the Annual *Conference of the Middle European Cooperation in Statistical Physics (MECO)*
- Organizer of the Workshop *CompPhys18* – 19th International NTZ Workshop on *New Developments in Computational Physics*, ITP, Universität Leipzig, 29. November – 01. December 2018
- Organizer (with M. Weigel, Coventry University, UK) of the CECAM Workshop *New Methods in Monte Carlo Simulations: Parallel, Adaptive, Irreversible*, CECAM-HQ-EPFL, Lausanne, Switzerland, 02.–04. September 2019
- Organizer of the Workshop *CompPhys19* – 20th International NTZ Workshop on *New Developments in Computational Physics*, ITP, Universität Leipzig, 28.–30. November 2019
- Editor "Computational Physics", Central European Journal of Physics, Krakow, Poland
- Member of Editorial Board, Condens. Matter Phys., Lviv, Ukraine
- External Reviewer for Deutsche Forschungsgemeinschaft (DFG); Humboldt-Stiftung (AvH); Studienstiftung des deutschen Volkes; Fond zur Förderung der wissenschaftlichen Forschung (FWF), Österreich; The Royal Society, UK; The Engineering and Physical Sciences Research Council (EPSRC), UK; Israel Science Foundation, Israel; National Science Foundation (NSF), USA; Natural Sciences and Engineering Research Council of Canada (NSERC), Canada; The Jeffress Memorial Trust, Bank of America, Virginia, USA; Universität Mainz, Germany; The University of Warwick, England, UK; Coventry University, England, UK; CECAM, Lausanne, Switzerland
- Referee for Physical Review Letters, Physical Review B, Physical Review E, Journal of Chemical Physics, Europhysics Letters, Physics Letters A, Physics Letters B, The European Physical Journal B, Physica A, Proceedings of the Royal Physical Society, Journal of Physics A, Computer Physics Communications, JSTAT, Canadian Journal of Physics, Condens. Matter Phys., PLOS ONE, New Journal of Physics, International Journal of Modern Physics C

12.29 External Cooperations

Academic

- Institute of Physics, Jagiellonian University, Kraków, Poland
  Prof. Dr. Piotr Białas, Dr. Leszek Bogacz, Prof. Dr. Zdzisław Burda
- CEA/Saclay, Service de Physique Théorique, France
  Dr. Alain Billoire
- Institut für Physik, Universität Mainz, Germany
  Prof. Dr. Kurt Binder, Andreas Nußbaumer, Prof. Dr. Friderike Schmid
- Institut für Theoretische Physik, Universität Heidelberg, Germany
  Dr. Elmar Bittner

- Laboratoire de Physique des Matériaux (UMR CNRS No 7556), Université de Lorraine, Nancy, France
  Prof. Dr. Bertrand Berche, Dr. Christophe Chatelain, Dr. Olivier Collet, Prof. Dr. Malte Henkel, Prof. Dr. Dragi Karevski
- Groupe de Physique des Matériaux (UMR CNRS No 6634), Université de Rouen, France
  Dr. Pierre-Emmanuel Berche
- SUPA, School of Physics and Astronomy, University of Edinburgh, Scotland, UK
  Dr. Richard A. Blythe, Prof. Dr. Martin R. Evans, Dr. Bartłomiej Wacław
- P.J. Šafárik University, Košice, Slovak Republic
  Dr. Michal Borovský
- Istituto Nazionale di Fisica Nucleare, Sezione di Milano-Bicocca, Milano, Italy
  Prof. Dr. Pablo Butera
- Institute of Physical Chemistry and Electrochemistry, Leibniz Universität Hannover, Germany
  Prof. Dr. Jürgen Caro
- Applied Mathematics Research Centre, Coventry University, England, UK
  PD Dr. Christian von Ferber, Dr. Nikolaos G. Fytas, Prof. Dr. Ralph Kenna, Dr. Thierry Platini, Dr. Martin Weigel
- Jülich Supercomputing Centre (JSC), Forschungszentrum Jülich, Germany
  Prof. Dr. Peter Grassberger
- IAC-1, Universität Stuttgart, Germany
  Prof. Dr. Rudolf Hilfer, Prof. Dr. Christian Holm
- Max Planck Institute for Polymer Research, Mainz, Germany
  Dr. Hsiao-Ping Hsu, Prof. Dr. Kurt Kremer
- Complex Systems Division, Department of Theoretical Physics, Lunds Universitet, Lund, Sweden
  Prof. Dr. Anders Irbäck
- Department of Mathematics and the Maxwell Institute for Mathematical Sciences, Heriot-Watt University, Edinburgh, Scotland, UK
  Prof. Dr. Desmond A. Johnston
- Inst. für Theoretische Physik, FU Berlin, Germany
  Prof. Dr. Hagen Kleinert
- Department of Physics, University of Athens, Zografou, Greece
  Prof. Dr. Anastasios Malakis
- Atominstitut, TU Wien, Austria
  Prof. Dr. Harald Markum
- Jacobs Universität Bremen, Germany
  Prof. Dr. Hildegard Meyer-Ortmanns, Darka Labavić
- Institute of Physics, Polish Academy of Sciences, Warsaw, Poland
  Dr. Panagiotis E. Theodorakis

- Applied Mathematics, Universitat Pompeu Fabra, Barcelona, Spain
  Prof. Dr. Ramon Villanova
- CERN (PH-SFT), Geneva, Switzerland
  Dr. Sandro Wenzel
- Department of Engineering of Physics, Ankara University, Ankara, Turkey
  Prof. Dr. Handan Arkın-Olgar, Mustafa Bilsel, Dogukan Hazar Özbey, Buket Taşdizen
- Dept. of Physics, Hacettepe University, Ankara, Turkey
  Prof. Dr. Tarik Çelik, Gökhan Gökoğlu
- Dept. of Physics Engineering, Hacettepe University, Ankara, Turkey
  Prof. Dr. Fatih Yaşar
- Institute for Condensed Matter Physics, National Academy of Sciences, Lviv, Ukraine
  Dr. Viktoria Blavatska, Prof. Dr. Yurij Holovatch
- Yerevan Physics Institute, Yerevan, Armenia
  Prof. Dr. David B. Saakian
- Alikhanyan National Science Laboratory, Yerevan, Armenia
  Prof. Dr. Nerses Ananikyan, Dr. Nikolay Izmailyan
- Landau Institute for Theoretical Physics, Chernogolovka, Russia
  Dr. Lev Yu. Barash, Prof. Dr. Lev N. Shchur
- National Research University Higher School of Economics, Moscow, Russia
  Prof. Dr. Evgeni Burovski, Maria Guskova
- Center for Simulational Physics, The University of Georgia, Athens, USA
  Prof. Dr. Michael Bachmann, Prof. Dr. David P. Landau
- Dept. of Physics, Florida State University, Tallahassee, USA
  Prof. Dr. Bernd A. Berg
- Dept. of Chemistry and Biochemistry, University of Oklahoma, Norman, USA
  Prof. Dr. Ulrich H.E. Hansmann
- Los Alamos National Laboratory, Los Alamos, USA
  Dr. Christoph Junghans
- Dept. of Physics and Astronomy, Texas A&M, College Station, USA
  Prof. Dr. Helmut G. Katzgraber
- Dept. of Physics, Virginia Tech, Blacksburg, USA
  Prof. Dr. Michel Pleimling, Prof. Dr. Royce K.P. Zia
- Physics Department, Carnegie Mellon University, Pittsburgh, USA
  Prof. Dr. Robert H. Swendsen
- University of North Georgia, Dahlonega, USA
  Dr. Thomas Vogel
- Banaras Hindu University, Varanasi, India
  Prof. Dr. Sanjay Kumar
- Jawaharlal Nehru Centre for Advanced Scientific Research (JNCASR), Jakkur, India
  Prof. Dr. Subir K. Das

- School of Physical Sciences, Jawaharlal Nehru University, New Delhi, India
  Manoj Kumar, Prof. Dr. Sanjay Puri
- Department of Physics, Indian Institute of Technology, Hauz Khas, New Delhi, India
  Prof. Dr. Varsha Banerjee
- Computational Chemistry Unit Cell (CCUC), Department of Chemistry, Chulalongkorn University, Bangkok, Thailand
  Prof. Dr. Supot Hannongbua, Dr. Oraphan Saengsawang
- Metallurgy and Materials Science Research Institute (MMRI), Chulalongkorn University, Bangkok, Thailand
  Prof. Dr. Rungroj Chanajaree
- Department of Chemistry, Faculty of Science, Ramkhamhaeng University, Bangkok, Thailand
  Dr. Tatiya Chokbunpiam
- Faculty of Applied Science and Engineering, Khon Kaen University, Nong Khai Campus, Nong Khai, Thailand
  Prof. Dr. Tawun Remsungnen
- Laboratory of Statistical and Computational Physics, Institute of Physics, Academia Sinica, Nankang, Taipei, Taiwan
  Prof. Dr. Chin-Kun Hu
- Zhejiang Institute of Modern Physics, Zhejiang University, Hangzhou, P.R. China
  Prof. Dr. He-Ping Ying, Prof. Dr. Bo Zheng
- The University of Tokyo, Tokyo, Japan
  Prof. Dr. Nobuyasu Ito
- Nagoya University, Nagoya, Japan
  Dr. Tetsuro Nagai, Prof. Dr. Yuko Okamoto

12.30 Publications

Journals

K.S. Austin, M. Marenz, W. Janke: *Efficiencies of Joint Non-Local Update Moves in Monte Carlo Simulations of Coarse-Grained Polymers*, Comput. Phys. Commun. **224**, 222–229 (2018)

N.G. Fytas, J. Zierenberg, P.E. Theodorakis, M. Weigel, W. Janke, A. Malakis: *Universality from Disorder in the Random-Bond Blume-Capel Model*, Phys. Rev. E **97**, 040102(R)-1–6 (2018)

J. Gross, J. Zierenberg, M. Weigel, W. Janke: *Massively Parallel Multicanonical Simulations*, Comput. Phys. Commun. **224**, 387–395 (2018)

W. Janke: *Generalized Ensemble Computer Simulations of Macromolecules*, invited Ising Lecture Notes 2016, in *Order, Disorder and Criticality: Advanced Problems of Phase Transition Theory*, Vol. 5, ed. Y. Holovatch (World Scientific, Singapore, 2018), pp. 173–225

W. Janke, J. Zierenberg: *From Particle Condensation to Polymer Aggregation*, invited Plenary Talk, International Conference *Computer Simulations in Physics and beyond (CSP2017)*, 09.–12. October 2017, Moscow, Russia, J. Phys.: Conf. Ser. **955**, 012003-1–10 (2018)

M. Kumar, R. Kumar, M. Weigel, V. Banerjee, W. Janke, S. Puri: *Approximate Ground States of the Random-Field Potts Model from Graph Cuts*, Phys. Rev. E **97**, 053307-1–10 (2018)

S. Majumder, H. Christiansen, W. Janke: *Scaling Laws During Collapse of a Homopolymer: Lattice Versus Off-Lattice*, J. Phys.: Conf. Ser. **955**, 012008-1–6 (2018)

S. Majumder, S.K. Das, W. Janke: *Universal Finite-Size Scaling Function for Kinetics of Phase Separation in Mixtures with Varying Number of Components*, Phys. Rev. E **98**, 042142-1–13 (2018)

N. Oberthür, J. Groß, W. Janke: *Two-Dimensional Monte Carlo Simulations of Coarse-Grained Poly(3-hexylthiophene) (P3HT) Adsorbed on Striped Substrates*, J. Chem. Phys. **149**, 144903-1–12 (2018)

S. Schnabel, W. Janke: *Distribution of Metastable States of Ising Spin Glasses*, Phys. Rev. B **97**, 174204-1–10 (2018)

F.P. Spitzner, J. Zierenberg, W. Janke: *The Droplet Formation-Dissolution Transition in Different Ensembles: Finite-Size Scaling from Two Perspectives*, SciPost Phys. **5**, 062-1–24 (2018)

R. Stübel, W. Janke: *Finite-Size Scaling of Monte Carlo Simulations for the FCC Ising Antiferromagnet: Effects of the Low-Temperature Phase Degeneracy*, Phys. Rev. B **98**, 174413-1–8 (2018)

in press

L. Shchur, L. Barash, M. Weigel, W. Janke: *Population Annealing and Large Scale Simulations in Statistical Mechanics*, Communications in Computer and Information Science (CCIS) **965**, 354–366 (2019)

H. Christiansen, S. Majumder, W. Janke: *Phase Ordering Kinetics of the Long-Range Ising Model*, Phys. Rev. E **99**, 011301(R)-1–5 (2019)

H. Christiansen, M. Weigel, W. Janke: *Accelerating Molecular Dynamics Simulations with Population Annealing*, Phys. Rev. Lett. **122**, 060602-1–5 (2019)

S. Majumder, H. Christiansen, W. Janke: *Dissipative Dynamics of a Single Polymer in Solution: A Lowe-Andersen Approach*, J. Phys.: Conf. Ser. **1163**, 012072-1–6 (2019)

W. Janke, H. Christiansen, S. Majumder: *Coarsening in the Long-Range Ising Model: Metropolis versus Glauber Criterion*, invited Plenary Talk at the International Conference on *Computer Simulation in Physics and beyond (CSP2018)*, 24.–27. September 2018, Moscow, Russia, J. Phys.: Conf. Ser. **1163**, 012002-1–10 (2019)

H. Christiansen, M. Weigel, W. Janke: *Population Annealing Molecular Dynamics with Adaptive Temperature Steps*, J. Phys.: Conf. Ser. **1163**, 012074-1–6 (2019)

S. Schnabel, W. Janke: *Distribution of Metastable States of Spin Glasses*, in *Computer Simulation Studies in Condensed-Matter Physics XXXI*, eds. D.P. Landau, M. Bachmann, S.P. Lewis, H.-B. Schüttler, J. Phys.: Conf. Ser. **1252**, 012001-1–6 (2019)

S. Majumder, U.H.E. Hansmann, W. Janke: *Pearl-Necklace-Like Local Ordering Drives Polypeptide Collapse*, Macromolecules **52**, 5491–5498 (2019)

Talks

H. Christiansen, S. Majumder, W. Janke: *Efficient Method of Simulating with Long-Range Interactions: The Case of Coarsening in the Ising Model*, DPG Frühjahrstagung 2018, TU Berlin, Germany, 12.–16. March 2018

H. Christiansen, M. Weigel, W. Janke: *Application of Population Annealing to Molecular Dynamics Simulations for Protein Folding*, Annual BuildMoNa Conference 2018, Universität Leipzig, Germany, 20. March 2018

H. Christiansen, M. Weigel, W. Janke: *Population Annealing for Molecular Dynamics Simulations of Protein Folding*, Soft Matter Day 2018, Universität Leipzig, Germany, 06. July 2018

H. Christiansen, S. Majumder, W. Janke: *Coarsening and Ageing in the Long-Range Ising Model*, Statistical Physics Seminar, Université de Lorraine Nancy, France, 15. November 2018

H. Christiansen, M. Weigel, W. Janke: *Accelerating Molecular Dynamics Simulations with Population Annealing*, 19th International NTZ-Workshop on *New Developments in Computational Physics – CompPhys18*, Universität Leipzig, Germany, 29. November – 01. December 2018

W. Janke: *Stochastic Approximation Monte Carlo vs Wang-Landau Algorithm*, 31st Annual CSP Workshop on *Recent Developments in Computer Simulation Studies in Condensed Matter Physics*, The University of Georgia, Athens, Georgia, USA, 19.–23. February 2018

W. Janke: *Thermodynamically Stable Phases for Semiflexible Polymers Characterized by Knots of Specific Topologies*, APS March Meeting, Los Angeles, California, USA, 05.–09. March 2018

W. Janke: *Scaling Behavior of Self-Avoiding Walks on Critical Percolation Clusters in Two to Seven Dimensions from Exact Enumeration*, DPG Frühjahrstagung 2018, TU Berlin, Germany, 11.–16. March 2018

W. Janke: *From Particle Condensation to Polymer Aggregation*,
2nd Changchun and Halle-Leipzig Discussion Seminar on Polymer Science, Universität Halle, Germany, 11. April 2018

W. Janke: *Long-Range Power-Law Correlated Percolation in Two and Three Dimensions*, Conference of the Middle European Cooperation in Statistical Physics – MECO43, Krakow, Poland, 01.–04. May 2018

W. Janke: *Coarsening Dynamics of the Long-Range Ising Model*, invited plenary talk, 3rd International Conference on *Computer Simulations in Physics and beyond (CSP2018)*, National Research University Higher School of Economics, Moscow, Russia, 24.–27. September 2018

R. Kumar: *Computer Simulation Studies of Frustrated Spin Systems*, PhD thesis defence, Coventry University, Coventry, UK, 07. December 2018

S. Majumder, H. Christiansen, W. Janke: *Dissipative Dynamics of a Single Polymer in Solution: A Lowe-Andersen Approach*, 3rd International Conference on *Computer Simulations in Physics and beyond (CSP2018)*, National Research University Higher School of Economics, Moscow, Russia, 24.–27. September 2018

S. Majumder, H. Christiansen, W. Janke: *Dissipative Dynamics of a Single Polymer in Solution: A Lowe-Andersen Approach*, 19th International NTZ-Workshop on *New Developments in Computational Physics – CompPhys18*, Universität Leipzig, Germany, 29. November – 01. December 2018

M. Marenz: *Morphologies of Semiflexible Polymers in Bulk and Spherical Confinement*, PhD thesis defence, Universität Leipzig, Germany, 13. June 2018

M. Mueller: *Nonstandard Finite-Size Effects at Discontinuous Phase Transitions – Degenerate Low-Temperature States and Boundary Conditions*, PhD thesis defence, Universität Leipzig, Germany, 01. February 2018

S. Paul, S.K. Das: *Dimension Dependence of Clustering Dynamics in Models of Ballistic Aggregation and Freely Cooling Granular Gas*, 19th International NTZ-Workshop on *New Developments in Computational Physics – CompPhys18*, Universität Leipzig, Germany, 29. November – 01. December 2018

S. Schnabel, W. Janke: *Distribution of Metastable States of Spin Glasses*, 31st Annual CSP Workshop on *Recent Developments in Computer Simulation Studies in Condensed Matter Physics*, The University of Georgia, Athens, USA, 19.–23. February 2018

S. Schnabel, W. Janke: *Simulation of a Large Polymer with Untruncated Interaction Near the Collapse*, 19th International NTZ-Workshop on *New Developments in Computational Physics – CompPhys18*, Universität Leipzig, Germany, 29. November – 01. December 2018

Posters

H. Christiansen, S. Majumder, W. Janke: *Coarsening in the Long-Range Interacting Ising Model*, Conference of the Middle European Cooperation in Statistical Physics – MECO43, Krakow, Poland, 01.–04. May 2018

J. Gross, J. Zierenberg, M. Weigel, W. Janke: *Massively Parallel Multicanonical Simulations*, DPG Frühjahrstagung 2018, TU Berlin, Germany, 12.–16. March 2018

S. Kazmin, W. Janke: *Critical Exponent ν of the Ising Model in Three Dimensions with Long-Range Correlated Disorder*, 19th International NTZ-Workshop on *New Developments in Computational Physics – CompPhys18*, Universität Leipzig, Germany, 29. November – 01. December 2018

F. Müller, S. Schnabel, W. Janke: *Non-Flat Histogram Techniques for Spin Glasses*, DPG Frühjahrstagung 2018, TU Berlin, Germany, 12.–16. March 2018

F. Müller, M. Ivanov, N. Oberthür, J. Gross, W. Janke: *Nanopatterns of Macromolecules*, 19th International NTZ-Workshop on *New Developments in Computational Physics – CompPhys18*, Universität Leipzig, Germany, 29. November – 01. December 2018

F. Müller, M. Ivanov, N. Oberthür, J. Gross, W. Janke: *Nanopatterns of Macromolecules*, SFB-Transregio 102, 6th Miniworkshop, Universität Halle, Germany, 09. July 2018

F.P. Spitzner, J. Zierenberg, W. Janke: *Two Perspectives on the Droplet Condensation-Evaporation Transition*, DPG Frühjahrstagung 2018, TU Berlin, Germany, 12.–16. March 2018

J. Zierenberg, W. Janke: *Parallel Multicanonical Simulations and their Application*, APS March Meeting, Los Angeles, California, USA, 05.–09. March 2018

12.31 Graduations

Doctorate

- Marco Müller
  Nonstandard Finite-Size Effects at Discontinuous Phase Transitions – Degenerate Low-Temperature States and Boundary Conditions
  01. February 2018
- Martin Marenz
  Morphologies of Semiflexible Polymers in Bulk and Spherical Confinement
  13. June 2018
- Ravinder Kumar
  Computer Simulation Studies of Frustrated Spin Systems
  07. December 2018

Diploma

- Hans-Joachim Lange
  Kollaps von Homopolymeren auf zweidimensionalen Gittern
  29. March 2018

Master

- Simon Schneider
  The 3D Gonihedric Ising Model and its Phase Diagram for $\kappa \neq 0$
  11. January 2018

- David Nicolai Oberthür
  Two-Dimensional Monte Carlo Simulations of Coarse-Grained Poly(3-Hexylthiophene) Polymers on Striped Substrates
  18. January 2018
- Ronja Stübel
  Finite-Size Scaling of Monte Carlo Simulations for the FCC Ising Antiferromagnet: Effects of the Low-Temperature Phase Degeneracy
  27. February 2018
- Lisa Fiedler
  HP Polymers under Investigation – A Coarse-Grained Approach to Study Protein Folding
  07. June 2018
- Dimitrij Tschodu
  Machine Learning the q-State Potts Model
  12. July 2018

Bachelor

- Adrian Häußler
  Exact Enumeration of a Lattice Polymer in Confinement

- Jakob Bürgermeister
  Finite-Size Scaling of the Three-Dimensional Lennard-Jones Gas
  28. June 2018
- Michel Michalkow
  Applications of the Bond-Propagation Algorithm
  05. October 2018

12.32 Guests

- Kseniia Shapovalova
  Far Eastern Federal University, Vladivostok, Russia
  DAAD Michail-Lomonosov-Programm
  01. October 2017 – 31. March 2018
- Dr. Fabian Senf
  Leibniz-Institut für Troposphärenforschung e.V., AG Satellitenfernerkundung
  NTZ/DFH-UFA Seminar (25. January 2018)
  Statistical Physics Approaches for Deep Convection in the Tropical Atmosphere
  25. January 2018
- Prof. Dr. Ulrich H.E. Hansmann
  University of Oklahoma, Norman, USA
  24.–25. April 2018
- Prof. Dr. Jaroslav Ilnytskyi
  ICMP, National Academy of Sciences of Ukraine, Lviv, Ukraine

NTZ/DFH-UFA Colloquium (16. May 2018)
Patchy Ligand Shell Nanoparticles: Modelling and Micronetwork Formation
16. May 2018

- Dr. Martin Weigel
  Coventry University, England, UK
  18.–20. June 2018
- Franz Paul Spitzner
  Max Planck Institute for Dynamics and Self-Organization, Göttingen, Germany
  21.–22. June 2018
- Dr. Johannes Zierenberg
  Max Planck Institute for Dynamics and Self-Organization, Göttingen, Germany
  NTZ/DFH-UFA Seminar (21. June 2018)
  Homeostatic Plasticity and External Input Shape Neural Network Dynamics
  21.–22. June 2018
- Dogukan Hazar Özbey
  Faculty of Engineering, Ankara University, Turkey
  ERASMUS internship
  01. July – 01. September 2018
- Prof. Dr. Subir K. Das
  Jawaharlal Nehru Centre for Advanced Scientific Research, Bangalore, India
  07.–09. October 2018
- Prof. Dr. Peter Grassberger
  FZ Jülich, Germany
  NTZ/DFH-UFA Colloquium (18. October 2018)
  Self-Repelling Biased Walks on Arbitrary Graphs and YAMMI (Yet Another Monte-carlo Method for dummIes
  18.-19. October 2018
- Dr. Elmar Bittner
  Universität Heidelberg, Germany
  29. November – 01. December 2018
- Dr. Nikolaos Fytas
  Coventry University, England, UK
  An Overview of Recent Numerical Results on the Random-Field Ising Model
  29. November – 01. December 2018
- Prof. Dr. Peter Grassberger
  FZ Jülich, Germany
  Does KPZ Describe Pushed Interfaces with Quenched Disorder?
  29. November – 01. December 2018
- Prof. Dr. Ulrich H.E. Hansmann
  University of Oklahoma, Norman, OK, USA
  Conformational Transitions in Prions and Amyloids
  29. November – 01. December 2018
- Prof. Dr. Alexander Hartmann
  Universität Oldenburg, Germany

Phase Transition in Detecting Causal Relationships from Obervational and Interventional Data
29. November – 01. December 2018

- Prof. Dr. Malte Henkel
Université de Lorraine Nancy, France
Axiomatic Construction of Quantum Langevin Equations
29. November – 01. December 2018
- Dr. Hsiao-Ping Hsu
MPI Polymer Research, Mainz, Germany
Indication of Chain Retraction in Highly Entangled Polymer Melts after a Large Step Deformation
29. November – 01. December 2018
- Dr. Fred Hucht
Universität Duisburg-Essen, Germany
A Multiplicative Monte Carlo Rate for Nonequilibrium Dynamics
29. November – 01. December 2018
- Prof. Dr. Ferenc Igloi
Wigner Research Centre, Budapest, Hungary
Quantum Relaxation and Metastability of Lattice Bosons with Cavity-Induced Long-Range Interactions
29. November – 01. December 2018
- Prof. Dr. Nobuyasu Ito
The University of Tokyo, Japan
Simulation of Quantum Computer
29. November – 01. December 2018
- Dr. Nikolay Izmailyan
Alikhanyan National Science Laboratory, Yerevan, Armenia
Specific Heat and Partition Function Zeros for the Dimer Model on the Checkerboard B Lattice: Finite-Size Effects
29. November – 01. December 2018
- Prof. Dr. Desmond A. Johnston
Heriot-Watt University, Edinburgh, Scotland, UK
Fractons
29. November – 01. December 2018
- Prof. Dr. Werner Krauth
Ecole Normale Supérieur, Paris, France
Irreversible, Totally Asymmetric Markov Chains in Statistical Physics
29. November – 01. December 2018
- Dr. Eunsang Lee
Martin-Luther Universität Halle, Germany
Thermodynamics of Supramolecular Polymers with Hydrogen Bonding Ends
29. November – 01. December 2018
- Prof. Dr. Jutta Luettmer-Strathmann
University of Akron, Ohio, USA

Steady State of a Protein-Ligand System in a Temperature Gradient
29. November – 01. December 2018

- Prof. Dr. Arnulf Möbius
IFW Dresden, Germany
29. November – 01. December 2018
- Dr. Gergö Roósz
TU Dresden, Germany
Quench Dynamics of the Disordered Quantum Ising Chain
29. November – 01. December 2018
- Dr. Timur Shakirov
Martin-Luther Universität Halle, Germany
Aggregation of Short Polyethylene Chains
29. November – 01. December 2018
- Paul Spitzner
Max Planck Institute for Dynamics and Self-Organization, Göttingen, Germany
Inferring Dynamical Properties of Subsampled Networks
29. November – 01. December 2018
- Prof. Dr. Mark P. Taylor
Dept. of Physics, Hiram College, USA
Entropy Reduction and Entropy Driven Folding for Confined Polymers
29. November – 01. December 2018
- Dr. Martin Weigel
Coventry University, England, UK
Approximate Ground States of the Random-Field Potts Model from Graph Cuts
29. November – 01. December 2018
- Dr. Johannes Zierenberg
Max Planck Institute for Dynamics and Self-Organization, Göttingen, Germany
Extending the Dynamic Range by an Ensemble of Neural Networks
29. November – 01. December 2018

13

Quantum Field Theory and Gravity

13.1 Introduction

The focus of investigation in the group of Quantum Field Theory and Gravity consists of three main strands: (1) Quantum field theory in curved spacetimes (Prof. Dr. R. Verch, Dr. T.-P. Hack, Dr. M. B. Fröb), (2) mathematical structure of gauge field theories and their quantization (Prof. Dr. G. Rudolph (retired), Dr. M. Schmidt) and (3) quantum fields under the influence of external conditions (PD Dr. M. Bordag).

In quantum field theory in curved spacetimes, several research fields are pursued, such as mathematical and conceptual foundations of local covariant quantum field theory and of the early epoch of cosmology, characterization of locally thermal states and their application to the Unruh effect, and in cosmology; and furthermore some aspects of quantum field theory on spacetimes that contain closed timelike curves. New contributions are directed towards black hole thermodynamics and the measurement problem in connection with local covariance. In the research on gauge theories, one focus is on the topological structure of gauge orbit spaces. A complementary line of research is devoted to a better understanding of gauge field theories on lattices. In quantum field theory under the influence of external conditions, a central research field is the influence of boundaries, as in the Casimir effect, and singular potentials and their role in quantization. Some of the effects studied in this line of research have concrete applications in experiments.

Prof. Dr. Rainer Verch

13.2 Causal pathologies in quantum field theory

R. Verch, J. Tolksdorf*

*Max Planck Institute for Mathematics in the Sciences, Leipzig

Analogue models for states in the presence of closed timelike curves which are popular in quantum information theory are studied within quantum field theory together with J. Tolksdorf (Max Planck Institute for Mathematics in the Sciences).

[1] J. Tolksdorf and R. Verch: *Quantum physics, fields and closed timelike curves: The*

D-CTC condition in quantum field theory, Commun. Math. Phys. **357** (2018) no.1, 319, doi:10.1007/s00220-017-2943-5

13.3 Thermal and non-equilibrium steady states in quantum field theory

R. Verch, T.-P. Hack, N. Pinamonti*, K. Sanders†

*Università degli studi di Genova, Italy
†City University of Dublin, University College, Dublin

Non-equilibrium steady states of the interacting scalar field in four spacetime dimensions have been constructed and investigated with T.-P. Hack.

Constraints for equilibrium states have been investigated together with N. Pinamonti and K. Sanders.

[1] T.-P. Hack and R. Verch: *Non-equilibrium steady states for the interacting Klein-Gordon field in 1+3 dimensions*, preprint, arXiv:1806.00504 [math-ph]
[2] N. Pinamonti, K. Sanders and R. Verch: *Local incompatibility of the microlocal spectrum condition with the KMS property along spacelike directions in quantum field theory on curved spacetime*, preprint, arXiv:1806.02124 [math-ph] (Letters in Mathematical Physics, in press)

13.4 Measurement and covariance in quantum field theory

R. Verch, A. G. Passegger, C. J. Fewster*

*University of York, England

The measurement problem is investigated in the model-independent framework of general local covariant quantum field theory, in the operator algebraic approach. It is, among other desiderata, aimed to shed light on the locality aspects arising in measuring the Hawking effect.

[1] C. J. Fewster and R. Verch: *Quantum fields and local measurements*, preprint, arXiv:1810.06512 [math-ph]

13.5 Quantum field theory and cosmology

R. Verch, M. B. Fröb*, T.-P. Hack, M. Hänsel, I. Khavkine†

*University of York, England
†Czech Academy of Sciences, Prague, Czech Republic

Fundamental aspects of stability in cosmology (pertaining to solutions to the semiclassical Friedmann equations) are under investigation together with M. Hänsel.

The localisation, infrared properties and completeness of observables in the theory of inflationary perturbations are investigated by M. Fröb, T.-P. Hack and I. Khavkine (Czech Academy of Sciences) [1].

[1] M. B. Fröb, T.-P. Hack and I. Khavkine: *Approaches to linear local gauge-invariant observables in inflationary cosmologies*, Class. Quant. Grav. **35** (2018) no. 11, 115002, doi:10.1088/1361-6382/aabcb7

13.6 Perturbative quantum gravity and cosmology

M. B. Fröb

Non-local gauge-invariant observables in perturbative quantum gravity are proposed for spacetimes of high symmetry, such as flat space or cosmological (inflationary) backgrounds. The perturbative expansion of these observables is considered, and one-loop quantum corrections due to gravitons are determined. Physical consequences for the theory of inflation are discussed.

[1] M. B. Fröb: *One-loop quantum gravitational backreaction on the local Hubble rate*, Class. Quant. Grav. **36** (2019) no. 09, 095010, doi:10.1088/1361-6382/ab10fb

13.7 Stability of black holes and dynamical Hawking-radiation

R. Verch, T.-P. Hack, F. Kurpicz, N. Pinamonti*

*Università degli studi di Genova, Italy

The dynamical stability of black holes is investigated by considering the backreaction of quantum fields on non-stationary black hole backgrounds. A related project is the analysis of Hawking-radiation of quantum fields on non-stationary black hole backgrounds which model evaporating black holes.

13.8 Structure of the gauge orbit space and study of gauge theoretical models

G. Rudolph, T. Diez E. Fuchs, H. Grundling*, J. Huebschmann†, P. Jarvis‡, J. Kijowski§, M. Schmidt

*University of Sydney, Australia
†Université de Lille, France
‡University of Tasmania, Hobart, Australia
§University of Warsaw, Poland

1. The investigation of gauge theories in the Hamiltonian approach on finite lattices with emphasis on the role of nongeneric strata was continued.

   As a further step towards a generalization of the results of [1] on stratified Kähler quantization to larger lattices, based on the defining relations derived in [2], the multiplicative structure of the algebra of quasicharacters for SU(2) has been analyzed. Using this, the Hilbert space costratification of SU(2)-quantum gauge theory on a finite spatial lattice in the Hamiltonian approach has been constructed [3].

2. Based on [4] and [5], in collaboration with H. Grundling, the investigation of the structure of the algebra of observables and its representations for specific models of quantum lattice gauge theory in terms of gauge invariant quantities was continued.

3. Investigation of infinite-dimensional symplectic structures and their application in gauge theories has been continued, with emphasis on

   - an extension of the classical slice theorem to inifinite dimensions [6],
   - the study of a new variational principle for relativistic field theories with symmetries [7],
   - the extension of classical singular symplectic cotangent bundle reduction theory to infinite dimensions [8],
   - the study of the Yang-Mills moduli space [9].

4. The investigation of the deformation quantization and homological reduction of classical lattice gauge theory in collaboration with Markus Pflaum (U Boulder) has been continued.

[1] J. Huebschmann, G. Rudolph, M. Schmidt: Commun. Math. Phys. **286**, Nr. 2 (2009) 459–494
[2] F. Fürstenberg, G. Rudolph, M. Schmidt: *Defining relations for the orbit type strata of* SU(2)*-lattice gauge models*, J. Geom. Phys. **119** (2017) 66–81
[3] E. Fuchs, P. Jarvis, G. Rudolph, M. Schmidt: *The Hilbert space costratification for the orbit type strata of* SU(2)*-lattice gauge theory*, J. Math. Phys. **59** (2018) 083505
[4] J. Kijowski, G. Rudolph: J. Math. Phys. **43** (2002) 1796
J. Kijowski, G. Rudolph: J. Math. Phys. **46** (2005) 032303; Rep. Math. Phys. **55** (2005) 199
P. Jarvis, J. Kijowski, G. Rudolph: J. Phys. A **38** (2005) 5359
[5] H. Grundling, G. Rudolph: Commun. Math. Phys. **318** (2013) 717 ; Commun. Math. Phys. **349** (2016) 1163
[6] T. Diez, G. Rudolph: *Slice theorem and orbit type stratification in infinite dimensions*, arXiv:1812.04698, Differ. Geom. Appl. (in print)

[7] T. Diez, G. Rudolph: *Clebsch-variational principle and geometric constraint analysis of relativistic field theories*, arXiv:1812.04659
[8] T. Diez, G. Rudolph: *Singular symplectic cotangent bundle reduction of gauge field theory*, arXiv:1812.04707
[9] T. Diez, J. Huebschmann: *Yang-Mills moduli spaces over an orientable closed surface via Fréchet reduction*, J. Geom. Phs. **132** (2018) 393

13.9 Dispersion forces and dissipation

M. Bordag

With increasing precision of Casimir and van der Waals force measurements, the question of the influence of dissipation becomes increasingly interesting. Sources of dissipation are primarily ohmic losses in the interacting bodies. The intriguing question is how such losses will influence the groundstate of a quantum system, which by definition is the lowest state (in energy) and cannot loose energy any further. In order to gain understanding in this question we consider a typical setup from first principles by coupling the internal degrees of freedom of the interacting bodies to heat bathes. We derive a representation of the free energy as an integral over real frequencies, which can be viewed as an generalization of the 'remarkable formula' introduced by Ford et al. 1985. As application we calculate free energy and entropy for a one dimensional periodic chain of delta and delta prime functions. Especially we consider the transition to Matsubara representation for a spectrum with allowed and forbidden bands.

13.10 Funding

Stability in cosmology
M. Hänsel
Universität Leipzig

Measurement and covariance in quantum field theory
A.G. Passegger
IMPRS fellowship, MPI-MIS

Stability of black holes
F. Kurpicz
IMPRS fellowship, MPI-MIS

Symplektische Reduktion im Unendlichdimensionalen mit Anwendung auf das Cauchy-Problem der Yang-Mills Gleichung
T. Diez
IMPRS fellowship, MPI-MIS

Quanteneffekte klassischer Phasenraumsingularitäten in Gittereichmodellen
M. Schmidt
DFG project SCHM 1652/2-1

13.11 Organizational Duties

Prof. Dr. Rainer Verch

- Ansprechpartner, Forschungsprofilbereich "Mathematical and Computational Sciences", Universität Leipzig
- Berufungsbeauftragter des Rektorats
- Book Series Editor, Fundamental Theories of Physics (Springer)
- Referee for DFG, AvH Stiftung, Studienstiftung d. Deutschen Volkes
- Referee: Ann. H. Poincaré, Commun. Math. Phys., Found. Phys., Class. Quantum Grav., J. Geom. Phys., SIGMA, Proc. Roy. Soc.

Prof. Dr. G. Rudolph

- Referee: Class. Quant. Grav., J. Math. Phys., J. Geom. Phys., J. Phys. A, Rep. Math. Phys., Commun. Math. Phys.
- Referee for the German Research Council (DFG) and the Alexander von Humboldt Foundation

Priv.-Doz. Dr. Michael Bordag

- Referee: J. Phys. A, Phys. Rev. D, J. Math. Phys.

Dr. T.-P. Hack

- Referee for AvH Stiftung
- Referee: Ann. H. Poincaré, Class. Quantum Grav., Phys. Lett. B, Gen. Rel. Grav., Math. Rev. (AMS)

Dr. M. B. Fröb

- Referee: Phys. Rev. D, Gen. Rel. Grav, J. High Energy Phys., Class. Quantum Grav., Int. J. Mod. Phys. D, Ann. H. Poincaré

Dr. Matthias Schmidt

- Referee: J. Phys. A and Int. J. Mod. Phys. A

13.12 External Cooperations

Academic

- Mathematisches Institut, Universität Göttingen
  Prof. Dr. D. Bahns
- Dipartimento di Matematica, Università di Trento, Italy
  Prof. Dr. Romeo Brunetti
- Institut f. Theoretische Physik, Universität Göttingen
  Prof. Dr. D. Buchholz
- Department of Mathematics, University of York, England
  Prof. Dr. C. J. Fewster
- II. Institut f. Theoretische Physik, Universität Hamburg
  Prof. Dr. K. Fredenhagen

- Department of Mathematics, University of York, England
  Dr. A. Higuchi
- Department of Mathematics, Czech Academy of Sciences, Prague, Czech Republic
  Dr. I. Khavkine
- Department of Mathematics, University of York, England
  Dr. K. Rejzner
- Dipartimento di Matematica, Università degli studi di Genova, Italy
  Prof. Dr. N. Pinamonti
- School of Mathematical Sciences, City University Dublin, Ireland
  Dr. Ko Sanders
- Max Planck Institute for Mathematics in the Sciences, Leipzig
  PD Dr. J. Tolkstorf
- Institut für Mathematik, Universität Paderborn
  Prof. Dr. Ch. Fleischhack
- Polish Academy of Sciences, Center for Theoretical Physics, Warsaw, Poland
  Prof. Dr. J. Kijowski, Dr. Sz. Charzynski
- University of Boulder, Colorado, USA
  Prof. Dr. Markus Pflaum
- University of Tasmania, Hobart, Australia
  Prof. Dr. P. Jarvis
- Université des Sciences et Technologies de Lille, France
  Prof. Dr. J. Huebschmann
- University of New South Wales, Sydney, Australia
  Prof. H. Grundling
- National University, Dnepropetrovsk, Ukraine
  Prof. V. Skalozub
- Central Astronomical Observatory at Pulkovo of the Russian Academy of Science, Russia
  Prof. V. M. Mostepanenko
- Baylor University, Texas, USA
  Prof. K. Kirsten
- VIK Dubna, Russia
  Dr. V. Nesterenko, Dr. I. Pirozhenko
- Departamento de Fisica Teórica Atómica y Óptica, Universidad de Valladolid, Spain
  Prof. Dr. J. M. Muñoz-Castañeda

13.13 Publications

Journals

J. Tolksdorf, R. Verch: *Quantum physics, fields and closed timelike curves: The D-CTC condition in quantum field theory*, Commun. Math. Phys. **357** (2018) no.1, 319

M.B. Fröb, T.P. Hack, I. Khavkine: *Approaches to linear local gauge-invariant observables in inflationary cosmologies*, Class. Quant. Grav. **35** (2018) no.11, 115002

M.B. Fröb: *One-loop quantum gravitational backreaction on the local Hubble rate*, Class. Quant. Grav. **36** (2019) no. 09, 095010

E. Fuchs, P. Jarvis, G. Rudolph, M. Schmidt: *The Hilbert space costratification for the orbit type strata of* SU(2)*-lattice gauge theory*, J. Math. Phys. **59** (2018) 083505

T. Diez, J. Huebschmann: *Yang-Mills moduli spaces over an orientable closed surface via Fréchet reduction*, J. Geom. Phs. **132** (2018) 393–414

M. Bordag: *Free energy and entropy for thin sheets*, Phys. Rev. D **98** (2018) no.8, 085010

M. Bordag, K. Kirsten: *On the entropy of a spherical plasma shell*, J. Phys. A **51** (2018) no.45, 455001

M. Bordag, I.G. Pirozhenko: *Dispersion Forces Between Fields Confined to Half Spaces*, Symmetry **10** (2018) no.3, 74

M. Bordag, G.L. Klimchitskaya, V.M. Mostepanenko: *Nonperturbative theory of atom-surface interaction: corrections at short separations*, J. Phys.: Condens. Matter, **30** (2018) no.5, 055003

M. Bordag: *Vacuum and Thermal Energies for Two Oscillators Interacting Through A Field*, Theor. Math. Phys. **195** (2018) no.3, 834

in press

N. Pinamonti, K. Sanders, R. Verch: *Local incompatibility of the microlocal spectrum condition with the KMS property along spacelike directions in quantum field theory on curved spacetime*, Lett. Math. Phys. (2019)
arXiv:1806.02124 [math-ph]

T. Diez, G. Rudolph: *Slice theorem and orbit type stratification in infinite dimensions*, Differ. Geom. Appl. (2019)
arXiv:1812.04698 [math-DG]

M. Bordag, J.M. Muñoz-Castañeda, L. Santamaría-Sanz: *Vacuum energy for generalised Dirac combs at* $T = 0$, Front. Phys. (2019)
arXiv:1812.09022 [math-ph]

preprints

C.J. Fewster, R. Verch: *Quantum fields and local measurements*
arXiv:1810.06512 [math-ph]

K. Fredenhagen, T.P. Hack, N. Pinamonti: *Thermodynamics of Quantum Fields in Non-stationary Spacetimes*
arXiv:1809.08557 [gr-qc]

T.P. Hack, R. Verch: *Non-equilibrium steady states for the interacting Klein-Gordon field in 1+3 dimensions*
arXiv:1806.00504 [math-ph]

M. Bordag, V. Skalozub: *Photon dispersion relations in A_0-background*
arXiv:1809.08117 [hep-ph]

M. Bordag: *Entropy in some simple one-dimensional configurations*
arXiv:1807.10354 [quant-ph]

Talks

Prof. Dr. R. Verch: Invited talk, Conference "Progress and Visions in Quantum Theory in View of Gravity", MPI-MIS, Leipzig, 01-05 October 2018

Prof. Dr. R. Verch: Invited talk, RTG Workshop "Methods of Gravity", ZARM, Universität Bremen, 10-12 September 2018

Prof. Dr. R. Verch: Invited Lecturer, Summer School "The black hole information paradox", RTG "Methods of Gravity", Universität Bremen, 03-07 September 2018

Prof. Dr. R. Verch: Invited Workshop participation, BIRS Workshop 18w5015 "Physics and Mathematics of Quantum Field Theory", Banff International Research Center, Canada, 29 July - 3 August 2018

Prof. Dr. R. Verch: Invited research collaboration, Prof. C. J. Fewster, Dep. of Mathematics, University of York, England, 02-06 July 2018

Prof. Dr. R. Verch: Invited talk, Conference "AQFT: Where operator algebra meets microlocal analysis", Cortona, Italy, 04-08 June 2018

Priv.-Doz. Dr. M. Bordag: JINR, Dubna, Russia, "Effective $\gamma\gamma G$ vertex and scattering of photons in quark-gluon plasma", 17 April 2018

Priv.-Doz. Dr. M. Bordag: NSU, Trondheim, Norway, "On the entropy of a spherical plasma shell", 11 June 2018

Priv.-Doz. Dr. M. Bordag: ITP Leipzig, "On the entropy of a spherical plasma shell", 25 June 2018

Priv.-Doz. Dr. M. Bordag: University St. Petersburg, Russia, "On the entropy of a spherical plasma shell", 25 August 2018

Priv.-Doz. Dr. M. Bordag: University of Kaliningrad, Russia, "On the entropy of a spherical plasma shell", 17 September 2018

Dr. M. Fröb: Invited talk "New results for the operator product expansion", BIRS Workshop 18w5015 "Physics and Mathematics of Quantum Field Theory", Banff International Research Center, Canada, 29 July - 3 August 2018

Dr. M. Fröb: Invited research collaboration, Dr. I. Khavkine, Czech Academy of Sciences, Prague, Czech Republic, 11-14 November 2018

Dr. M. Fröb: Invited talk "Algebraic structures in the perturbative quantization of gauge theories", Seminar of the Czech Academy of Sciences, Prague, Czech Republic, 14 November 2018

13.14 Graduations

Master

- Sebastian Knappe
  Quantum Constraints and Costratification of Gauge Theories
  January 2018
- Maik Wessling
  Analytical properties of states of low energy
  August 2018
- Dorian Nothaaß
  Dirac quantum inequalities and wormhole spacetimes
  September 2018

13.15 Guests

- Prof. Dr. Nicola Pinamonti
  Università degli studi di Genova, Italy
  1 November 2017 - 28 February 2018
  Funding: DAAD
- Prof. Dr. C. J. Fewster
  University of York, England
  1-5 October 2018
- Prof. Dr. Peter Jarvis
  University of Tasmania, Hobart, Australia
  October/November 2018 Funding: Alexander von Humboldt Foundation

14

Theory of Condensed Matter

14.1 Introduction

Research of the division is predominantly devoted to nonequilibrium phenomena and pattern formation in soft, biological, and active matter. A common theme is the presence of strong fluctuations and stochastic dynamics on the microscale. The emergence of the mesoscopic structure and transport is to be understood ("Soft Mesoscopics"). Modern analytic methods of statistical physics and computer simulations complement and stimulate each other. Cooperations with mathematicians, theoretical and experimental physicists, geologists, biologists, and medical researchers in Germany, Europe and around the world are well established. In particular, related experimental work is currently in progress at the Peter Debye Institute.

The studied phenomena range from structure formation by wind-blown sand resulting in ripples and dunes, through non-equilibrium dynamics of hot nanoparticles, microswimmers, proteins and polymers, droplet-size distributions growing in the bulk or on surfaces, stochastic models for transport in cells, the viscoelastic and inelastic mechanics of the cytoskeleton under strong external fields, etc. The applied methods comprise a broad statistical mechanics toolbox including dynamical-systems theory, discrete, continuous-time and delay stochastic processes, liquid-state theories, fluctuating hydrodynamics, various systematic coarse-graining techniques, massively parallel numerical simulations on CPUs and GPUs, and even some experiments (e.g. on droplets growth) and field work (e.g. with colleagues from geoscience).

Klaus Kroy, Jürgen Vollmer

14.2 Aeolian sand sorting and megaripple formation

M. Lämmel, A. Meiwald, H. Yizhaq[*], H. Tsoar[†], I. Katra[†], K. Kroy

[*]Department of Solar Energy and Environmental Physics, Blaustein Institutes for Desert Research, Ben-Gurion University of the Negev, Sede Boqer Campus, Beér Sheva, Israel
[†]Department of Geography and Environmental Development, Ben-Gurion University of the Negev, Beér Sheva, Israel

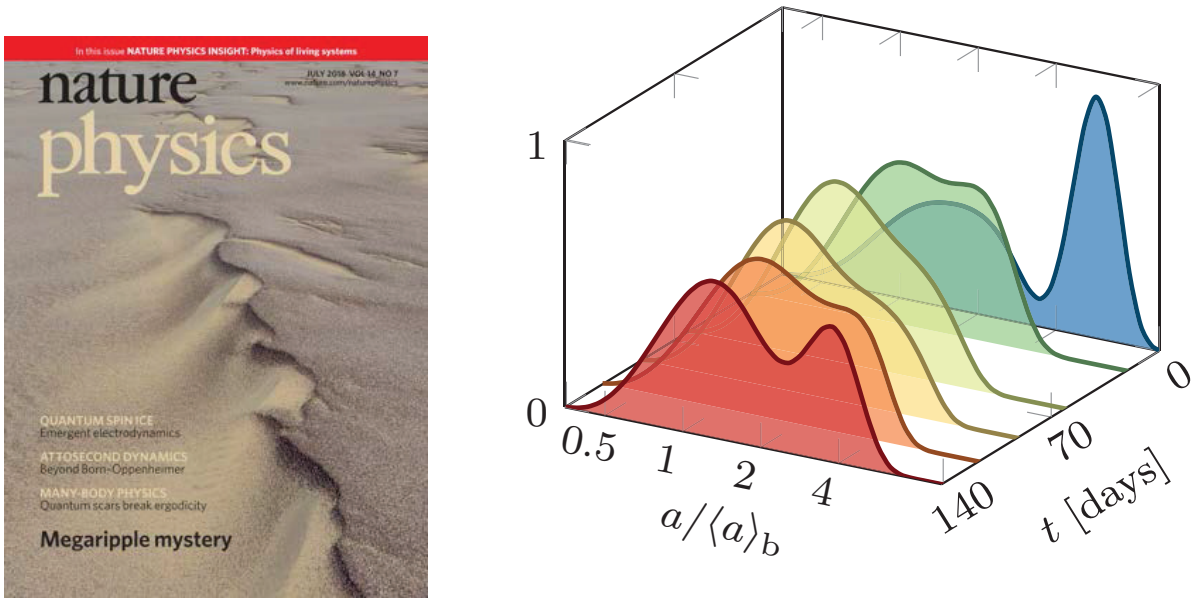

Figure 14.1: *Left panel:* Our megaripple mystery [1] received a lot of attention in various popular science portals. *Right panel:* Our theory predicts that megaripple growth depends sensitively on the co-evolving bimodal grain-size distribution and that megaripples are actually morphologically better characterized as (highly volatile) mini-dunes made from the coarse grains.

Sand is blown across beaches and deserts by turbulent winds. This seemingly chaotic process creates two dominant bedforms: decametre-scale dunes and centimetre-scale ripples, but hardly anything in between. By the very same process, grains are constantly sorted. Smaller grains advance faster, while heavier grains trail behind. Here, we argue that, under erosive condi- tions, sand sorting and structure formation can conspire to create distinct bedforms in the 'forbidden wavelength gap' between aeolian ripples and dunes. These so-called megaripples are shown to co-evolve with an unusual, predominantly bimodal grain-size distribution. Combining theory and field measurements, we develop a mechanistic understanding of their formation, shape and migration, as well as their cyclic ageing, renewal and sedimentary memory, in terms of the intermittent wind statistics. Our results demonstrate that megaripples exhibit close similarities to dunes and can indeed be mechanistically characterized as a special type of ('reptation') dune. See Fig. 14.1.

[1] M. Lämmel *et al.*: Nat. Phys. **14** (5), 759-765 (2018)

14.3 Polarization of Janus swimmers with spatially heterogeneous activity

S. Auschra, N. Söker*, P. Cervenak, V. Holubec†, M. Heber, F. Chichos*, K. Kroy

*Peter-Debye Institute for Soft Matter Physics, University of Leipzig

†Charles University, Faculty of Mathematics and Physics, Department of Macromolecular Physics, V Holešovičkách 2, CZ-180 00 Praha, Czech Republic

Janus particles fuelled by laser heating are paradigmatic autophoretic microswimmers. Their dynamics under constant driving has been well characterized [1–3]. We consider situations in which the particle's propulsion strength fluctuates in space, due to a variable fuel supply.

Specifically, we analyze a Janus sphere's spatial and orientational distribution under the influence of a simple prescribed spatial activity variation $v(r) = v_0\Theta(r-a)$, with the propulsion speed v_0 and the Heaviside function $\Theta(x)$, as depicted in the left panel of Fig. 14.2. A simple 2-state run-and-tumble process [4] captures the observed features,

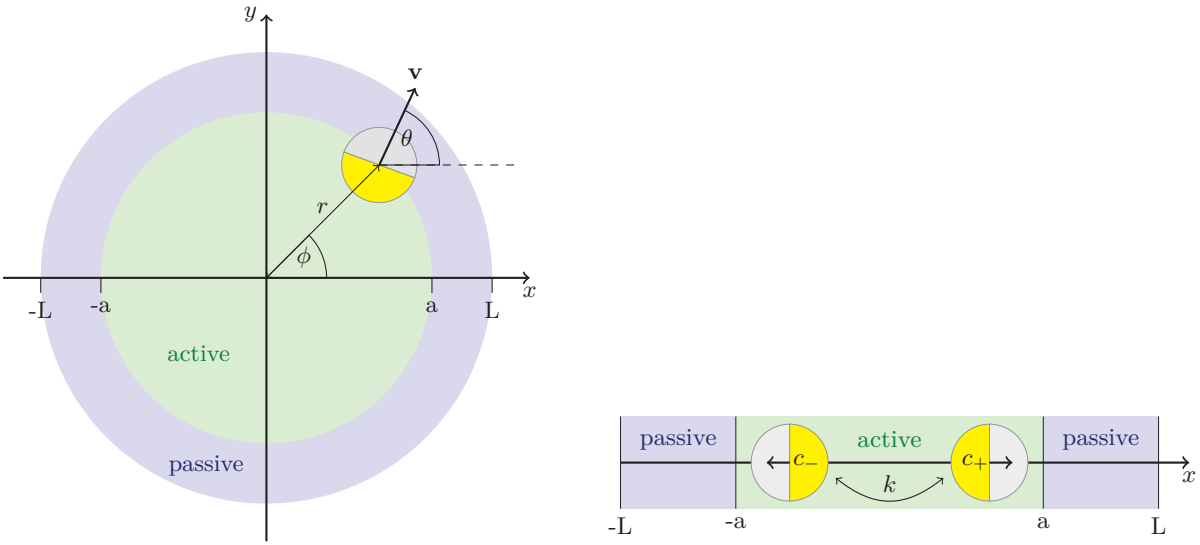

Figure 14.2: *Left panel:* General setup of a Janus sphere confined in two spatial dimensions. Depending on the particle's position (r, ϕ) it either propels actively at a velocity v if the swimmer is found inside the green region, otherwise it behaves like an ordinary Brownian particle. The orientation of the Janus sphere is described by the angle θ. *Right panel:* General setup of the 2-state model. The Janus swimmer translates only along the x-direction. Moreover, we allow for only two orientational states, denoted by the probability densities $c_\pm$ for each state. The rate of change at which the orientation flips is given by k. Again, the particle is driven actively only within the green region. Otherwise is just undergoes pure thermal diffusion.

qualitatively, and provides some analytical insights. As sketched in the right panel of Fig. 14.2 we consider a single Janus sphere confined to one spatial dimension and allow for only two directional states denoted by $c_+(x)$ and $c_-(x)$. From the continuity equations for $c_\pm(x)$ in the steady state the following set of equations for the *density* $\rho \equiv c_+ + c_-$ and the *polarization* $P \equiv c_+ - c_-$ can be derived in dimensionless form

$$\rho'(x) = \mathcal{A}\Theta(a-x)P(x) \tag{14.1}$$

$$P''(x) = \left[1 + \mathcal{A}^2\Theta^2(a-x)\right]P(x) - \mathcal{A}\delta(a-x)\rho(x), \tag{14.2}$$

where $\delta(x)$ denotes the Dirac delta function, and the emerging activity parameter $\mathcal{A}$ is defined as $v_0/(2kD)$, with the diffusion coefficient D and the flipping rate k of the particle orientation. This set of equations can be solved within the active $(x \leq a)$ and

passive region ($a < x \leq L$) separately. The respective solutions are then matched by appropriate conditions. The analytical solutions for the density ρ and the (normalized) polarization P/ρ for moderate and relatively high activity parameters are depicted in Fig. 14.3. We find depletion in regions of higher activity and polarization in activity

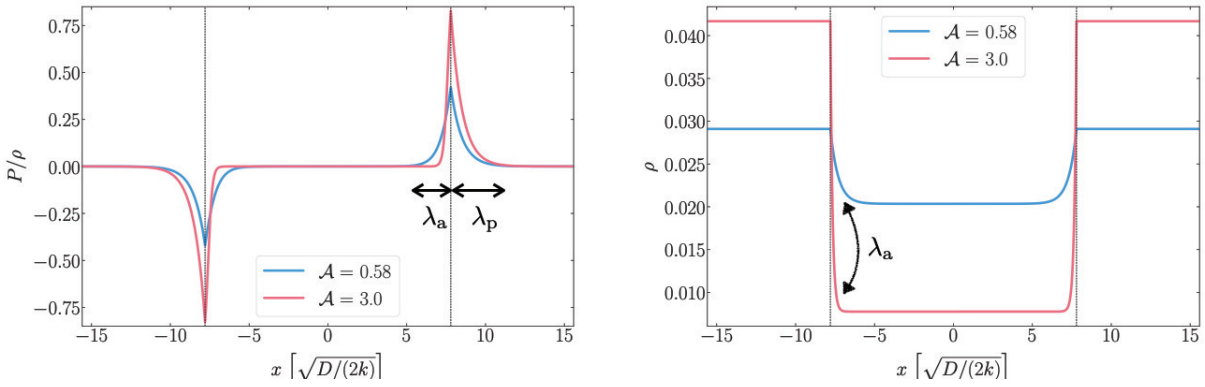

Figure 14.3: The left panel depicts the analytical solution of the 2-state model for the (normalized) polarization P/ρ and the right panel shows the corresponding density ρ. Both quantities are plotted for a gentle and a relatively high activity parameter $\mathcal{A}$ in the scenario of the simple activity profile $v(x) = v_0\Theta(a - x)$. The polarization's and densitiy's characteristic decay lengths λ_p and λ_a are given in Eq. (14.3).

gradients. The associated characteristic length scales λ_a and λ_p of the polarization and density inhomogeneities are given by

$$\lambda_p = \sqrt{\frac{D}{2k}}, \quad \frac{\lambda_p}{\lambda_a} = \sqrt{1 + \frac{v_0^2}{2kD}}. \tag{14.3}$$

Using Brownian dynamics simulations and a powerful numerical solver for Fokker-Planck equations [5], we can extend the simple 2-state model to higher spatial dimensions and allow for continuous rotational diffusion. With that, we can qualitatively reproduce the experimental observations.

[1] A. Bregulla, F. Cichos: Faraday Discuss. **184**, 381-391 (2015)
[2] H. Jiang, N. Yoshinaga, M. Sano: PRL **105**, 268302 (2010)
[3] A. Würger: Rep. Prog. Phys. **73**, 126601 (2010)
[4] M. J. Schnitzer: Phys. Rev. E **48**, 2553-2568 (1993)
[5] V. Holubec, K. Kroy, S. Steffenoni: "Physically consistent numerical solver for time-dependent Fokker-Planck equations", arXiv:1804.01285 (in press)

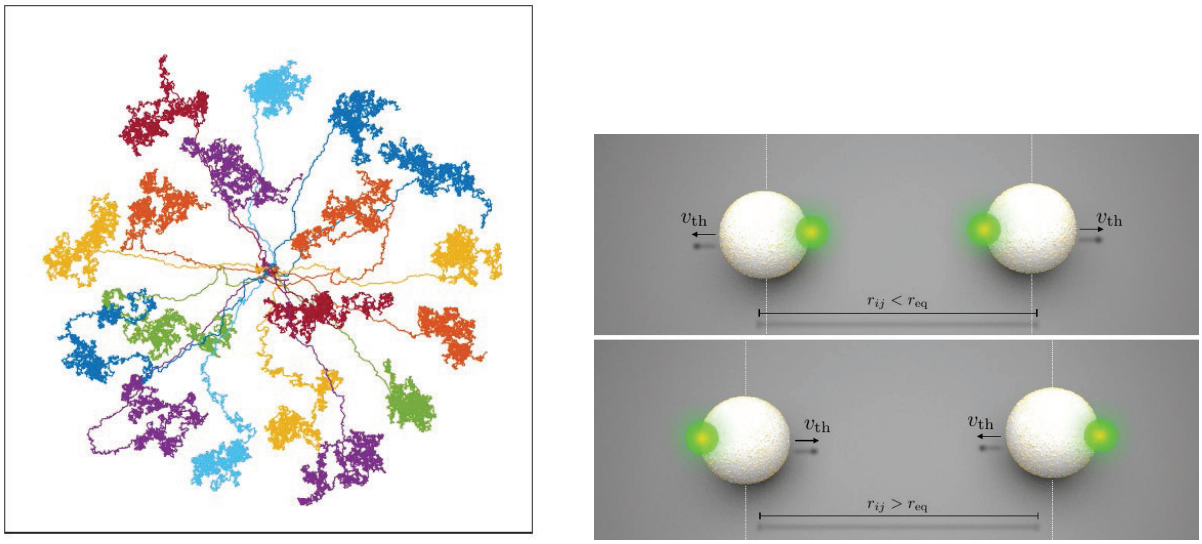

Figure 14.4: *Left panel:* A single stochastic trajectory of N = 18 particles. At long times, the particles form molecular-like, vibrating structures that become unstable for large delays. *Right panel:* Brownian particles used in the experiments of [1] are symmetrically decorated by gold nanoparticles. If they become asymmetrically heated by a laser, the particles start to move due to arising thermophoretic forces.

14.4 Brownian Molecules Formed by Delayed Harmonic Interactions

D. Geiß, V. Holubec*,

*Charles University, Faculty of Mathematics and Physics, Department of Macromolecular Physics, V Holešovičkách 2, CZ-180 00 Praha, Czech Republic

A time-delayed response of individual living organisms to information exchange within groups or swarms leads to the formation of complex collective behaviors. A recent experimental setup [1], employing synthetic microswimmers, allows to realize and study such behavior in a controlled way, in the lab. Motivated by these experiments, we study a system of N Brownian particles interacting via a harmonic, time-delayed potential. For N < 4, we model the problem analytically by linear stochastic delay differential equations, and for N > 3 we use Brownian dynamics simulations. The particles form molecular-like structures which become increasingly unstable with the number of particles and the length of the delay. We evaluate the entropy fluxes in the system and develop an appropriate time-dependent transition state theory [2] to characterize transitions between different isomers of the molecules.

[1] U. Khadka, V. Holubec, H. Yang, F. Cichos: Nat. Commun. **9**:3864 (2018)
[2] J. T. Bullerjahn, S. Sturm, K. Kroy: Nat. Commun. **5**:4463 (2014)

14.5 Bottom-up Inelastic Cell Mechanics

C. Huster, K. Kroy

In our modelling approach to the mechanics of cytoskeletal networks we combine two important concepts in bio-mechanics. First, the bottom-up approach to biomechanics [1] that traces back the mechanical response of living matter to its macromolecular constituents. And secondly, the idea that the mechanics of biological systems transcends the viscoelastic dynamics of semiflexible polymers (at least) by one very essential ingredient, namely the slow (un-) binding dynamics of weak reversible crosslinkers [2].

A general framework for inelastic biomechnics is developed which can be used for interpreting existing inelastic models as well as for the construction of new models. Further, the results of experiments using different techniques and probing different systems ranging from single biopolymers, over polymer networks to cells and cellular aggregates can be analyzed and compared. We thereby aim at a coherent minimalistic description of the universal rheological properties of biomaterials in the liner and non-linear range. In the framework simple models for semiflexible polymers and weak reversible bonds can be combined systematically using interaction rules. A description on the level of the mesoscopic building blocks can than be related to a model on the continuum level employing integration and distribution rules. The developed models are currently used to interpret experimental data measured in various biophysics labs. One example is illustrated

[1] A. R. Bausch, K. Kroy: Nat. Phys. **2**, 231–238 (2006)
[2] M. Gralka, K. Kroy: Biochim. Biophys. Acta Mol. Cell Res. **11**, 3025–3037 (2015)

14.6 Physically consistent numerical solver for time-dependent Fokker-Planck equations

V. Holubec*, K. Kroy, S. Steffenoni

*Charles University, Faculty of Mathematics and Physics, Department of Macromolecular Physics, V Holešovičkách 2, CZ-180 00 Praha, Czech Republic

Many natural phenomena exhibit a timescale separation between slow and fast degrees of freedom. The variables varying slowly in space or time can then be characterized by a self-contained coarse-grained dynamics, which is for not too extreme coarse-graining perceptibly perturbed by fluctuations arising from the noisy dynamics of the fast variables. The Fokker-Planck equation (FPE) represents a most comprehensive description of such time-separated phenomena. It predicts not only the average dynamics of the slow variables but directly addresses, in a technically manageable way, their complete probability distribution, which includes the relevant information about the fluctuations of the slow degrees of freedom induced by the fast ones. To achieve this, all of the slow variables need to be resolved explicitly in a so-called Markovian description, such that the remaining fast variables evolve without perceptible memory of the past dynamics.

We describe a simple thermodynamically consistent matrix numerical method for solving over-damped FPEs with time-dependent coefficients [1]. Not only can the method resolve the transition and long-time behavior of probability distributions described by the FPE, but it is also naturally applicable to computations of moment-generating functions and large-deviation functions for various types of functionals

defined along the trajectories of the stochastic process described by the FPE. The key strategy is to approximate the FPE by a master equation with transition rates in configuration space that obey a local detailed balance condition for arbitrary discretization. Its time-dependent solution is obtained by a direct computation of the time-ordered exponential, representing the propagator of the FPE, by summing over all possible paths in the discretized space. The method thus not only preserves positivity and normalization of the solutions but also yields a physically reasonable total entropy production, regardless of the discretization. To demonstrate the validity of the method and to exemplify its potential for applications, we compare it against Brownian-dynamics simulations of a heat engine based on an active Brownian particle trapped in a time-dependent quartic potential.

[1] V. Holubec, K. Kroy, S. Steffenoni: "Physically consistent numerical solver for time-dependent Fokker-Planck equations", arXiv:1804.01285, in the press for Physical Review E

14.7 Cycling tames power fluctuations near optimum efficiency

V. Holubec*, A. Ryabov*

*Charles University, Faculty of Mathematics and Physics, Department of Macromolecular Physics, V Holešovičkách 2, CZ-180 00 Praha, Czech Republic

According to the laws of thermodynamics, no heat engine can beat the efficiency of a Carnot cycle. This efficiency traditionally comes with vanishing power output and practical designs, optimized for power, generally achieve far less. Recently, various strategies to obtain Carnot's efficiency at large power were proposed. However, a thermodynamic uncertainty relation implies that steady-state heat engines can operate in this regime only at the cost of large fluctuations that render them immensely unreliable. Here, we demonstrate that this unfortunate trade-off can be overcome by designs operating cyclically under quasi-static conditions. The experimentally relevant yet exactly solvable model of an overdamped Brownian heat engine is used to illustrate the formal result. Our study highlights that work in cyclic heat engines and that in quasi-static ones are different stochastic processes.

[1] V. Holubec, A. Ryabov: Phys. Rev. Lett. **121** (12), 120601 (2018)

14.8 Diffusing Up the Hill: Dynamics and Equipartition in Highly Unstable Systems

M. Šiler*, O. Brzobohatý*, P. Jákl*, A. Ryabov†, V. Holubec†, P. Zemánek*, R. Filip‡

*Institute of Scientific Instruments of the Czech Academy of Sciences, Královopolská 147, 612 64 Brno, Czech Republic
†Charles University, Faculty of Mathematics and Physics, Department of Macromolecular Physics, V Holešovičkách 2, 180 00 Praha 8, Czech Republic
‡Department of Optics, Palacký University, 17. listopadu 1192/12, 771 46 Olomouc, Czech Republic

Stochastic motion of particles in a highly unstable potential generates a number of diverging trajectories leading to undefined statistical moments of the particle position. This makes experiments challenging and breaks down a standard statistical analysis of unstable mechanical processes and their applications. A newly proposed approach takes advantage of the local characteristics of the most probable particle motion instead of the divergent averages. We experimentally verify its theoretical predictions for a Brownian particle moving near an inflection in a highly unstable cubic optical potential. The most-likely position of the particle atypically shifts against the force despite the trajectories diverge in the opposite direction. The local uncertainty around the most-likely position saturates even for strong diffusion and enables well-resolved position detection. Remarkably, the measured particle distribution quickly converges to the quasi-stationary one with the same atypical shift for different initial particle positions. The demonstrated experimental confirmation of the theoretical predictions approves the utility of local characteristics for highly unstable systems which can be exploited in thermodynamic processes to uncover energetics of unstable systems.

[1] M. Šiler *et al.*: Phys. Rev. Lett. **121** (23), 230601 (2018)

14.9 Brownian motion surviving in unstable cubic potential and Maxwell's demon behind

L. Ornigotti*, A. Ryabov†, V. Holubec†, R. Filip*

*Palacký University, Department of Optics, 17. listopadu 1192/12, 771 46 Olomouc, Czech Republic
†Charles University, Faculty of Mathematics and Physics, Department of Macromolecular Physics, V Holešovičkách 2, 180 00 Praha 8, Czech Republic

Trajectories of an overdamped particle in a highly unstable potential diverge so rapidly, that the variance of position grows much faster than its mean. Description of the dynamics by moments is therefore not informative. Instead, we propose and analyze local directly measurable characteristics, which overcome this limitation. We discuss the most probable particle position (position of the maximum of the probability density) and the local uncertainty in an unstable cubic potential, both in the transient regime and in the long-time limit. The maximum shifts against the acting force as a function of time and temperature. Simultaneously, the local uncertainty does not increase faster than the observable shift. In the long-time limit, the probability density naturally attains a quasi-stationary form. We explain this process as a stabilization via the measurement-feedback mechanism, the Maxwell demon, which works as an entropy

pump. Rules for measurement and feedback naturally arise from basic properties of the unstable dynamics. Observed thermally induced effects are inherent in unstable systems. Their detailed understanding will stimulate the development of stochastic engines and amplifiers and later, their quantum counterparts.

[1] L. Ornigotti, A. Ryabov, V. Holubec, R. Filip: Phys. Rev. E **97** (3), 032127 (2018)

14.10 Effects of noise-induced coherence on the performance of quantum absorption refrigerators

V. Holubec[*], T. Novotný[†]

[*]Charles University, Faculty of Mathematics and Physics, Department of Macromolecular Physics, V Holešovičkách 2, CZ-180 00 Praha, Czech Republic
[†]Department of Condensed Matter Physics, Faculty of Mathematics and Physics, Charles University, Ke Karlovu 5, CZ-121 16 Prague, Czech Republic

We study two models of quantum absorption refrigerators with the main focus on discerning the role of noise-induced coherence on their thermodynamic performance. Analogously to the previous studies on quantum heat engines we find the increase in the cooling power due to the mechanism of noise-induced coherence. We formulate conditions imposed on the microscopic parameters of the models under which they can be equivalently described by classical stochastic processes and compare the performance of the two classes of fridges (effectively classical vs. truly quantum). We find that the enhanced performance is observed already for the effectively classical systems, with no significant qualitative change in the quantum cases, which suggests that the noise-induced-coherence enhancement mechanism is caused by static interference phenomena.

[1] V. Holubec, T. Novotný: J. Low Temp. Phys. **192** (3-4), 147-168 (2018)

14.11 Anomalous shift of the most probable position of a particle in an unstable optically created potential

M. Šiler[*], L. Ornigotti[†], O. Brzobohatý[*], P. Jákl[*], A. Ryabov[‡], V. Holubec[‡], P. Zemánek[*], R. Filip[†]

[*]Institute of Scientific Instruments of the Czech Academy of Sciences, Královopolská 147, 612 64 Brno, Czech Republic
[†]Department of Optics, Palacký University, 17. listopadu 1192/12, 771 46 Olomouc, Czech Republic
[‡]Charles University, Faculty of Mathematics and Physics, Department of Macromolecular Physics, V Holešovičkách 2, 180 00 Praha 8, Czech Republic

Description of stochastic motion of a particle in an unstable potential is a challenging topic since even small number of diverging trajectories leads to undefined statistic moments of particle position. This breaks down the standard statistical analysis of unstable mechanical processes and their applications. Therefore, we employ a different approach taking advantage of the local characteristics of the most-likely particle motion instead of the average motion. We experimentally verify theoretical predictions for a Brownian particle moving near an inflection in a cubic optical potential. Notably, the most-likely position of the particle atypically shifts against the force despite the trajectories diverge in opposite direction. In this work we study the influence of the analytical formula used for quantification of the most likely particle position parameters in the case where only limited number of trajectories is available.

[1] M. Šiler *et al.*: Proc. SPIE 10976, 21st Czech-Polish-Slovak Optical Conference on Wave and Quantum Aspects of Contemporary Optics, 109760E (2018)

14.12 Anomalous Scaling Exponents for Breath Figures

D. Dernbach, L. Stricker*, J. Vollmer

*Polymer Physics, ETH Zürich

The analysis of the size distribution of droplets condensing on a substrate (breath figures) is a test ground for scaling theories. In [1] we showed that a faithful description of these distributions must explicitly deal with the growth mechanisms of the droplets. This finding established a gateway connecting nucleation and growth of the smallest droplets on surfaces to gross features of the evolution of the droplet size distribution. In this work we observed that that droplet growth involves an anomalous scaling exponent that is not universal. The behaviour was confirmed also in a numerical model for three-dimensional droplets on a one-dimensional substrate (fiber) [2]. In Leipzig we are presently exploring the connection between the anomalous scaling exponent of the scaling theory and scaling exponents that characterize fractal properties of the arrangement of the droplets on the substrate. Establishing an exact solution of the latter models will allow us to settle issues about the origin of the non-universality. In parallel to this theoretical work, we restart experiments where the droplets evolution is tracked by video microscopy and batch image processing.

[1] J. Blaschke, T. Lapp, B. Hof, and J. Vollmer: Phys. Ref. Lett. **109**, 068701 (2012).
[2] L. Stricker, J. Vollmer: Phys. Rev. E **92**, 042406 (2015).

14.13 Stochastic Thermodynamics for Markov processes

A. Wachtel*, A. Gamba†, M. Zamparo†, B. Conti‡, L. Rondoni‡, J. Vollmer

*Physics and Materials Science Research Unit, University of Luxembourg
†Dept. of Applied Science and Technology, Politechnico di Torino

‡Dept. of Mathematical Sciences, Politecnico di Torino

Unlike macroscopic engines, the molecular machinery of living cells is strongly affected by fluctuations. Stochastic thermodynamics uses Markovian jump processes to model the random transitions between the chemical and configurational states of these biological macromolecules. We have developed a theoretical framework [1] providing a simple algorithm for the determination of macroscopic currents and correlation integrals of arbitrary fluctuating currents. It also allows us to explicitly calculate cumulants to any given order. The effectiveness of the model was demonstrated by discussing energy conversion and nonequilibrium response in different models for the molecular motor kinesin [2]. With A. Wachtel we succeeded to employ graph theory in order to explicitly work out all derivatives that were still present in formal expressions in Refs. [1, 2]. With M. Zamparo and A. Gamba I worked out an application to domain drift and diffusion in cell polarization processses. With B. Conti and L. Rondoni the results have been extended to deal with time-discrete Markov processes. The latter step is crucial to make contact to ergodic theory in order to discuss the microscopic foundations of stochastic thermodynamics.

[1] A. Wachtel, J. Vollmer, and B. Altaner: Phys. Rev. E **92**, 042132 (2015)
[2] B. Altaner, A. Wachtel, and J. Vollmer: Phys. Rev. E **92**, 042133 (2015)

14.14 Anomalous Transport

L. Rondoni*, M. Tayyab*, C. Mejédá-Monasterio†, C. Giberti‡, J. Vollmer

*Dept. of Mathematical Sciences, Politecnico di Torino
†Technical University of Madrid
‡Dept. of Science and Engineering Methods, Univ. Modena Reggio E.

The Slicer Map (SM) is a one-dimensional non-chaotic dynamical system that shows sub-, super-, and normal diffusion as a function of its control parameter. The Lévy-Lorentz gas (LLg) is a random walk on the line in which the scatterers are randomly distributed according to a Lévy-stable probability distribution. Rondoni and coworkers established [1] that both model share the same scaling of the moments of the position distributions. In Ref. [2] we derive analytic expressions for the position-position correlations of the SM and, on the ground of this result, we formulate some conjectures about the asymptotic behaviour of position-position correlations of the LLg, for which the information in the literature is minimal. The numerically estimated position-position correlations of the Lévy-Lorentz show a remarkable agreement with the conjectured asymptotic scaling. In collaboration with C. Mejía-Monasterio we checked that the correspondence can be extended to a deal with the moments and position-autocorrelations to a considerable number of billiards that show anomalous transport in settings with and without chaotic motion. We hence conjecture that the correspondence hints towards a universality class of anomalous diffusion [3].

[1] L. Salari, L. Rondoni, C. Giberti, and R. Klages: Chaos **25**, 073113 (2015).

[2] C. Giberti, L. Rondoni, M. Tayyab, and J. Vollmer: "Equivalence of position-position auto-correlations in the Slicer Map and the Lévy-Lorentz gas", Nonlinearity (to appear 2019), arXiv:1709.04980.
[3] J. Vollmer, L. Rondoni, M. Tayyab, C. Giberti, and C. Mejía-Monasterio: "On a universality class of anomalous diffusion", arXiv:1903.12500.

14.15 Funding

DFG "Non-isothermal Brownian Motion"
K. Kroy
DFG, KR 3381/4-1

DFG SPP 1726 "Thermophoretic Propulsion and Interaction of Hot Brownian Swimmers"
K. Kroy in collaboration with F. Cichos
DFG, KR 3381/5-1

Humboldt Foundation "Optimal control of information-driven hot micro-swimmers"
Viktor Holubec (Humboldt postdoc position)

Czech Science Foundation "Stochastic thermodynamics of molecular systems: from classical to quantum"
Viktor Holubec, 17-06716S

International Max Planck Research Schools (IMPRS) "Mathematics in the Sciences"
Daniel Gein

International Max Planck Research Schools (IMPRS) "Mathematics in the Sciences"
Stefano Steffenoni

14.16 Organizational Duties

K. Kroy
- Member of the graduation grants committee of the University
- Study counselor for physics
- Member of the Faculty Council
- Scientific Member of the International Max Planck Research School "Mathematics in the Sciences"
- Editorial Board Member at Scientific Reports
- Referee for Nature Commun., Phys. Rev. Lett., Phys. Rev. E, J. Chem. Phys., Biophysical Journal, Physica A, and various funding organizations

Jürgen Vollmer
- Member of the Lehrteam
- Board member of the "Dynamics Days Europe" Advisory Board
- Associate Editor of Frontiers in Interdisciplinary Physics

14.17 External Cooperations

Academic

- Ben-Gurion University of the Negev, Israel
  Prof. Dr. Hezi Yizhaq, Prof. Dr. Itzhak Katra, Prof. Haim Tsoar
- Max-Planck Institut für Kolloid- und Grenzflächenforschung, Potsdam-Golm
  Dr. Kerstin Blank
- Max-Planck Institut des Lichts, Erlangen und Biotechnology Center TU Dresden
  Prof. Dr. Jochen Guck
- Institute for Experimental Physics - Ulm University
  Prof. Dr. Kay-E. Gottschalk
- University of Luxembourg
  Dr. Artur Wachtel
- ETH Zürich
  Dr. Laura Stricker
- Politecnico di Torino
  Prof. Dr. Lamberto Rondoni and collaborators, Prof. Dr. Andrea Gamba and collaborators
- Technical University of Madrid
  Prof. Dr. Carlos Mejédá-Monasterio
- Universitá di Modena e Reggio E.
  Prof. Dr. Claudio Giberti

14.18 Publications

Journals

M. Lämmel, A. Meiwald, H. Yizhaq, H. Tsoar, I. Katra, K. Kroy: *Aeolian sand sorting and megaripple formation*, Nat. Phys. **14**(5), 759-765, 2018

T. Golde, C. Huster, M. Glaser, T. Händler, H. Herrmann, J. Käs, J. Schnauß: *Glassy dynamics in composite biopolymer networks*, Soft Matter **14**(39), 7970–7978, 2018

C. Huster, K. Nagel, S. Spange, J. Prehl: *A reactive bond fluctuation model (rBFM) for twin polymerization: Comparison of simulated morphologies with experimental data*, Chem. Phys. Lett. **713**, 145–148, 2018

V. Holubec, A. Ryabov: *Cycling tames power fluctuations near optimum efficiency*, Phys. Rev. Lett. **121** (23), 120601, 2018

M. Šiler, L. Ornigotti, O. Brzobohatý, P. Jákl, A. Ryabov, V. Holubec, P. Zemánek, R. Filip: *Diffusing Up the Hill: Dynamics and Equipartition in Highly Unstable Systems*, Phys. Rev. Lett. **121** (12), 120601, 2018

L. Ornigotti, A. Ryabov, V. Holubec, R. Filip: *Brownian motion surviving in unstable cubic potential and Maxwell's demon behind*, Phys. Rev. E **97** (3), 032127, 2018

V. Holubec,T. Novotný: *Effects of noise-induced coherence on the performance of quantum absorption refrigerators*, J. Low Temp. Phys. **192** (3-4), 147-168, 2018

Books

K. Kroy, F. Cichos: *Hot Brownian Motion*, In: A. Bunde, J. Caro, J. Kärger, G. Vogl (eds) *Diffusive Spreading in Nature, Technology and Society*. Springer, Cham, 2018

in press

V. Holubec, K. Kroy, S. Steffenoni: *Physically consistent numerical solver for time-dependent Fokker-Planck equations*, arXiv:1804.01285, in the press for Physical Review E

J. Sapudom, L. Kalbitzer, X. Wu, S. Martin, K. Kroy, T. Pompe: *Fibril bending stiffness of 3D collagen matrices instructs spreading and clustering of invasive and non-invasive breast cancer cells*, in the press for Biomaterials

C. Giberti, L. Rondoni, M. Tayyab, J. Vollmer: *Equivalence of position-position auto-correlations in the Slicer Map and the Lévy-Lorentz gas*, Nonlinearity (2019) [arXiv:1709.04980]

D. Geiss, R. Lilow, F, Fabis, M. Bartelmann: *Resummed Kinetic Field Theory: Using Mesoscopic Particle Hydrodynamics to Describe Baryonic Matter in a Cosmological Framework*, JCAP05(2019)017, [arXiv:1811.07741]

Talks

V. Holubec: *Effects of noise-induced coherence on the performance of quantum absorption refrigerators*, TAMU-PQE Follow-on Workshop, College Station, Texas, USA, January 2018

K. Kroy: *Why is the desert not flat? The interesting physics of windblown sand*, Hauptvortrag, Leibniz Network MMS, IOM Leipzig, Germany, February 2018

V. Holubec: *Diverging, but negligible power at Carnot efficiency: theory and experiment*, DPG Spring Meeting 2018, Berlin, Germany, April 2018

K. Kroy: *Aeolian sand sorting and megaripple formation*, EGU General Assembly, Wien, Austria, April 2018

K. Kroy: *Why is the desert not flat? The interesting physics of windblown sand*, Physikalisches Kolloquium, Universität Greifswald, Germany, May 2018

K. Kroy: *Soft dynamic landscapes emerging from turbulent particulate flows*, NECD Conference, Potsdam, Germany, October 2018

K. Kroy: *Hot Brownian particles for your nonequilibrium-statistical-mechanics playground*, Theorie-Kolloquium, Humboldt Universität Berlin, Germany, November 2018

K. Kroy: *Warum ist die Wüste nicht flach? Physisch-Geographisches Kolloquium*, Universität Leipzig, Germany, Dezember 2018

Posters

C. Huster and K. Kroy: *Inelastic bottom-up cell mechanics*, Anual BuildMoNa Converence, Leipzig, Germany, March 2018

14.19 Graduations

Master

- Katharina Tholen
  A Survey on nonlinear Microrheology
  August 2018
- Benjamin Streitz
  Discrete-Element Simulation Framework For Adherent Cells
  September 2018

Bachelor

- Wei Liu
  Effektive Temperaturen geheizter Januskugeln
  June 2018
- Markus Heber
  Simulation Brownscher Dynamik von Heissen Janusschwimmern in Inhomogenen Medien
  December 2018

14.20 Guests

- Prof. Dr. Karel Netocny
  Institute of Physics AS CR
  06.03.2018
- Dr. Muhammad Tayyab
  Politecnico di Torino
  April 2018
- Prof. Dr. Lamberto Rondoni
  Politecnico di Torino
  June 2018
- Prof. Dr. Thomas Ihle
  University of Greifswald
  05.07.2018
- Prof. Dr. Ido Regev
  Ben Gurion University of the Negev
  August 2018

- Beatrice Conti
  Politecnico di Torino
  December 2018

15

Theory of Elementary Particles

15.1 Introduction

Our group is interested in the properties of matter at very high energies (small scales) or under other extreme conditions, covering a broad variety of research topics ranging from the study of elementary particles and their properties to the study of quantized matter fields in the presence of strong gravitational fields. The underlying theme of our research and teaching activity is the theory of such quantized fields in its various manifestations, and applications, including:

1. Quantum fields on discrete spacetimes (lattices) and their numerical and theoretical study
2. Quantum fields on curved spacetimes and in the presence of background (gauge) fields
3. Applications of ideas from integrable systems to the study of quantum gauge theories
4. Dualities and relation with classical General Relativity

Quantum field theories on lattices are discretized counterparts of continuum models describing elementary particles in quantum field theoretic models such as the standard model of particle physics. They were introduced in order to investigate certain non-perturbative features of these models in a controlled approximation. A substantial fraction of the current work being done in this area are numerical simulations and the development of new theoretical methods leading to improved numerical schemes. Our group is participating in this endeavor.

Quantum gauge theories such as the standard model can also be treated as continuum field theories, and can thereby be studied using for instance by perturbative methods. The task of finding improved ways of handling perturbative calculations is an important aspect of quantum field theory and is actively pursued in our group from a variety of different viewpoints, including operator product expansion techniques, methods from integrability, renormalization group methods, holographic ideas, and more.

We also pursue the quest to generalize quantum field theory to curved spacetime (QFTCS), which is inspired by the ideas and principles of General Relativity. On account

of its classical treatment of the metric, QFTCS cannot be a fundamental theory of nature. However, QFTCS is expected to provide an accurate description of quantum phenomena in a regime where the effects of curved spacetime may be significant, but effects of quantum gravity itself may be neglected. In particular, it is expected that QFTCS should be applicable to the description of quantum phenomena occurring in the early universe and near (and inside of) black holes, provided that one does not attempt to describe phenomena occurring so near to singularities that curvatures reach Planckian scales and the quantum nature of the spacetime metric would have to be taken into account. Quantum field theory in curved spacetimes has provided important physical insights into the quantum nature of black holes, indicating that they should, if left alone, gradually evaporate due to the emission of quanta whose energies are distributed thermally at the famous Hawking temperature.

In parallel to direct approaches to quantum field theory via perturbative, or numerical, techniques, there are now also more indirect approaches via so-called "holographic dualities", or methods from "operator algebras". Holographic dualities typically establish a connection with a quantum field theory living on some sort of boundary of a space and a classical, gravitational, theory living in the higher dimensional space itself. This type of duality is believed to probe rather different regimes of quantum field theory (strong coupling, "large N"), and is hence complementary to other methods. At the technical level, it motivates studies into higher dimensional gravity theories, which turn out to have a rather rich mathematical structure. The study of such structures is another research topic in our group. Operator algebraic methods become useful e.g. when trying to apply concepts from quantum information theory in the context of quantum field theories, such as entanglement, relative entropies etc.

We are very happy that in autumn 2018 Daniela Cadamuro joined our group with her DFG funded Emmy-Noether project "The quantum stress-energy tensor", in which she investigates the properties of the stress-energy tensor in interacting quantum fields, in particular w.r.t. quantum energy inequalities, Section 15.13. This complements very well our work on the stress-energy tensor in conformal field theory, Section 15.3, and on QFTCS. See https://home.uni-leipzig.de/tet/?page_id=2507 for more information on the project.

More information under https://home.uni-leipzig.de/tet/

Prof. S. Hollands

15.2 Higher dimensional black holes

S. Hollands V. Toomani

The idea that there might exist extra dimensions beyond the evident three space and one time dimension is an old one which was already brought up in the early days of General Relativity. It has since become a major ingredient in many fundamental theories of nature, not only those with an eye on a "unification of forces", but also more recently "holographic theories" wherein the introduction of a higher dimensional geometry is in some sense only a formal trick in order to study theories on the boundary [1].

A concrete and sensible starting point is to consider theories of the same general type as General Relativity, such as e.g. various Kaluza-Klein, or supergravity theories,

on a higher dimensional manifold, and to ask about the nature of their solutions. Of particular interest are solutions describing black holes, and among these, stationary black hole solutions are of special interest, because they are expected to be the end point of the (classical) evolution of a dynamical black hole spacetime.

The task is then to classify, ideally, all stationary black hole spacetimes satisfying the vacuum Einstein equations on a n-dimensional manifold, with say, asymptotically flat (or alternatively Kaluza-Klein) boundary conditions at infinity. In $n = 4$ dimensions the answer to this question is provided by the famous black hole uniqueness theorems, see e.g. [2] and references. These theorems state that the only such solutions are provided by the Kerr-family of metrics, and these are completely specified by their angular momentum and mass. Unfortunately, already in $n = 5$, the analogous statement is demonstrably false, as there exist different asymptotically flat black holes—having event horizons of different topology—with the same values of the angular momenta and charges[1]. Nevertheless, one might hope that a classification is still possible if a number of further invariants of the solutions are also incorporated. This turns out to be possible [4, 5], at least if one restricts attention to solutions which are not only stationary, but moreover have a comparable amount of symmetry as the Kerr-family, namely the symmetry group. The purpose of this project is to sharpen this classification using the powerful methods of integrable models (associated linear problems, inverse scattering method) combined with geometric inequalities of the type developed in [6].

In fact, in a setting where the symmetry group is abelian and has $n - 2$ dimensions, the metric will, in a sense, depend non-trivially only on two remaining coordinates, and the Einstein equations will consequently reduce to a coupled system of PDE's in these variables. These equations happen to be of a type to which the powerful methods of integrability are available (see e.g. [7]), and our current goal is to investigate the consequences one can draw using such methods to the classification problem of black holes in higher dimensions. The starting point of such investigations is a dimensional reduction to a 2-dimensional manifold $\hat{M}$ of orbits [4, 5], see fig. 15.1.

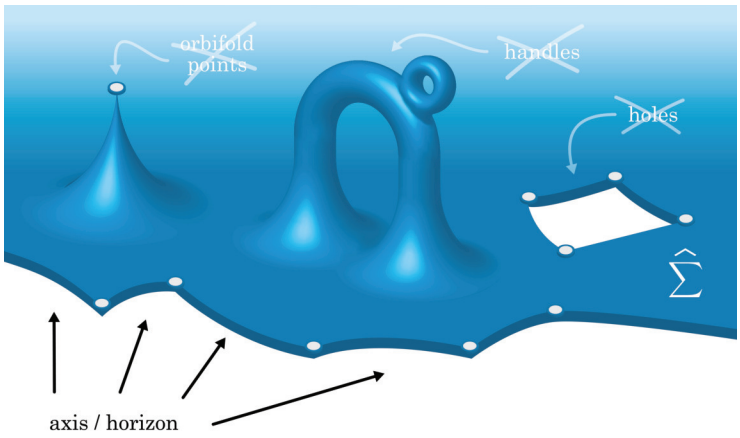

Figure 15.1: Orbit space $\hat{M} = \hat{\Sigma}$.

Then one must study the dynamical fields and their boundary conditions on such

[1]For a review of exact black hole solutions in higher dimensions, see e.g. [3].

a manifold using the Einstein equations and their integrable structure to gain further information.

[1] J. M. Maldacena, "The Large N limit of superconformal field theories and supergravity," Int. J. Theor. Phys. **38**, 1113 (1999) [Adv. Theor. Math. Phys. **2**, 231 (1998)] doi:10.1023/A:1026654312961, 10.4310/ATMP.1998.v2.n2.a1
[2] P. T. Chrusciel, J. Lopes Costa and M. Heusler, "Stationary Black Holes: Uniqueness and Beyond," Living Rev. Rel. **15**, 7 (2012) doi:10.12942/lrr-2012-7 [arXiv:1205.6112 [gr-qc]].
[3] R. Emparan and H. S. Reall, "Black Holes in Higher Dimensions," Living Rev. Rel. **11**, 6 (2008)
[4] Hollands, S. and Yazadjiev, S.: "Uniqueness theorem for 5-dimensional black holes with two axial Killing fields," Commun. Math. Phys. **283**, 749 (2008)
[5] S. Hollands and S. Yazadjiev, "A Uniqueness theorem for stationary Kaluza-Klein black holes," Commun. Math. Phys. **302**, 631 (2011) doi:10.1007/s00220-010-1176-7 [arXiv:0812.3036 [gr-qc]].
[6] S. Hollands, "Horizon area-angular momentum inequality in higher dimensional spacetimes," Class. Quant. Grav. **29**, 065006 (2012) doi:10.1088/0264-9381/29/6/065006 [arXiv:1110.5814 [gr-qc]].
[7] G. Neugebauer and R. Meinel, "Progress in relativistic gravitational theory using the inverse scattering method," J. Math. Phys. **44**, 3407 (2003) doi:10.1063/1.1590419 [gr-qc/0304086].

15.3 Probability distributions for the quantum stress tensor

C.J. Fewster* S. Hollands

*University of York

The vacuum state – or any other state of finite energy – is not an eigenstate of any smeared (averaged) local quantum field. The outcomes (spectral values) of repeated measurements of that averaged local quantum field are therefore distributed according to a non-trivial probability distribution. In [1], we have studied probability distributions for the smeared stress tensor in two dimensional conformal quantum field theory. One accomplishment of the paper was to provide a new general method for this task based on the famous conformal welding construction in complex analysis. Secondly, we extended a known moment generating function method of Fewster, Ford and Roman [2]. Our analysis provided new explicit probability distributions for the smeared stress tensor in the vacuum for various infinite classes of smearing functions. All of these turned out to be given in the end by a shifted Gamma distribution, pointing, perhaps, at a distinguished role of this distribution in the problem at hand.

Being more specific, the averaged "chiral half" of the energy density operator is

$$\Theta(f) = \int_{-\infty}^{\infty} \Theta(u) f(u)\, \mathrm{d}u, \tag{15.1}$$

where $\Theta(u)$ is the energy density operator on a light-ray (i.e., more properly speaking, the generator of translations in a light-like direction). Considering as a smearing function e.g. a Gaussian, $f(u) = \mathrm{e}^{-\tau^2 u^2}/(\tau\sqrt{\pi})$ one can consider repeated measurements of $\Theta(f)$ in the vacuum state. The results are statistically distributed according to a probability distribution that will be called the *vacuum distribution of* $\Theta(f)$. The moments of this distribution can be organized into generating functions that are constrained by conformal Ward identities. At least in principle this permits the moment generating function and probability distribution to be obtained in closed form. In [2] it was shown (for Gaussian f) that the vacuum distribution has the *shifted Gamma probability density*

$$\mathrm{d}\nu_f(\lambda) = \rho(\lambda;\alpha,\beta,\sigma)\mathrm{d}\lambda := \vartheta(\lambda+\sigma)\frac{\beta^\alpha(\lambda+\sigma)^{\alpha-1}}{\Gamma(\alpha)}\exp(-\beta(\lambda+\sigma))\,\mathrm{d}\lambda, \tag{15.2}$$

where ϑ is the Heaviside function and the parameters α, β and σ are

$$\alpha = \frac{c}{24}, \qquad \beta = \pi\tau^2, \qquad \sigma = \frac{c}{24\pi\tau^2}. \tag{15.3}$$

Evidently, the vacuum distribution is supported in the half-line $[-\sigma,\infty)$; on general grounds [2], the infimum of the support is equal to the optimal quantum energy inequality (QEI) [3] for $\Theta(f)$,

(15.4)

with the infimum taken over all physically acceptable normalized states Ψ.

In our paper [1] , a more general and geometric method for computing the probability distribution was introduced, and concrete forms of that distribution were found for several families of smearing functions f in the case of the vacuum state, highest weight states. However, our method also applies to other states such as thermal states and gives for general f an algorithm for determining the probability distribution that can be implemented numerically.

[1] C. J. Fewster and S. Hollands, "Probability distributions for the stress tensor in conformal field theories," Lett. Math. Phys. **109**, no. 4, 747 (2019) doi:10.1007/s11005-018-1124-6

[2] C. J. Fewster, L. H. Ford and T. A. Roman, "Probability distributions of smeared quantum stress tensors," Phys. Rev. D **81**, 121901 (2010) doi:10.1103/PhysRevD.81.121901 [arXiv:1004.0179 [quant-ph]].

[3] C. J. Fewster and S. Hollands, "Quantum energy inequalities in two-dimensional conformal field theory," Rev. Math. Phys. **17**, 577 (2005) doi:10.1142/S0129055X05002406 [math-ph/0412028].

15.4 Quantum information theory and quantum fields

K. Sanders*, S. Hollands, O. Islam†

*Dublin City University
†Leeds U

A typical state of a quantum field theory (QFT) exhibits entanglement between spacelike separated regions. In Minkowski space this is due to the Reeh-Schlieder theorem, which has partial extensions to curved spacetimes [2]. In order to quantify the amount of entanglement of a state between two given regions, one may adopt the notion of entanglement entropy as used in quantum mechanics (QM). Computing entanglement entropies is difficult, even for free fields [3], but the results show some interesting features. E.g., when space is divided into two regions by a boundary surface S, the entanglement entropy of the vacuum is divergent and the coefficient of the leading divergent order is proportional to the area of S ("area law").

Unfortunately, the existing computations have a number of drawbacks: they often only work for ground states (using path integrals), and they introduce regulators and subtle computational tricks whose physical and mathematical meaning is sometimes unclear (e.g. the replica method). In our group, we investigate quantum information theoretic questions about QFT using operator algebraic techniques in general and the "algebraic approach to QFT" pioneered by Haag and collaborators. The language of operator algebras is particularly natural in this context because many concepts from quantum information theory have a natural formulation in operator algebraic terms, such as the notion of a channel, local operation, reduced (sub-) system, various entropies, entanglement measures, and many other topics, see [4] for an exposition of some of these ideas to a theoretical physics audience.

Among other topics, we are interested in the following questions [6, 7]:

- Definition and study of entanglement measures, in particular ones based on the relative entropy of Araki [1]. This definition is based in an essential way on the notion of the "modular operator", a mathematical tool which has its origin in the theory of v. Neumann algebras.

- Computations of relative entropies and entanglement measures in free quantum field theory (for previous work, see e.g. [5]).

- Upper and lower bounds on entanglement measures and relative entropies in the context of conformally invariant quantum field theories, in particular in low dimensions.

- Investigations of general properties of the modular flow and operator in general quantum field theory. In particular, we investigate the question whether the "modular flow" has an approximate geometrical meaning near the bounding surface S of a region of a general shape[8]. We are also interested in the conceptually important question of computing this modular for thermal states, vacuum states, and general regions in particular theories such as chiral conformal field theories.

[1] H. Araki, Publ. Res. Inst. Math. Sci. **11** (1975/76), 809–833
[2] K. Sanders, Commun. Math. Phys. **288** (2009), no.1, 271–285
[3] S.N. Solodukhin, Living Rev. Relativity **14** (2011), no.8

[4] E. Witten, "APS Medal for Exceptional Achievement in Research: Invited article on entanglement properties of quantum field theory," Rev. Mod. Phys. **90**, no. 4, 045003 (2018) doi:10.1103/RevModPhys.90.045003 [arXiv:1803.04993 [hep-th]].
[5] C. Weedbrook, S. Pirandola, R. García-Patrón, N.J. Cerf, T.C. Ralph, J.H. Shapiro and S. Lloyd, Rev. Mod. Phys. **84** (2012), no.2, 621–669
[6] S. Hollands and K. Sanders, "Entanglement measures and their properties in quantum field theory," arXiv:1702.04924 [quant-ph].
[7] S. Hollands, O. Islam and K. Sanders, "Relative entanglement entropy for widely separated regions in curved spacetime," arXiv:1711.02039 [math-ph].
[8] S. Hollands, "Relative entropy close to the edge," arXiv:1805.10006 [hep-th].

15.5 Yangians and symmetric correlators

R. Kirschner, J. Fuksa, A.P. Isaev, D. Karakhanyan

We have studied Yang-Baxter relations with the symmetry of the the orthosymplectic Lie super-algebras, in particular the RLL relations involving the fundamental R-matrix. The work is based on the classical results [1–3] and continues recent work [4, 5].

The concept of Yangian symmetric correlators has been proposed as a tool for the calculation of amplitudes in gauge field theories, where the Yangian of the type $s\ell_4$ applies [6, 7]. We have studied now in detail such symmetric correlators in the simpler case of type $s\ell_2$. Symmetric correlators can be used to define integral operators obeying Yang-Baxter relations. The latter can be used to solve completely the spectral problem of those operators. An application to the kernels of the evolution equation of generalized parton distributions has been pointed out.

[1] A.B. Zamolodchikov and Al.B. Zamolodchikov, "Factorized S Matrices in Two-Dimensions as the Exact Solutions of Certain Relativistic Quantum Field Models," Annals Phys. **120** (1979) 253.
[2] B. Berg, M. Karowski, P. Weisz and V. Kurak, "Factorized U(n) Symmetric s Matrices in Two-Dimensions," Nucl. Phys. B **134** (1978) 125.
[3] N.Yu. Reshetikhin, Integrable models of quantum one-dimensional models with $O(n)$ and $Sp(2k)$ symmetry, Theor. Math. Fiz. **63** (1985) 347-366.
[4] D. Chicherin, S. Derkachov and A. P. Isaev, "The spinorial R-matrix," J. Phys. A **46** (2013) 485201. arXiv:1303.4929 [math-ph].
[5] A. P. Isaev, D. Karakhanyan, R. Kirschner, "Orthogonal and symplectic Yangians and Yang-Baxter R operators," Nucl. Phys. **B904** (2016) 124147, arXiv:1511.06152
[6] D. Chicherin and R. Kirschner, *Yangian symmetric correlators,* Nucl. Phys. B **877** (2013) 484 doi:10.1016/j.nuclphysb.2013.10.006 [arXiv:1306.0711 [math-ph]].
[7] D. Chicherin, S. Derkachov and R. Kirschner, *Yang-Baxter operators and scattering amplitudes in N=4 super-Yang-Mills,* Nucl. Phys. B **881** (2014) 467 doi:10.1016/j.nuclphysb.2014.02.016 [arXiv:1309.5748 [hep-th]].

15.6 High-spin parton splitting in generalised Yang-Mills theory

R. Kirschner, G. Savvidy

The generalised Yang-Mills theory [1] involves gauge bosons of higher spin, based on a consistent extension of the Poincare group [2]. As in ordinary gauge field theory the tree-level amplitudes can be calculated from the action as well as by the BCFW rules [3] related to $s\ell_4$ Yangian symmetry.

Following the hypothesis [4] that the high-spin gluons contribute to the structure of hadrons in analogy to the ordinary gluons, we calculate the corresponding Lipatov-Altarelli-Parisi parton splitting kernels. Relying on results of [5] derived by Yangian symmetry we obtain a convenient universal form of the splitting kernels in dependence on the helicities of the involved partons.

[1] G. Savvidy, *Non-abelian tensor gauge fields.* Int. J. Mod. Phys. A **21** (2006) 4931 and 4959.
[2] I. Antoniadis, L. Brink and G. Savvidy, *Extensions of the Poincare group,* J. Math. Phys. **52** (2011) 072303 doi:10.1063/1.3607971 [arXiv:1103.2456 [hep-th]].
[3] R. Britto, F. Cachazo, B. Feng and E. Witten, *Direct proof of tree-level recursion relation in Yang-Mills theory,* Phys. Rev. Lett. **94** (2005) 181602 [arXiv:hep-th/0501052].
[4] G. Savvidy, *Asymptotic freedom of non-Abelian tensor gauge fields,* Phys. Lett. B **732** (2014) 150.
[5] J. Fuksa and R. Kirschner, *Correlators with $s\ell_2$ Yangian symmetry,* Nucl. Phys. B **914** (2017) 1 doi:10.1016/j.nuclphysb.2016.10.019 [arXiv:1608.04912 [hep-th]].

15.7 Hadron physics using background from lattice QCD

H. Perlt, A. Schiller

It is well known that the sea quark and gluon content of hadrons (Fig. 15.2) can be traced back to flavor singlet hadron matrix elements, following the operator product expansion. The calculation of these matrix elements is one of the greatest technical challenges left in lattice QCD. This is due to the fact that the lattice calculation of so-called "disconnected diagrams" is extremely noisy and gives a poor signal. An improved determination of these disconnected contributions is one of the main aims of this project.

For that we have proposed an alternative to the conventional three-point function technique for the study of hadron matrix elements in lattice QCD. By adapting the so called Feynman-Hellmann theorem (FH) to the lattice setting, we were able to isolate matrix elements in terms of energy shifts in the presence of appropriate weak external background fields. Our spin results contribute to a solution of the so called spin crisis of the proton and allow for a direct comparison of our lattice form factor results to experimental measurements at JLab. The HPC system JUQUEEN has been used to generate part of the necessary lattice configurations at different lattice couplings, quark masses, sizes and background fields. Among the results let us to mention here:

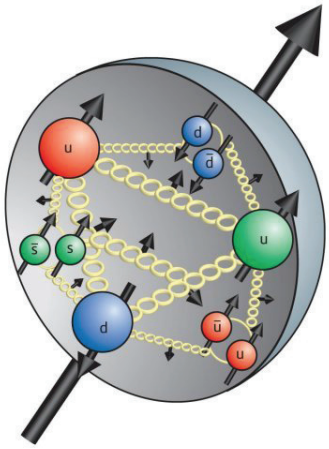

Figure 15.2: Schematic view of the proton with spin arrows of the quarks and gluon (from http://www.quantumdiaries.org/wp-content/uploads/2012/03/SPT78-proton.jpg).

- Calculation of spin distributions in the hadrons including the sea quark content [1, 2] (see Fig. 15.3).

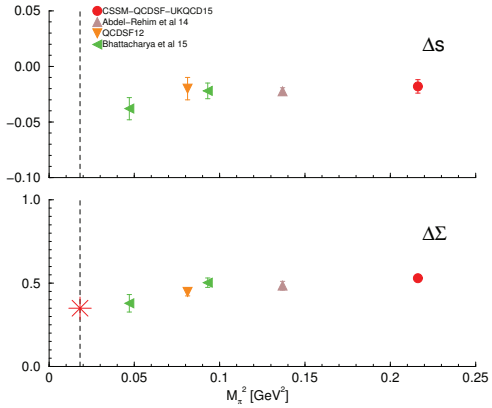

Figure 15.3: Strange quark and total quark spin for various lattice pion masses (in red our collaboration).

- Elastic form factors at large momentum transfer unreachable by standard lattice techniques [3–5] (see Fig. 15.4).
- Determination of the flavor-singlet axial-vector and scalar renormalisation constants [7].

[1] A. J. Chambers *et al.* [QCDSF and UKQCD Collaborations], Phys. Rev. D **90** (2014) 014510 [arXiv:1405.3019 [hep-lat]].
[2] A. J. Chambers *et al.*, Phys. Rev. D **92** (2015) no.11, 114517 [arXiv:1508.06856 [hep-lat]].
[3] A. J. Chambers *et al.*, PoS LATTICE **2015** (2016) 125 [arXiv:1511. [hep-lat]].
[4] A. Chambers *et al.*, PoS LATTICE **2016**, 168 (2017).

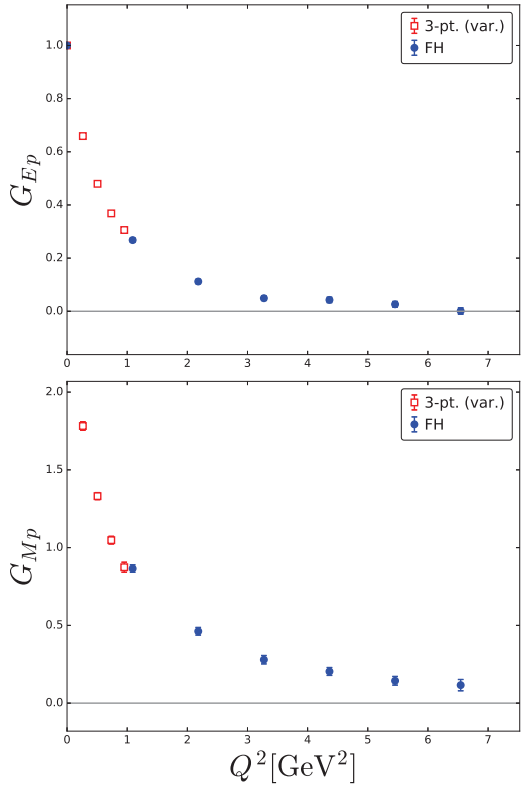

Figure 15.4: Electric and magnetic form factor vs. momentum transfer Q^2 compared to a standard variational three-point method [6].

[5] A. J. Chambers *et al.* [QCDSF and UKQCD and CSSM Collaborations], Phys. Rev. D **96**, no. 11, 114509 (2017) [arXiv:1702.01513 [hep-lat]].
[6] J. Dragos *et al.*, Phys. Rev. D **94** (2016) no.7, 074505 doi:10.1103/PhysRevD.94.074505 [arXiv:1606.03195 [hep-lat]].
[7] A. J. Chambers *et al.* [QCDSF Collaboration], Phys. Lett. B **740** (2015) 30 [arXiv:1410.3078 [hep-lat]].

15.8 Nucleon structure functions from lattice forward Compton amplitude

H. Perlt, A. Schiller

Traditionally, parton distribution functions (PDFs) are obtained from global fits to the experimental data. However, there are gaps in the experimental coverage, and hence it is highly desired to have robust results from numerical simulations in lattice QCD. So far lattice calculations have been limited to a few low Mellin moments of selected PDFs. Though providing useful information, both as benchmarks of lattice QCD calculations and as constraints in global fits, this is insufficient to reconstruct the total momentum dependence of the structure functions without significant model dependence.

Our approach is based on the computation of the structure functions from the forward Compton scattering amplitude [1]. Here, one has to compute the current-current correlator

$$T_{\mu\nu}(p,q) = \int \mathrm{d}^4x\, \mathrm{e}^{iqx} \langle p,s|TJ_\mu(x)J_\nu(0)|p,s\rangle \tag{15.5}$$

at large q^2, which involves the time ordered product of electromagnetic currents J_μ sandwiched between states of momentum p and spin s. We started with the calculation of the structure function F_1. Its relation to the Compton scattering amplitude is given by ($\omega = 2pq/q^2$)

$$T_{33}(p,q) = \mathcal{F}_1(\omega,q^2) = 4\omega \int_0^1 dx\, \frac{\omega x}{1-(\omega x)^2}\, F_1(x,q^2) \tag{15.6}$$

The Compton amplitudes can be computed most efficiently, including disconnected contributions, by a simple extension of existing implementations of the Feynman-Hellmann technique to lattice QCD [2]. We consider local vector and axial vector currents only. The corresponding renormalisation constants Z_V, Z_A are known [3]. No further renormalisation is needed. To compute the Compton amplitude T_{33} from the Feynman-Hellmann relation, we introduce the perturbation to the Lagrangian

$$\mathcal{L}(x) \to \mathcal{L}(x) + \lambda \mathcal{J}_3(x)\,, \quad \mathcal{J}_3(x) = Z_V \cos(\vec{q}\cdot\vec{x})\, e_q\, \bar{q}(x)\gamma_3 q(x)\,, \tag{15.7}$$

where q is the quark field, $q = u,d,s$ in our case, to which the photon is attached, and e_q is its electric charge. Note that λ has dimension mass. Taking the second derivative of the nucleon two-point function $\langle N(\vec{p},t)\bar{N}(\vec{p},0)\rangle_\lambda \simeq C_\lambda\, \mathrm{e}^{-E_\lambda(p,q)\,t}$ with respect to λ on both sides, we obtain

$$-2E_\lambda(p,q)\, \frac{\partial^2}{\partial\lambda^2} E_\lambda(p,q)\,\Big|_{\lambda=0} = T_{33}(p,q)\,. \tag{15.8}$$

Only one insertion is needed to compute $E_\lambda(p,q)$ for all momenta p at any value of q and parameter λ. Varying q^2 will allow us to test the twist expansion and, in particular, isolate twist-four contributions. A conventional calculation of the four-point function $\langle p,s|J_\mu(x)J_\nu(0)|p,s\rangle$, in contrast, would involve all-to-all quark propagators twice consecutively, which is not practical.

After a successfull test calculation with mock data[1] (which were taken from experiments) we made a first run with data from lattice simulation. It turns out that the second derivative of the nucleon energy can be computed rather accurately. In a proof-of-principle study we have computed (15.8) from $O(900)$ configurations generated at the SU(3) symmetric point [4] on a $32^3\times 64$ lattice with lattice spacing $a \approx 0.074$ fm generated at rather heavy quark masses, $m_\pi = m_K = 465$ MeV. First results are presented in Figs. 15.5 and 15.6, where the contribution from

$$\mathcal{F}_1(0,q^2) = -2\, E_\lambda(0,q)\, \partial^2 E_\lambda(0,q)/\partial\lambda^2\,\Big|_{\lambda=0} \tag{15.9}$$

has been subtracted. We used momenta $\vec{p} = (2,-1,0), (-1,1,0), (1,0,0), (0,1,0), (2,0,0), (-1,2,0), (1,1,0), (0,2,0), (2,1,0), (1,2,0)$, from left to right, and $\vec{q} = (3,5,0)$, in lattice units. For our lattice this translates into $q^2 \approx 9.3\ \mathrm{GeV}^2$. Z_V has been taken from [3]. The

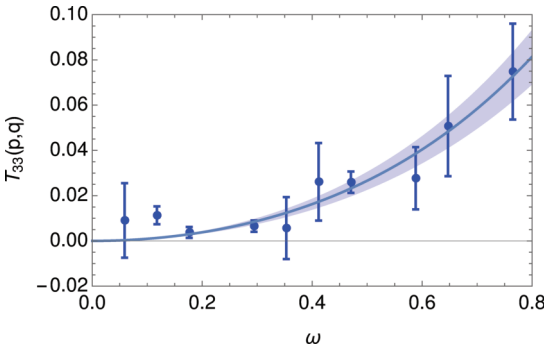

Figure 15.5: The proton Compton amplitude $T_{33}(p,q)$ for the lattice described in the text. The solid line shows a sixth order polynomial fit (giving $\chi^2/\text{dof} = 0.9$), and the shaded area shows the error.

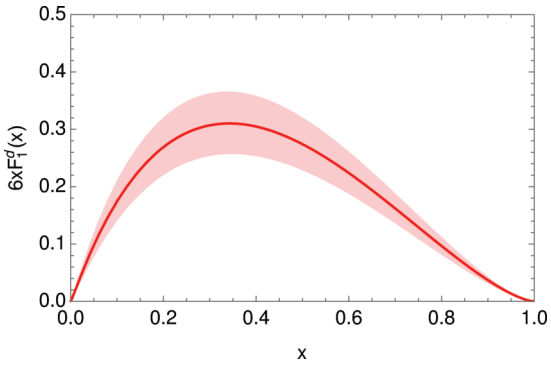

Figure 15.6: The structure function $F_1^{u-d}(x)$ as obtained from the Compton amplitude shown in Fig. 15.5. The shaded area shows the error.

precision for lattice momenta $\vec{p}^2 = 1$ and 2 is already quite impressive. We emphasise that the lattice computation has been done away from the physical point. However, one recognises already a fairly good agreement in the shape compared to the result of the mock data in [1]. We should be able to improve on the precision of the data at higher momenta by employing 'momentum smearing' techniques, which has not been attempted here.

[1] A. J. Chambers, R. Horsley, Y. Nakamura, H. Perlt, P. E. L. Rakow, G. Schierholz, A. Schiller, K. Somfleth, R. D. Young, J. M. Zanotti, Phys. Rev. Lett. **118** (2017) no.24, 242001, [arXiv:1703.01153 [hep-lat]].

[2] R. Horsley, R. Millo, Y. Nakamura, H. Perlt, D. Pleiter, P.E.L. Rakow, G. Schierholz, A. Schiller, F. Winter, J.M. Zanotti, Phys. Lett. B **714** (2012) 312 [arXiv:1205.6410 [hep-lat]].

[3] M. Constantinou, R. Horsley, H. Panagopoulos, H. Perlt, P. E. L. Rakow, G. Schierholz, A. Schiller and J. M. Zanotti, Phys. Rev. D **91** (2015) 1, 014502 [arXiv:1408.6047 [hep-lat]].

[4] W. Bietenholz *et al.* [QCDSF Collaboration], Phys. Rev. D **84** (2011) 054509 [arXiv:1102.5300 [hep-lat]].

15.9 Generalized Wentzell boundary conditions and quantum field theory

J. Zahn

Quantum Field Theory in the presence of boundaries has technologically relevant applications, the Casimir effect, but is also important for recent developments in high energy physics, in particular holography (the AdS/CFT correspondence). The goal of the project is to study exotic boundary conditions involving second order derivatives, known in the mathematical literature as *generalized Wentzell boundary conditions*.

These occur for example for a spinning string with a mass attached to the boundary [1], but also in the context of the AdS/CFT correspondence [2].

In our project [3], we investigate different aspects of these boundary condition. As a first step, we establish well-posedness of the wave equation at the classical level, including a proof of causal propagation. We then quantize the system and in particular discuss holographic aspects.

[1] J. Zahn, "The excitation spectrum of rotating strings with masses at the ends," JHEP **1312**, 047 (2013).
[2] K. Skenderis, "Lecture notes on holographic renormalization," Class. Quant. Grav. **19**, 5849 (2002).
[3] J. Zahn, "Generalized Wentzell boundary conditions and quantum field theory," Annales Henri Poincare **19**, no. 1, 163 (2018).

15.10 Semi-classical energies of rotating strings

J. Zahn

For several reasons, the Nambu-Goto string is an interesting model: It exhibits diffeomorphism invariance, making it a toy model for (quantum) gravity. It also provided motivation for the Polyakov string, which led to string theory as a candidate for a fundamental theory. Furthermore, it constitutes a phenomenological model for QCD (Quantum Chromo-Dynamics) vortex lines connecting quarks, i.e., for the description of hadrons.

It is well-known that in the covariant quantization of the open Nambu-Goto string, the *intercept* a is a free parameter, only constrained by the fact that the theory is consistent only for $a \leq 1$ and $D \leq 25$ or $a = 1$ and $D = 26$. Furthermore, the ground state energies $E_{\ell_{1,2}}$ for a given angular momentum $\ell_{1,2} > 0$, say in the $1-2$ plane, lie on the *Regge trajectory*

$$E^2_{\ell_{1,2}} = 2\pi\gamma(\ell_{1,2} - a),$$

with γ the string tension. In other approaches to quantization, the critical dimension $D = 26$ with intercept $a = 1$ are singled out. One way to compute a for $D < 26$ is to use the effective action of Polchinski and Strominger [1]. With this, the result $a = 1$ is obtained for any dimension D [2].

Another approach to string theory in non-critical dimensions is via perturbation theory around classical solutions [3], using concepts from quantum field theory on curved space-times. It is a priori not clear that the two approaches yield the same result. The second approach has the advantage that also the case of masses at the endpoints can be treated, a model which is particularly interesting in the context of QCD phenomenology [4]. With our method [5], we find $a = 1$ for any D, consistent with the results found in [2]. We can also treat the closed string with our methods [6], with results again in agreement with those of [2].

[1] J. Polchinski and A. Strominger, "Effective string theory," Phys. Rev. Lett. **67**, 1681 (1991).

[2] S. Hellerman and I. Swanson, "String Theory of the Regge Intercept," Phys. Rev. Lett. **114**, no. 11, 111601 (2015).
[3] D. Bahns, K. Rejzner and J. Zahn, "The effective theory of strings," Commun. Math. Phys. **327**, 779 (2014).
[4] J. Sonnenschein and D. Weissman, "Rotating strings confronting PDG mesons," JHEP **1408**, 013 (2014).
[5] J. Zahn, "Semiclassical energy of open Nambu-Goto strings," Phys. Rev. D **97**, no. 6, 066028 (2018).
[6] M. Kozon and J. Zahn, "The semi-classical energy of closed Nambu-Goto strings," arXiv:1610.02813 [hep-th].

15.11 Background independence in gauge theories

M. Taslimi Tehrani, J. Zahn

In Quantum Field Theory (QFT), one frequently considers the quantum fluctuations around classical field configurations. Examples are:

- Spontaneous symmetry breaking in the Standard Model, where one considers quantum fluctuations around a non-trivial classical configuration of the Higgs field;
- The background field method, which is an efficient tool, for example, for the computation of the renormalization group flow;
- Perturbative Quantum Gravity, where one has to use a non-trivial background metric, providing the necessary structure for the formulation of a QFT.

Hence, the issue of *background independence* is of high conceptual importance. It is particularly interesting in gauge theories, where the gauge fixing introduces an explicit background dependence.

Previous treatments of the topic are not completely satisfactory, as they are either in a formal Riemannian path integral framework with no clear relation to the Lorentzian space-times one is ultimately interested in, or only treat the background field as an infinitesimal perturbation, and thus miss non-perturbative effects. Furthermore, they are not "operational" in that they do provide a means to consistently assign "the same" observable to different backgrounds.

As there is no preferred (vacuum) state for generic backgrounds, it is advantageous to address the issue of background independence in the algebraic approach. We directly (perturbatively) construct the algebras of observables for the different background configurations, using locally covariant renormalization techniques developed in the context of QFT on curved space-times [1]. Background independence for us then means that we can unambiguously identify observables on different backgrounds (at least for infinitesimally close backgrounds). As suggested in [2], this can be formulated in the spirit of *Fedosov quantization* [3]: One considers the bundle of observable algebras over the manifold of background configurations and constructs a flat connection on it. The sections that are flat, i.e., covariantly constant, w.r.t. this connection provide a

consistent assignment of an observable to each background. We show [4] that in the case of Yang-Mills theory in four space-time dimensions such a flat connection indeed exists.

[1] S. Hollands and R. M. Wald, "Local Wick polynomials and time ordered products of quantum fields in curved space-time," Commun. Math. Phys. **223**, 289 (2001).
[2] S. Hollands, "Background independence in Quantum Field Theory," unpublished notes (2011).
[3] B. v. Fedosov, "A Simple geometrical construction of deformation quantization," J. Diff. Geom. **40**, no. 2, 213 (1994).
[4] M. Taslimi Tehrani and J. Zahn, "Background independence in gauge theories," arXiv:1804.07640 [math-ph].

15.12 Quantum integrable models

H. Bostelmann*, D. Cadamuro, Y. Tanimoto†

*York U
†Rome "Tor Vergata" U

Integrable models are a special class of 1 + 1-dimensional QFTs, where the two-particle scattering process characterizes the theory completely. They are constructed as an *inverse scattering problem*, specifically, given a function S_2 as a mathematical input, one constructs the corresponding QFT having this two-particle scattering function. There are several simplifications when considering integrable theories. First of all, unlike most interacting field theories they can be represented on a Fock space, with the interacting vacuum given by the usual Fock vacuum, allowing for explicit computations. Further, they are amenable to a treatment in a non-perturbative setting [1], avoiding to deal with formal power series whose convergence is generally unknown.

Physically, they are toy models for interaction, but share interesting common features with interacting theories in higher dimensions. For example, the nonlinear $O(N)$ sigma models [2] are linked to experimentally realizable situations in condensed matter systems. They can also be regarded as simplified analogues of four-dimensional nonabelian gauge theories, inasmuch as they share crucial features with them, including renormalizability, asymptotic freedom, and the existence of instanton solutions. Then there are models that can support a representation of a gauge group or a group of internal symmetries, for example, the 1 + 1 dimensional $SU(N)$-symmetric models (such as the chiral Gross-Neveu and principal chiral models) which are of importance in physics as toy models of quantum field theory with relations to both gauge and string theory, and have been analyzed both in general and in the limit $N \to \infty$. Finally, the Ising model is widely known also for its counterpart in statistical mechanics in the context of lattice spin systems. Therefore, integrable systems provide a "landscape" of possible interactions, that one can use as a testbed for ideas and techniques in more realistic models.

In our group we are interested in the rigorous construction of such models, and in the structure of their local observables [6]. In particular, we study models [3–5] where

the two-particle scattering function has poles inside the so called "physical strip", since these poles are believed to correspond to "bound states" of particles; examples of such theories are the Sine-Gordon and Thirring models.

[1] Gandalf Lechner, "Construction of Quantum Field Theories with Factorizing S-Matrices," Commun. Math. Phys. **277**, 821–860 (2008).
[2] Hrachya M. Babujian, Angela Foerster, and Michael Karowski, "Exact form factors of the $O(N)$ σ-model," Journal of High Energy Physics **2013**, 1–53 (2013).
[3] Daniela Cadamuro, Yoh Tanimoto, "Wedge-Local Fields in Integrable Models with Bound States," Commun. Math. Phys. **340**, 661–697 (2015).
[4] Daniela Cadamuro, Yoh Tanimoto, "Wedge-Local Fields in Integrable Models with Bound States II: Diagonal S-Matrix," Annales Henri Poincaré **18**, 233–279 (2017).
[5] Daniela Cadamuro, Yoh Tanimoto, "Wedge-local observables for factorizing S-matrix with gap in the coupling constant," Rev. Math. Phys. **30**, 1850010 (2018).
[6] Henning Bostelmann, Daniela Cadamuro, "Towards an explicit construction of local observables in integrable quantum field theories," ArXiv:1806.00269 (2018).

15.13 Quantum energy inequalites

H. Bostelmann*, D. Cadamuro, C.J. Fewster*

*York U

The classical energy conditions, originally motivated by the Penrose-Hawking singularity theorems of general relativity, are violated by quantum fields. A reminiscent notion of such conditions are the so called quantum energy inequalities (QEIs), which are however not known to hold generally in quantum field theory.

Mathematically, QEIs are lower bounds for the smeared energy density, $T^{00}(g^2) = \int dt\ g^2(t)T^{00}(0,t)$ of the form

$$\langle \varphi, T^{00}(g^2)\varphi\rangle \geq -c_g\|\varphi\|^2 \tag{15.10}$$

for all suitably regular state vectors φ and all real-valued test functions g, where $c_g > 0$ is a constant depending only on g. There is also a slightly weaker form of this inequality which can include a mild dependence on the energy content of the quantum state.

QEIs of the form (15.10) have been proved for free fields (both in flat and curved spacetimes) and conformal fields (see [1] for a review), excluding situations where interaction (scattering) between particles is present. Weaker forms of quantum inequalities have been proved for certain "classically positive" expressions in [2], but without a clear relation to the energy density.

Only recently, a state-independent QEI has been established for the massive Ising model [3], which represents the first result to our knowledge of a QEI in a self-interacting situation. Partial results have been obtained later in a larger class of "scalar" integrable systems, including the sinh-Gordon model [4].

In our group we are interested in investigating QEIs in quantum field theories with self-interaction, generalizing progressively the type of interaction. The aim is to study the dependence of QEI on the type of particle interaction, as well as on other

model parameters, and to exhibit possible counterexamples and edgecases to QEIs by considering a range of explicitly tractable models.

This is part of the DFG funded Emmy Noether project *"The quantum stress-energy tensor"* https://home.uni-leipzig.de/tet/?page_id=2507 .

[1] Christopher J. Fewster, "Energy inequalities in quantum field theory," Preprint math-ph/0501073 (2005).
[2] Henning Bostelmann, Christopher J. Fewster, "Quantum Inequalities from Operator Product Expansions," Commun. Math. Phys. **292**, 761–795 (2009).
[3] Henning Bostelmann, Daniela Cadamuro, and Christopher J. Fewster, "Quantum Energy Inequality for the Massive Ising Model," Phys. Rev. D **88**, 025019 (2013).
[4] Henning Bostelmann, Daniela Cadamuro, "Negative energy densities in integrable quantum field theories at one-particle level," Phys. Rev. D **93**, 065001 (2016).

15.14 Funding

Investigation of the hadron structure with the Feynman–Hellmann theorem
H. Perlt
PE 2792/2-1

DFG Emmy-Noether fellowship "The quantum stress-energy tensor"
D. Cadamuro
CA 1850/1-1

MPG Vorhaben "Kooperation zur Stärkung der Mathematischen Physik"
S. Hollands (jointly with Prof. F. Otto, director MPI MiS)
M.FE.A.MATN0003

15.15 Organizational Duties

Prof. S. Hollands
- Group leader
- Group speaker
- Speaker of the International Max Planck Research School (IMPRS) Mathematics in the Sciences
- Kolloquium organizer
- Co-Organization of "Physics and Mathematics of Quantum Field Theory", workshop at Banff International Research Station (Canada), July 29 – August 3, 2018

Dr. A. Schiller
- Referee Phys. Rev. D
- Referee Europhysics Journal C

Dr. J. Zahn
- Erasmus coordinator
- Referee: Ann. Henri Poincaré, European Physical Journal C, Journal of Physics A, Letters in Mathematical Physics

Dr. D. Cadamuro
- Emmy Noether group leader
- Referee: Communications in Mathematical Physics, Physics Letters A
- Editor of the *Springer Proceedings in Mathematics and Statistics* for the Workshop on "Macroscopic Limits of Quantum Systems", Technische Universität München, March 30 - April 1, 2017 (2018)

15.16 External Cooperations

Academic

- DESY Hamburg
  Prof. G. Schierholz (QCDSF collaboration)
- Edinburgh U., UK
  Dr. R. Horsley (QCDSF collaboration)
- Liverpool U., UK
  Dr. P.E.L. Rakow (QCDSF collaboration)
- Adelaide U., Australia
  Dr. J. Zanotti (QCDSF collaboration)
- Cyprus U. Nikosia
  Prof. H. Panagopoulos and collaborators
- Jena U.
  Dr. A. Sternbeck
- Dubna, Russia
  Dr. E.-M. Ilgenfritz
- U Chicago, USA
  Prof. R. M. Wald
- Kinki U., Japan
  Prof. A. Ishibashi
- U Michigan, USA
  Prof. D. Garfinkle
- Dublin City U, Ireland
  Dr. J. Sanders
- York U., UK
  Dr. M. Fröb
- Dubna, Russia
  Prof. A. Isaev (Heisenberg-Landau grant)
- St. Petersburg, Steklov Inst., Russia
  Dr. S.E Derkachov
- Yerevan Phys. Inst., Armenia
  Dr. D. Karakhanyan

- Nottingham U, UK
  Dr. A. Schenkel
- U. York, UK
  Dr. H. Bostelmann and Prof. C. J. Fewster
- U. Rome "Tor Vergata", Italy
  Dr. Y. Tanimoto
- TU München, Germany
  Dr. W. Dybalski
- Cardiff U., UK
  Dr. G. Lechner
- U. Leeds, UK
  Prof. S. Ruijsenaars, O. Islam

15.17 Publications

Journals

D. Cadamuro, Y. Tanimoto: *Wedge-local observables for factorizing S-matrix with gap in the coupling constant*, Reviews in Mathematical Physics **30**, 1850010 (2018)
arXiv:1612.02073

P. Duch: *Weak adiabatic limit in quantum field theories with massless particles*, Annales Henri Poincare **19**, no. 3, 875 (2018)
doi:10.1007/s00023-018-0652-z, arXiv:1801.10147

C.J. Fewster, S. Hollands: *Probability distributions for the stress tensor in conformal field theories*
doi:10.1007/s11005-018-1124-6, arXiv:1805.04281

M.B. Fröb, M. Taslimi Tehrani: *Green's functions and Hadamard parametrices for vector and tensor fields in general linear covariant gauges*, Phys. Rev. D **97**, no. 2, 025022 (2018)
doi:10.1103/PhysRevD.97.025022, arXiv:1708.00444

S. Hollands: *Action principle for OPE*, Nucl. Phys. B **926**, 614 (2018)
doi:10.1016/j.nuclphysb.2017.11.013, arXiv:1710.05601

S. Hollands, G. Lechner: *$SO(d,1)$ -Invariant Yang-Baxter Operators and the dS/CFT Correspondence*, Commun. Math. Phys. **357**, no. 1, 159 (2018)
doi:10.1007/s00220-017-2942-6, arXiv:1603.05987

S. Hollands, O. Islam, K. Sanders: *Relative entanglement entropy for widely separated regions in curved spacetime*, J. Math. Phys. **59**, no. 6, 062301 (2018)
doi:10.1063/1.5017093, arXiv:1711.02039

D. Karakhanyan, R. Kirschner: *Orthogonal and symplectic Yangians - linear and quadratic evaluations*, Nucl. Phys. B **933** (2018) 14
doi:10.1016/j.nuclphysb.2018.05.022, arXiv:1712.06849

R. Kirschner: *QCD at high energies and Yangian symmetry*, Universe **4** (2018) no.11, 124
doi:10.3390/universe4110124, arXiv:1810.03549

S. Pottel: *BPHZ renormalization in configuration space for the $\mathcal{A}^4$-model*, Nucl. Phys. B **927**, 274 (2018)
doi:10.1016/j.nuclphysb.2017.12.020, arXiv:1709.10194

J. Zahn: *Generalized Wentzell boundary conditions and quantum field theory*, Annales Henri Poincaré **19**, no. 1, 163 (2018)
doi:10.1007/s00023-017-0629-3, arXiv:1512.05512

J. Zahn: *Semiclassical energy of open Nambu-Goto strings*, Phys. Rev. D **97**, no. 6, 066028 (2018)
doi:10.1103/PhysRevD.97.066028, arXiv:1605.07928

Books

D. Cadamuro, M. Duell, W. Dybalski, S. Simonella: *Macroscopic Limits of Quantum Systems*, Munich, March 30 - April 1, 2017, Springer Proceedings in Mathematics & Statistics (2018)

S. Hollands, K. Sanders: *Entanglement measures and their properties in quantum field theory*, SpringerBriefs in Mathematical Physics, Springer International Publishing (2018)

in press

D. Cadamuro, W. Dybalski: *Relative normalizers of automorphism groups, infravacua and the problem of velocity superselection in QED*
arXiv:1807.07919, accepted for publication in Commun. Math. Phys.

Talks

D. Cadamuro: *Lower bounds for the energy density in quantum integrable models*, talk at the seminar "Mathematics and Physics of local quantum field theories", Humboldt-Universität zu Berlin, Germany, January 2018

D. Cadamuro: *An introduction to algebraic quantum field theory*, talk at the seminar "maths bites trento", University of Trento, Italy, March 2018

D. Cadamuro: *Removing velocity superselection with infravacuum representations*, talk at the "Mathematical Physics seminar", University of York, UK, June 2018

D. Cadamuro: *Construction of Haag-Kastler nets for factorizing S-matrices with poles. part I*, talk at workshop "Physics and Mathematics of Quantum Field Theory", Banff International Research Station for Mathematical Innovation and Discovery, Canada, July – August 2018

D. Cadamuro: invited guest at the CRM-SIMONS Program "Mathematical challenges in many-body physics and quantum information", Centre de recherches mathématiques (CRM), Montréal, Canada, October 2018

D. Cadamuro: *Lower bounds for the energy density in quantum integrable models*, talk at conference "Progress and Visions in Quantum Theory in View of Gravity: Bridging foundations of physics and mathematics", Max Planck Institute for Mathematics in the Sciences, Leipzig, Germany, October 2018

D. Cadamuro: *Lower bounds for the energy density in quantum integrable models*, talk at the "Mathematical Phyics seminar", TU München, Germany, November 2018

S. Hollands: *Entanglement and modular theory*, talk at conference "Quantum Information and Operator Algebras", Rome, Italy, February 2018

S. Hollands, invited guest at the Centro Atomico Balseiro, Bariloche, Argentina, March 2018

S. Hollands: *Perturbative renormalization of YM_4 on curved Lorentzian spacetimes*, talk at workshop "Quantum fields, scattering and spacetime horizons: mathematical challenges", Les Houches, France, May 2018

S. Hollands: *Renormalization of Yang-Mills theories*, talk at workshop "Physics and Mathematics of Quantum Field Theory", Banff International Research Station, Canada, May 2018

S. Hollands: *Symmetry in General Relativity*, theory colloquium at CERN, Geneva, Switzerland, September 2018

S. Hollands: *Probability distribution of the stress tensor in CFT*, seminar talk at EPFL Lausanne, Switzerland, September 2018

S. Hollands: *Probability distribution of the stress tensor in CFT*, talk at workshop "Energy conditions in quantum theory and gravity", York, UK, September 2018

S. Hollands: *Perturbative QFT in D=4*, talk at workshop "Quantum field theory, renormalisation and stochastic partial differential equations", Issac Newton Institute, Cambridge, UK, October 2018

S. Hollands: *Entanglement measures and modular theory*, talk at workshop "AQFT, Modular Techniques, and Rényi Entropy", AEI Golm, Germany, October 2018

R. Kirschner: *QCD at high energies and Yangian symmetry*, talk at "7th Intern. Conference on New Frontiers in Physics", Kolymbari, Greece, July 2018

R. Kirschner: *Orthogonal and symplectic Yangians - representations of the quadratic evaluations*, talk at "32nd International Colloquium on Group Theoretical Methods in Physics", Prague, Czech Republic, July 2018

M. Taslimi Tehrani: *Background independence in gauge theories*, talk at conference "Progress and Vision in Quantum Theory in View of Gravity", Leipzig, Germany, October 2018

J. Zahn: *Global anomalies on Lorentzian space-times*, talk at workshop "Local Quantum Physics 41", Göttingen, Germany, February 2018

J. Zahn: *The current density in QED in external potentials*, talk at workshop "Pair creation", Jena, Germany, October 2018

15.18 Graduations

Doctorate

- Steffen Pottel
  Bogoliubov-Parasiuk-Hepp-Zimmermann renormalization in configuration space
  May 2018
- Mojtaba Taslimi Tehrani
  Aspects of gauge theories in Lorentzian curved space-times
  November 2018

Master

- Sebastian Drawert
  Der gravitative Memory-Effekt drehimpulsbehafteter Quellen
  March 2018
- Marek Kozon (external)
  Semi-classical energy of elliptic Nambu-Goto string
  September 2018
- Ludwig A. Hoffmann
  Positivity of Bondi mass in odd dimensions
  November 2018

Bachelor

- Narek Papoyan
  Angle-resolved time delay in quantum mechanical scattering
  April 2018
- Sami Abdallah
  Gauge theoretic formulation of General Relativity
  September 2018

15.19 Guests

- Dr. Stephen Green
  AEI Golm
  January 29–31, 2018.
- Dr. Pawel Duch
  U Cracow
  March 19–23, 2018.

- Dr. Ko Sanders
  Dublin City U
  May 2–14, 2018.
- Dr. Asger Ipsen
  HU Berlin
  June 4, 2018.
- Prof. Robert M. Wald
  U Chicago
  June 11–15, 2018.
- Prof. Jürg Fröhlich
  ETH Zürich
  June 11–14, 2018.
- Prof. Christoph Kopper
  Ecole Polytechnique
  June 13–15, 2018.
- Dr. Michal P. Heller
  AEI Golm
  October 29, 2018.
- Dr. Federico Faldino
  U Genova
  November 11–14, 2018.
- Dr. Yoh Tanimoto
  U Roma "Tor Vergata"
  December 3 –7, 2018.
- Prof. Gerrit Schierholz
  DESY
  December 4–5, 2018
- Dr. Gandalf Lechner
  U Cardiff
  December 17 – 21, 2018.
- Dr. David Karakhanyan
  Yerevan Physics Institute
  October 15 – December 8, 2018.

Author Index

E

F

G

H

I

J

K

L

M

N

O

P

Q

R

S

T

V

W

Y

Z

CELEBRATING 5 YEARS

ACS Photonics

DECEMBER 2018
VOLUME 5
NUMBER 12
pubs.acs.org/photonics

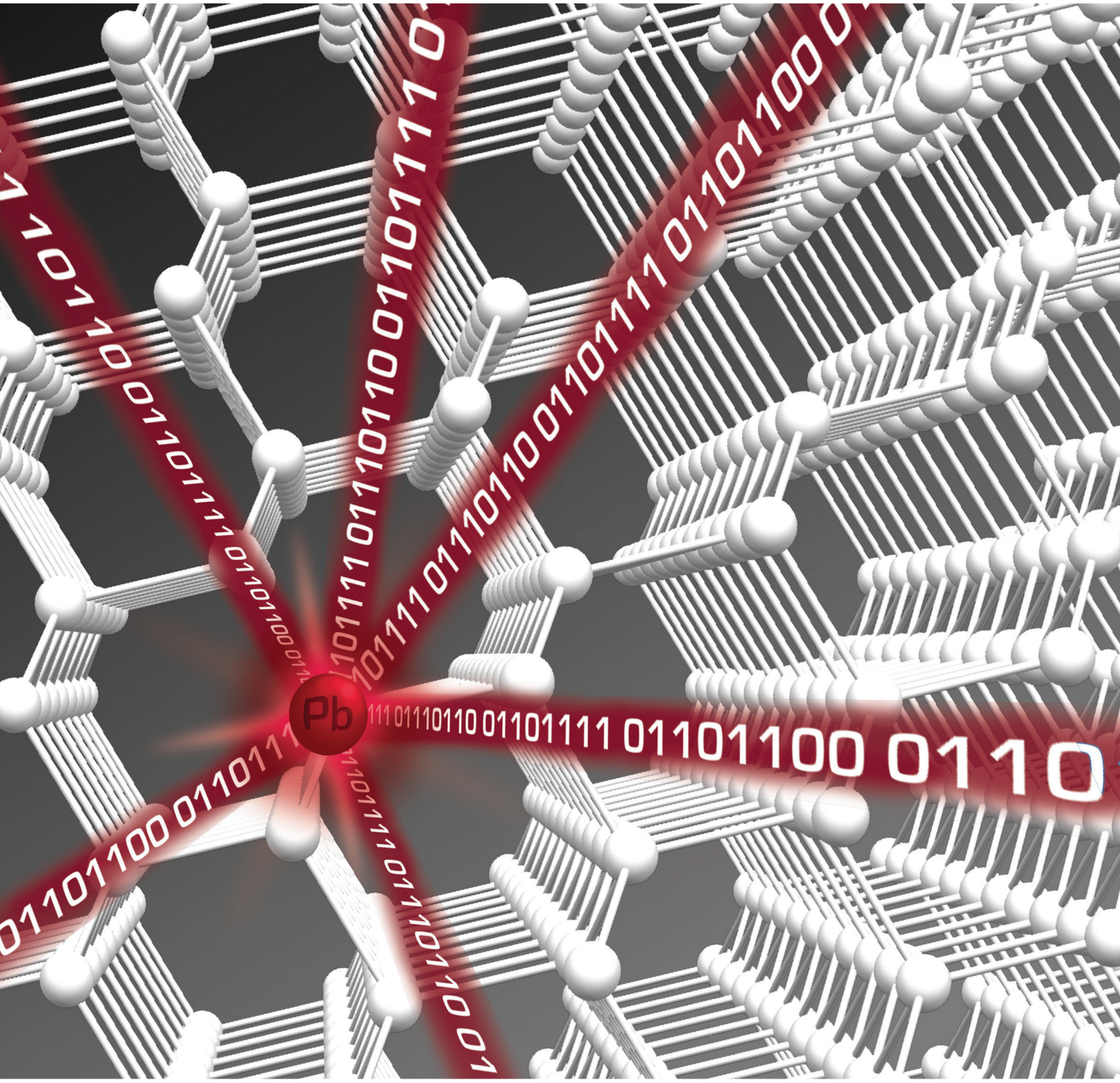

ACS Publications
Most Trusted. Most Cited. Most Read.

www.acs.org